DOE/ER/13000--T13

Stanford Synchrotron Radiation Laboratory

SSRL
Activity Report 1989

Arthur Bienenstock
Director

Herman Winick
Deputy Director

SSRL Report 90/01

Editor - Katherine Cantwell
Technical Production - Carol Mitchell

STANFORD SYNCHROTRON RADIATION LABORATORY

ACTIVITY REPORT FOR 1989

ABOUT THE STANFORD SYNCHROTRON RADIATION LABORATORY

SSRL is a national facility supported primarily by the Department of Energy for the utilization of synchrotron radiation for basic and applied research in the natural sciences and engineering. It is a user-oriented facility which welcomes proposals for experiments from all researchers.

The synchrotron radiation is produced by the 3.5 GeV storage ring, SPEAR, and the 15 GeV storage ring, PEP, operated by the Stanford Linear Accelerator Center (SLAC). SPEAR is dedicated to the production of synchrotron radiation during 50% of its operations time or about 4 months per year. Operation on PEP is generally parasitic with the high energy physics program. Starting in the fall 1990 SPEAR will be fully dedicated to synchrotron radiation operation, and is expected to operate 6 - 9 months each year.

SSRL currently has 25 experimental stations on the SPEAR and PEP storage rings. There are 166 active proposals for experimental work from 126 institutions involving approximately 519 scientists. There is normally no charge for use of beam time by experimenters.

Additional information for prospective users is contained in the booklet "SSRL User Guide". Further information about the facility may be obtained by writing or telephoning Katherine Cantwell at SSRL, SLAC Bin 69, P.O. Box 4349, Stanford, CA 94309 -0210 - telephone (415) 926-3191.

This report summarizes the activity at SSRL for the period January 1, 1989 to December 31, 1989.

SSRL is operated by the Department of Energy, Office of Basic Energy Sciences, Division of Chemical Sciences. Support for research by SSRL staff is provided by tht Office's Division of Material Science. The SSRL Biotechnology Program is supported by the NIH, Biomedical Resource Technology Program, Division of Research Resources.

Stanford Synchrotron Radiation Laboratory
1989 ACTIVITY REPORT

TABLE OF CONTENTS

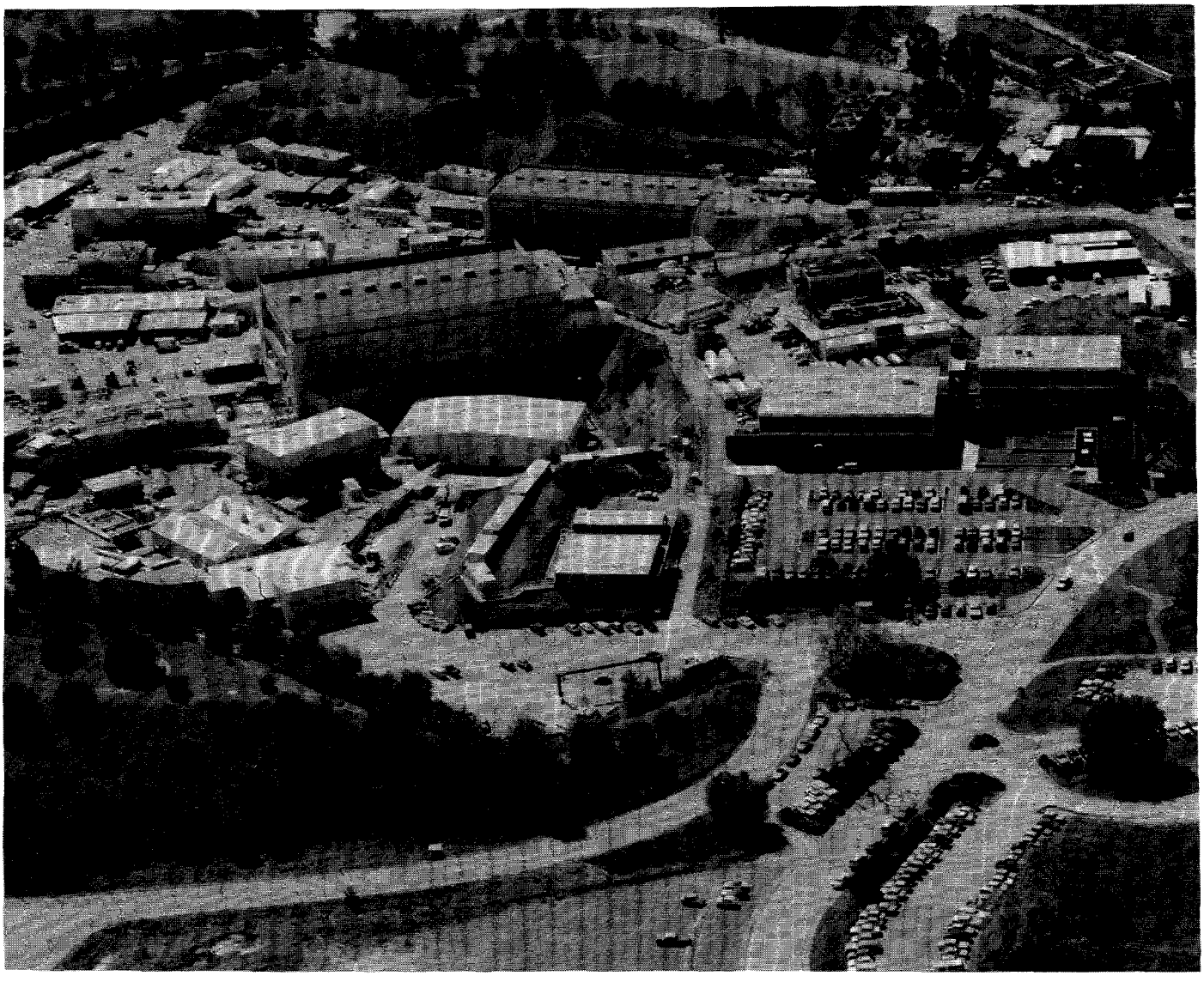

Overview of SSRL

-Photo by Joe Faust

The SPEAR ring is shown on the left side of the picture. SSRL has 23 stations housed in the two building (131,120) adjacent to the north and south arcs of the ring. The large white building in the center is the shelter for the new 3 GeV injector. The building (LOS) on the far right houses the scientific, administrative and engineering staffs.

ACTIVITY REPORT 1989

INTRODUCTION

The April, 1990 SPEAR synchrotron radiation run was one of the two or three best in SSRL's history. High currents (100 milliamps) were accumulated, ramping went easily, lifetimes were long (averaging 23 hours), beam dumps were infrequent and the average current was 42.9 milliamps. In the one month of operation, 63 different experiments involving 208 scientists from 50 institutions received beam. The end-of-run summary forms completed by the experimenters indicated high levels of user satisfaction with the beam quality and with the outstanding support received from the SSRL technical and scientific staffs.

These fine experimental conditions result largely from the SPEAR repairs and improvements performed during the past year and described in Section I. Also quite signficant was Max Cornacchia's leadership of the SLAC staff.

SPEAR's performance this past April stands in marked contrast to that of the January-March, 1989 run which is also described in Section 1. It is, we hope, a harbinger of the operation which will be provided in FY '91, when the SPEAR injector project is completed (Section II) and SPEAR is fully dedicated to synchrotron radiation research.

Over the coming years, SSRL intends to give highest priority to increasing the effectiveness of SPEAR and its various beam lines. The beam line and facility improvements performed during 1989 are described in Section III.

In order to concentrate effort on SSRL's three highest priorities prior to the March-April run: (1) to have a successful run, (2) to complete and commission the injector, and (3) to prepare to operate, maintain and improve the SPEAR/injector system, SSRL was reorganized. In the new organization, all the technical staff is contained in three groups: Accelerator Research and Operations Division, Injector Project and Photon Research and Operations Division, as described in Section IV. Responsibility for safety and quality assurance, as well as scheduling and proposal review, resides in the Director's office.

In spite of the limited effectiveness of the January-March, 1989 run, SSRL's users made significant scientific progress, as described in Section V of this report.

Arthur Bienenstock
Director

Section I

Laboratory Operations

I. LABORATORY OPERATIONS

Two factors had very strong influences on SSRL's operations in 1989. These were: the concurrent operation of the SLAC Linear Collider for Z_o production, which placed severe limits on SPEAR injection and maintenance and the expectation that the SPEAR storage ring, with a new independent injector, will become completely dedicated to synchrotron radiation research in 1990. Thus, if it receives sufficient funding, SSRL will be able to operate SPEAR for a very large portion of 1991. SSRL should be in a position, at last, to provide its users with a steady stream of photons for research. Hence, emphasis was placed on converting SPEAR into a ring which can run reliably and effectively through maintenance, improvements and modifications. Only one experimental run was provided.

SPEAR OPERATIONS

January 23 - March 17 Run - This run, which was plagued by operational and weather-related problems, was scheduled for 145 shifts. Only 63 shifts, or 43%, were delivered to users. Only slightly over half of these shifts were at initial currents above 25 mA. The electron energy was 3.3 GeV in order to enhance studies of human patients being conducted under the angiography program. In the final hours of the run, with the cooperation of SLAC and all of the SSRL users on site, these studies were successfully completed and significant progress was made. *(See Experimental Progress Report No. 1046B).*

During the run problems were experienced with several ring components including the beam position monitoring system, RF system, power supplies and beam line control systems. The failure of a ceramic window in one of the RF cavities caused the ring to be vented and resulted in 13 days of down time.

These difficulties were exacerbated by limited injection. Due to the demands of the SLAC Linear Collider (SLC) program, as discussed in the 1987 Activity Report, injection to SPEAR was available only at 12 hour intervals. This made it very difficult to diagnose and cure the various component problems.

Immediately after the run, B. Richter, Director of SLAC, chaired a series of meetings to identify and correct the most serious problems in anticipation of a scheduled summer run. In particular, it was clear that an RF transformer must be repaired and that alignment of the beam lines and storage ring should occur. This work was started.

The Cornacchia Report - Max Cornacchia, the newly appointed Head of Storage Rings at SLAC, then led a more detailed study of SPEAR which produced recommendations, costs, and time estimates for the work involved to make SPEAR a reliably operating synchrotron radiation facility. This study involved technical, engineering and scientific staff from SLAC and SSRL.

In summary, the report stated: "The priorities given to major SPEAR improvement projects described in this report came from a consideration of the operational problems caused by the subsystems, their projected lifetime, safety implications and the estimated impact on SSRL running resulting from the work necessary to replace the subsystems. These items are, in order of priority: replacement of the ion pump cable plant, addition of RF isolators, fabrication of a spare klystron, miscellaneous RF improvements, upgrading of the low conductivity water (LCW) system, upgrading of the general cable plant, replacement/upgrade of the magnet power supplies and improvement of the instrumentation and control (I&C) system."

The report also cited a high priority need for accelerator physics studies once the machine was operational and the need for a self-consistent alignment of the storage ring and beam lines to reduce orbit deviations.

Cancellation of the Summer Run - After receipt of the Cornacchia Report the decision was made to cancel the summer run for three reasons. The run was not expected to be significantly more successful than the January-March run with the limited injection to be provided by SLAC and SPEAR's performance status. The run would interfere significantly with a critical SLAC Linear Collider (SLC) run. SSRL had to assure that it had sufficient funding to initiate the major SPEAR up-grade program required for effective and full-time operation.

SPEAR Improvement Projects - Starting in the late spring several improvement projects were undertaken by the SSRL and SLAC staffs. These included work on the RF system, a power supply upgrade, a rebalancing of the low conductivity water (LCW) system, orbit control improvements, new vacuum

control systems for Beam Lines 1 and 2, a new high voltage ion pump distribution system, and alignment of the beam lines relative to the storage ring, as well as a number of smaller maintenance and improvement tasks. Highlights of the major projects are described below.

RF System: There were three significant RF problems during the winter run: a cavity window failure, frequent reflected power trips, and intermittent RF transformer difficulties. The window failure was attributed to accidentally overpowering a klystron, a condition which is now prevented by software controls. Renewing the nitride coating of both cavities and rebuilding the cavity tuners addressed the second problem. The problematic RF transformer was completely rebuilt. A transformer shelter is being erected by SSRL to help prevent future weather-related problems.

Power Supplies: There were two areas of power supply problems. The power supplies which drive the beam steering system were giving spurious outputs causing beam dumps. When this system was thoroughly tested, a manufacturing error was discovered and repaired. The power supplies which drive the bend magnets and quadrupoles were found to have problems tracking with each other during the ramp. Software, which will be tested with beam in March 1990, has been refined to correct this problem.

Low Conductivity Water (LCW): A substantial number of trips caused by inadequate flow in parts of the vacuum and the magnet LCW systems occurred during the run. The entire system has been extensively reexamined by SLAC and SSRL personnel. It was determined that the total flow was actually sufficient, but a flow balancing problem existed. The vacuum LCW has now been completely rebalanced and stabilized.

For some time SLAC has been concerned that SPEAR LCW transients caused problems in the SLC system. These problems were traced to four switches in the SLC arcs. Delays have been put on these switches which should eliminate this problem. These improvements should reduce the perturbations of the SLAC site LCW system caused by SPEAR, and provide stable and adequate LCW flow for SPEAR and SSRL components during dedicated running.

Delays have also been put on all the flow circuits as to make them less sensitive to power dips or minor perturbations in the LCW system.

In addition to rebalancing the system, the booster pump control system was improved. This system, which controls the return water pressure, was discovered to be insufficiently sensitive to regulate the flow. The resulting variations in supply pressure were causing trips.

The magnet LCW system is a larger problem, and will be tackled after the spring 1990 run. The problem is basically one of plumbing. Hose connections to the magnet busses fail frequently and will be replaced with new connecting hardware.

Alignment: A large effort has been invested in evaluating and correcting mechanical misalignments of both the beam lines and the storage ring. The process began during the winter run with the discovery that the upstream apertures of Beam Line 2 were 6 mm below the plane of the storage ring. This motivated a program to align all of the beam lines, which was accomplished during the summer of 1989. The beam lines in the South Arc had maintained their position quite well, but those in the North Arc had dropped with respect to SPEAR. The amount of the displacement appears to increase with time, leading to problems with new beam lines located near older ones. Before October 17 all beam lines had been completely aligned.

The Richter magnitude 7.1 earthquake of October 17 was not kind to SSRL. At first glance it appeared that, on a local scale, the relative motion of beam line components was less than one millimeter. When, however, the storage ring realignment process began in late November, it was apparent that there had been substantial motion on a more global scale, requiring another full realignment of the beam lines as well as the storage ring. The earthquake caused the storage ring to tilt as a plane, with an elevation difference from one side to the other of 5 mm. When the insertion devices were surveyed, some were found to have undergone larger motions than would have been expected when compared with adjacent magnets. The plane of the storage ring was redefined to the mean quadrupole elevation and aligned with respect to this new plane [Figure 1]. This had the advantage of minimizing the amount of motion necessary to correct the vertical position of the beam line components.

FIGURE 1

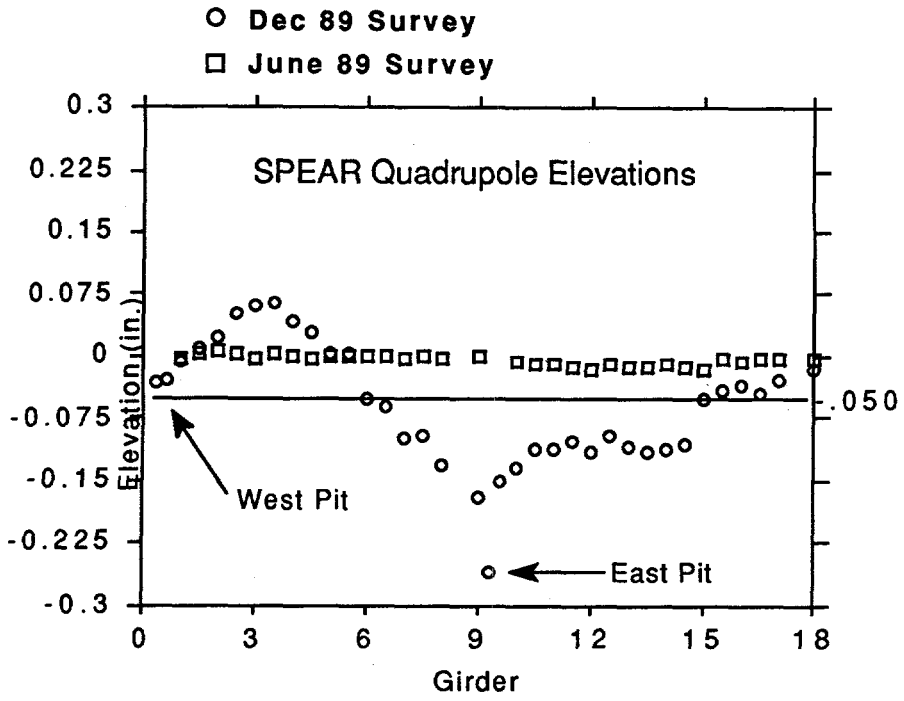

The October earthquake caused significant misalignment of the SPEAR storage ring as shown in the December 1989 survey. The ring has now been realigned to a new plane (solid line).

Unfortunately, the nature of the horizontal alignment of the magnets precludes a quantitative assessment of potential problems caused by the earthquake. It is difficult to separate the movement of the individual magnets from the movement of the references. All that can be determined is that there has not been a significant motion of one magnet girder with respect to another. The recalibration of the horizontal references would best be done during a long shut-down after the High Energy Physics Mark III Detector has been removed. In the meantime, the beam lines will be realigned to the local magnet geometry of their sources.

Electron Beam Position Monitors (BPM's): The lack of a complete set of beam position monitors severely hampered the machine operators in establishing orbits. Newly designed electron beam position monitors have been installed to replace defective units on each end of the insertion devices on Beam Lines 6 and 10. As a result, SSRL now has the means of locating the SPEAR electron beam position as it enters and leaves the insertion devices on these beam lines. This more complete distribution of BPM's around the machine should greatly improve closed orbit distortions and facilitate reproducing orbits and photon beam steering.

Beam Line 1 and 2 Control Systems: SSRL's original Beam Line 1 and 2 control systems, now 15 years old, have been replaced to eliminate faults which have shut down the SPEAR beam. Starting in the summer of 1989 a new vacuum control system was designed, fabricated, installed and tested. The new system utilizes modular construction and plug-in P.C. cards to allow ease of maintenance and trouble-shooting, expedite repairs and provide flexibility for modifications as required. This new system should serve as a prototype for future SSRL beam lines.

Ion Pump High Voltage Distribution System: The SPEAR ion pump high voltage distribution system was recabled. The motivations for this were safety, (the distributed ion pumps in the ring dipoles had to be started by vacuum technicians present in the ring housing while the magnets were powered) and improved operation (individual ion pumps could not be monitored while beam was stored or while the ring magnets were powered). Now each individual pump has its own cable running from the ring through a high voltage terminal cabinet to the SPEAR power supply building. From the power supply building vacuum technicians have electrical access to all vacuum pumps in the storage ring.

A major goal of the March 1990 run is to test and commission the improvements described above.

Scheduling of SSRL Users at Other Facilities: In response to the shortage of beam time at SSRL, three other U.S. synchrotron radiation laboratories (NSLS, CHESS and the SRC) offered to accommodate SSRL users on the basis of their existing SSRL proposals. SSRL and it users are extremely grateful for this cooperation. The NSLS accommodated 41 SSRL experiments this fall. Four groups ran at the SRC and another 8 are being accommodated at CHESS.

PEP OPERATIONS

SSRL has two synchrotron radiation beam lines on the 15 GeV storage ring PEP. These lines operate parasitically when PEP is run for high energy physics *(see 1988 Activity Report)*. After the successful December 1988 run, when four synchrotron radiation user groups took data, a planned down time until the fall was scheduled, to allow work on the SLAC Linear Collider. A high energy physics run on PEP was expected to start in October 1989 and continue until the end of the year.

Cancellation of Fall PEP Run: This planned fall PEP run was another casualty of the October 17 earthquake, which caused an 8 mm peak-to-peak variation in the machine elevation. The present schedule calls for a PEP start-up in May 1990. The storage ring will be realigned by that time.

BEAM AND SPEAR USAGE TABLES

The following tables and graphs contain statistics on SPEAR running, experimental use and characteristics of SSRL stations. For earlier information, previous Activity Reports should be consulted.

Table 1 and the accompanying graph show the number of SPEAR shifts scheduled and delivered since dedicated running commenced in 1979.

Table 2 and the accompanying graph illustrate the use of beam at SSRL for experimental purposes.

Table 3 lists the characteristics of the 25 SSRL SPEAR and PEP experimental stations and Table 4 shows the number of shifts requested versus the number of shifts actually scheduled for dedicated time.

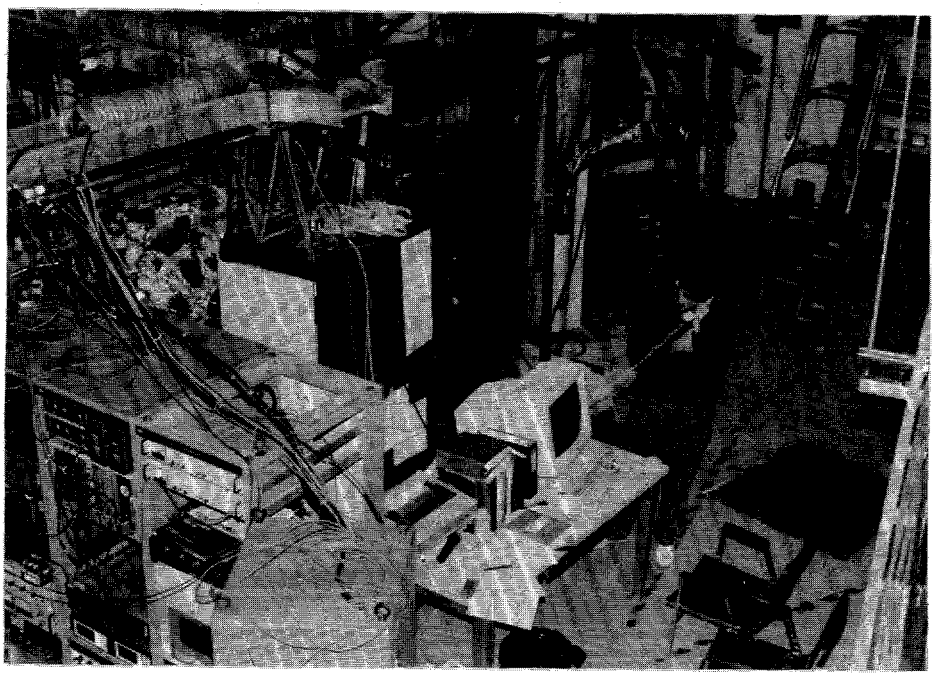

TABLE 1

BEAM TIME STATISTICS/DEDICATED TIME

DEDICATED RUN	SCHEDULED HOURS	DELIVERED HOURS	%DELIVERED
10/20-11/05/79	152	95.3	62
12/03-12/21/79	352	299.4	85
02/08-03/05/80	472	366.3	77
04/16-05/19/80	764	588.2	76
06/30-07/30/80	726	320.4	44
09/29-10/14/80	336	194.9	58
12/02-12/22/80	440	309	70
01/26-03/03/81	792	600.9	76
05/16-06/30/81	988	727	73
11/18-12/21/81	546	363.6	66
01/08/-02/22/82	748	612.5	81
03/09-04/26/82	995	830.9	83
10/15-11/05/82	473	316	66
12/27-02/22/83	1050	825.6	78
05/09-06/30/83	1195	960.3	80
11/07-12/23/83	857	662.8	77
03/21-04/30/84	835	674.3	80
01/10-02/21/85	905	606.6	67
03/15-07/22/85	1502	1056.5	70
10/14-11/11/85	416	203.7	48
04/11-06/30/86	1550	1106.5	71
11/17-12/24/86	752	527	70
01/02-02/07/87	696	522	75
03/18-05/02/87	1112	769	69
10/26-12/24/87	1360	801	59
01/23-03/17/89	1160	504	43

The history of dedicated time at SSRL/SPEAR since its inception in 1979 is shown. Until 1986 SSRL received one-half of the SPEAR operating time in a mode dedicated to synchrotron radiation while the other half was used for colliding beam physics. There has been no colliding beam physics on SPEAR in the last few years. Dedicated shifts have been limited by SSRL budgetary considerations, construction and the SLC schedule.

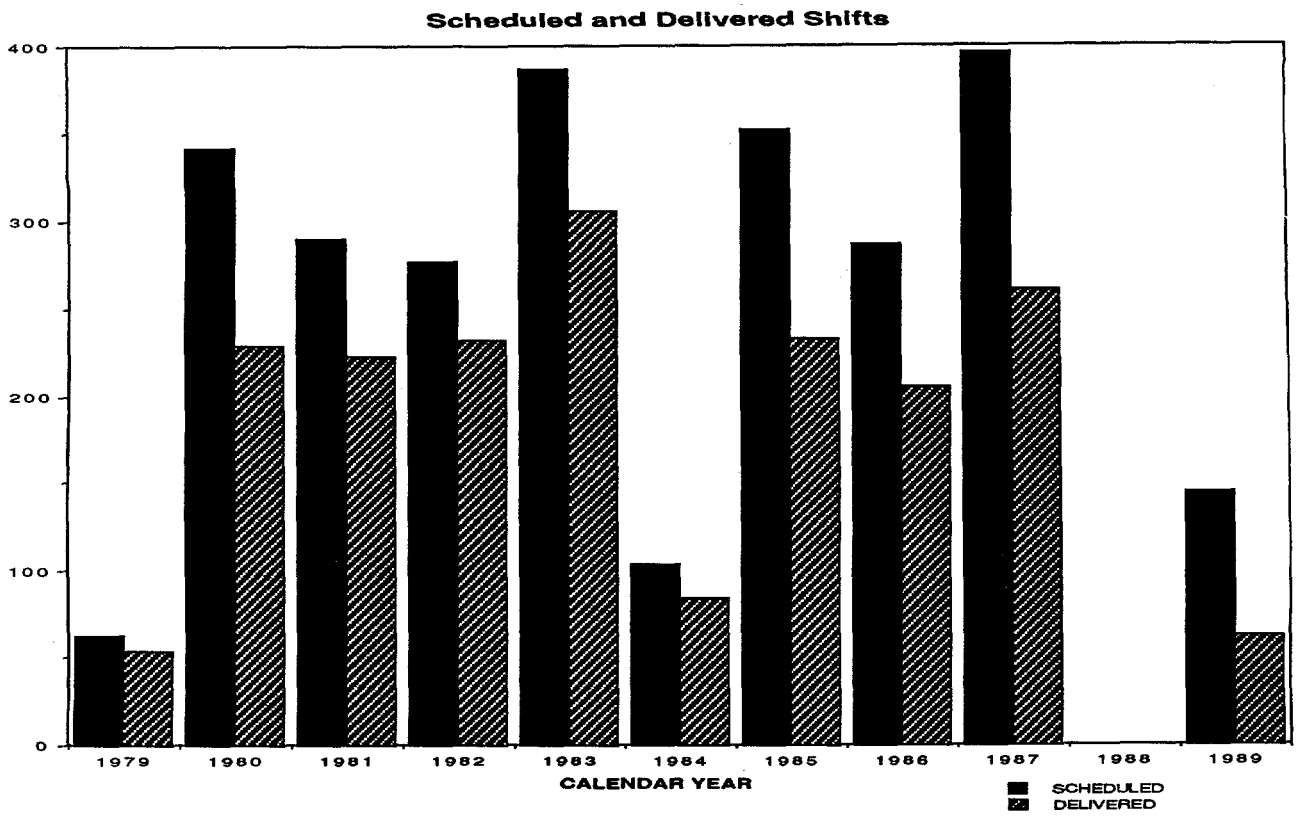
Scheduled and Delivered Shifts
400
300
200
100
0
1979
1980
1981
1982
1983
1984
1985
1986
1987
1988
1989
CALENDAR YEAR
SCHEDULED
DELIVERED

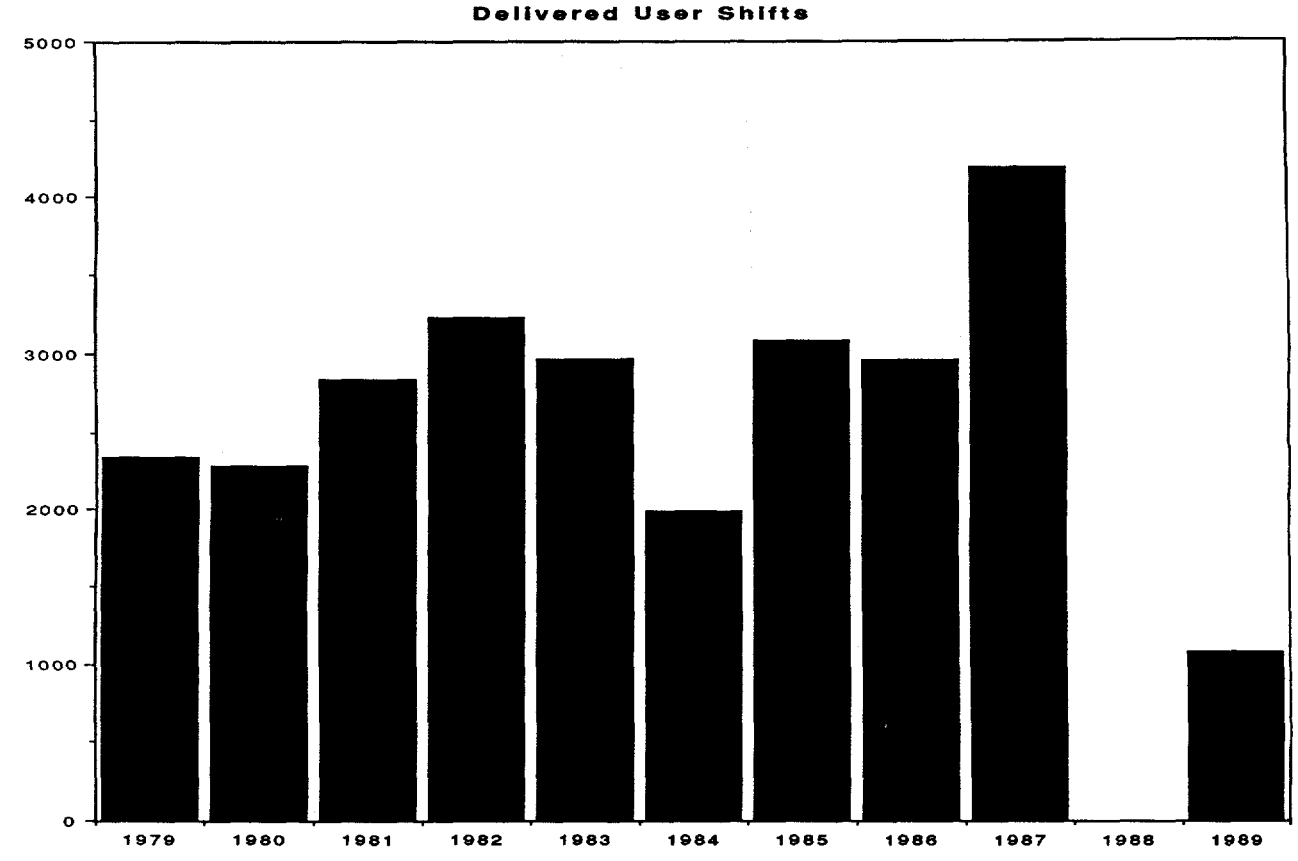
Delivered User Shifts
5000
4000
3000
2000
1000
0
1979
1980
1981
1982
1983
1984
1985
1986
1987
1988
1989

USER SHIFTS BY EXPERIMENTAL STATION **TABLE 2**
Calendar 1989

Experimental Station	1/23/89 - 3/17/89	
Beam Line 1		
1-1	57	
1-2	42	(15)*
1-4	40	
1-5	4	(33)
Beam Line 2		
2-1	57	
2-2	48	(7)
2-3	47	
Beam Line 3		
3-1	57	
3-2	46	
3-3	48	
3-4	54	
Beam Line 4		
4-1	49	
4-2	43	
4-3	44	
Beam Line 5		
5-2	0	(30)
Beam Line 6		
6-1	0	(30)
6-2	45	
Beam Line 7		
7-1	55	
7-2	45	
7-3	48	
Beam Line 8		
8-1	52	
8-2	52	
Beam Line 10		
10-2	50	(8)
TOTAL Shifts Used	**964**	**(123)**
Proposals Run	**88**	

**( ) = facility characterization time*

In 1989, 964 8-hour shifts were used by experimenters for data acquisition on SSRL's 23 operating SPEAR stations. Additional shifts were used for beam line check out between experimenters. A total of 123 shifts were used by SSRL staff, PRT members and collaborators for characterization, upgrading and commissioning time. In 1989 both the new soft x-ray line on 6-1 and the multi-undulator on Beam Line 5 were being commissioned.

TABLE 3

CHARACTERISTICS OF SSRL EXPERIMENTAL STATIONS

SSRL presently has 25 experimental stations 23 of which are located on SPEAR and two on PEP. 12 of these stations are based on insertion devices while the remainder use bending magnet radiation.

	Horizontal Angular Acceptance (Mrad)	Mirror Cut Off (keV)	Monochromator	Energy Range (eV)	Resolution ΔE/E	Approximate Spot Size HgtxWdth (mm)	Dedicated Instrumentation
INSERTION DEVICES STATIONS							
WIGGLER LINES - X-RAY							
End Stations							
4-2 (8-Pole)							
Focused	4.6	10.2	Double Crystal	2800-10200	~$5x10^{-4}$	2.0 x 6.0	
Unfocused	1.0		Double Crystal	2800-45000	~10^{-4}	2.0 x 20.0	
6-2 (54-Pole)							
Focused	2.3	22	Double Crystal	2800-21000	~$5x10^{-4}$	2.0 x 6.0	
Unfocused	1.0		Double Crystal	2800-45000	~10^{-4}	2.0 x 20.0	
7-2 (8-Pole)							6-circle Diffractometer
Focused	4.6	10.2	Double Crystal	2800-10200	~$5x10^{-4}$	2.0 x 6.0	
Unfocused	1.0		Double Crystal	2800-45000	~10^{-4}	2.0 x 20.0	
10-2 (31-Pole)							
Focused	2.3	22	Double Crystal	2800-21000	~$5x10^{-4}$	2.0 x 6.0	
Unfocused	1.0		Double Crystal	2800-45000	~10^{-4}	2.0 x 20.0	
Side Stations							
4-1	1.0		Double Crystal	2800-45000	~$5x10^{-4}$	2.0 x 20.0	
4-3							2-circle Diffractometer
Focused	1.0 Variable		Double Crystal	2800-20000	~10^{-4}	0.3 x 20	
UnFocused	1.0		Double Crystal	2800-45000	~10^{-4}	2.0 x 20.0	
7-1	1.0		Curved Crystal	6000-13000	~$8x10^{-4}$	0.6 x 3.0	Rotation Camera
7-3	1.0		Double Crystal	2800-45000	~10^{-4}	2.0 x 20.0	
Undulator Lines - VUV/Soft X-Ray							
5 multiple undulators	1.5		Rowland Circle-Multiple Grating	10-1200	Δλ =.013–.13Å	6.0 x 8.0	Commissioning
6-1			6m SGM	200-1000	~$2x10^{-4}$	≤1mm²	
Undulator Lines - X-Ray							
PEP 1B							
Focused	1.7	22	Double Crystal	12000-22000	2 x 10^{-5}	0.5 x 3	
Unfocused	FULL		Double Crystal	12000-50000	~10^{-5}	0.6 x 6.0	6-circle Diffractometer
PEP 5B							
Focused	1.7	22	Double Crystal	12000-22000	2 x 10^{-5}	0.5 x 3	
Unfocused	FULL		Double Crystal	12000-50000	~10^{-5}	0.6 x 6.0	

	Horizontal Angular Acceptance (Mrad)	Mirror Cut Off (keV)	Monochromator	Energy Range (eV)	Resolution ΔE/E	Approximate Spot Size HgtxWdth (mm)	Dedicated Instrumentation
BENDING MAGNET STATIONS							
X-Ray							
1-4	2.0		Curved Crystal	6700-10800	0.3×10^{-3}	0.25 x 0.5	SAS Detector
1-5	1.0		Double Crystal	2800-30000	$\sim 10^{-4}$	3 x 20	Area Detector/CAD-4
2-1 (Foc.)	4.8	8.9	Double Crystal	2800-8900	$\sim 5 \times 10^{-4}$	1 x 4	
2-2	1.0-6.1		None	3200-30000		4 x 22 - 4 x 134	
2-3	1.0		Double Crystal	2800-30000	$\sim 5 \times 10^{-4}$	3 x 20	
VUV/Soft X-Ray							
1-1	2.0		Grasshopper	64-1000	$\Delta\lambda = .1\text{-}.2$Å	1.0 x 1.0	
1-2	4.0		6m TGM	8-90	$\sim 2 \times 10^{-3}$	1.0 x 2.0	
3-1	2.0		Grasshopper	25-1000	$\Delta\lambda = .05\text{-}2$ Å	1.0 x 1.0	
3-2	4.0		Seya-Namioka	5-40	$\Delta\lambda = .2\text{-}6$ Å	2 x7	
3-3	8-10	4.5	UHV Double Crystal (Jumbo)	800-4500	$\sim 5 \times 10^{-4}$	1.5 x 2.5	
3-4	0.6		Multilayer	0-3000	White or $\Delta\lambda/\lambda = .6\%$	2 x 8	Vaccum Diffractometer/ Litho. Expo.Station
8-1	12		6m TGM	8-180	$\sim 9 \times 10^{-3}$	$\leq 1 mm^2$	Angle Resolved e- Spectrometer
8-2	5.0		6m SGM	150-1000	$\sim 3 \times 10^{-4}$	$\leq 1 mm^2$	Angle Resolved e- Spectrometer

TABLE 4

DEDICATED DEMAND vs. ACCOMMODATION ON SSRL EXPERIMENTAL STATIONS

January 1989-March 1989

Station	Shifts Requested	Shifts Assigned	Over-Subscription	Proposals Requesting	Proposals Assigned	%Assigned
Wigglers Lines						
End Stations						
4-2	503	126	466%	13	4	31%
6-2*	191	42	455%	4	3	75%
7-2 Diffractometer	242	126	200%	14	7	50%
10-2*	66	42	151%	4	2	50%
Side Stations						
4-3 Diffractometer	125	108	116%	7	5	71%
7-3,4-1	570	242	226%	45	14	31%
7-1 Rotation Camera	110	126	115%	10	10	100%
Bending Magnet X-ray Lines						
1-4 SAS	91	126	72%	4	4	100%
1-5 Area Detector	119	126	94%	11	4	36%
2-1 Focused	114	72	158%	14	6	43%
2-2 White	240	108	222%	11	6	55%
2-3 EXAFS	12	108	11%	2	8**	400%
VUV/Soft X-ray Lines						
Grasshoppers (1-1, 3-1)	246	198	124%	8	5	63%
Double Crystal (3-3)	119	126	94%	4	3	75%
TGM's (1-2, 8-1*)	124	132	94%	8	6	75%
SGM (8-2*)	107	42	255%	3	1	33%
Lithography (3-4)	85	126	67%	4	4	100%
Seya (3-2)	70	126	56%	3	3	100%

**PRT line - general user time only shown*

*** 2-3 was run in white-radiation mode part of the time to accommodate overdemand from 2-2.*

Demand for experimental time on the SSRL branch lines varies considerably. The percentage of proposals receiving beam time is often higher than the percentage of shifts accommodated since most experimenters do not receive the full allotment of shifts requested. Demand is also limited by perceived availability of beam time. Experimenters have indicated that they could use much more time if it were available. In addition, many new groups have been discouraged from starting programs based on synchrotron radiation at SSRL since the time available is so limited. This situation should improve once SPEAR becomes dedicated to synchrotron use.

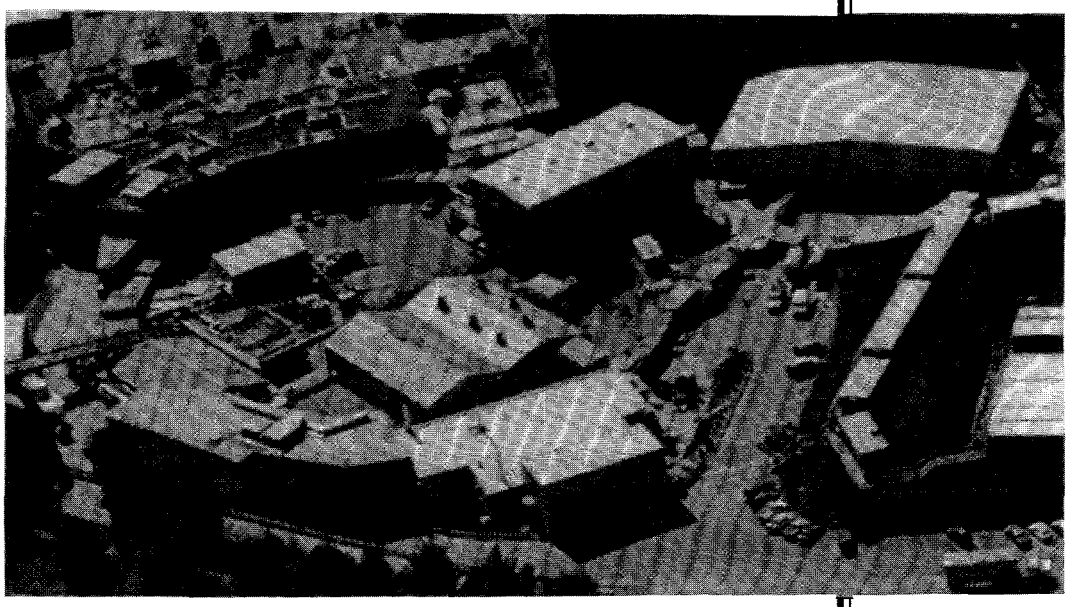

Section II

The 3 GeV Injector & Accelerator Research

II THE 3 GEV INJECTOR & ACCELERATOR RESEARCH

THE 3 GEV INJECTOR

SSRL is in the final stages of constructing a 3 GeV booster synchrotron as an injector for SPEAR This injector will make the SPEAR storage ring independent from the SLAC Linear Accelerator. After authorization of the project by the DOE in February of 1988, most of the first year's effort was spent on detailed technical designs, fabrication of prototype components and construction of conventional facilities. During 1989 activities concentrated on the procurement, fabrication, and assembly of injector subsystems. Many components were designed or specified by injector personnel, while fabrication occurred in industry, or SLAC shops, but primarily in-house within specially formed project groups. Assembly and test of sub-systems was also performed by the injector group. By year's end most of the main components were fabricated and installed. In particular, the main magnets with their supports, the vacuum chamber, the first linac modulator and all linac DLWG sections had been installed. Completion of the installation phase is projected for the first quarter of 1990 followed by a six month commissioning phase.

LINAC System

Microwave Gun - In collaboration with Varian Associates, a microwave gun has been developed to produce a high intensity electron beam as the first step of the accelerator chain comprising the injector project. The main feature of this type of electron source is its small beam emittance and high intensity. First tests show a beam current which exceeds, by at least a factor of two, the required intensity for the injector project. The electron source for the gun consists of a cathode immersed in the field of an RF cavity. Electrons emerging from the cathode through thermionic emission become accelerated immediately by a high RF field of the order of 50 MV/m and the repelling electrostatic forces within an intense electron beam are compensated very quickly. As a consequence the electron beam from a microwave gun has a much higher brightness than from ordinary sources. Three linac modulators have been constructed at SSRL, each driving one klystron connected to a ten foot long S-band accelerating section. The accelerator sections were manufactured at the High Energy Physics Laboratory in Beijing. One of the sections has now been powered up to 30 MW or an accelerating field of 18 MeV/m.

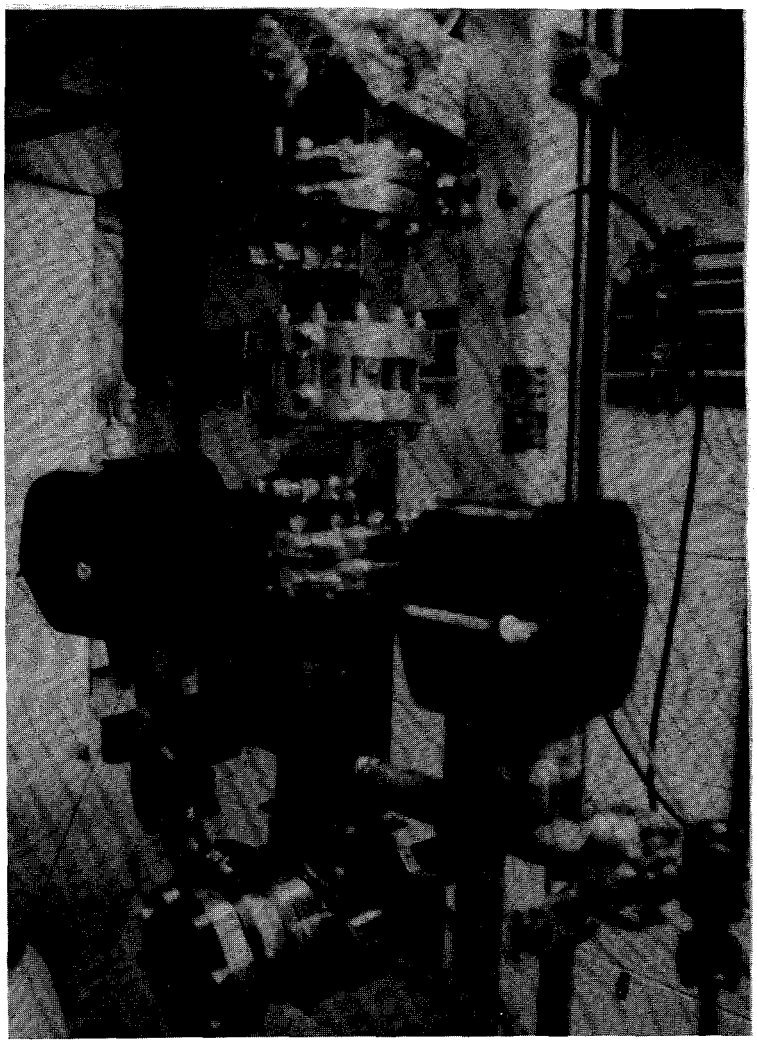

Microwave Gun

Booster System

Booster Ring Magnet System - The ring magnets for the booster were designed and assembled at SSRL. In order to allow cycling the booster at 10 Hz all ring magnets are constructed from laminations of magnetic steel. The final choice of material was based on prototype tests performed with a variety of materials under realistic operating conditions. All magnet cores have been stacked, assembled with coils delivered by industry and tested by the injector magnet group. To allow efficient installation and alignment all magnets are preassembled and prealigned resting on precision locators on rigid girders. This preassembly

was done in the magnet assembly area and included the installation of the vacuum chamber and bussing. The completed girders were then transported to the ring tunnel for final installation.

Main Magnet Power Supply - To minimize the interference of the cycling operation of the booster with other sensitive facilities at the SLAC site a White circuit was chosen to power the main magnets. In such a circuit the magnets are connected in parallel with capacitor banks to form a resonant circuit tuned to the operating frequency of the booster. The losses of this circuit are then compensated by energy pulses via magnetic chokes. All the magnets are designed for cycling up to 3.5 GeV at 10 or 15 Hz and the White circuit can also be configured to oscillate at 10 or 15 Hz.

Vacuum System - Due to the cyclical magnetic fields in synchrotrons, special vacuum chamber designs are needed to avoid eddy current losses. In some machines cermanic chambers have been used. For this injector the technique pioneered by DESY, constructing the vacuum chambers of 0.3 mm thin stainless steel tubes strengthened by external metallic ribs, was used. This construction method proved very successful and has been incorporated into the injector design. All the magnet chambers have been fabricated, installed and pumped down.

Booster Accelerating System - In order to minimize the maintenance complexity it was decided to duplicate the SPEAR RF system for the booster. One of the original four accelerating cavities of SPEAR has been recommissioned for the booster ring.

Beam Transport System

Injection/Extraction System - The injection and extraction transport systems are designed, and fabrication complete. The magnets which transport electrons from the booster to SPEAR have been measured and are installed. Installation of the transport components from the injector LINAC to the booster synchrotron has begun. The kicker magnets for injecting electrons into the booster and for extracting them out of the booster are ferrite picture frame magnets mounted inside the booster vacuum. They are built up from standard modules: 2 units for injection, 4 units for extraction. Construction of the kicker pulsers is underway. The injection septum is a DC horizontal deflecting magnet. The extraction septum will be a pulsed Lambertson type magnet.

Design work is underway to allow SPEAR to inject at full energy. This requires modification of the SPEAR injection components, including the septum magnet.

Project Schedule

It is expected that all injector components will be installed by the spring of 1990, and after a six month commissioning period, a dedicated, full energy injector for SPEAR should be available in October 1990.

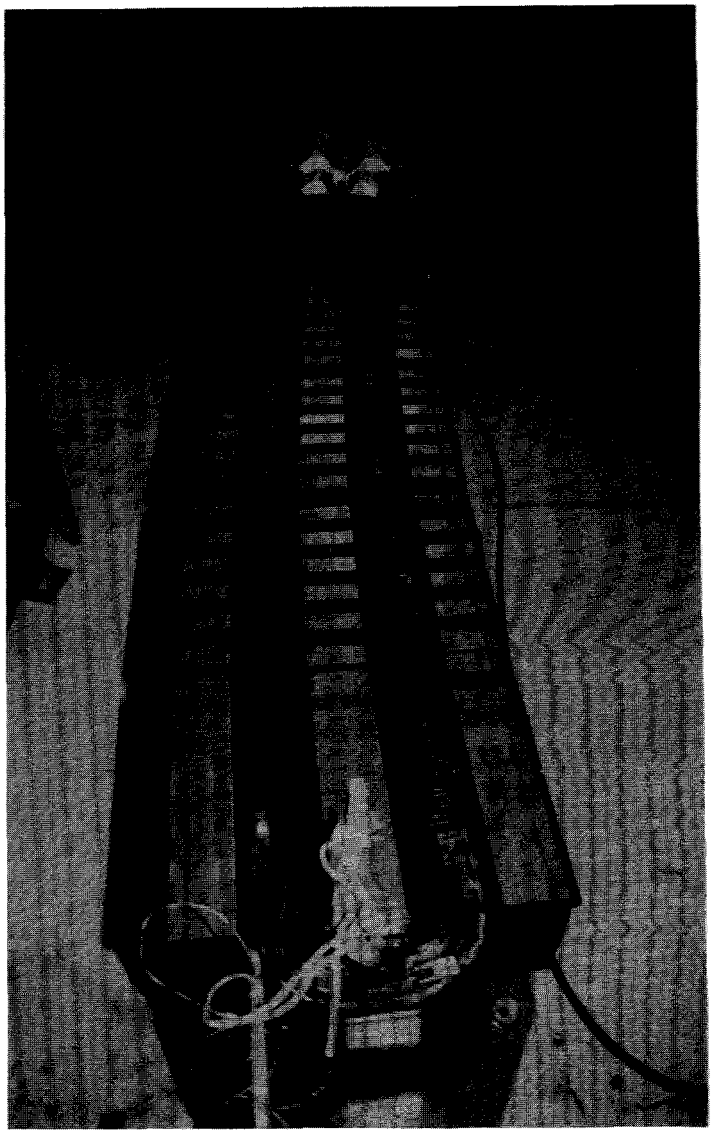

Bending Magnet Engineering Model with Coil (Top Half Removed)

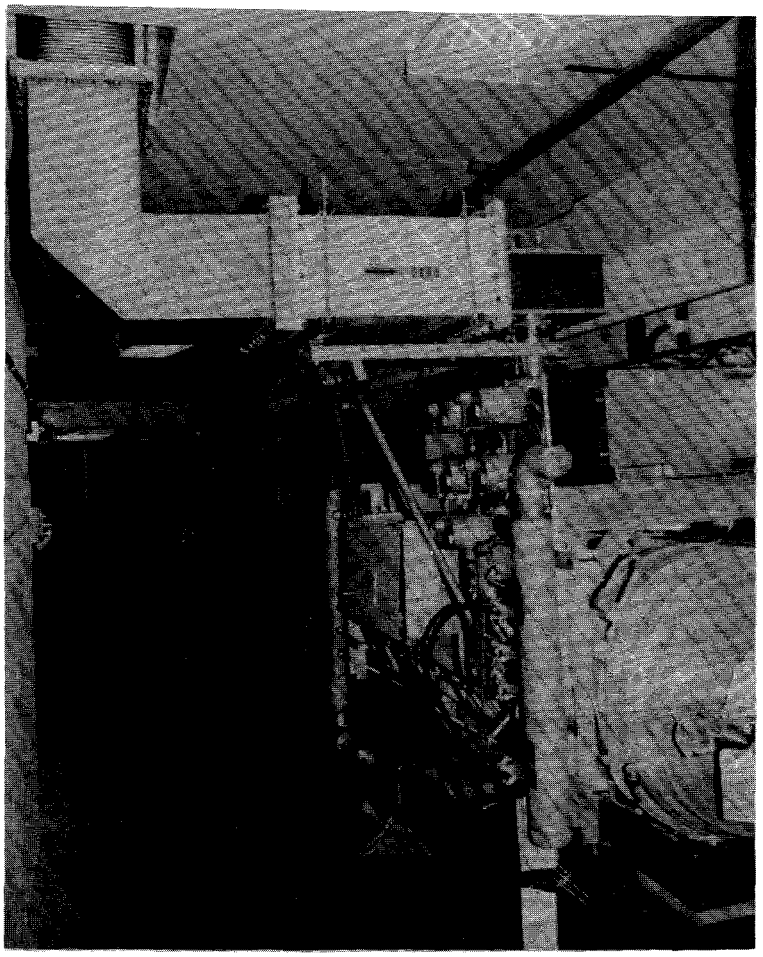

385 MHz RF Cavity
in Ring Tunnel

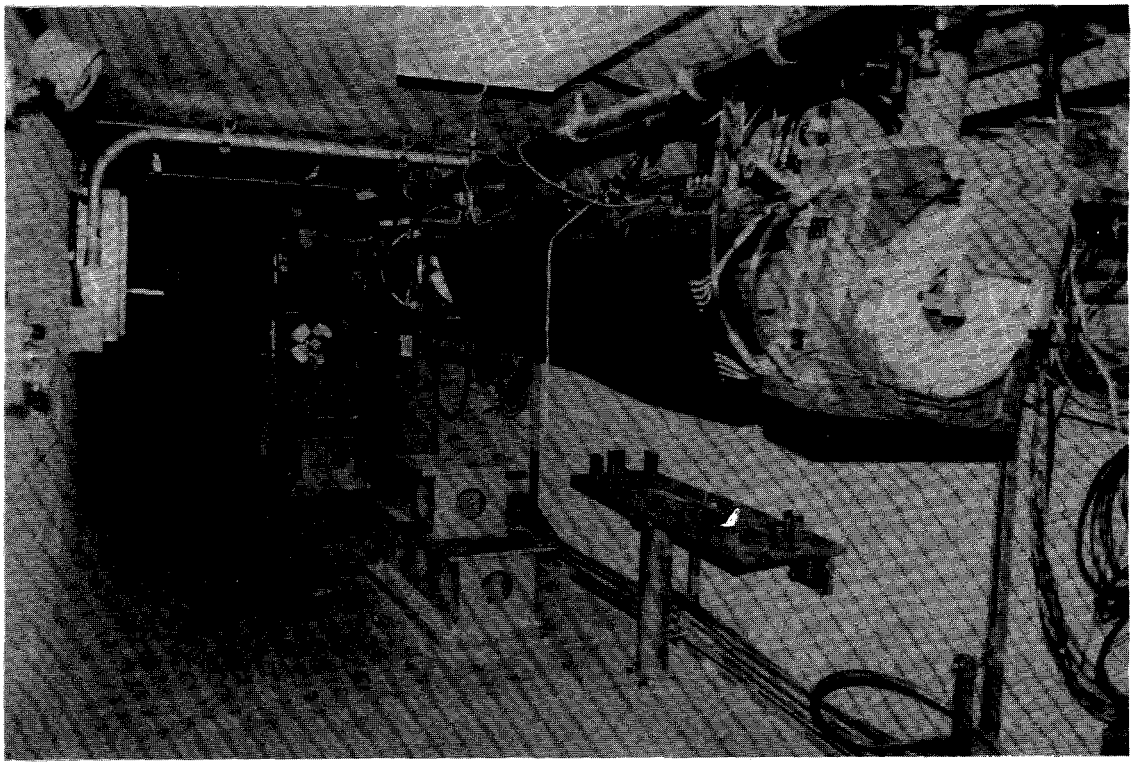

Beam Transport Line from Booster to SPEAR

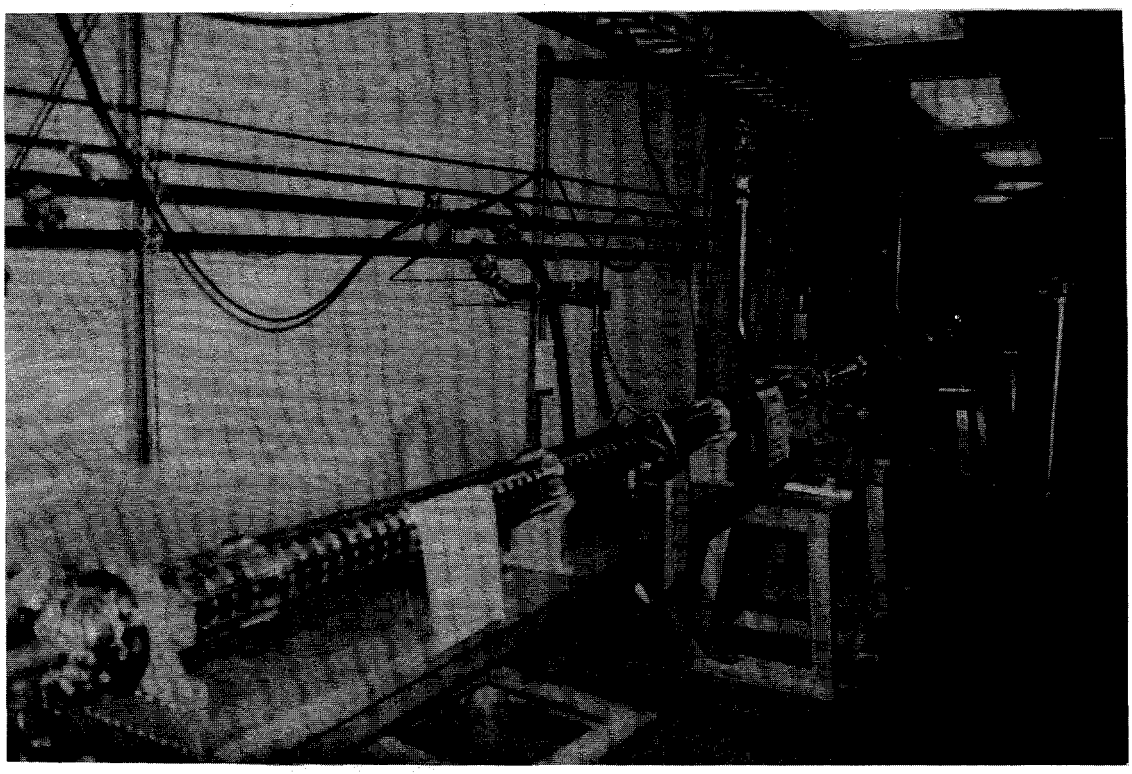

New Linac Sections in Linac Tunnel

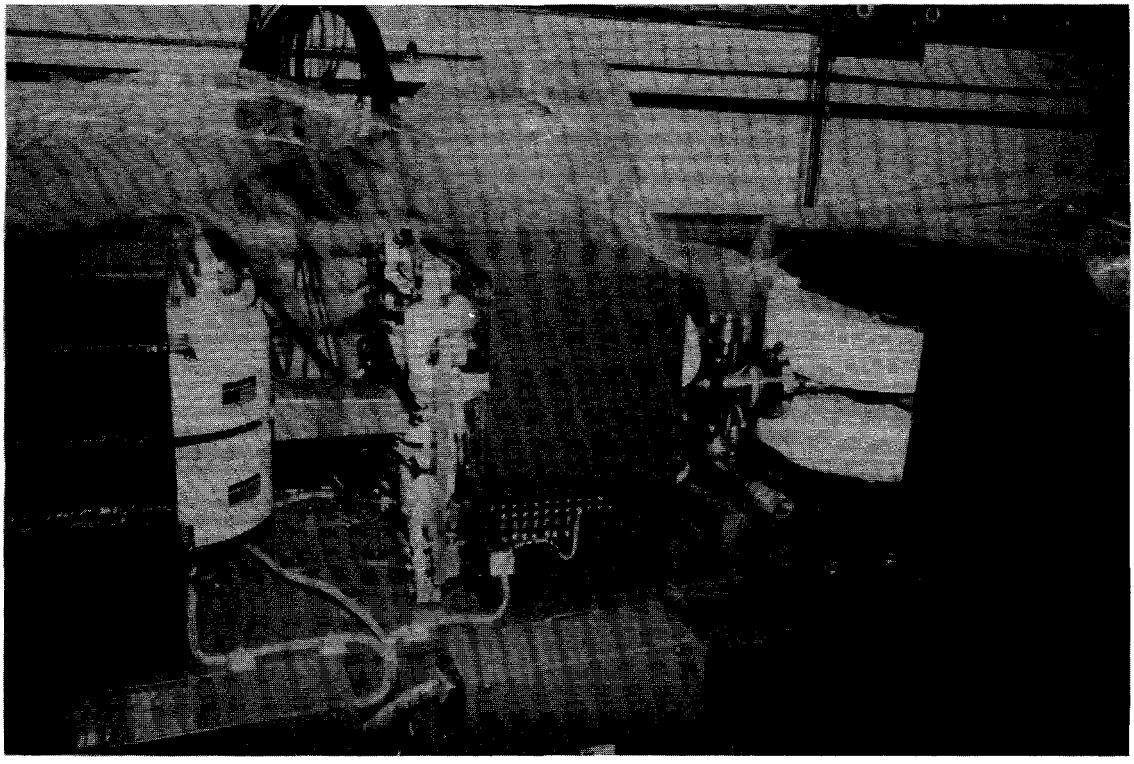

Ring Bending Magnet, Quadrupole, Vacuum Chamber

ACCELERATOR RESEARCH PROJECTS

SPEAR Studies

Accelerator research projects have been pursued in connection with the training of graduate students. Specific emphasis is given in combining theoretical studies with practical hands-on experience with accelerator systems and the design, fabrication and testing of new accelerator components.

Major accelerator research efforts concentrated on the design of the ring lattice and stability studies for the new 3 GeV injector, and the beam transport lines between the pre-injector linac and the booster as well as between the booster and SPEAR.

A low emittance configuration for SPEAR has been developed to reach a factor of 3 smaller beam emittance. This requires a third injection kicker in SPEAR which is part of the injector project. Injection studies and stability simulations have been performed and experimental verification is expected to occur during the injector commissioning.

With the transition of SPEAR to a dedicated synchrotron radiation source, consideration is now being given to hardware modifications to the long interaction region straight sections to enable them to accommodate long undulators. Preliminary studies indicate that it should be possible to revise the present straight sections so that the free straight section length is increased from the present 2.5 meters to 10 meters or more. Emphasis is placed on developing an optics for a 5 meter long undulator which will be the source for a proposed 1-4 keV beam line.

PEP Studies

Accelerator physics research on PEP has diminshed due to the higher priority of SPEAR and the injector, the limited operation time of PEP and the uncertainty of PEP's future as SLAC develops a proposal for modifying PEP to function as a B-meson factory.

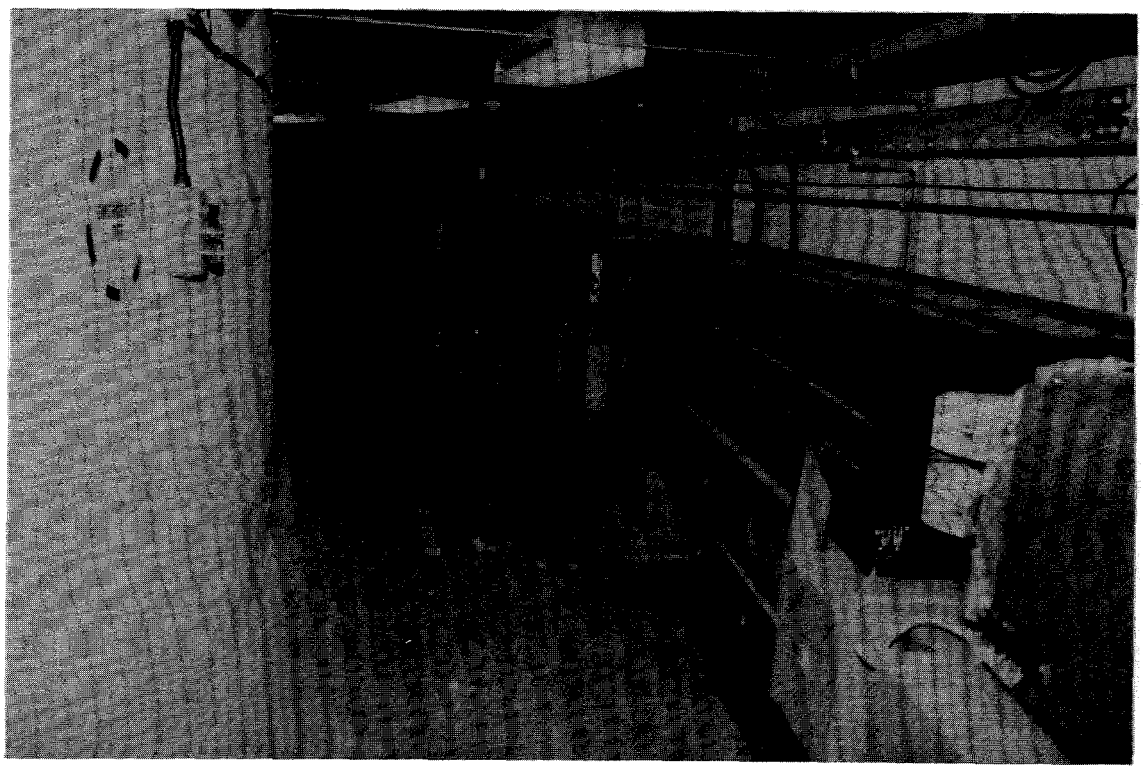

3 GeV Booster Ring

Some work continues on the development of a longitudinal feedback system for PEP.

Feedback systems have been found necessary to reach high currents with stable beams in many light sources. SSRL is presently developing a system to combat longitudinal instabilities in PEP. Such systems are likely to be needed also on SPEAR, particularly when the low emittance mode is implemented.

The work that has been done includes detailed characterization of the frequency response of the cavity, comparison of phase detection with energy detection, the design of a stripline monitor and the choice of a suitable location for it in the PEP ring, the exploration of different placements of the cavity in the ring, the possible impact of the cavity on PEP operations and the development of the feedback electronics.

The detailed plan for the system was developed in consultation with many laboratories (SSRL, SLAC, LBL, NSLS, Argonne, DESY and Hiroshima Univeristy). The cavity is scheduled for installation into the PEP ring in March 1990. The first tests for the longitudinal feedback systems are anticipated for summer 190.

Also, reports have been completed on the use of the PEP emittance control wigglers as sources of circular polarized hard x-rays and on the modificationsneeded to PEP if it were to become a dedicated light source. These reports are available from SSRL. The work on PEP as a source of circular polarized x-rays will be published in the proceedings of SRI-89.

General Accelerator Physics Studies

Detailed theoretical studies of optimum microwave gun designs have been undertaken leading to the construction of such electron sources for the injector project. Systematic measurements of beam parameters and comparison with theory will follow in the coming year.

Fundamental limits of beam optical aberrations have been studied. As a consequence the feasibility of a storage ring with a beam emittance of 0.04 nanometers has been established. This emittance is a factor of one hundred smaller than that for the APS or ALS and would produce fully spatially coherent radiation down to wavelengths of 3Å.

The simulation programs, PATRICIA and PATPET, have been further developed. These programs, which allow the simulation of particle motion in the presence of a variety of perturbations, are now being used in a number of laboratories throughout the world.

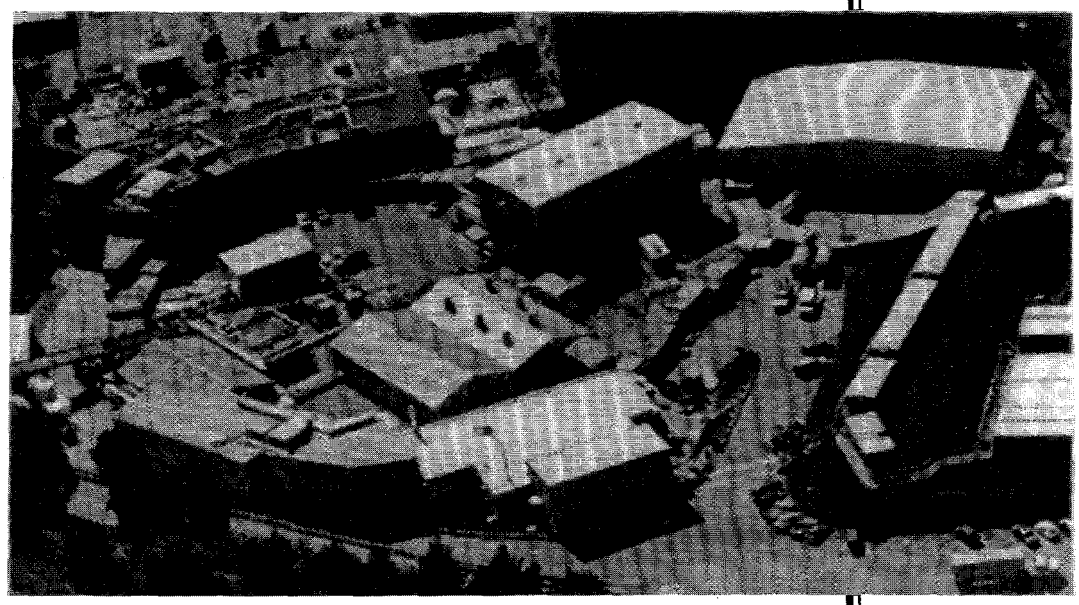

Section III

Experimental Facilities

III EXPERIMENTAL FACILITIES

Experimental facilities at SSRL are of two types: general facility stations and participating research team (PRT) stations. General facility stations have been funded by various government agencies, principally the DOE, NIH and NSF and are open to the user community on a competitive basis for 100% of their operating time.

SSRL has three operational PRT's with a fourth in the process of developing a branch line. All present PRT's are three party collaborations with SSRL as one of the parties. The two outside institutions receive 2/3rds of the available beam time while the last third is reserved for the SSRL general users. The PRT arrangements are for a 3 year period. Renewal is based on review by an ad hoc committee, appointed by the Stanford University Dean of Research, which considers scientific merit, contributions to graduate student education and to the SSRL user community.

X-RAY FACILITIES

There are 13 x-ray stations located on six beam lines at SSRL. Two of these are PRT lines (wiggler lines 6 and 10). The other 11 are SSRL facility stations. Of the facility lines, two (Beam Lines 4 and 7) have wigglers as sources for six stations and the other two (Beam Lines 1 and 2), serving five stations, have bending magnet sources. There are also two x-ray beam lines on the PEP storage ring, each serving a single experimental station.

Improvements to Existing Experimental Stations

Beam Line 1: The two x-ray branch lines on Beam Line 1 are a Small Angle Scattering line (1-4) and an EXAFS line (1-5), which can also be run in a mode dedicated to a Protein Crystallography Area Detector. A major upgrade to Station 1-4 was started in 1988 and has continued this year. During 1989 a commercial version of the original photodiode array detector was purchased. This detector has been customized for low temperature operation and beam stops were added. IBM donated a PC which is used to operate the detector. A valve to allow changing the sample-to-detector distance without exposing the cold array to ambient air has been added. Finally, the monochromator has been fitted with absolute encoders to better monitor its configuration.

On the EXAFS line the older racks were replaced with taller versions in order to consolidate the controls and free more area for setup space.

Beam Line 2: Several upgrades were made to the three branch lines on Beam Line 2. During the last run it was determined that the 2-1 mirror had finally reached the end of its useful life; a new mirror has been ordered. An additional driver chassis has been constructed for remote operation of the diffractometers on the white light line (2-2), thus alleviating the need for connector changes when switching from one diffractometer to the other. A spectrum analyzer to monitor the Fourier components of the photon beam noise has been installed as part of the dedicated diagnostics port on this beam line.

Branch Line 4-3: The hutch table was modified to increase the tilt range of the diffractometer to match the larger range of angles allowed by the new 4-3 mirror.

Branch Line 7-2: In 1989 this branch line moved into the microVax era. During the winter run the new version of SUPER had its baptism, and after some initial frantic debugging, proved to be a very successful control package. It is expected that SUPER will become the standard program to control all diffractometers at SSRL and is also being used with ithe x-ray generator. The on-line HELP file is available as an ASCII file and can be transmitted to interested users.

General X-ray Facility Improvements

Although much of the efforts of the x-ray staff were directed to the SPEAR improvement projects described in Section1, several other tasks were completed during the long 1989 shutdown. An extensive survey of all of the electrical outlets in both experimental halls was undertaken, and all wiring brought up to current safety standards. A bar-code inventory control system for x-ray equipment was implemented.

The first crystals to be completely cut and polished in-house were finished. The ϕ orientation of these three sets of Si(220) crystals was chosen to complement the already existing crystals.

Two new sample positioners and their support chassis were constructed.

In addition, a number of x-ray staff members went to the NSLS to provide support for SSRL users running on NSLS Beam Line X19A. Standard SSRL sample positioners were also sent to Brookhaven for use by SSRL users.

Crystal Cooling Project: Recent research at several synchrotron radiation laboratories has shown that the performance of a typical double-crystal silicon monochromator suffers when the power density on the first crystal reaches a few watts per square millimeter. Thermal gradients in the crystal cause its surface to pillow slightly, and the consequent warping of the crystal planes reduces the transmitted flux. Since the power density at SSRL's wiggler lines 6-2 and 10-2 can reach this level, and since significantly higher values will be achieved on future beam lines, SSRL has been studying methods for more efficient cooling of monochromator crystals.

In 1989 we began studying a technique developed at LLNL for the cooling of integrated circuits. This technique uses numerous tiny water cooling channels cut directly into the crystal. During the past year, in collaboration with scientists from Livermore, methods for cutting the cooling channels and attaching the associated plumbing without introducing strain have been developed. Several prototype crystal assemblies are now ready for testing at a synchrotron beam line, which should occur during the spring of 1990.

VUV FACILITIES

There are currently ten VUV or soft x-ray branch lines at SSRL. Four of these facilities were built by PRT's and the general user community has access to 33% of the time on these lines. The facilities being scheduled for users are: two TGM's (1-2 and 8-1), two grasshopper monochromators (1-1 and 3-1), a Seya-Namioka monochromator (3-2), an in-vacuum double crystal monochromator (3-3), a SGM (8-2) and the lithography/optics line (3-4). Two PRT branch lines, 6-1 and 5, are in the final stages of commissioning.

Improvements to Existing Experimental Stations

Branch Line 1-1: The old grasshopper was operated with the new elliptical M1 mirror installed in late 1988. The new mirror reduced the spot size from 90 μ to 40 μ , with a resulting factor of three increase in flux through the entrance slit. With the small spot size, and the cantilever design of the new mirror holder, vibration of the mirror caused intensity fluctuations that did not damp out until one second after the monochromator stopped scanning. A modification to the mirror holder was made to hold the end of the M1 mirror and to make fine *in situ* adjustments of the focus at the entrance slit. Also, the scanning motor was changed to a smoother operating 5 phase stepper. It is now expected that the dead time due to mirror vibrations should be negligible, and the spot size at the entrance slit should be reduced to an estimated 25 μ, with a further increase in flux.

Branch Line 1-2: The new TGM on Branch Line 1-2 was opened to users in the 1989 run. The first VUV beam line with a microVAX workstation for monochromator control and data acquisition, it operated with the EXP and AUTO data acquisition and analysis packages. During the run, it was confirmed that the 2400 l/mm grating is of poor quality, and will have to be replaced. Thus, the range of the monochromator is limited from 7 to 90 eV. The roll motion on the M0 was reassembled to ease the alignment of the beam into the monochromator. This adjustment, however, cannot completely remove the cant built into the 15 year old copper M0 mirror. To correct this a SiC mirror has been ordered (with the assistance of LANL) which will greatly increase the flux through the monochromator. A permanent I_0 section and pneumatic exit valve have been added after the refocusing mirror. The section has a metal pneumatic exit valve.

Branch Line 3-1: A microVAX workstation is being installed on the new grasshopper. It will be operating with the EXP and AUTO data acquisition and analysis packages.

Branch Line 3-2: The main bearing for the grating rotation galled during the last run. It was rebuilt and modified to prevent reoccurence of the problem.

Branch Line 3-3: A new fused silica mirror was been received to replace the one that has been in use on Jumbo since 1979.

BIOTECHNOLOGY FACILITIES

The research and user support in the Biotechnology area at SSRL are funded jointly by the NIH Division of Research Resources and the core SSRL DOE operations budget. Two specialized branch lines for protein crystallography (1-5 Area Detector and 7-1 Rotation Camera) exist as well as a variety of supporting equipment and instrumentation.

The current NIH grant is in its last budget year. A 5-year renewal proposal was submitted in May 1989. As part of the proposal review process, the SSRL Biotechnology Resource had a site visit in November. The Special Study Section gave a very favorable review and rating of the proposal, and it is now clear from NIH that the SSRL Biotechnology Resource will receive continued funding at the present level or higher. Major projects/instrumentation included in the proposal are an imaging plate detector system for use in crystallography and small angle scattering, an additional area detector for the system on Branch Line 1-5, acquisition of a Ge detector array system for XAS studies, implementation of a harmonic rejection/focusing mirror for Branch Line 7-3 (XAS), and a low-energy enhancement to Branch Line 6-2 including an in-vacuum monochromator and a Ni-coated mirror with an energy cutoff at about 6 keV.

Facilities for X-ray Absorption Spectroscopy: Continued progress in the development of HgI_2 detector arrays was achieved through careful characterization of a 5-element array under realistic operation conditions at SSRL. With an improved front end design the detectors maintained nearly ideal spectrometric behavior to input count rates in excess of 100 kHz.

The "rapid turnaround" station for XAS measurements was put in use for the first time. Due to the limited amount of beam time, only two such users were accommodated. After the successful use during the winter run of the new motorized alignment rails for XAS measurements, an additional rail was manufactured and assembled. Two rails are now dedicated to Branch Line 7-3 and to the rapid turnaround EXAFS station, respectively, while a third rail is available on request for the remaining XAS beam lines. A design effort has been successfully completed in the construction and assembly of a single crystal XAS alignment system to be used with the motorized rail system. It consists of a κ arc (rotation 0-100° and a ϕ rotation stage (full rotation). The system includes a movable laser-based beam/crystal alignment module attached to the rail through a standard slide.

Facilities for Protein Crystallography: During the past year a permanent radiation enclosure for the area detector data acquisition system on Branch Line 1-5 has been built. This new enclosure, which is the size of a small room, replaces the portable hutch that has been in use since the area detector system was first built. The enclosure is large enough to permit the future addition of a liquid nitrogen cryostat for low temperature crystallographic data collection. It will also provide enough space to accommodate an additional area detector at a future data which would greatly enhance the efficiency of multi-wavelength anomalous scattering data collection. Furthermore, the diffractometer has now been mounted directly onto the concrete floor slab for additional mechanical stability, and there is now adequate space for users to walk around the instrument for alignment purposes. This will make the system far more convenient to use.

The liquid nitrogen cryostat, that was built last year for the rotation camera system on Beam Line 7-1, has been further refined and tested on protein samples. This cryostat is now available to visiting user groups as part of the rotation camera system. A translation stage has been added to the rotation camera crystal monochromator so that a different region of the monochromator crystal can be used without opening the monochromator tank should the crystal become damaged by the x-ray beam.

A computer-controlled single-crystal goniometer for white beam Laue diffraction, incorporating a very fast x-ray shutter system, is under construction. When complete, this instrument will be used to perform time-resolved studies in protein crystallography using an Imaging Plate Detector system.

Facilities for Small Angle Scattering: A major improvement to the SAXS camera has been completed with the integration of a new detector into the system. This detector, a quadrant detector (obtained from Dr. A. Gabriel, EMBL, Grenoble), is of gas chamber type with spatial resolution in one dimension, but with a sensitive area covering a 60 degree quadrant. Integration of signals along 60 degree arcs provides a very significant improvement in signal-to-noise ratio at higher Q values when compared with single-wire

linear detectors. The new detector is most applicable to isotropic scattering experiments, but can also be used with oriented samples if some degree of mosaic spread is present. A fully motorized X-Z translation stage has been constructed to allow remote centering of the detector in the x-ray beam. As a separately moving component of the camera, the detector allows the existing alignment rail, motorized stages, and defining slits to be used for positioning samples and controlling the beam size. A sample-to-detector helium path has been manufactured to eliminate air scattering. I_1 (transmitted intensity) measurement is achieved using a design in which I_1 photons hit a flourescent screen mounted on the beam stop and the emitted light collected by a fiber optic cable and transmitted to a photomultiplier tube for measurement.

PRT EXPERIMENTAL FACILITIES

Improvements to Existing Experimental Stations

Beam Line 5 *(Xerox/Stanford University/SSRL)* - During the early shifts of SPEAR storage ring operation in 1989, the new monochromator on the multi-undulator Beam Line 5 took its first spectra. Performance during initial commissioning confirmed that the design and fabrication goals have been met. This is illustrated in Figure 2 which shows the observed transmitted flux compared to the calculated values.

FIGURE 2

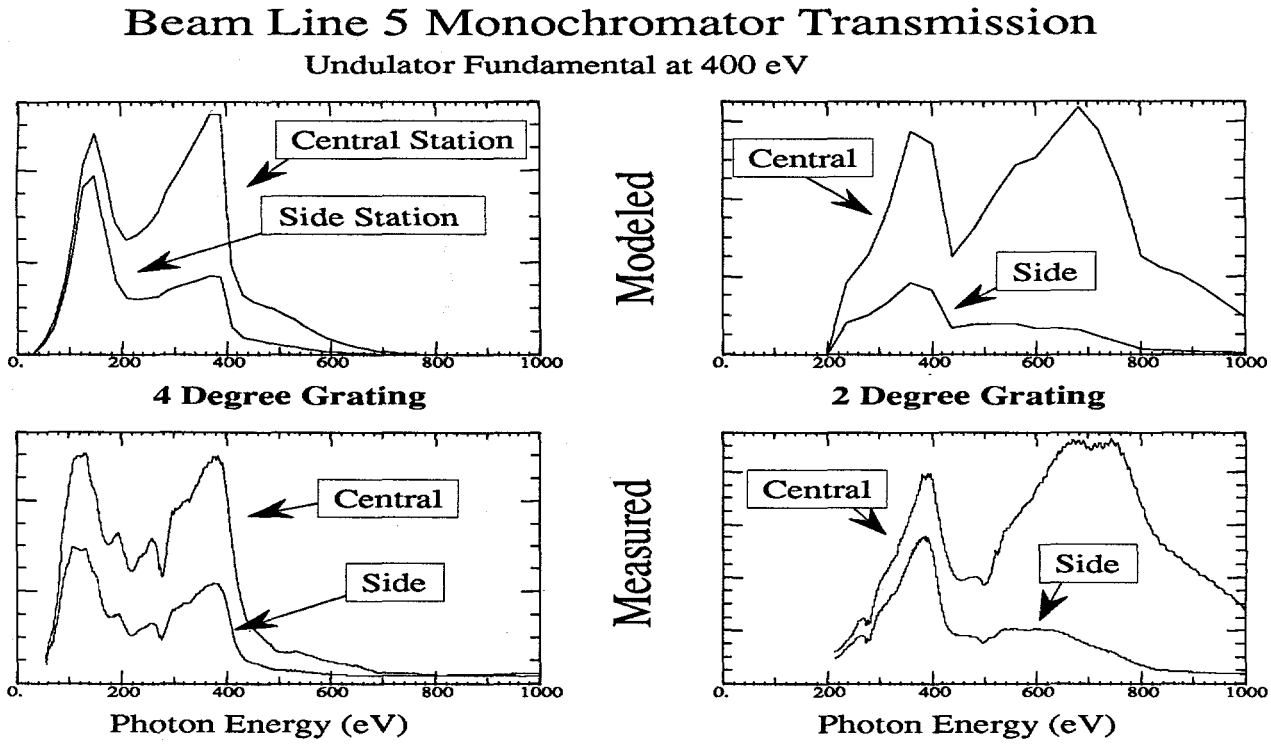

Observed Transmission vs. Calculated Values, Beam Line 5. The functional form of the observed transmitted flux of the beam line at a fixed undulator setting is compared to calculated values. The transmission of both the 2° and 4° gratings, as well as both the end station and side station are shown. The total electron yield from gold was used as a measure of the transmitted flux. The calculated transmitted flux includes the calculated spectral distribution of the source and the reflectivity of the mirrors, and assumes a grating efficiency function based on measurements of previous gratings purchased from Astron The peak in transmitted flux at about 120 eV is due to a peak in reflectivity of the optics, while the 400 and 800 eV peaks are due to the undulator fundamental and 2nd harmonic. The qualitative agreement and overall function form of the transmitted flux confirms that scattered light is not a serious problem. In addition, the side deflecting mirrors demonstrate predicted reflectivity performance, which results in usable side station flux up to 800 eV.

FIGURE 3

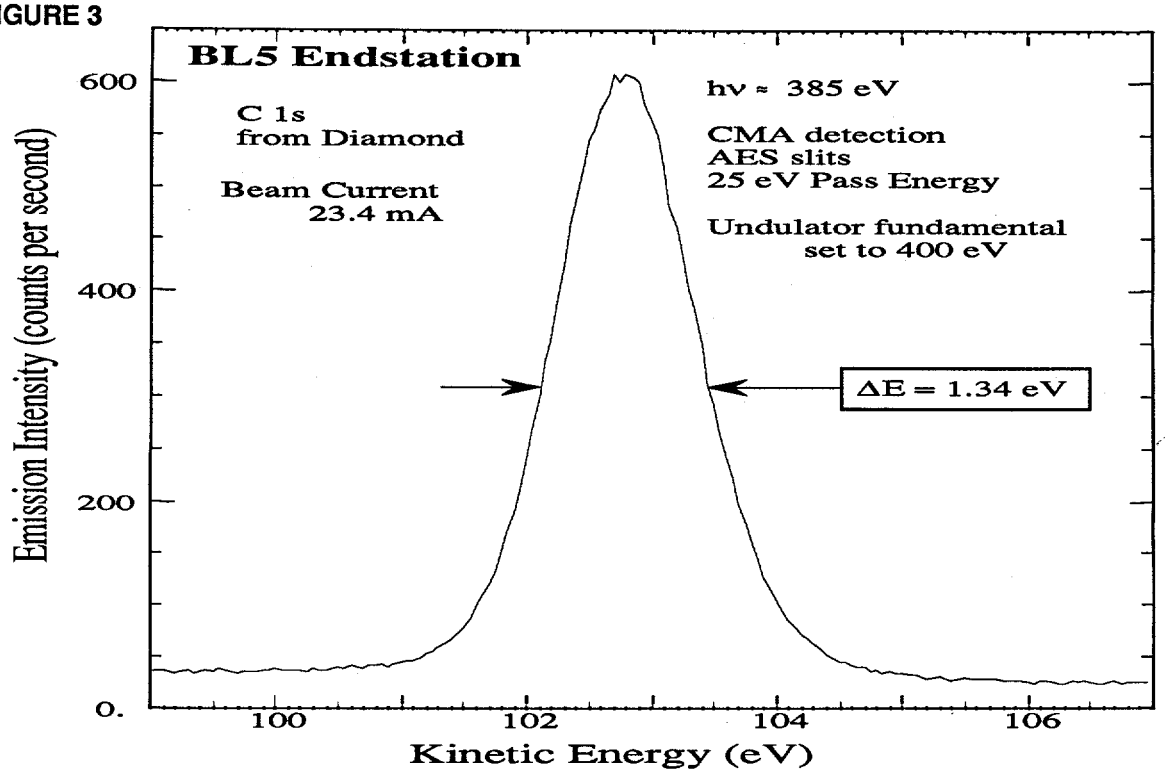

The Carbon 1s Photoemission Spectra at 385 eV on Beam Line 5

Operation of the beam line was limited to fixed undulator gaps for this initial run. Early in the run it was discovered that the exit slit had jammed open. Ironically, the monochromator resolution was limited by this stuck slit to that of the grasshoppers at SSRL. Shown in Figure 3 is the carbon 1s photoemission spectrum from diamond at an excitation photon energy of about 385 eV. The peak width is almost entirely due to the monochromator, as the natural linewidth of the C 1s is much less than 1 eV. The apparent monochromator resolution confirms that the slit opening is stuck at an opening of roughly 50 μ. In comparison to carbon 1s photoemission measurements made on the new grasshopper, Branch Line 3-1, (March 1982) at similar photon energies (and operating at the same photon resolution) it is estimated that the Beam Line 5 photon flux at 400 eV is about a factor of 20 more intense (normalized to beam current). Final optimization of the beam line during April, 1990 may alter (i.e., improve) this figure.

After the run the 1 and 2 meter gratings of the monochromator were replaced with new specifically figured Astron gratings. These gratings were optically aligned for optimum instrument resolution using a mercury lamp technique. Extensive characterization of the instrument's optical performance was made, particularly, flux measurements as a function of slit width, determination of zero order positions for the various optical elements, determination of the slit position as a function of encoder position, and extensive exercise of the mechanical motions and repeatability of position. Various improvements were also made to the electronics systems and monochromator software. Undulator control capability from the beam line has also been implemented, utilizing direct communciation with the SPEAR control computer.

Beam Line 8 *(University of California/National Laboratories/SSRL)* - Very good spectral resolutions have been measured for TGM Beam Line 8-1 using an electron time-of-flight spectrometer. For the G2 grating (822 gr/mm), FWHM linewidths of 39 meV and 85 meV were obtained for the Kr $4s^{-1}$ line at 27.52 eV and the Xe ($4d_{5/2}$-6p) line at 65.11 eV, respectively. A FWHM linewidth of 41 meV was obtained at 65.11 eV using the G1 grating (2400 gr/mm). These results were derived by subtracting in quadrature an instrumental spreading of 20 meV. The electron spectrometer data yielded negligible higher-order light for G1 above 110 eV. This is

consistent with an estimated factor of five suppression of higher orders in this energy range by prefocusing mirror roll off. Below 100 eV, higher-order contributions to the G1 output did not exceed 20%. Very little higher-order contributions were observed for G2 above 35 eV. In contrast, very significant higher-order contributions were observed for G2 below 35 eV and for G3 (288 gr/mm) through its entire range. A suitable mirror roll-off device, such as SiC at 20° with a sharp roll off above 90 eV, is recommended for TGM operation below 35 eV. Prefilters now installed on the branch line include In, Sn, Al, Si, Be/C, B, and C.

A new multipurpose sample chamber was installed on SGM Branch Line 8-2 and tested during the spring 1989 run. It includes a 150-nm Al vacuum barrier for operation at 10^{-6} Torr, a well-shielded flux monitor mounted near a pair of Huber adjustable entrance slits, a translatable filter holder, a calibrated NBS-style diode featuring a Au cathode that can be inserted into the beam near the chamber exit, and computer-coupled rotation stages for multilayer reflectivity measurements. A large (1 x 1 cm) GaAsP detector was mounted on the detector arm which, despite its size, had adequately low dark current. A nearly ideal focus was obtained at the chamber center (less than 1 x 3 mm), thus verifying excellent exit mirror performance. Two new I_o monitors both performed very well. A new channeltron-amplified I_o monitor located upstream of the window section gave similar results to a gold mesh I_o monitor located in the scattering chamber near the entrance slits. The unamplified gold mesh is very well shielded yielding dark currents that were a factor of 5 or 10 lower than previous designs.

FIGURE 4

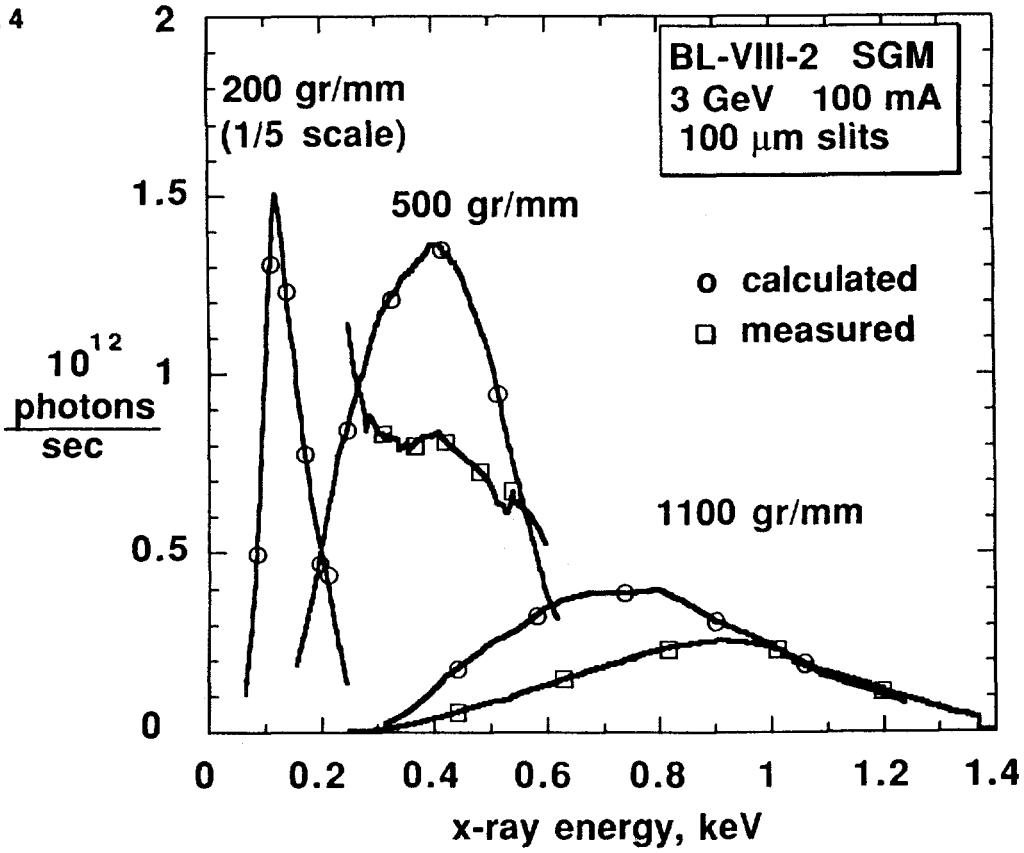

Calculated SGM Throughput Compared to Au Diode Results, Branch Line 8-2. The calculated results are based on a 3 GeV, 100-mA SPEAR bending magnet spectrum, ideal grating efficiency, and ideal Pt reflectivity at 2.5° and 2° (first and exit mirrors); measured results were corrected for transmission through the 150-nm Al window. Increases in measured flux for the 500-gr/mm case below 300 eV and above 550 eV are due to second-order and zero-order contributions, respectively. The second order component is preferentially transmitted through the Al window and has not been subtracted. These results are in satisfactory agreement considering the corrections required and the preliminary status of the grating efficiency calculations.

FIGURE 5

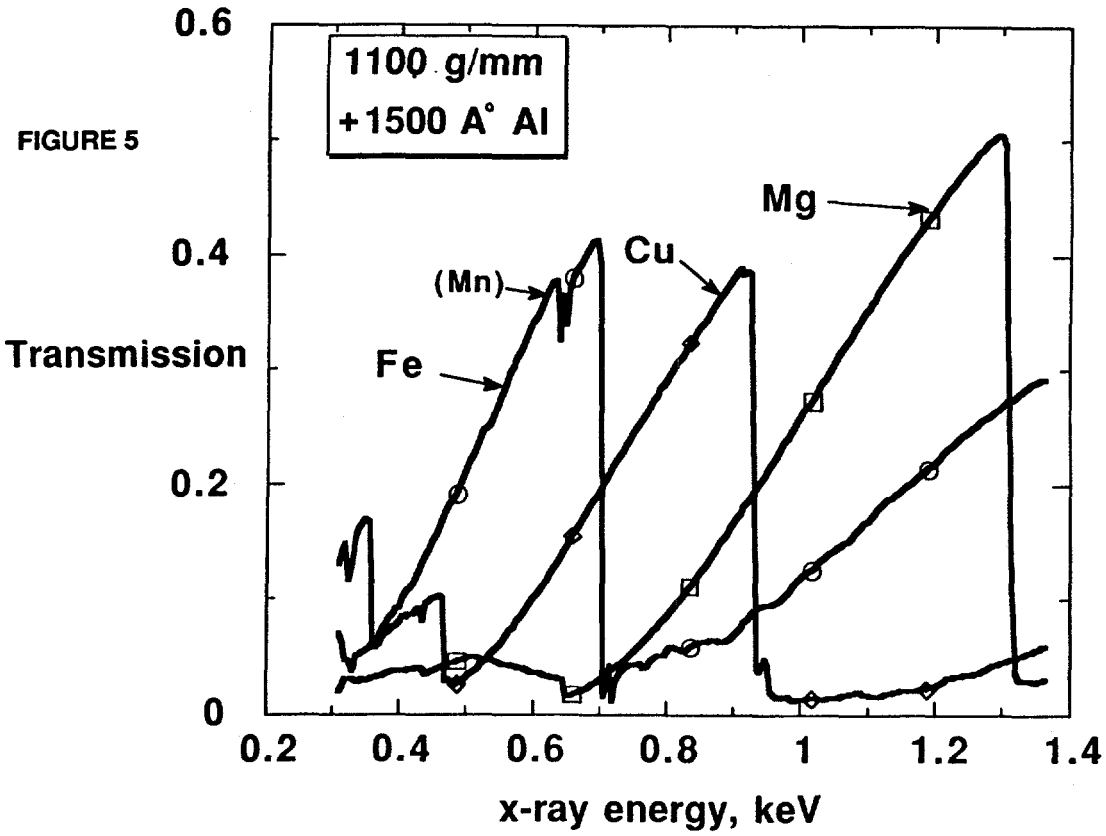

Measured Transmission Results for Typical Station 8-2 Gratings

FIGURE 6

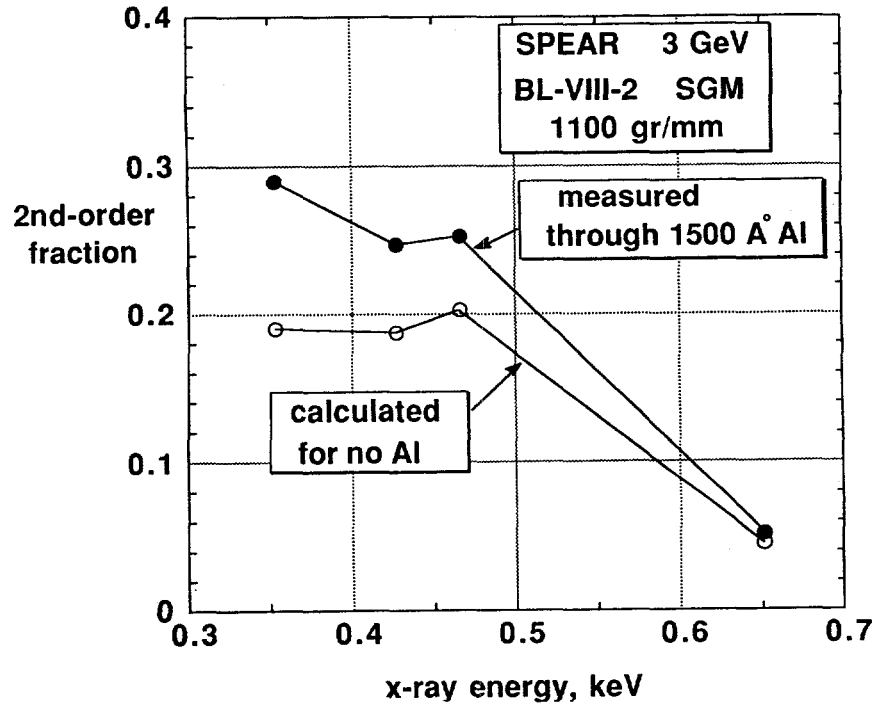

Second Order Results from the 1100 gr/mm Grating. The second-order results obtained for the SGM 1100-gr/mm grating based on Fe, Ni, Cu, and Mg edges are shown. Each value has been corrected for the moderate detector sensitivity difference at the two edges. Corrections for third and higher orders are negligible. Note the evidence for rather weak third-order at 434 eV (311 eV) for Mg (Cu). These results suggest that above 600 eV this grating range is relatively free from second- or higher-order contributions and that the second-order fraction is somewhat reduced if the vacuum barrier is not required.

Good data on prefilter transmission and monochromator plus window output was obtained using an NBS style gold x-ray diode. Absolute calibration of the detectors was done at LLNL using proton-induced K and L lines in the range of interest, Figure 4 shows calculated SGM throughput compared to results obtained using the Au diode. These results are in satisfactory agreement considering the corrections required and the preliminary status of the grating efficiency calculations.

Prefilters installed in SGM Branch Line 8-2 include C, Ag, V, Fe, Ni, Cu, and Mg. Figure 5 shows measured transmission results for typical filters. Note that higher orders are exaggerated in Figure 5 because the first-order amplitude has been reduced by the vacuum barrier. Filter transmission data has been used to determine absolute second-order contributions. Figure 6 shows second-order results obtained for the SGM 1100-gr/mm grating based on Fe, Ni, Cu, and Mg edges. These results suggest that above 600 eV this grating range is relatively free from second- or higher-order contributions and that the second-order fraction is somewhat reduced if the vacuum barrier is not required.

Beam Line 10 *(University of California/National Laboratories/SSRL)* - During the spring 1989 run the flux of Branch Line 10-2 in the focused mode was determined. With SPEAR operating at 3.3 GeV and 59 mA ring current, the measured flux at 10 keV photon energy was 3.4×10^{12} photons/sec for a wiggler field of 1.0 Tesla.

In 1989 a new tandem diffraction hutch was installed on Branch Line 10-2. This hutch is shielded to handle white light and can accommodate a 1.5 m radius swing. A large (48" x 72") optical table top is being installed in the front hutch for EXAFS, imaging, and other experiments.

The beam movement and energy drift problems encountered during the 1989 run have been diagnosed and solved - the energy drift by eliminating false pulses sent to the monochromator motor drive during scanning and the horizontal beam movement by correcting the off-parallel alignment of the plates housing the monochromator crystals and crystal holders. As a result of the earthquake, Branch Line 10-2 dropped ~.1" with respect to the SPEAR plane. Realignment has been completed.

To obtain photons in the 1-3 keV region, modifications were made to allow operation without the Be window module. This included installation of a differential pump section to serve as a transition region from UHV to HV and modifications of the monochromator to enable operation at high vacuum (10^{-7} Torr). Rh-C multilayers (2d = 80 Å and 2d = 40 Å) and a beryl crystal will be used as dispersive elements. A HV experimental chamber is also available. A schematic drawing of the modified beam line is shown in Figure 7. A protocol for the change-over from hard to soft x-rays has been developed. Tests and characterization of the modifications will be conducted during the spring 1990 run. Because the present monochromator cooling is probably insufficient for operation at the full wiggler field, the initial measurements will be made with operation in undulator mode.

We are also implementing a quick scan EXAFS capability. R. Frahm (HASYLAB) is collaborating with LLNL to install this new capability and to perform time-resolved EXAFS measurements of thin film growth processes and interface formation in the time domain of seconds.

PRT Facilities Under Development

Branch Line 6-1 *(LBL/SSRL/EXXON)* - During the last dedicated SPEAR run a new Spherical Grating Monochromator (SGM) saw its first synchrotron light at the LBL/EXXON/SSRL 54-pole wiggler Station 6-1. This monochromator and two premirrors, designed and fabricated by LBL for high resolution and high flux requirements, had been installed at SSRL in 1988.

The monochromator is based on a Rowland Circle geometry with a large radius (R=55 m) and movable slits. The first optical component, a movable and water-cooled plane mirror, horizontally reflects a part of the wiggler beam onto a second mirror, a toroid. This focuses vertically on the entrance and horizontally on the exit slit of the monochromator. The grating chamber may accommodate three large (65 mm x180 mm) water-cooled metal gratings. These gratings were not available for the winter run. They are now nickel-coated and polished, but the ruling process will still take several months. Instead, a single fused silica grating (600 l/mm, no cooling) from Ferranti Astron of outstandingly high quality (very small surface roughness and slope errors) was installed.

FIGURE 7

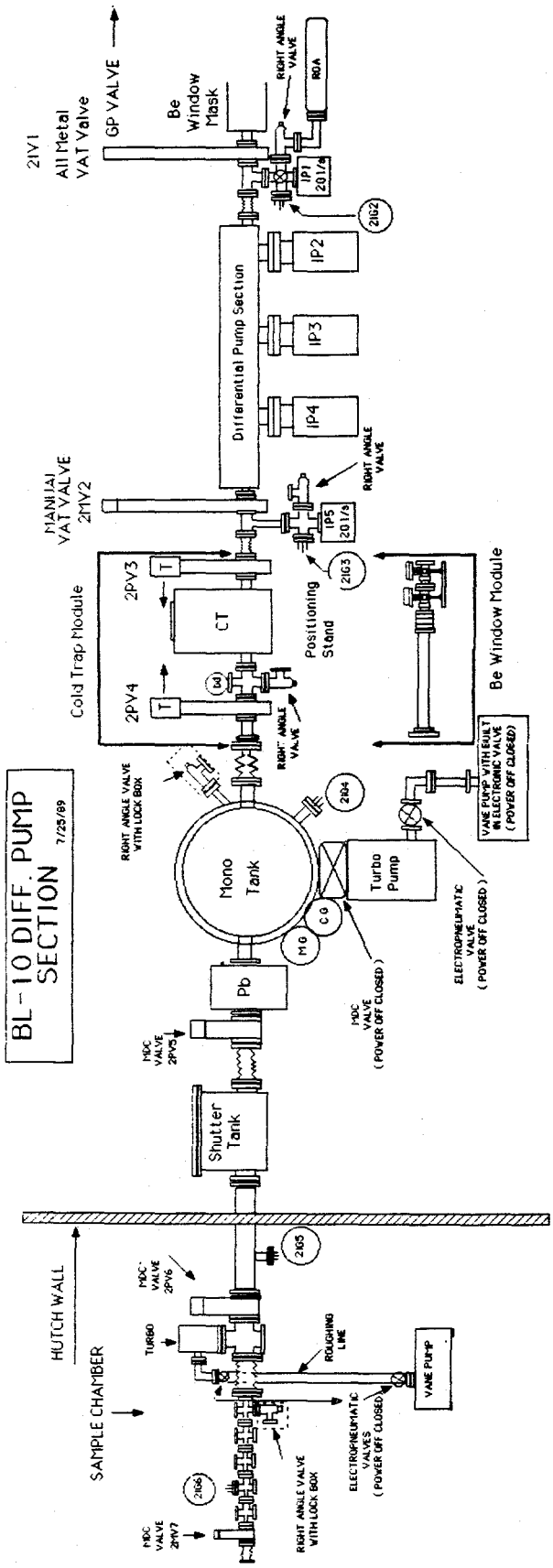

Schematic Drawing of Line 10-2

The first output data of the monochromator taken with an aluminum photodiode show an unusually low stray light contribution, which confirms the quality of the grating. The energy range of this grating covers 180 eV to 820 eV. The absolute photon flux is calculated to be $1x10^{11}$ Phot/sec/100 mA at 440 ev with 0.5 eV resolution (i.e., 100 μ slits).

Two strong peaks which are visible in the output spectrum at 220 eV and 440 eV were identified as the 1st and 2nd harmonic of the 54-pole wiggler (0.5 T). This means that, for future applications, the wiggler could be used to increase the photon flux in small, selected energy ranges.

For a fine alignment of the monochromator, and hence improvement of its resolution, the photodiode was replaced by an ion chamber (supplied with 0.01 Torr nitrogen). The ion yield from nitrogen displays five clearly resolved vibrational final states structures at the $1s\text{-}2p^*$ resonance at about 401 eV. This demonstrates that the achieved instrumental resolution at the end of the run was already less than the lifetime broadening, which is about 130 meV for N 1s vacancies.

A deconvolution using Lorentzian functions for the lifetime width and with Gaussian functions for the monochromator resolution shows a width of 80 meV for the monochromator resolution, i.e., at 400 eV a resolving power of 5000. This is the second best resolution ever achieved with a monochromator covering the K-edges of the elements C, N, O, and F. (C.T.Chen and F. Sette, Bell Labs claim 10,000 for their new SGM with an 800 l/mm grating at NSLS).

It is worth mentioning that the measurements at SSRL were performed under "low intensity" conditions, which means the wiggler was mainly operated at 0.5 T and the mirror M0 was only modestly inserted into the wiggler fan, (an intensity of 4-9% was subtracted from the x-ray Branch Line 6-2).

It is expected that the photon flux and the resolving power can be improved further during the next SPEAR run.

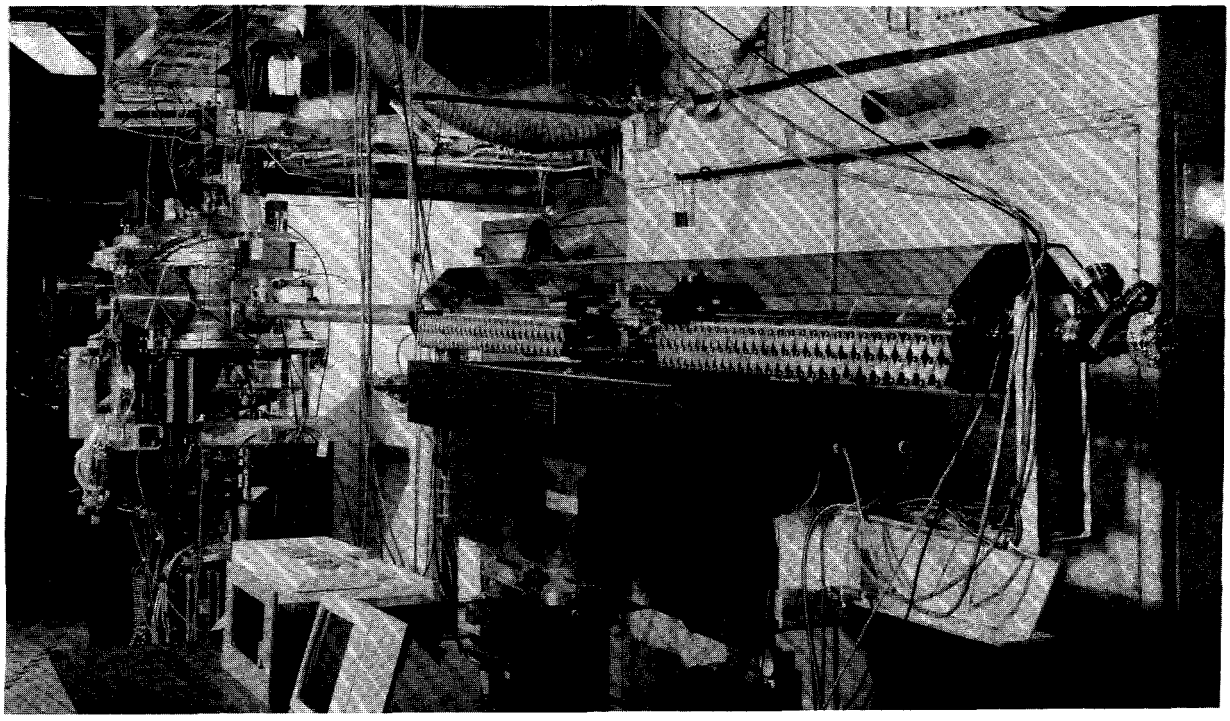

An overview of the Branch Line 6-1 Spherical Grating Monochromator (SGM) built by Lawrence Berkeley Laboratory (LBL) with assistance from SSRL. Seen from left to right are the toroidal condensing mirror, the grating chamber and the moveable slit exit.

Branch Line 10-1 *(IBM/Stanford University/SSRL)* - During the year the front end components of Beam Line 10 were modified to accept the components for the new 10-1 station. The mirrors and monochromator will be delivered in the first half of 1990. For specific details of the branch line see the 1988 Activity Report. The expected date for first light in this line is October 1990.

SUPPORT FACILITIES

Computational Facilities - Preparations for the conversion of all PDP-11 beam line data acquisition systems to VAXstations have continued. Programming for the base-level driver system (called VAX motors) is fully complete and programming for higher-level user-interface software for specific applications is ongoing. The first major application of the new hardware/software control system will be for EXAFS applications on Branch Line 7-3 during the coming Spring 1990 run. Following full debugging and documentation, all remaining systems are expected to be converted to VAXstation control by the end of Summer, 1990.

Biochemical Laboratory. One major addition was made to the lab in 1989, a refrigerated Beckman GPKR centrifuge with rotors.

User Clean Room: The clean room vacated by the vacuum group, on their move to Building 137, has been set up for use by staff and users. It has benches, tools, spot welder, fume hood for cleaning small parts and a limited supply of hardware that can be signed out.

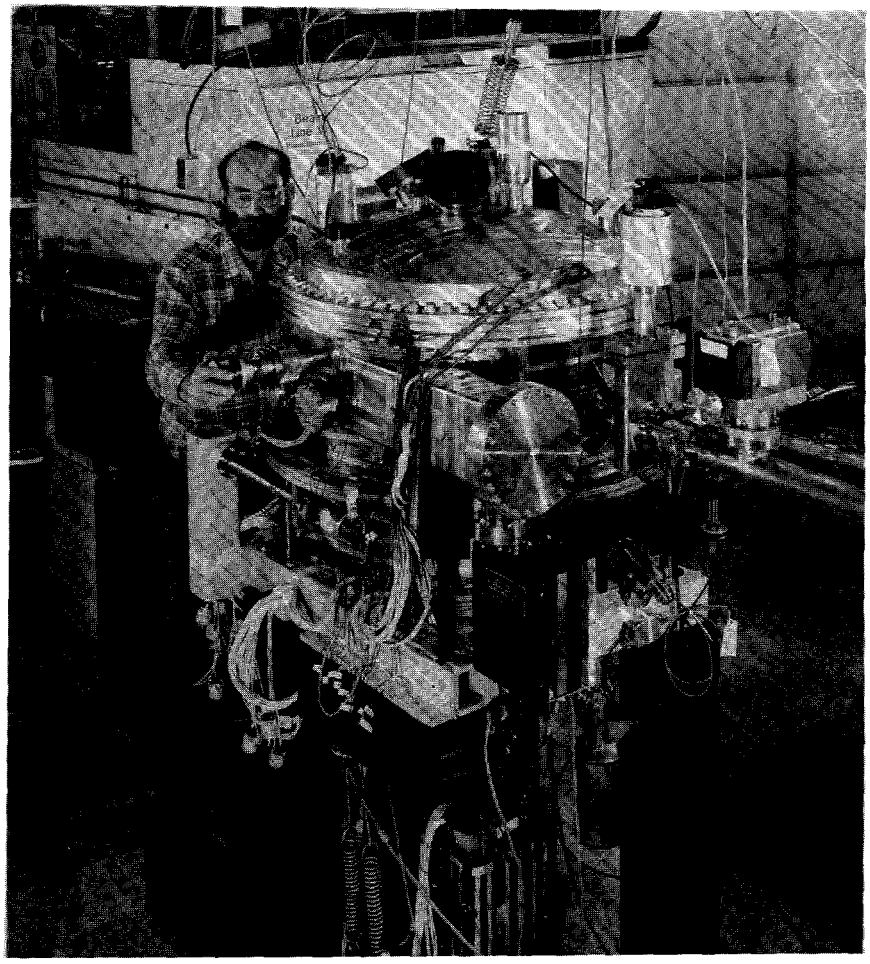

The grating chamber with facility for three interchangeable, water-cooled gratings. Underneath black covers are a HP laser interferometer and stepping motor from the Orasis Corporation, which precisely control the angle of the grating. Standing next to the chamber is assembly technician Bill Gath.

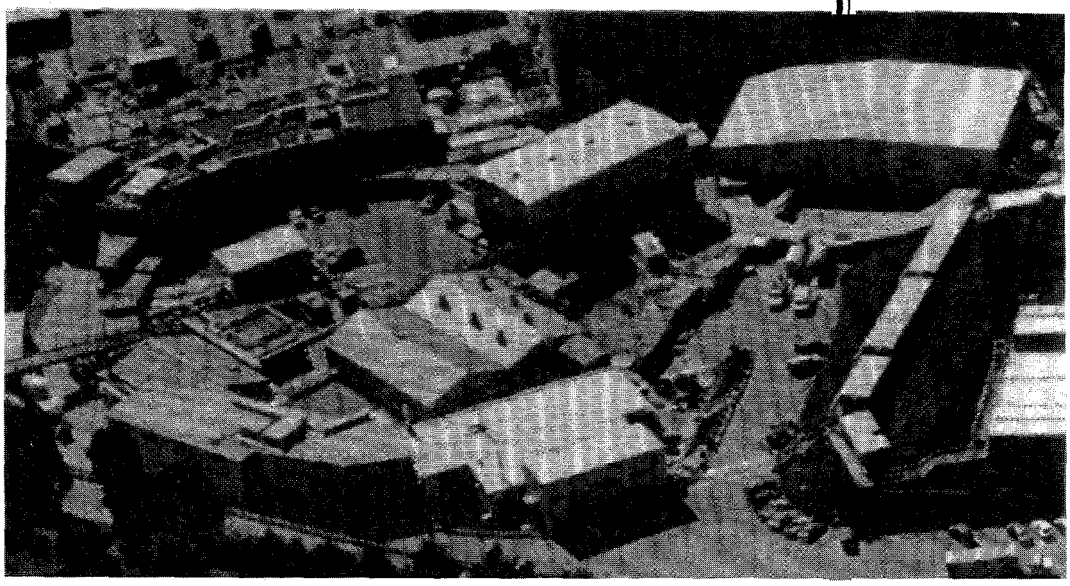

Section IV

SSRL Organization

IV SSRL ORGANIZATION

On December 22, 1989, SSRL Director A. Bienenstock announced a reorganization of the SSRL technical staff which became effective January 2, 1990. The goals of the reorganization were to focus effort on SSRL's three highest priorities: to complete and commission the injector, to prepare to operate and maintain SPEAR and the injector and to have a successful spring 1990 experimental run. In the new organization, all the technical staff is contained in three groups:

1. Accelerator Research and Operations Division
2. Injector Project
3. Photon Research and Operations Division.

Responsibility for safety and quality assurance resides in the Director's Office.

The functions of the Accelerator Research & Operations Division are: accelerator operations, accelerator physics research, engineering, technical resources and user support. The Photon Research & Operations Division is responsible for: beam line management, beam line development, research using synchrotron radiation and user support. At the completion of the injector project personnel from this project will be incorporated into the other divisions as appropriate. In addition, there is a Computational and Administrative Resources Division.

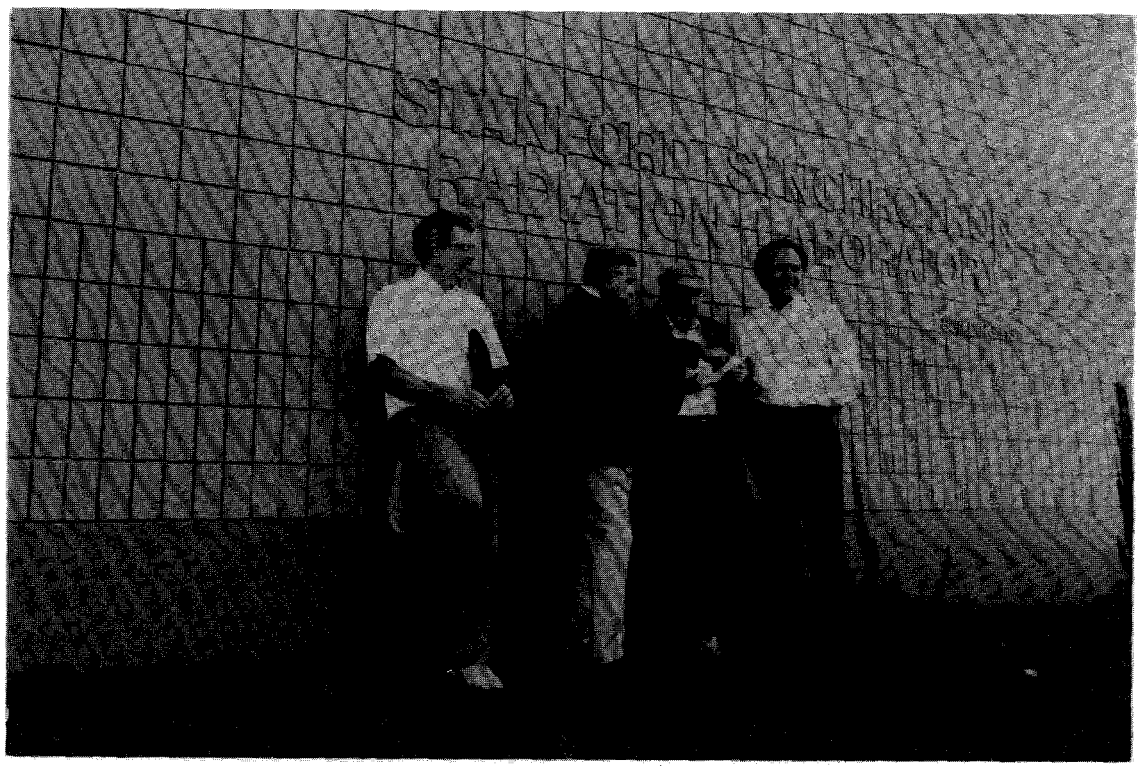

Piero Pianetta (Associate Director Photon Research Division), Arthur Bienenstock (Director), Herman Winick (Deputy Director) and Ron Gould (Associate Director Computional and Administrative Resource Division).

SSRL EXPERIMENTAL STATIONS

RESPONSIBLE PERSONNEL

BRANCH LINE		RESPONSIBLE PERSON(S)
1-1	Grasshopper	A. Waldhauer
1-2	TGM	M. Rowen
1-4	SAS	H. Tompkins
1-5	Unfocused Bend Magnet	H. Tompkins
1-5AD	Area Detector	P. Phizackerley/H. Bellamy
2-1	Focused Bend Magnet	H. Tompkins
2-2	White Radiation	Z. Rek
2-3	Unfocused Bend Magnet	H. Tompkins
3-1	Grasshopper	A. Waldhauer
3-2	Seya - Soft X-ray	F. Coffman
3-3	Jumbo - Soft X-ray	M. Rowen
3-4	Lithography	P. Pianetta
4-1	8-Pole Wiggler	H. Tompkins
4-2	8-Pole Wiggler	H. Tompkins
4-3	8-Pole Wiggler (Materials Diffraction)	H. Tompkins
5	Mutli-Undulator.	R. Carr/F. Coffman
6-1	54- Pole Wiggler - SGM	A. Waldhauer *(SSRL)*, P. Heimann *(LBL)*
6-2	54- Pole Wiggler	J. Arthur *(SSRL)*, G. George *(EXXON)*, P. Ross *(LBL)*
7-1	8-Pole Wiggler (Rotation Camera)	P. Phizackerley/M. Soltis
7-2	8-Pole Wiggler (Scattering)	J. Arthur
7-3	8-Pole WIggler	H. Tompkins
8-1	SGM	M. Rowen *(SSRL)*, G. Tirsell *(LLNL)*, J. Tobin *(LLNL)*
8-2	TGM	M. Rowen *(SSRL)*, S. Williams *(UCLA)*
10-2	31- Pole Wiggler	J. Arthur *(SSRL)*, J. Wong *(LLNL)*
PEP1B		H. Tompkins
PEP 5B		H. Tompkins

INSTRUMENTATION/FACILITY RESPONSIBILITIES

MATERIALS DIFFRACTOMETER: S. Brennan, H. Tompkins
PERKIN-ELMER CHAMBER: M. Rowen
VG SAMPLE CHAMBER: M. Rowen
AREA DETECTOR: P. Phizackerley, H. Bellamy
ROTATION CAMERA: P. Phizackerley, M. Soltis
CAD-4 DIFFRACTOMETER: M. Soltis
COMPUTER SYSTEMS: T. Cox
7-2 SPECTROMETER: S. Brennan, H. Tompkins
BIOCHEMISTRY LABORATORY: B. Hedman, R. Mayer
DARKROOMS: M. Soltis, Z. Rek
BEAM LINE STEERING: R. Hettel
EXAFS EQUIPMENT AND SOFTWARE: B. Hedman, R. Mayer
SAS CAMERA (BIOTECH): S. Wakatsuki
EXAFS CONSULTANT: B. Hedman
SCATTERING CONSULTANT: S. Brennan
RT-11 SOFTWARE CONSULTANT: S. Brennan
TOPOGRAPHY EQUIPMENT: Z. Rek
RAPID TURNAROUND EXAFS FACILITIES: B. Hedman, R. Mayer
MIRROR COATING/METROLOGY LABORATORY: D. Ernst

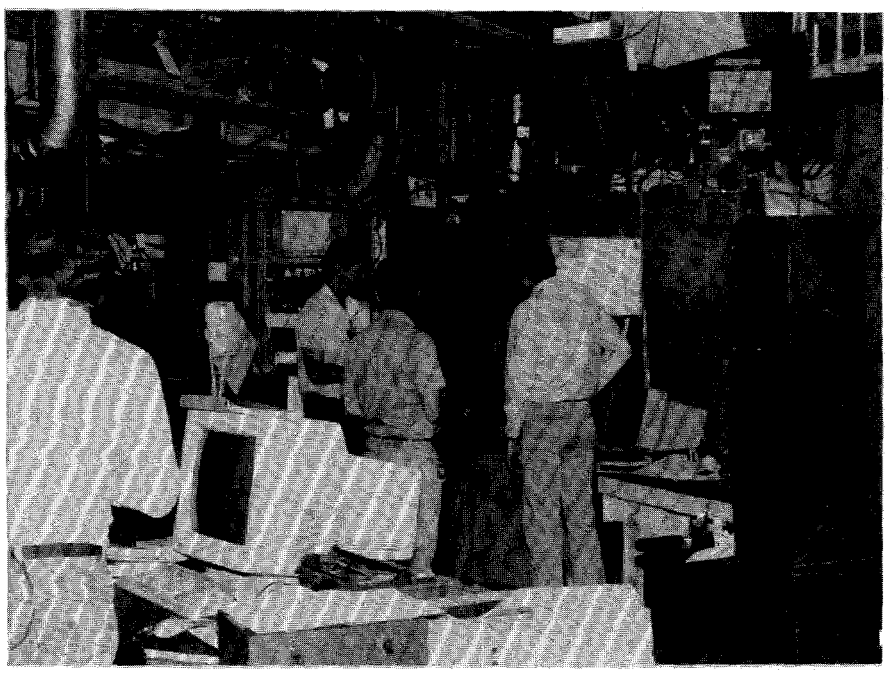

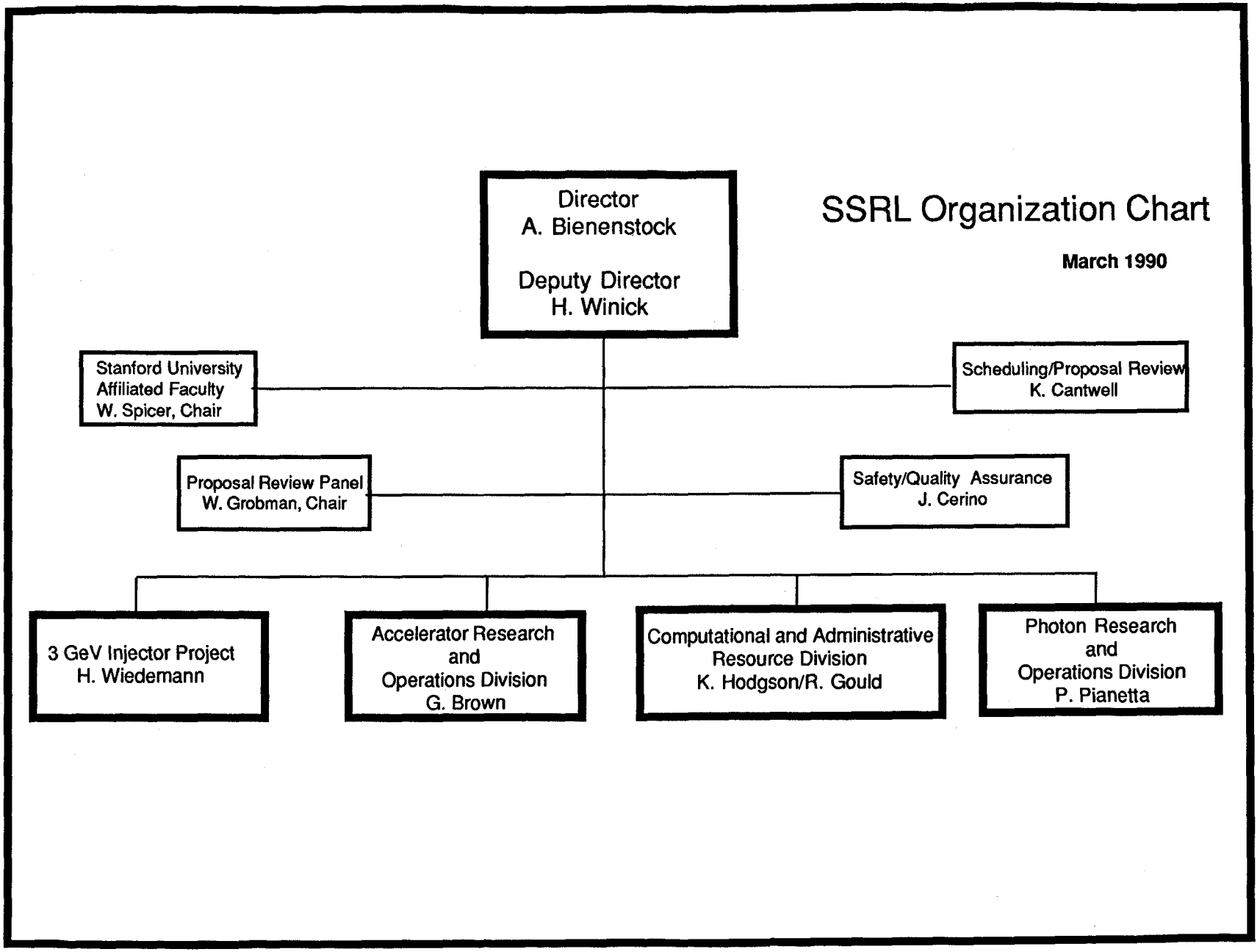
SSRL Organization Chart
March 1990
Director
A. Bienenstock
Deputy Director
H. Winick
Stanford University
Affiliated Faculty
W. Spicer, Chair
Scheduling/Proposal Review
K. Cantwell
Proposal Review Panel
W. Grobman, Chair
Safety/Quality Assurance
J. Cerino
3 GeV Injector Project
H. Wiedemann
Accelerator Research
and
Operations Division
G. Brown
Computational and Administrative
Resource Division
K. Hodgson/R. Gould
Photon Research
and
Operations Division
P. Pianetta

SSRL ADVISORY BOARDS

PROPOSAL REVIEW PANEL

A main task of the Proposal Review Panel is the review and rating of scientific proposals to SSRL based largely on reports obtained from outside (non-panel) referees. The panel met on January 14, 1989 and on July 20 and 21, 1989 at SSRL and rated the new proposals which had been received in September 1988 and March, 1989 respectively.

As of December 31, 1989 SSRL has received a total of 2107 proposals of which 166 are presently active.

The Proposal Review Panel meets twice yearly, generally in June and January. Deadlines for receipt of proposals for consideration at the next meeting are the first of September and the first of March of each year.

The panel members in 1989 were:

Biology Sub-panel
Don Engelman, Yale University
Wayne Hendrickson, Columbia University
William Orme-Johnson, MIT

Materials Sub-panel
G. Slade Cargill, IBM Research Center
Howard Birnbaum, University of Illinois
Russell Chianelli, EXXON
Denis McWhan, AT&T Bell Laboratories (term ended 1/89)
Peter Pershan, Harvard University (term started 7/89)

VUV Sub-panel
Charles Fadley, University of Hawaii
Warren Grobman, IBM Watson Research Center *(Chairperson)*
Torgny Gustafsson, Rutgers University

SCIENCE POLICY BOARD

The Science Policy Board reviews all aspects of SSRL operation, development and plans for the future. It reports to Stanford University President Donald Kennedy. The Board met once during this reporting period, on May 4-5, 1989. A joint meeting with the SLAC Science Policy Committee was held during the meeting. Members of the 1989 Board were:

B. McDaniel, Cornell University *(Chairperson)*
C. Barrett, Intel
P. Chaudhari, IBM
E. Ginzton, Varian
E. Knapp, University Research Associates
W. Kohn, University of California-Santa Barbara
V. Narayanamurti, Sandia Laboratories
W. Orme-Johnson, MIT
Y. Petroff, LURE
P. Wolff, MIT
M. Wrighton, MIT

SSRL USERS ORGANIZATION

Members of the Executive Committee of the SSRLUO were appointed at the 16th Annual SSRL Users Group Meeting as follows:

Stephen Laderman, Hewlett-Packard *(Chairperson)*
Brad Pate, Washington State University *(Vice-Chairperson)*
Troy Barbee, LLNL
Gordon Brown, Stanford University
Phil Heimann, LBL
Janet Kahn, Stanford University
Paul King, Stanford University
Marjorie Olmstead, University of California
David Templeton, LBL
Al Thompson, LBL
Katherine Cantwell *(Secretary-SSRL Liaison)*

The Users Organization is responsible for organizing the annual users conference. The 16th Users Conference was held October 17th - 18th, chaired by Steve Laderman and Fred Senf.

Section V

Experimental Progress Reports

V. EXPERIMENTAL PROGRESS REPORTS

MATERIALS PROPOSALS

BIOLOGY PROPOSALS

VUV PROPOSALS

Materials Progress Reports

X-RAY ABSORPTION STUDIES OF DISORDERED SYSTEMS

E.D. Crozier and D.T. Jiang
Physics Department, Simon Fraser University, Burnaby, B.C., Canada V5A 1S6

R.Ingalls, J. Freund and B. Houser
Physics Department, University of Washington, Seattle, WA, 98195

This activity report summarizes experiments done at SSRL on beamline IV-1 during our February 1989 run and work sponsored by SSRL at NSLS on beamline X-23A, September 1989. At SSRL we continued our glancing- incidence EXAFS investigations of the structure of buried films, obtaining high quality data on films grown by molecular beam epitaxy which were only a few monolayers thick. We also continued our high pressure study of the 12 gPa phase transition in Fe. Our experiments at NSLS were done in conjunction with C.E. Bouldin. They involved high pressure measurements to study: asymmetry effects in RbBr; the mixed valent transition in $TlReO_4$; the pressure-induced displacement of niobium atoms in $KTaO_3$; and multiple scattering effects in the high T_c superconductor $YBa_2Cu_3O_{7-\delta}$. We also initiated an XAS study of the intercalation of Li into MnO_2

MBE Films

Ni epitaxially grown on the (001) face of iron single crystals shows interesting magnetic and structural properties. Although the first 6ML (monolayers) of Ni have been shown to be ferromagnetic, additional layers exhibit large cubic in-plane magnetic anisotropy. In earlier work we applied the glancing incidence XAS technique to examine the changes in the short range structure with the number of monolayers of Ni grown. We have extended this work to a study of the epitaxially grown multilayer system: 10 ML of Au/ 9ML of Ni/9 ML of Fe which was itself grown on the (001) surface of a Ag single crystal. The 9 ML of Fe was chosen to reduce the magnetic contribution of the bulk iron of the earlier study. The Au was present as a passive overlayer to protect the Ni/Fe from oxidation during ferromagnetic resonance measurements. The Au permitted us to examine the extent to which the evanescent wave in the glancing incidence mode will penetrate surface films of high atomic number permitting study of underlying films of smaller atomic number.

Both Ni and Fe K-edge XAS spectra were obtained for angles above and below the critical angle for total reflection. Neither the Ni nor the Fe XANES/EXAFS are characteristic of their normal bulk structures. As shown in Fig. 1, the Ni K-edge XANES shows a dramatic progressive change with increasing angle of incidence. The Ni EXAFS reveals that for angles less than the critical angle there is a contraction of 0.05 Å in the nearest neigbour distance relative to angles greater than the critical angle. These data suggest that the interaction of Ni atoms at the Au-Ni interface is different from that at the Ni-Fe interface. There are also angular dependent changes in the Fe spectra. These changes are somewhat unexpected. RHEED patterns and RHEED oscillations taken during film growth indicate that Au grows expitaxially on the Ni without interdiffusion and similarly for Ni on Fe. This needs to be reconciled with the XANES/EXAFS spectra. Our present analysis has been simple. A more detailed analysis involving Ni, Au and Fe atoms will have to be done to give a better specification of the structures of the multilayers.

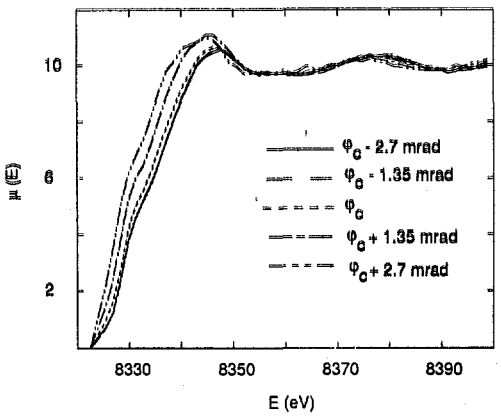

The data are also of interest from an experimental viewpoint. The angular dependent changes observed in the K-edge XANES of Ni and Fe demonstrate that the glancing incidence XAS technique may be able to provide both electronic and structural information for interfaces that are buried under a thin overlayer of atomic number higher than that of the underlayer. In addition, the data at glancing incidence were collected using simultaneously two or three modes of detection: total electron yield with a He gas flow detector, fluorescence and/or reflectivity. This provided an efficient means of determining the reproducibility of the data.

High Pressure Studies

A series of XAFS experiments were performed on samples subjected to static pressures in the range 0 to 20 gPa. The work focussed on pressure induced atomic disorder and structural phase changes.

A study of rubidium bromide was undertaken. Like most of the other alkali halides, RbBr undergoes a B1-B2 transition under pressure which is clearly visible in the XAFS. Data analysis shows that the second and third cumulants, i.e. quantities related to the second and third moments of the bond lengths, depend on pressure. We are working on a lattice model to explain these dependences and expect to relate them to the first and second perturbations of the pair potentials between the atoms.

Measurements were performed on niobium impurities in $KTaO_3$. The niobium atoms substitute for tantalum and are known to be displaced in the [111] directions at a pressure of 1 bar. It has been inferred through susceptibility measurements that pressure induces the niobium to move on-center. When fully analyzed, our absorption spectra will tell whether movement of the niobium is indeed occuring, or whether there is some other structural transition responsible for the changes in susceptibility.

We also examined the compound $TlReO_4$. According to Jayaraman this compound has the scheelite structure at 1 bar but undergoes subtle structural transitions at approximately 0.5, 1.9 and 9.7 gPa. The latter has been speculated to have a simultaneous valence change of the Re ion from 7^+ to 5^+. The present experiment reached 16 gPa, and focussed on the Re-L_{III} XANES, with full EXAFS spectra only taken at selected pressures. The 9.7 gPa

transition primarily manifested itself as a pronounced narrowing and slight shift of the "white line" of the Re-L_{III} edge. Analysis of the XAFS is in progress. Further work must involve careful comparison with other Re compounds in its various valence states, as well as the Tl L-edges, which should also indicate a valence change from 1^+ to 3^+.

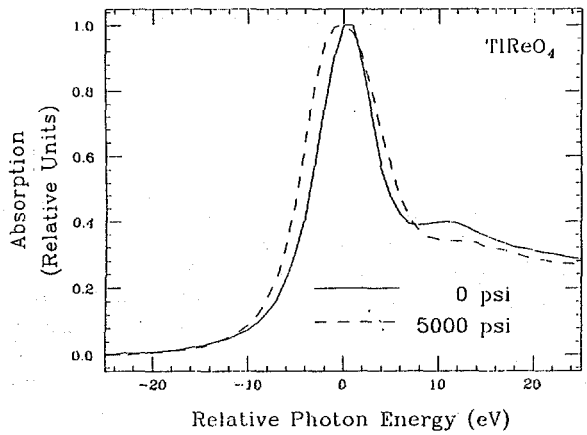

We continued our high pressure study of high T_c superconductors. X-ray diffraction suggests that pressure causes a monotonic compression of the unit cells of both $La_{1.85}Sr_{.15}CuO_4$ and $YBa_2Cu_3O_{7-\delta}$. However, the limited number of Bragg reflections observed prevented definitive comment on changes within the unit cell. Our earlier XAS results for $La_{1.85}Sr_{.15}CuO_4$ showed that at room temperature compression causes the Cu-O octahedra to rotate. At the same time our analysis of $YBa_2Cu_3O_{7-\delta}$ indicated that the Cu-O-Cu bonds begin to bend at about 10 kbar. In this case, the analysis is complicated due to focussed multiple scattering and we were unable to distinguish whether the bending occurs in the linear chains, the puckered sheets, or both. In an attempt to clarify the multiple scattering analysis, pressure-dependent measurements were made at room temperature on two samples of $YBa_2Cu_3O_x$: one with x= 6.95 containing the linear chains and the other with x=6.10 which does not contain the linear chains. Analysis is in progress.

The x-ray absorption spectrum of metallic iron was studied as a function of pressure to 9.0 gPa, together with metallic copper, which served as a pressure calibrant. This portion of our work was covered by proposal 1047M and was done at SSRL during our February run. The purpose was for comparison with an earlier uncalibrated run in which the iron by itself was taken to approximately 20 gPa. This experiment, in which the iron transforms from the bcc structure to the hcp structure at 12 gPa, is important for studying phase transition mechanisms from a local standpoint. It must still be carried to higher pressures.

Li Intercalated MnO_2

We also initiated an XAS study of the intercalation of Li into MnO_2. Li intercalated MnO_2 is used in the manufacture of light-weight, high energy density batteries. MnO_2 exists in a number of crystal structures, all characterized as "tunnel" compounds. In the intercalation process, which occurs when the electrochemical cell discharges, Li atoms are inserted reversibly into the tunnels, producing Li_xMnO_2. It is presumed that insertion of the Li causes a decrease in the valence of Mn from Mn^{4+} to Mn^{3+}. Conduction then occurs via electrons hopping from one site to another in the ionic Li_xMnO_2 which would explain the small dc electrical conductivity. From a practical viewpoint it is important to understand the conduction mechanism in detail, since this may lead to methods of increasing the conductivity, the low value of which is one of the limiting factors in battery performance.

XANES spectroscopy was used to study the valence state. The 1 eV decrease that we observe in the onset of absorption at the Mn K-edge of $Li_{3/7}MnO_2$ relative to pyrolusite (pure β-MnO_2) is consistent with a decrease in the Mn valence (Fig.3). A similar decrease is observed in

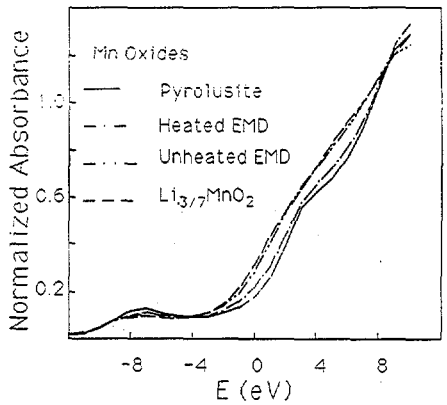

the edge features of unheated electrolytic manganese oxide (EMD or γ-MnO_2) relative to heated EMD. Unheated EMD contains the Mn^{3+} ions resulting from the presence of H^+ ions through the incorporation of water in the "tunnels", whereas heated EMD presumbaly contains predominantly Mn^{4+} ions. The interpretation of the XANES features must also include the structural changes indicated by the Mn K-edge EXAFS. The magnitude of the Fourier transform of $k\chi(k)$ (Fig. 4) shows that replacement of the protons in unheated EMD by Li^+ produces a substantial decrease in the strength of the Mn-Mn "corner" peak associated with

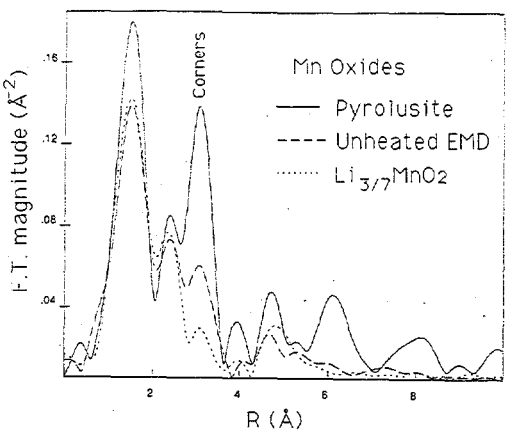

linkage of Mn oxygen octahedra via the common corner oxygen. Detailed analysis is in progress. Further experiments will involve EXAFS/XANES measurements of the *in-situ* intercalation of Li into an electrochemical cell to study changes as a function of the charge state of the battery.

SODIUM K-EDGE XAFS INVESTIGATION OF COAL ASH

Naresh Shah, Frank E. Huggins, Gerald P. Huffman, Sudipa Mitra, Anup Shah

Institute for Mining and Minerals Research, University of Kentucky, Lexington, KY 40506-0107

INTRODUCTION

The alkali elements, sodium and potassium, can be major contributors to deposition and fouling problems in coal combustion units because of the ease with which certain forms of these elements, notably NaCl and carboxyl-bound Na^+ or K^+ in coal macerals, are volatilized from coal. Deposits are formed as volatilized alkalies condense on cooler surfaces of water wall tubes and superheater elements in the form of thin, viscous alkali-rich surface films that also facilitate capture of ash particles in flue gases. Fluxing properties of these alkalies enhance sintering and the formation of stronger deposits. Deposits in turn reduce heat transfer rates and thereby the efficiency of the combustor. Condensation of alkalies on fly ash and formation of thin viscous films on fly ash particles increase the probability of particle-particle adherence on collision and fouling problems of the combustor. Increasing alkali content in coal leads to increased fouling in combustors [1]. Although U.S. coals on average contain equal quantities of sodium and potassium, selective deposition of sodium on a controlled-temperature superheater surface has been observed. In this investigation, we have used XAFS spectroscopy as a direct probe to understand the presence and formation of alkali phases in both a power production scale and a laboratory scale combustor.

EXPERIMENTAL

Sodium K-edge XAFS experiments were performed in March 1989 on beam-line III-3 (JUMBO) at SSRL. The ring was operated at 3.3 GeV and the current was highly variable at that time due to operational problems. A beryl double crystal monochromator was used for incident X-ray energy selection. The entire beamline and monochromator were kept at machine vacuum. There was a 10 mil (254 μm) thick Be window at the end of the beamline (after the monochromator). Absorption by this window caused substantial flux loss at the Na K-edge energy region, but it had to be used to avoid any contamination in the beam line as well as in the storage ring due to outgassing of samples. The sample chamber was attached to the end of the beamline and was evacuated to 10^{-6} to 10^{-7} torr by using a turbo molecular pump. To avoid repeated cycling of the vacuum chamber to atmospheric pressure for sample changes, several samples were mounted on a stainless steel strip and were moved in and out of the beam path with a linear motion feed-through attachment to the vacuum chamber. To dissipate any charge buildup on the sample due to photo-electron ejection from the sample, samples were prepared by pressing the powder into indium metal foil. These samples were mounted on the sample strip and the sample strip was grounded to the vacuum chamber to neutralize charge build up. The sample strip was positioned at 45° to both the incident beam and the detector to optimize the solid angle. Due to the unavailability of a suitable vacuum compatible solid-state x-ray detector, it was decided to measure fluorescent electron yield. A channeltron electron multiplier was used to measure the XAFS signal. In addition to the significant signal loss due to the Be window, the XAFS signal was poor due to very high background signal. Indium M edges (444-827 eV) are close to the Na K edge (1071 eV) and so the indium foil also fluoresces in Na XAFS region. Moreover, Na loading in the samples was quite low (less than 10%) and the matrices of most of the samples were made up of higher (than Na) atomic weight atoms (e.g. Al, Si, S, Cl, K, and Ca). A heavier matrix can greatly reduce the signal from lighter fluorescing element. This matrix problem was present even in the case of standard compounds, e.g. Na feldspar ($NaAlSi_3O_8$). All samples were run with 4 seconds per point acquisition time and typically 4 to 5 scans were made and averaged to improve signal to noise ratio. Although scans were made up to 400 eV above the Na K edge, the EXAFS data were too poor for any analysis.

RESULTS

Figure 1 shows the Na K-edge XANES spectra of various standard Na compounds, that could be present in coal ash and slag deposits. Figure 2 shows Na K-edge XANES for two series of samples. The Fireside and Tubeside samples were actual deposits from the Belle River Station of Detroit Edison power plant formed while burning Decker (WY) subbituminous coal. From the edge step height, it can be concluded that there is a higher sodium concentration on the tubeside than on the fireside, which is an indication of the importance of sodium in initiating the deposit. Despite the poor signal-to-noise, the XANES spectra of both deposits are consistent with formation of a sodium aluminosilicate phase. However, other minor Na phases could be hidden in the noise. A second series of samples was obtained from a laboratory-scale, self-sustained combustor run with a Beulah (ND) lignite at the University of Arizona combustion facility. The ash from Beulah coal run was collected on a series of size-separation filters. Impactor 5 (IM5) collects ash particles in the size range 2.1-3.3 μm, while impactor 8 (IM8) collects ash particles in the 0.43-0.65 μm size range. Sample IM8, which had the higher content of sodium in the ash analysis, showed a larger edge height than sample IM5, as expected. XANES of both these samples were relatively featureless and quite different from all the standards we had analyzed. Although we can not confirm formation of any specific phase at this time, we can conclude that none of the standard phases we have measured is significantly present in the samples.

CONCLUSIONS

We have successfully shown feasibility of obtaining Na K-edge XANES for coal ash. Even with poor running conditions, high degree of flux loss in the Be window, poor detection capabilities, and high background signal from the substrate, we were able to get informative data. We have been able to identify presence of a sodium aluminosilicate phase in deposits obtained from a power plant combustion facility.

ACKNOWLEDGEMENT

We are grateful to Dr. Piero Pianetta and Mike Rowen, SSRL, for their help with experimental setup. This work was supported by U.S. DOE through Physical Sciences, Inc.

REFERENCE

1 W.T. Reid, Chemistry of Coal Utilization, 2nd Supplementary Volume, Ed: M.A. Elliott, (1981) p. 1389.

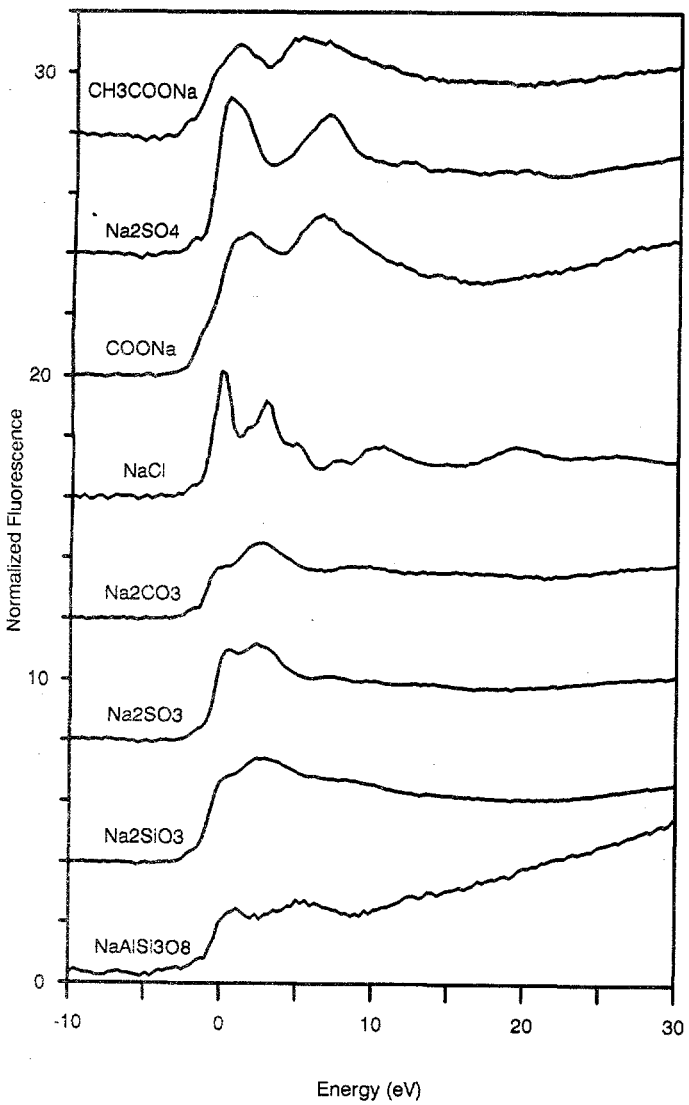

Figure 1. Na K-edge XANES of standards.

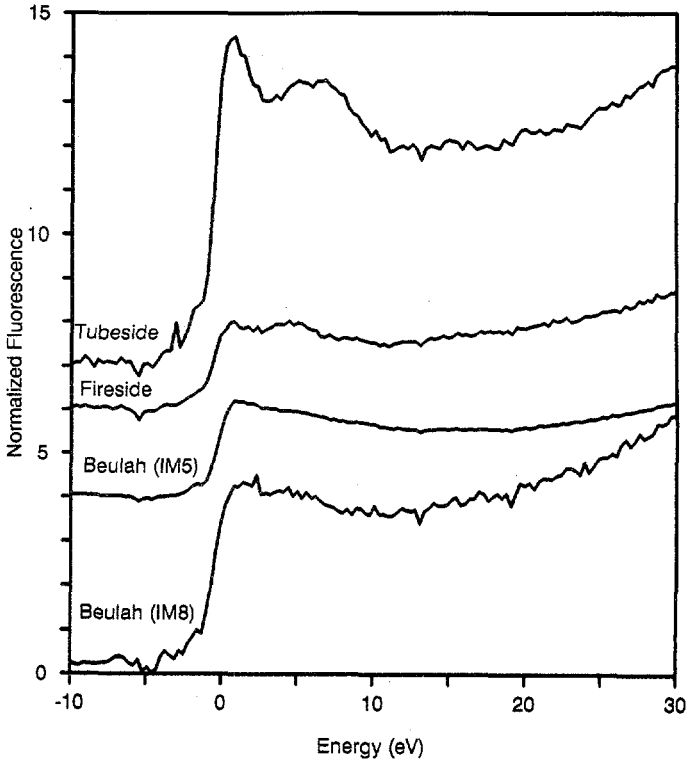

Figure 2. Na K-edge XANES of coal ashes and deposits.

AN XAFS INVESTIGATION OF CHLORINE IN U.S. COALS

F. E. Huggins[1], G. P. Huffman[1], F. W. Lytle[2] and R. B. Greegor[2]

[1]Institute for Mining and Minerals Research, University of Kentucky, Lexington, KY 40506
and [2]The Boeing Company, Seattle, WA 98124

INTRODUCTION

The chlorine contents of most U.S. coals are typically less than 0.3 wt%, except for certain coals from the Illinois basin in which the chlorine contents may be as high as 1.0 wt% [1]. Such high chlorine coals can give rise to severe corrosion problems in coal utilization. However, relatively little is known about how chlorine occurs in coals from the Illinois Basin or from other seams in the U.S. Based largely on indirect observations made mostly on British and Indian high chlorine coals, chlorine has been postulated to occur in coal as alkali or alkaline-earth chlorides (NaCl, KCl, $CaCl_2$, etc.), as organic chlorides, as hydrochlorides, and as chloride ions in the water associated with coal [2,3]. In this investigation, we have used XAFS spectroscopy as a direct probe of the chlorine environment in coal to establish how this element occurs in U.S. coals.

EXPERIMENTAL

Chlorine K-edge XAFS experiments were performed in January 1987 on beam-line VII-3 at SSRL. XAFS spectra were recorded in fluorescent geometry. The chlorine K edge in sodium chloride (NaCl) at 2826 eV and the argon K edge (from air contamination in the beam path) at 3205 eV were used as primary standards. The latter edge was present in every spectrum and served as an effective internal calibration point, but its presence limited the chlorine EXAFS region to only about 380 eV. Further details are given elsewhere [4].

RESULTS

XAFS data were collected for coals from eight different U.S. seams (chlorine contents varied from 0.04 to 0.84 wt%) and, additionally, from a number of Illinois #6 coals that had been subjected to an aqueous leaching process to remove some of the chlorine [5]. These data (Fig. 1) showed that the chlorine XANES fingerprint from the coals was relatively universal and unaltered by aqueous leaching, despite removal of over 70% of the chlorine from the coal [4]. Furthermore, this characteristic XANES spectrum was quite unlike any of the standard inorganic or organic chlorides commonly thought to be present in coal, although two of the coals did clearly contain a minor fraction (<25%) of the chlorine as NaCl [4]. The XANES of chlorine in the coal resembled those of chlorine in saturated NaCl solution, $CaCl_2.6H_2O$, and organic hydrochlorides. These three substances do have some structural and bonding features in common that are, no doubt, reflected in similar XANES spectra: (i) chlorine is present in these substances as chloride anions, (ii) the bonding is relatively weak and largely ionic in character, and (iii) the chlorine-oxygen or chlorine-nitrogen distances are long: between 3.0 and 3.3 Å. Hence, the chlorine in coals will likely be similar in structure and bonding because of the similarity of its XANES to these materials. Analysis of the EXAFS region was possible for some of the coals with higher chlorine contents and the best agreement for the phase-shift for chlorine in coal was found for a Cl-H_2O distance of 3.03 Å when modelled by the experimentally derived phase-shift for $CaCl_2.6H_2O$, in which the chlorine anion is surrounded by six water molecules at an average distance of 3.15 Å [6].

CONCLUSIONS

XAFS spectroscopy has proved extremely informative in establishing how chlorine occurs in U.S. coals. The data are consistent with chloride anions in the moisture associated with coal being the major form-of-occurrence of chlorine. This finding is in agreement with the latest work on British coals obtained by much less direct methods [2].

REFERENCES

1 H.J. Gluskoter and R.R. Ruch, Fuel 50, 65-76, (1971).
2 N.J. Hodges, W.R. Ladner and T.G. Martin, J. Inst. Energy, 56, 158-169 (1983).
3 J.N. Chakrabarti, in: Analytical Methods for Coal and Coal Products, Vol. 1, Academic Press, NY, 1978, 323-345.
4 F.E. Huggins, G.P. Huffman, F.W. Lytle and R.B. Greegor, ACS Div. Fuel Chem., Preprints, 34(2), 551-558 (1989).
5 H.L. Chen and M. Pagano, Fuel Proc. Technol., 13, 261-269, (1986).
6 R.W.G. Wyckoff, Crystal Structures, Vol. 3, J. Wiley & Sons, New York, 1963.

ACKNOWLEDGEMENTS

We are grateful to Professor Han Lin Chen of Southern Illinois University for providing us with samples of raw and leached Illinois #6 coals. This work was supported by the U.S. DOE under Contract No. DE-FG22-86 PC90520 and the Electric Power Research Institute under Contract No. RP-8803-20.

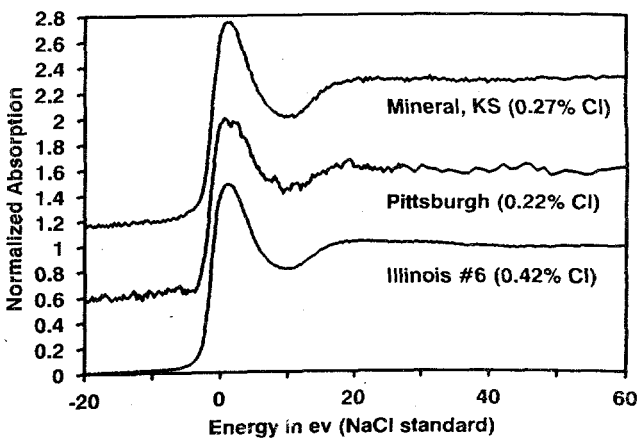

Fig. 1: Chlorine XANES spectra of three U.S. coals

Characterization of the Coordination Environment of Divalent Iron in Silicate Crystals, Glasses and Liquids as a Function of Temperature and Composition Using X-ray Absorption Spectroscopy

William E. Jackson, Glenn A. Waychunas, Gordon E. Brown, Jr., and Jean-Marie Combes
Center for Materials Research and Department of Geology
Stanford University, Stanford, CA 94305

Introduction

The main purpose of this research program is to define the structural role of Fe^{2+} in crystalline and amorphous silicates as a function of composition and temperature up to and above the temperature of fusion (T_f) in the compounds studied. Iron in its 2+ oxidation state is the most abundant transition metal in the Earth and is an important component in slags and natural silicate liquids. The local environment of Fe^{2+} in silicate crystals and liquids is not always predictable because the ion can adopt octahedrally coordinated, tetrahedrally coordinated or, in certain cases, other types of coordination geometry (e.g. square-planar, 7- or 8-coordinated) depending on a number of variables. When octahedrally coordinated, Fe^{2+} is thought to behave as a classical network modifier in silicate glasses and liquids, whereas when tetrahedrally coordinated, it may behave as a network former or a molecular complex. In general, the greater the ratio of network formers to network modifiers in a silicate liquid, the greater its bulk polymerization. The degree of tetrahedral polymerization in such a liquid affects certain of its bulk physical properties, such as viscosity and density, and can profoundly affect crystallization. For example, the configurational entropy contribution to the entropy of fusion tends to decrease with increasing polymerization of the liquid for common silicates. It is expected that the high configurational entropy associated with Fe_2SiO_4 liquid, which is primarily responsible for the difficulty in forming glass of this composition, is a consequence of structural changes in long range order (> ~ 4 A) and perhaps even short range order (4 A <) at the melting point (see, for example, Jeanloz, 1985).

There exists, however, little direct structural information on the coordination environment of Fe^{2+} in silicate liquids. This information has previously been difficult to obtain because of the redox potential of Fe^{2+} at high temperatures and the typically high T_f associated with iron silicates (e.g. Fe_2SiO_4, T_f = 1478 K). Indeed, most past studies of Fe^{2+} in silicate 'liquids' have actually been performed on the quenched glasses which do not necessarily have the same average structure as the corresponding liquid. The need to examine the structure of liquids *in situ* is necessary due to the possibility of structural rearrangements within the liquid during quench. The low glass transition temperatures associated with extremely depolymerized liquids suggest a major degree of structural rearrangement in the liquid during glass formation and, hence, the greatest difference between the glass and liquid structure.

Our past research (e.g. Waychunas et al., 1987, 1988) has focussed on defining the coordination environment of Fe^{2+} in polymerized 'feldspar' -composition glasses and corresponding liquids using Mossbauer, EXAFS and XANES spectroscopy. Fe^{2+} was found to occupy network-forming, tetrahedral sites in glasses and liquids of $M_2FeSi_3O_8$ compositions (M= Li, Na, K, Rb). Few spectroscopic methods are capable of yielding direct information on the structural environment of Fe^{2+} in silicate liquids at high temperature. X-ray absorption spectroscopy using a high intensity synchrotron source is one of the few methods that can help overcome problems such as the need to examine liquids in ceramic containers inside high temperature furnaces, and that can also provide estimates of bond lengths, coordination numbers, and information on oxidation state. This application of EXAFS spectroscopy is not without significant problems, however, including the effect of thermal motion on EXAFS amplitudes and resolution, particularly at $k > 10$ A^{-1}, and the resultant loss of information on next-nearest neighbors around Fe^{2+}.

We are currently studying the local coordination environment of Fe^{2+} as a function of temperature and composition (polymerization) in a range of Fe^{2+}-bearing systems, including glasses and liquids using x-ray absorption spectroscopy and a special furnace assembly. The high-temperature samples being studied include the compositions Fe_2SiO_4, $CaFeSiO_4$, $CaFeSi_2O_6$, $Ca_{0.8}Fe_{1.2}Si_2O_6$, and compositions along the $Na_2FeSi_3O_8$ - $CaFeSi_3O_8$ join. Room temperature Fe K-EXAFS and K-XANES studies have been made on a unique glass of Fe_2SiO_4 composition, on glasses from the $Na_2FeSi_3O_8$ - $CaFeSi_3O_8$ join, and on selected crystalline silicates. We have also carried out XAS studies of well-characterized model compounds ($FeCO_3$, $Ca_3Fe_2Si_3O_{12}$, and $CaFeSi_2O_6$) in order to extract Fe-O phase and amplitude information.

Experimental

No data in this program have been obtained at SSRL since December 1987. In September 1989, room temperature and elevated temperature XAS studies were performed at the National Synchrotron Light Source on BL X19A (unfocussed, 2 X 20 mm photon spot size) and X23B (focussed, 1 X 1 mm spot size) using Si (111) monochromator crystals. Ring conditions were 2.5 GeV and 80 - 180mA. The high temperature data were collected in the fluorescence mode with a Lytle-type detector and a water-cooled, controlled-atmosphere furnace capable of sustaining temperatures up to 1750 K. The furnace assemblage consisted of a water-cooled Al jacket, Mo sample holder, Mo heating coils, alumina insulation, inert atmosphere (N_2), and an S-type thermocouple. Kapton film covered the incident and fluorescence photon ports. The oxygen partial pressure was controlled by the Mo and a N_2 atmosphere. Mossbauer spectroscopic analyses on the quenched samples indicate no more Fe^{3+} (plus an equal amount of Fe^0) than that produced by the slight incongruent melting of the samples (about 5% Fe^{3+}). The samples were contained in BeO crucibles aligned to expose the melt directly to the incident beam and fluorescence detector in order to eliminate any signal from the crucible-melt interface. The BeO crucibles proved to be refractory and inert even when in contact with the iron-bearing silicate liquids for over 3 hours at T > 1650 K. An average of 3-5 scans were collected for each high-temperature crystalline compound and melt.

Results and Discussion

Using Fe-O phase and amplitude information taken from the room temperature model compounds listed above, the structural environment of Fe^{2+} in the glasses was successfully modeled. The Fe K-EXAFS and K-XANES data are consistent with tetrahedral Fe^{2+} in all feldspar-composition glasses. These results confirm our earlier conclusions that Fe^{2+}, like Fe^{3+} (Brown et al., 1978), can be charge-balanced in tetrahedral coordination in fully polymerized silicate glasses.

Analysis of the Fe_2SiO_4 glass yielded the unexpected result of tetrahedral Fe^{2+} (Figure 1), which when taken in context of the high configurational entropy associated with Fe_2SiO_4 at T_f, is not too surprising. Tetrahedral Fe (II) and Si (IV) require an average oxygen coordination of *three*, as compared to an oxygen coordination of four in crystalline Fe_2SiO_4. This type of polymerization in the Fe_2SiO_4 liquid, may be related to Shiraishi's (1978) report of an anomalous maximum in viscosity at the Fe_2SiO_4 composition in melts along the FeO-SiO_2 join.

Analysis of the EXAFS spectra from high-temperature crystalline silicates and liquids is currently in progress and requires an understanding of the temperature effect on the Fe-O bond. High-temperature XAS studies and/or studies of disordered systems require knowledge of the asymmetric distribution function for the Fe-O pair as well as any anharmonic vibration effects (e.g. Eisenberger and Brown, 1979; DeCrescenzi, et al. 1981). This asymmetric distribution function and anharmonic vibration behavior are generally

accommodated in the modeling of the χ (k) function which must include the corrections to both phase and amplitude. Such modeling involves non-Gaussian Debye-Waller formulations and explicit G(r) functions for the Fe-O pair distribution, which correctly interprets the apparent bond length contraction and amplitude reduction seen in the EXAFS signal as a function of increasing temperature. To accurately model the asymmetric distribution function and anharmonic effects expected for the iron-bearing silicate liquids, we collected EXAFS data from Fe^{2+} and Fe^{3+} in the crystalline silicate model compounds as a function of temperature. To begin to correct for the anharmonic Fe-O bond vibrations, we are currently modeling the high-temperature Fe K-EXAFS collected from Fe^{3+} which resides in a centrosymmetric octahedral site in $Ca_3Fe_2Si_3O_{12}$ (Figure 2). Once the anharmonic contribution to the Fe-O bond vibration as a function of temperature has been approximated, corrections for a non-Gaussian distribution of distances can be extracted from the Fe K-EXAFS collected from crystalline Fe_2SiO_4. Crystalline Fe_2SiO_4 contains Fe^{2+} in two distorted octahedral sites. The EXAFS partial RDFs for Fe_2SiO_4 are seen in Figure 3. As expected, the EXAFS results give an apparent bond length contraction of approximately 0.07 A over the temperature change of 780 K (90 K to 870 K). To correct for this contraction, these EXAFS results will be modeled in light of the high-temperature x-ray structure refinements of crystalline Fe_2SiO_4 which suggest an Fe-O expansion of 0.02 - 0.03 A over a comparable temperature range (Smyth, 1975).

Despite the high-temperature corrections, the study becomes a bit problematic if we suppose Fe^{2+} changes its coordination environment from octahedral to tetrahedral in the liquid as the study of glassy Fe_2SiO_4 suggests. Such a coordination change will serve to change the distribution of oxygen distances, perhaps to a more Gaussian arrangement, as well as influence the the amplitude of the Fe-O bond vibration and, hence, the anharmonic contribution. Consequently, it is necessary to consider the phase and amplitude information for Fe^{2+} in tetrahedral coordination in high temperature solids as well. The phases studied by EXAFS as a function of temperature include $FeAl_2O_4$ (hercynite spinel), and the $M_2FeSi_3O_8$ glasses.

Some of the Fe K-EXAFS data currently being modeled, as described, are illustrated in Figure 4 which plots the partial RDFs for Fe_2SiO_4 as a function of temperature and physical state. The χ (k) functions are shown for crystalline Fe_2SiO_4 (298 K), liquid Fe_2SiO_4 (1520 K), and glassy Fe_2SiO_4 (298 K). It is apparent from the Fourier transform data alone that the EXAFS signal from the glass is markedly different from that of the liquid. In addition to the modeling of Fe_2SiO_4 liquid, we are modeling the effect on the Fe^{2+} coordination environment of a liquid with a pyroxene composition whose silica content is intermediate between that of olivine and feldspar. We are also examining the effect of substituting Ca^{2+} for Fe^{2+} in silicate liquids with the idea that the strong network modifying effect of Ca^{2+} (i.e. almost always occupies an octahedral or larger coordination environment) will cause Fe^{2+} to revert to octahedral coordination to satisfy the charge on nearby oxygens.

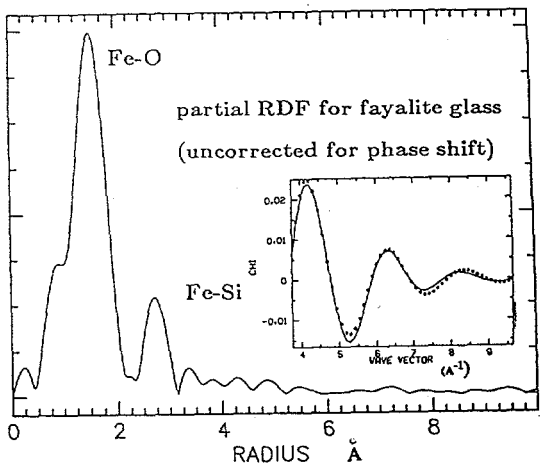

Figure 1. Partial radial distribution function for Fe^{2+} in Fe_2SiO_4 glass (uncorrected for phase shift). Inset: Using Fe-O phase and amplitude information extracted from Fe K-EXAFS data of $CaFeSi_2O_6$ (^{VI}Fe-O = 2.13 A) and $FeCO_3$ (^{VI}Fe-O = 2.14 A), the best least-squares fit to Fe K-EXAFS data collected from Fe_2SiO_4 glass yield: 3.36 (± 0.5) oxygens coordinating Fe^{2+} at an average distance of 2.01 (±0.02) A with a Debye-Waller parameter equal to 0.0127 A².

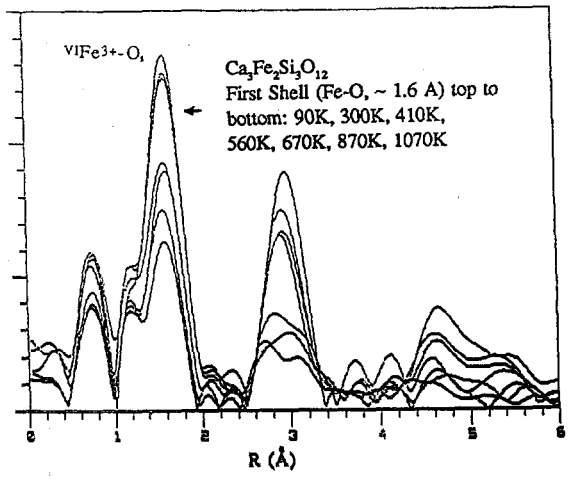

Figure 2. Partial RDFs for Fe^{3+} in the regular octahedral site (i.e. single Fe^{3+}-O distance) of crystalline $Ca_3Fe_2Si_3O_{12}$ as a function of temperature (uncorrected for phase shift). There is little shift in the Fe^{3+}-O distance over the whole temperature range. This is consistent within standard errors of the result from high-temperature XRD (Rakai, 1975).

Conclusions

Our Fe K-EXAFS studies of Fe (II) in feldspar and olivine-composition glasses indicate Fe (II) is tetrahedrally coordinated in both systems and probably serves as a network former in linking the SiO_4 tetrahedra. These results agree with our earlier studies, and may aid in the interpretation of the thermodynamic and viscosity data for silicate liquids.

By incorporating phase and amplitude information taken from model compounds as a function of temperature, we are beginning to model the effects of high-temperature on the Fe coordination environment. This information will help us constrain the structural differences between glasses and their corresponding melts as well as the structural rearrangements at T_f for important rock and magma forming silicates.

Acknowledgements

This work was supported by NSF grants EAR-8513488 and EAR-8917437. We acknowledge the general support of the SSRL and NSLS staff. In particular we thank Glenn Kerr (SSRL), and NSLS staff members Johnny Kirkland, (X23B), Rich Neiser (X23B), Steve Cramer (X19A), Charlie Yang (X19A) and Fulong Loo (X19A) for their assistance.

References

Brown, G.E., Jr., Keefer, K.D., Fenn, P.M. (1978) EXAFS Study of Iron-Bearing Silicate Glasses: Iron Coordination Environment and Oxidation State, Geol. Soc. Am. Abstr. With Programs 10: 373.

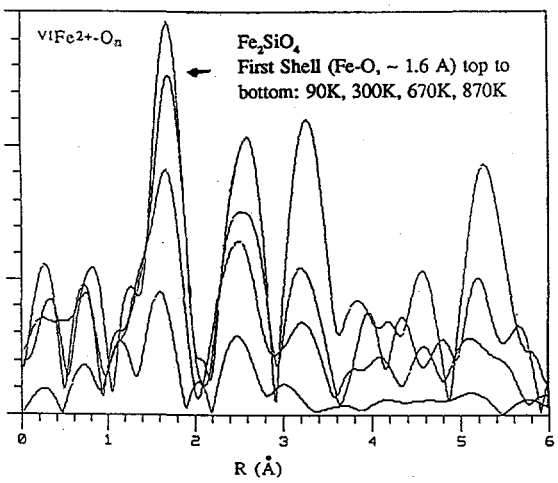

Figure 3. Partial RDFs for Fe^{2+} in the two distorted sites (i.e. highly non-Gaussian distribution of oxygen distances) of crystalline Fe_2SiO_4 as a function of temperature (uncorrected for phase shift). The apparent bond length contraction of 0.07 A over the temperature change is being modeled in in light of an actual 0.02 A expansion for this temperature change as determined from XRD (Smyth, 1975).

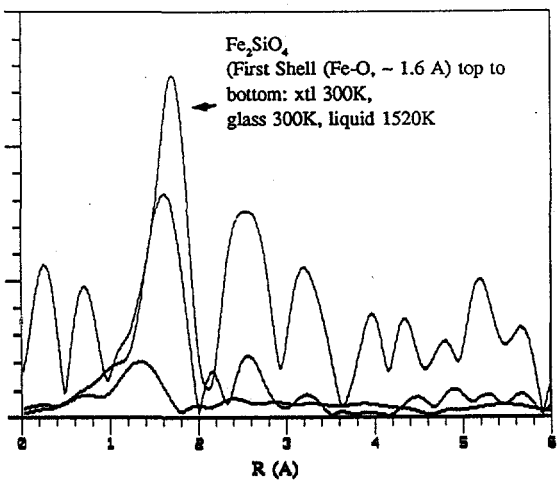

Figure 4. Partial RDFs for Fe_2SiO_4 (top to bottom): crystalline Fe_2SiO_4 (298 K), glassy Fe_2SiO_4 (298 K) and liquid Fe_2SiO_4 (1520 K) (uncorrected for phase shift). Note both decrease in amplitude and bond distance from the crystal to the liquid.

De Crescenzi, M., Balzarotti, A., Comin, F., Incoccia, L., Mobilio, S., Motta, N. (1981) EXAFS Measurements on Fe-B Metallic Glasses: Asymmetry of the Radial Distribution Function, Solid State Communications, Vol. 37, 921-923.

Eisenberger, P., and Brown, G.S. (1979) The Study of Disordered Systems by EXAFS: Limitations, Solid State Communications, Vol. 29, 481-484.

Jeanloz, R. (1985) Thermodynamics of Phase Transitions, In *Reviews in Mineralogy Vol. 14: Microscopic to Macroscopic*, Mineralogical Society of America 1985, 428p.

Rakai, R.J. (1975) Crystal Structure of Spessartine and Andradite at Elevated Temperatures, M.Sc thesis, Univ. British Columbia.

Shiraishi, Y., Ikeda, K., Tamura, A., and Saito, T. (1978) On the Viscosity and Density of the Molten FeO-SiO_2 System, Trans JIM, Vol. 19, 264-274.

Smyth, J.R. (1975) High Temperature Crystal Chemistry of Fayalite, American Mineralogist, Vol. 60, 1092-1097.

Waychunas, G.A., Brown, G.E., Jr., Jackson, W.E., and Ponader, C.W. (1988) Evidence from X-ray Absorption for Network-Forming Fe^{2+} in molten alkali silicates, Nature 332, 251-253.

Waychunas, G.A., Brown, G.E., Jr., Ponader, C.W., and Jackson, W.E. (1987) High-Temperature X-ray Absorption Study of Iron Sites in Crystalline, Glassy, and Molten Silicates and Oxides, SSRL Report 87/01, 139-141.

X-RAY ABSORPTION SPECTROSCOPY OF ION SORPTION COMPLEXES AT MINERAL/WATER INTERFACES

Proposal No. 999Mp

Peggy A. O'Day, Catherine J. Chisholm-Brause,
Ning Xu, Jean-Marie Combes, Gordon E. Brown, Jr., George A. Parks

School of Earth Sciences, Stanford University, Stanford, CA 94305

INTRODUCTION

The sorption of ions from aqueous solutions onto mineral surfaces controls the transport and partitioning of aqueous species in a wide variety of systems such as contaminent transport, nuclear waste disposal, ore deposition, electrochemical processes, corrosion control, solar energy conversion, and enhanced oil recovery. Quantitative descriptions of molecular level reactions are required to accurately predict the interaction of ions with mineral surfaces in macroscopic models. The quantitative structural information provided by synchrotron-based x-ray absorption spectroscopy (XAS) permits characterization of *in situ* sorption complexes at mineral/water interfaces at very low surface concentrations representative of natural conditions.

Our previous investigations focused on two aqueous ion/oxide systems: (1) Se oxyanion sorption on goethite (α-FeOOH)[1] (2) Pb(II) sorption on γ-Al_2O_3[2,3] and goethite[4]. In both of these systems, we were able to distinguish between inner sphere and outer sphere sorption complexes with XAS. In addition, XANES and EXAFS analyses of Pb(II) complexes on goethite and γ-Al_2O_3 indicate the presence of Pb atoms in the second coordination shell, suggesting that aqueous Pb complexes may form clusters on the mineral surface.

In order to investigate how mineral surfaces control the size and structure of sorption complexes, we have begun a detailed study of the sorption of Co(II) complexes onto a variety of natural and synthetic minerals. We previously reported results for cobalt sorption on γ-Al_2O_3[5,6]. In the past year, we have collected XAS data on cobalt sorbed to kaolinite, rutile, silica, and calcite. The samples studied by XAS cover a wide range of surface sorption densities in order to detect changes in the atomic structure of Co(II) complexes as a function of surface coverage. We have collected data on sorption samples estimated to have from about 10 to greater than 95 percent of a monolayer of oxygen-ligated surface cobalt atoms. Interpretation of the EXAFS data allows us to distinguish between surface adsorption, surface precipitation, and diffusion of metal ions into the solid. Our initial results show that Co(II) uptake by minerals occurs by surface adsorption and formation of inner sphere complexes[5,6,7]. Comparison of complex formation on different minerals suggests that surface clusters may be a common phenomenon of metal ion sorption, but mineral surfaces themselves strongly control the size of the cluster which forms[8,9].

EXPERIMENTAL

XAS data were collected at SSRL during the dedicated run in February and March, 1989, on beam lines VII-3 (wiggler field = 18kG) and II-1 (bending magnet line). Through SSRL, we obtained additional beamtime at the National Synchrotron Light Source (NSLS) in July, 1989, on beam line X-19A. On beam line VII-3, all cobalt spectra collected were not usable due to interference from unshielded high energy x-rays and spectra noise from shutter opening and closing on an adjacent beamline. Data collection on this line was limited to Kr *K*-, Se *K*-, and Np L_{III} - absorption edges. Absorption spectra were collected on cobalt sorption samples and iron model compounds on beam line II-1. However, the significantly lower intensity of the bending magnet beam in comparison with a wiggler beam resulted in a very low signal-to-noise ratio and poorly resolved EXAFS spectra. Usable data from this line were limited to a few high concentration sorption samples and model compounds. Spectra for cobalt sorbed to kaolinite, silica, and calcite were collected on NSLS X19-A. Although data quaility for lower concentration samples was better on this line than on II-1, it was still far inferior to high resolution data obtainable on SSRL wiggler lines (Figure 1). On all beamlines, data for sorption samples and

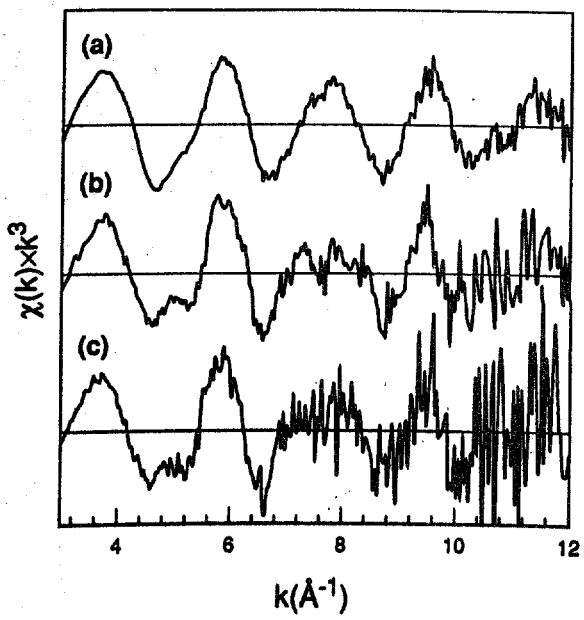

Figure 1. EXAFS spectra for Co(II) sorbed to kaolinite at a sorption density of about 1.2 μmoles/m^2 collected on three different beamlines. (a) SSRL wiggler line IV-1, (b) NSLS X-19A, (c) SSRL bending magnet line II-1. Sample (a) has a higher water content than (b) or (c) which accounts for the damping of the "beat" on the second oscillation at about k=5.

glasses were collected in fluorescence mode using a Lytle-type detector with the sample oriented at 45° to the incoming x-ray beam. Spectra for solid model compounds were collected in transmission mode with the sample oriented perpendicular to the x-ray beam.

Cobalt sorption samples were prepared by equilibration of the aqueous metal ion in nitrate solution with a solid mineral in amounts from 50-120g mineral/1000g aqueous solution, depending on the surface area of the mineral. The pH of the suspension was adjusted such that approximately 95% of Co(II) was removed from solution by uptake on the solid. Initial Co(II) solution concentrations ranged from 0.6 to 18 mM in order to obtain variable amounts of surface sorption density at 95% ion uptake from solution. The resulting sorption densities varied from 1.2 to 39 μmoles/m^2. The samples were centrifuged and the supernatent solution removed, leaving the mineral solid as a wet paste. The pastes were loaded and sealed in teflon sample cells with mylar windows. Samples were checked carefully before and after data collection to insure no drying of the pastes.

The Np sorption sample was prepared in a similar fashion using 1g goethite/1000g aqueous solution and an initial Np solution concentration of 5 mM. Adjustment of pH to 7.1 resulted in about 95% uptake from solution corresponding to a sorption density of 10^{-5} moles Np/m^2 goethite.

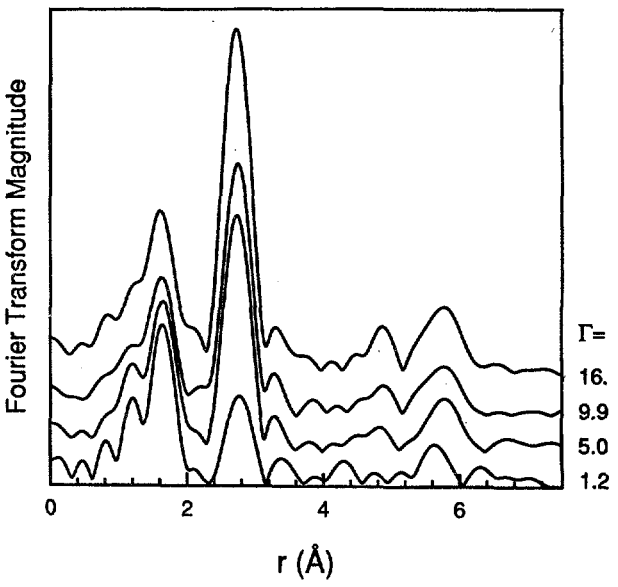

Figure 2. Radial structure functions for Co(II) sorbed to kaolinite at four different surface sorption densities (Γ) in μmoles/m^2. Note the reduction in the amplitude of the second peak as a function of decreasing surface coverage indicating fewer cobalt nearest neighbor atoms in the second coordination shell.

COBALT SORPTION ON MINERAL SURFACES

Co/Kaolinite

Four sorption samples representing surface adsorption densities of 16.0, 9.9, 5.0, and 1.2 μmoles/m^2 of Co(II) sorbed to kaolinite were studied by XAS. The kaolinite used was a chemically pure, moderately well-crystallized sample from Dry Branch, Georgia[10]. Analyses of the EXAFS spectra indicate that Co(II) is in octahedral coordination with oxygen, consistent with results from wet chemical analyses[11]. Fourier transforms of the EXAFS spectra give radial structure functions (rsf) (Figure 2) which show a progressive decrease in the amplitude of the second shell peak as a function of surface coverage. Best fits of the back-transforms of these peaks using empirical parameters from $Co(OH)_2$ indicate cobalt atoms in the second coordination shell at 3.11 to 3.13 Å. The number of cobalt atoms progressively decreases from about six to two as the surface coverage decreases. In addition, the fit to the experimental data is generally improved with inclusion of either Al or Si, representing an atom from the kaolinite surface, in the EXAFS model. Use of theoretical parameters for Al or Si results in about 0.5 to 1 atom at 3.19 to 3.22 Å. A peak in the rsf at r = 5 to 6 (Figure 2) arises from a colinear arrangement of the central, second, and fourth coordination shell cobalt atoms as in $Co(OH)_2$[8,9]. Analyses of this peak (with empirical parameters from $Co(OH)_2$) indicate one to three fourth shell cobalt atoms at a distance of 6.21 to 6.23 Å from a central absorber, in contrast to six cobalt atoms at 6.35 Å in $Co(OH)_2$.

The results from XAS analyses suggest that sorption behavior of Co(II) on kaolinite is similar to that of cobalt on γ–Al_2O_3[7,8]. Bond distances for Co-O and Co-Co are similar in both systems; however, coordination numbers for second and fourth shell neighbor cobalt atoms are slightly lower (≃ 1 to 2 fewer atoms) for Co/kaolinite at the same surface sorption density. The presence of Al or Si atoms in the second coordination shell points to the formation of inner sphere complexes as in the Co/γ–Al_2O_3 system. Comparison of second and fourth shell distances and coordination numbers with those of $Co(OH)_2$ show that atomic distances are shorter and coordination numbers are lower for multinuclear sorption complexes on kaolinite, suggesting the lack of a well-ordered surface precipitate at coverages approaching a monolayer of cobalt atoms.

Co/Rutile

EXAFS analysis of Co(II) sorbed to rutile (TiO_2) at a surface sorption density of 1.3 μmoles/m^2 suggests formation of cobalt inner sphere complexes as in the γ–Al_2O_3 and kaolinite systems. However, best fits of the fourier back-transform of the second coordination shell (using parameters from $Co(OH)_2$) results in fewer second shell cobalt atoms (CN ≃ 1) and longer Co-Co interatomic distances (3.36 Å) than for cobalt sorbed to γ–Al_2O_3 and kaolinite. These results suggest that monomeric species or small clusters of cobalt atoms form on the rutile surface and they are structurally different from larger multinuclear complexes which form on γ–Al_2O_3 and kaolinite[5,8,9].

Co/Silica

Co(II) sorbed to silica (SiO_2) was examined by XAS at a surface sorption density of 9.9 μmoles/m^2. The silica used was ground quartz (MIN-U-SIL) with a surface area of approximately 0.2 m^2/g. Second shell cobalt coordination numbers from preliminary EXAFS analysis suggests that cobalt forms slightly smaller surface complexes on silica than on kaolinite or γ–Al_2O_3 at the same surface coverage, although second shell Co-Co distances are similar (3.11 Å). The absence of a fourth shell cobalt peak at high r indicates the lack of large multinuclear complexes containing colinear, equidistant cobalt atoms.

Co/Calcite

XAS data was collected on Co(II) sorbed to calcite at a sorption density of 39 μmoles/m^2. The EXAFS spectrum of the sorption sample shows a distinctive "beat" pattern which differs from that of hydrated $CoCO_3$ (solid). Preliminary analysis suggest that cobalt sorbed to the surface is not diffusing into solid calcite in significant amounts as proposed by previous workers for Cd^{2+} sorption on calcite surfaces[12].

NEPTUNIUM SORPTION ON GOETHITE

XAS data for Np sorbed to goethite was compared to absorption spectra for solid NpO_2 and an aqueous Np solution. XANES and EXAFS analyses suggest that Np is present on the goethite surface as a monomeric species in a bipyramidal oxygen coordination environment similar to that of aqueous NpO_2^+. Although it could not be determined whether the sorption complex is inner sphere or outer sphere, Np is clearly not forming a surface precipitate on goethite.

ACKNOWLEDGEMENTS

This research was supported in part by NSF grants EAR-8513488 and EAR-8805540. Karen Gruebel, George Redden, and Jim Leckie prepared Se sorption samples and assisted in data collection. We gratefully acknowledge the experimental assistance of Britt Hedman. We would especially like to thank the SSRL staff, in particular Glenn Kerr, C. Troxel, Jr., and Hal Tompkins, for special assistance during difficult times.

REFERENCES

(1) Hayes K.F., A.L. Roe, G.E. Brown, Jr., K.O. Hodgson, J.O. Leckie and G.A. Parks (1987) In situ x-ray absorption study of surface complexes at oxide/water interfaces: Selenium oxyanions on α–FeOOH, Science **238** 783-786.

(2) Chisholm-Brause, C.J., K.F. Hayes, A.L. Roe, G.E. Brown, Jr., G.A. Parks and J.O. Leckie (1990) Spectroscopic investigation of Pb(II) complexes at the γ–Al_2O_3/water interface, Geochimica et Cosmochimica Acta, in press.

(3) Chisholm-Brause, C.J., A.L. Roe, K.F. Hayes, G.E. Brown, Jr., G.A. Parks and J.O. Leckie (1989) XANES and EXAFS study of aqueous Pb(II) adsorbed on oxide surfaces, Physica B **158** 674-675.

(4) Roe, A.L., K.F. Hayes, C.J. Chisholm-Brause, G.E. Brown, Jr., G.A. Parks, K.O. Hodgson and J.O. Leckie (1990) In situ x-ray absorption study of lead surface complexes at the goethite/water interface, Langmuir, in press.

(5) Chisholm-Brause, C.J., G.E. Brown, Jr. and G.A. Parks (1988) EXAFS study of Co(II) complexes at oxide/water interfaces, (Abstract), EOS **69** 1482.

(6) Chisholm-Brause, C.J., G.E. Brown, Jr. and G.A. Parks (1989) EXAFS investigation of aqueous Co(II) adsorbed on oxide surfaces in-situ, Physica B **158** 646-648.

(7) O'Day, P.A., C.J. Chisholm-Brause, G.E. Brown, Jr. and G.A. Parks (1988) Characterization of Co(II) complexes at the kaolinite/water interface by x-ray absorption spectroscopy, (Abstract), EOS **69** 1482.

(8) O'Day, P.A., C.J. Chisholm-Brause, G.E. Brown, Jr. and G.A. Parks (1989) Synchrotron-based XAS study of Co(II) sorption complexes at mineral/water interfaces: Effect of mineral surfaces, 28th International Geological Congress Abstracts **2** 534.

(9) Brown, G.E., Jr., G.A. Parks and C.J. Chisholm-Brause (1989) In-situ x-ray absorption spectroscopic studies of ions at oxide-water interfaces, Chimia **43** 248-256.

(10) May, H.M., D.G. Kinniburgh, P.A. Helmke and M.L. Jackson (1986) Aqueous dissolution, solubilities and thermodynamic stabilities of common aluminosilicate clay minerals: Kaolinite and smectites, Geochimica Cosmochimica Acta **50** 1667-1677.

(11) Baes, C.F., Jr. and R.E. Mesmer (1976) *The Hydrolysis of Cations*, New York, Wiley, 489 p.

(12) Davis, J.A., C.C. Fuller and A.D. Cook (1987) A model for trace metal sorption processes at the calcite surface: Adsorption of Cd^{2+} and subsequent solid solution formation, Geochimica Cosmochimica Acta **51** 1477-1490.

W. Parrish,[1] C. Erickson,[1] N. Masciocchi,[2] H. Toraya,[3] and B. Gilles[4]

[1]IBM Research Division, Almaden Research Center, San Jose, California 95120-6099
[2]Istituto Chimica Strutturistica Inorganica, University Milano, I-20133 Milano, Italy
[3]Ceramic Eng. Res. Lab., Nagoya Inst. Technology, Asahigaoka, Tajimi 507, Japan
[4]C.E.N.G., 85X, 38041 Grenoble Cedex, France

Introduction

The reconstructed Beam Line II and the new white beam hutch were dedicated and began operation in February 1989. The hutch is greatly improved with much more room allowing installation of larger instrumentation, more efficient use and better alignment procedures with the adjustable table height. The adjacent beam pipe was moved farther away permitting the use of specimen chambers that were not possible previously.

Powder Diffraction

Powder data were collected for a number of crystal structure refinements. The first three listed below were done with Pearson VII profile fitting, a modified Rietveld method[6] and $\lambda = 1.535$Å.

$Na_2Al_2Ti_6O_{16}$. Space group C2/m, monoclinic, a = 12.1239(3), b = 3.7749(1), c = 6.4180(2)Å, $\beta = 107.59°$, R(Bragg) = 6.4%, $R_p = 3.4\%$, $R_{wp} = 4.3\%$. Partial ordering of Al^{3+} and Ti^{4+} in the two crystallographically non-identical octahedral sites.[7]

CuO. Space group C2/c, monoclinic, a = 4.6837(1), b = 3.4238(1), c = 5.1297(2)Å, $\beta = 99.4°$, y(0) = 0.4191(6), R(Bragg) = 3%, $R_p = 7.8\%$, $R_{wp} = 9.8\%$. The Cu valence was +1.9 rather than +2 probably due to the (small) contribution of the special oxygen in the Cu-O elongated octahedron to the valence charge.

$Nd_{1.85}Ce_{0.15}CuO_4$. Space group I4/mmm, tetragonal, a = 3.94698(4), c = 12.0795(1)Å, $R_p = 2.5\%$, $R_{wp} = 3.3\%$. The valence state of the Cu ion was +1.80 confirming its mixed valence character. A full time-of-flight neutron diffraction analysis was published during the preparation of our paper.[2]

Al_2O_3. Two routine runs were made for the International Center for Powder Diffraction round-robin to compare results from various laboratories using the same specimen.[1] One run was done in 1.7 hours and the other in 0.4 hours for the range 20°-80° using 1.535Å radiation. Both had very high figures-of-merit with F_N above 600 and M_N 1000, showing the high quality of the parallel beam method with long Soller slit optics.

$MnCrInS_4$. Space group Fd3m (spinel), cubic, a = 10.4297(5)Å, $\lambda = 0.748$Å, R(Bragg) = 1.5%, $R_w = 1.2\%$. The data were obtained in a previous run and analyzed by the two-step method.[8] The refined cation distribution was

$$(Mn_{.75}In_{.25})(Mn_{.12}In_{.38}Cr_{.5})_2S_4 .$$

Comparisons of the parallel beam and conventional x-ray tube focusing methods were published.[3,4]

Figure 1 is a synchrotron radiation powder pattern of the polymer poly-(p-hydrobenzoic acid) PHBA at room temperature.[9] This is an example of the high resolution, peak-to-background and symmetrical peak shapes that can be obtained with the method. They are used to supplement conventional data for indexing, lattice parameter determination and structure refinements. Although it is not possible to do a complete research program using the method because of the limited SSRL time available at present, selected patterns provide an important aid in interpreting conventional laboratory patterns.

Grazing Incidence Diffraction

New instrumentation for grazing incidence diffraction studies of thin films, multi-layer films and substrates was developed using a rotating anode X-ray tube.[5] It consists of two channel monochromator (Ge 220 for X-ray tube and Si 111 for synchrotron), one placed before and the other after the specimen. It was installed in the new hutch to test the advantages of the synchrotron parallel beam. Unfortunately excessive orbital shifts and unstable beam made it very difficult to align and keep it aligned long enough to record a pattern. It will be tried again when better beam conditions are available.

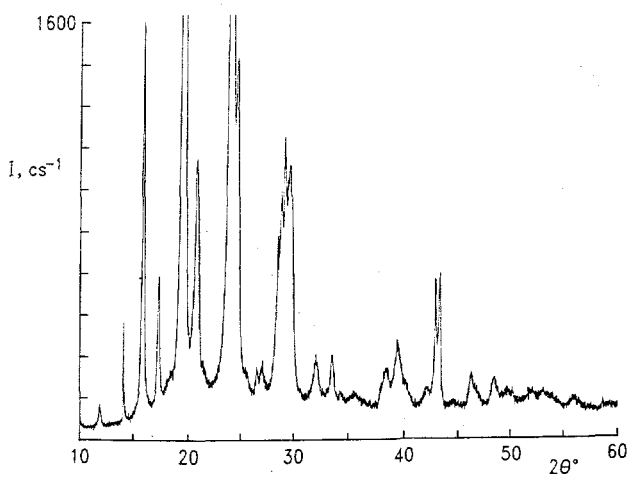

Figure 1

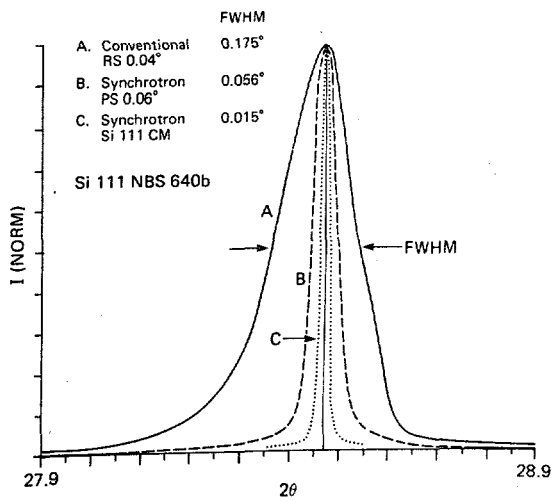

Figure 2

High Resolution

Figure 2 is an example of the very high resolution that can be obtained with the two channel monochromator arrangement with a powder sample. It shows the 111 reflection of silicon obtained with three methods: curve A with conventional X-ray tube focusing showing the beginning of separation of $CuK\alpha_2$ from $K\alpha_1$; curve B with our standard long Soller slit collimator; curve C with the new two channel monochromator method. The curves were normalized and clearly show the large reduction in width (FWHM). It should be noted, however, that the intensity is greatly reduced and recording time increased because 0.001° steps had to be used.

References

1. Huang, T. C., Parrish, W., Masaocchi, N. and Wang, P. M. (1990), *Adv. in X-Ray Anal.* **33**, in press.
2. Izumi, F., Matsui, Y., Takagi, H., Uchida, S., Tokura, Y. and Asano, H. (1989), *Physica C* **158**, 433-439.
3. Parrish, W. (1990), Int. Tables for Crystallography, Vol. C, Section 2.3.1, in press.
4. Parrish, W. and Hart, M. (1989), *Adv. in X-Ray Anal.* **32**, 481-488.
5. Parrish, W., Gilles, B., Hart, M. and Erickson, C. (1990), *Am. Cryst. Assoc.*, April 8, 1990.
6. Toraya, H. and Marumo, F. (1980), *Report Res. Lab. Eng. Mat., Tokyo Inst. Tech.* **5**, 55-64.
7. Toraya, H., Masciocchi, N. and Parrish, W. (1990), submitted for publication.
8. Will, G., Masciocchi, N., Parrish, W. and Lutz, H. D. (1990), *Zeit. f. Krist.*, in press.
9. Yoon, D., Masciocchi, N., Depero, L., Viney, C. and Parrish, W. (1990), *Macromolecules*, in press.

EXAFS Spectroscopy of Electrochemically Generated Species: Copper (BCP-S)$_2$ and Prussian Blue

Richard C. Elder and William R. Heineman
Department of Chemistry, University of Cincinnati
Cincinnati, OH 45221-0172

Copper(bcp-s)$_2$:

The combination of X-ray absorption spectroscopy with an electrochemical potential step technique allows oxidation state control while determiing the coordination chemistry of various transition metals (1). In some of our experiments, we probe the coordination environment of metal complexes contained within polymeric films, to understand the role of the polymer in the electrochemical process. Recently, the use of electrodes modified with semi-rigid polymer films for "solid-state" voltammetry has attracted considerable attention (2). Such electrochemical cells enable gas phase detection of electroactive species (3). The water soluble polymer poly(dimethyldiallylammonium chloride) or p(DMDAAC) may be used for this type of polymer modification.

In our EXAFS spectroelectrochemistry experiment, positively charged p(DMDAAC) not only physically contains the negatively charged metal complex in the X-ray beam, but also acts as the electrolyte during electrolysis, thus enabling a study of the complex's behavior only in the presence of the polymer. The negatively charged complex used in this investigation is $[Cu^{I}(bcp\text{-}s)_2]^{-3}$ where bcp-s = 2,9-dimethyl-4,7-diphenyl-1,10-phenanthroline disulfonic acid. The electrochemical cell utilized consists of a gold minigrid optically transparent thin-layer working electrode, two platinum foil auxiliary electrodes, and an oxidized silver wire reference electrode. These electrochemical cell components were then attachd to a Mylar window. The p(DMDAAC) containing $[Cu^{I}(bcp\text{-}s)_2]^{-3}$ was then cast onto the electrochemical cell and allowed to dry. In order to provide the required ionic-conductivity, the completed electrochemical cell was encased in a constant relative humidity chamber (Figure 1). While the polymer was maintained at a constant relative humidity, a cyclic voltammogram of the system was performed to locate the potential of the copper(I)/(II) redox couple and to confirm that this couple was electrochemically reversible.

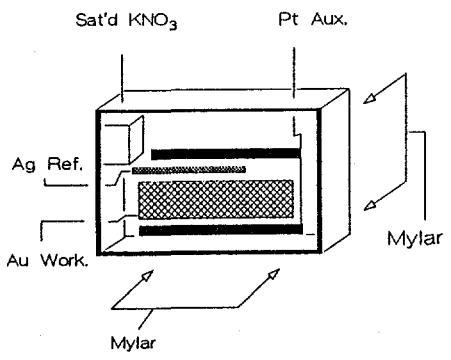

Figure 1

Confirmation of the stability of each oxidation state allows analysis of the structural characteristics of both the Cu^{I} and Cu^{II} states while in p(DMDAAC). The structures were determined from analysis of our EXAFS spectroelectrochemistry experiment, and compared to the results from solution. The model employed in this experiment was $[Cu^{I}(dmp)_2]BF_4$, where dmp = 2,9-dimethyl-1,10-phenanthroline. Since dmp and bcp-s have identical phenanthroline backbones, $[Cu^{I}(dmp)_2]BF_4$ should be an ideal model compound for Cu-N interaction in Cu(bcp-s)$_2$. When optimizing the filtered reverse Fourier transforms of $[Cu^{I,II}(bcp\text{-}s)_2]^{-3,-2}$ (measured in solution) with phase and amplitude functions of the model compound, the coordination number was observed to increase from 4 to 5. This is consistent with results obtained with $[Cu(dmp)_2]^{+,+2}$ in solution (4). Then optimizing the filtered reverse Fourier transform functions of Cu(bcp-s)$_2$ in p(DMDAAC) we observe no change in coordination number upon oxidation to the Cu^{II} species.

For the first time, we have evidence that the structural rearrangement, which follows electron transfer is different when in a polymer film than it is in solution. This is believed to be due to the electrostatic immobilization of the complex within the polymer film. Rearrangement of the complex to a 5-coordinate structure is believed to be energetically unfavorable when the complex is electrostatically paired through the sulfonated phenyl group to quaternary ammonium functionalities of the p(DMDAAC) matrix. This is due to the physical restrictions imposed upon the complex by the semi-rigid p(DMDAAC) matrix.

Prussian Blue:

Electrodes modified by hexacyanometalate films formed from various metals have been shown to have interesting electrochemical and spectral properties (5). Prussian blue (PB), one of these films, has been utilized as an important component of pigments in paints, lacquers, inks, and other color applications (6). An electrochemically generated and maintained PB film is potentially useful for implementation into electrochromic display devices. This is due to its thin-layer, electrochemical behavior and the extent of color change it exhibits, from blue to colorless, upon application of the appropriate potentials. Due to the complex environments about the iron centers, determination of the structures of these electrochemically generated materials is very difficult.

Mossbauer, infrared, and optical absorption spectroscopic investigations confirm the fact that the insoluble film is an iron(III) hexacyanoferrate, $\{Fe^{III}[Fe^{II}(CN)_6]\}^{-1}$. X-ray crystallography has been used to characterize the structure of the insoluble crystalline form of the complex (7). Evaluation of the structural report shows three different crystalline forms, each possessing four unique iron coordination environments. Upon first inspection, the iron coordination structure of PB appears to be too heterogeneous to practically analyze via EXAFS, yet there is distinct Fe↔Fe separation of 5.08 Å. This distance is associated with a characteristic Fe-C≡N-Fe linkage within the caged structure. The colinearity of the Fe-C≡N-Fe allows direct observation of the separation of the iron centers within the cage of PB at a distance not normally achievable with conventional room temperature EXAFS analysis (8). Although the structure of the PB form of the film is known, little or no information has been obtained concerning the in situ behavior of the electrochemically deposited material and the structure of its oxidized and reduced forms. EXAFS analysis allows evaluation of the distance between the iron atoms of the cage. Electrochemically generated forms of PB include the totally reduced Berlin green (BG) and its totally oxidized state Everitt's salt

(EVS). Most important of the electrochemical attributes of PB is that the various oxidation states are easily accessed and those products are stable over a long period of time, provided potential control is maintained.

Our investigations have involved the electrochemical deposition of PB onto a gold film electrode, 300 Å thick, vapor-deposited onto Mylar and then incorporated into a thin-layer EXAFS spectroelectrochemical cell. The gold film not only provides a suitable X-ray transparent electrode but a physical support for PB.

High quality X-ray fluorescence spectra were collected on each of the three generated oxidation states. The Fourier transforms of the EXAFS, (Figure 2A), indicate

Figure 2A

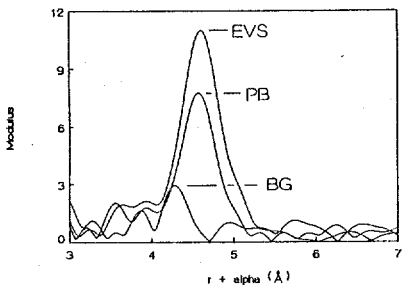

iron-iron interactions. The peak appears at a shorter distance, (∿4.5 Å), than the expected 5.08 Å due to the EXAFS phase shift, as expected. A marked decrease in amplitude of the Fe↔Fe peak at ∿4.5 Å is seen when comparing BG to PB to EVS. The decrease of the iron backscattering interaction is attributed to distortions of the cage structure of PB upon its reduction. Such distortion likely occurs when the cage has to incorporate hydrated cations to counterbalance the charge that accumulates upon decreasing the overall charge on iron. This is further supported by comparing the amplitudes of the back-transforms of the peaks associated with the Fe↔Fe backscattering interaction for the different oxidation states (Figure 2B). Upon decreasing the overall charge of the iron within the film, from EVS to PB and to BG, the peak magnitude descreases.

Figure 2B

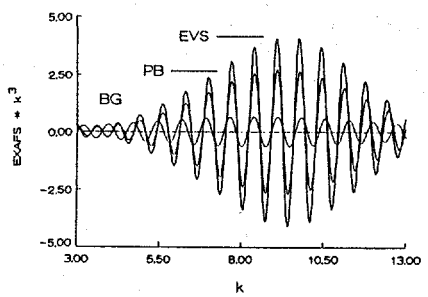

ACKNOWLEDGEMENTS

This work was supported by Air Force Grant AFOSR-88-0089. The X-ray spectroscopy and calculations reported here were performed by David H. Igo and Dr. Lee R. Sharpe.

REFERENCES

1. D.A. Smith, R.C. Elder and W.R. Heineman, J. Am. Chem. Soc., **106**, 3053-3054 (1986).
2. L. Geng, A. Reed, M.H. Kim. T.T. Woster, B.N. Oliver, J. Egekeze, R.T. Kennedy, J.W. Jorgenson, J.F. Parcher and R.W. Murray, J. Am. Chem. Soc., **110**, 1614-1619 (1989).
3. J.F. Parcher, C.J. Barbour and R.W. Murray, Anal. Chem., **61**, 584-589 (1989).
4. R.C. Elder, C.E. Lunte, A.F.M.M. Rahman, J.R. Kirchhoff, H.D. Dewald, W.R. Heineman, Electroanal. Chem., **240**, 361-364 (1988).
5. D. Ellis, M. Eckoff, V.D. Neff, J. Phys. Chem., **85**, 1225-1231 (1981).
6. H. Holtzman, Ind. Eng. Chem., **37**, 855 (1945).
7. H.J. Buser, D. Schwarzenbach, W. Petter, A. Ludi, Inorg. Chem., **16**, 2704-2710 (1977).
8. B.-K. Teo, J. Am. Chem. Soc., **103**, 3990-4001 (1981).

EXAFS Studies of (100) GaAs Treated with $[Ru^{II}(NH_3)_5H_2O]^{2+}$

S. R. Lunt, G. M. Miskelly, M. J. Sailor, P. G. Santangelo, B. J. Tufts and N. S. Lewis

Department of Chemistry and Chemical Engineering
California Institute of Technology
Pasadena, CA 91125

Keith O. Hodgson

Department of Chemistry
Stanford University
Stanford, CA 94305-5080

We have continued our investigations of the interactions of metal complexes with semiconductor surfaces. Previous work in our laboratory indicated that the adsorption of some transition metal complexes (e.g. $Co^{III}(NH_3)_6$, $RuCl_3$) onto GaAs surfaces results in improved semiconductor/liquid junction properties.[1,2] In the previous year, EXAFS and XPS investigations of GaAs powders exposed to a series of complexes of the type $Co^{III}(NH_3)_5X$ ($X=N_3^-, H_2O, NH_3$) in solutions of pH > 8 showed that an electron transfer reaction involving the cobalt ammines and the GaAs surface occured. The overall reacaction resulted in a layer $Co(OH)_2$ on the GaAs surface. EXAFS measurements also showed that an average of 5 Se atoms were incorporated into the inner shell of the cobalt in this layer upon exposure to the 1.0 M KOH-1.0 M K_2Se-0.1 M K_2Se_2 electrolyte solution used to GaAs/liquid junction solar cells.[3] Unfortunately, XPS and radioisotope analysis indicated that the inital $Co(OH)_2$ layer was about 40-60 Å thick which prohibited examination of the GaAs/metal ion interface and so no conclusions could be drawn about the precise nature of the bonding of the metal ions to the GaAs surface.

Another metal complex which improves the electrical properites of a GaAs/liquid junction solar cell is $[Ru^{II}(NH_3)_5H_2O]^{2+}$. The ammine ligands are substitutionally inert and so this compound is expected to react selectively with the GaAs surface via substitutuion of the aquo ligand. XPS analysis showed that the coverage of GaAs (100) surfaces exposed to this complex was less than a monolayer. Surface EXAFS experiments were undertaken to determine if this complex bonds directly to a surface Ga or As, or through a surface oxygen bridge.

SEXAFS experiments were conducted on GaAs (100) surfaces. The $[Ru^{II}(NH_3)_5H_2O]^{2+}$ was synthesized by Zn reduction of $[Ru^{III}(NH_3)_5H_2O]Cl_3$ in water (deareated with Ar). The solution was then filtered and a 1" X 1" etched wafer of GaAs was exposed to the solution for 30 min. The exposure was done under Ar and the wafer was placed in a Kapton covered cell which was continually purged with Ar during the course of the SEXAFS data collection. XPS of the sample after the experiment showed no detectable surface oxides.

The Ru Kα fluorescence was detected by two solid state Ge detectors. The spectra were analyzed using $Ru^{II}(NH_3)_6I_2$ as a model compound to determine scatteirng amplitudes and phase factors. The raw data and fourier transforms of the model compound and the ruthenium exposed GaAs are shown in figures 1 and 2. Fits of the first shell with the model parameters do not fit well at higher K values (figure 3) indicating the possibility that a heavier scatter, such as an As, may be present in the inner sphere of the ruthenium. However, further work with other model compounds (e.g. $[Ru(NH_3)_5AsPh_3]2+$) needs to be done before a firm conclusion can be drawn.

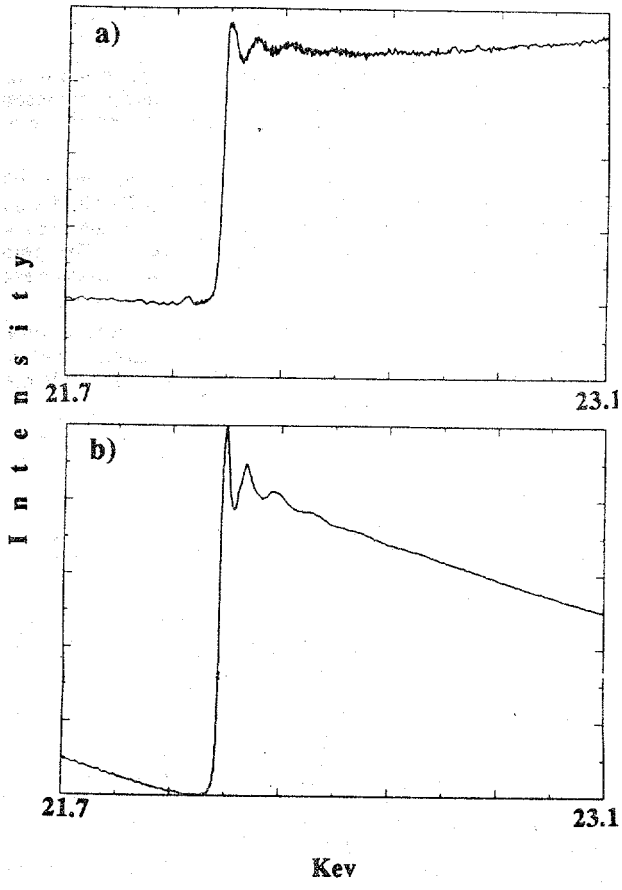

Figure 1. a) X-ray absorption data taken at room temperature for (100) GaAs which had been exposed to $[Ru^{II}(NH_3)_5H_2O]^{2+}$. The spectrum is an average of 25 scans and was collected in the fluorescence mode. b) X-ray absorption data taken at room temperature for $[Ru^{II}(NH_3)_6]I_2$. The data was collected in transmission mode.

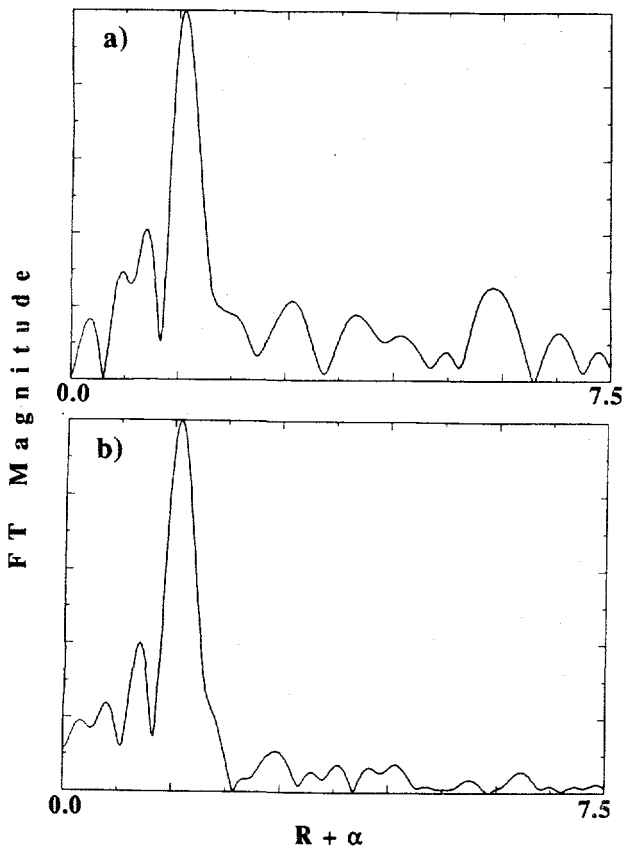

Figure 2. a) Fourier transform of EXAFS from data in figure 1a. b) Fourier transform of EXAFS from data in figure 1b.

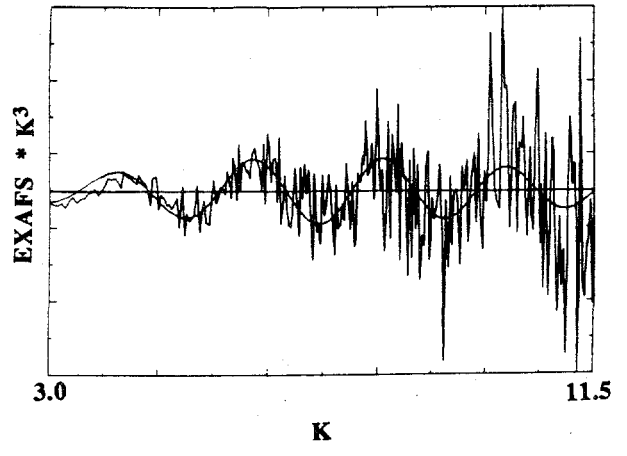

Figure 3. EXAFS data and best fit of first shell using model parameters from $[Ru^{II}(NH_3)_6]I_2$

Acknowledgements

We wish to thank Dr. M. D. E. Forbes of Caltech for help in this research and Dr. B. Hedman of SSRL for useful discussions. We also thank Dr. J. Gordon of IBM Almaden for the use of equipment and helpful discussions.

References

1. B. J. Tufts, I. A. Abrahams, P. G. Santangelo, G. R. Ryba, L. G. Casagrande, N. S. Lewis, Nature, **326**, 861 (1987).

2. I. A. Abrahams, B. J. Tufts, N. S. Lewis, J. Am. Chem. Soc., **109**, 3472 (1987).

3. B. J. Tufts, I. L. Abrahams, C. E. Caley, S. R. Lunt, G. M. Miskelly, M. J. Sailor, P. G. Santangelo, N. S. Lewis, B. M. Hedman, A. L. Roe, K. O. Hodgson, submitted.

ANALYSIS OF MUNICIPAL WASTEWATER-SLUDGE INCINERATOR EMISSION SAMPLES USING X-RAY ABSORPTION METHODS FOR THE DETERMINATION OF CHROMIUM AND NICKEL SPECIES

N.F. Mangelson*, L.B. Rees, J.E. Silk and M.W. Hill
Departments of Chemistry and Physics
Brigham Young University
Provo, Utah 84602

R.B. Greegor and F.W. Lytle
The Boeing Company
Seattle, Washington 98124

INTRODUCTION

Samples in this study were analyzed to determine chromium and nickel species present in ash samples. These data will be used with results from chemical analysis to establish emission standards for wastewater-sludge incinerators. Berry [1] has discussed the need to regulate toxic substances in the air. Fly-ash samples have been shown to have significant biological activity and cytotoxicity [2,3]. The toxic nature of the particulate matter is believed to be due in large part to inorganic compounds present in the fly ash. Since the toxicity of several elements is dependent on the chemical form in which the element is present [4,5], it is necessary to know the chemical species of elements in fly ash before meaningful risk-assessment analyses can be made.

Chromium in the Cr(VI) oxidation state and nickel subsulfide (Ni_3S_2) are suspected carcinogens. Sensitive chemical methods have been developed for determination of metal species, but some interferences may exist. Therefore, it is important to have a corroborative method of analysis. XANES and EXAFS are physical methods of metal speciation which avoid the necessity of chemical treatment before analysis.

EXPERIMENTAL

Municipal wastewater sludge from four sludge incinerator facilities was ashed in a laboratory furnace. Ash from each sample was placed on a quartz filter. Bulk ash was also prepared for analysis.

Nickel and chromium K-edge XRA spectra were taken at SSRL on beam line IV-1. Current of the 3.3 GeV electron beam varied from 1 to 55 microamps. A parallel crystal monochromator with silicon 220 crystals was used.

In a related study, bulk flyash from a municipal wastewater-sludge incinerator was collected at the inlet to the electrostatic precipitator and effluent particulate material was collected on quartz filters at the outlet of the precipitator.

Nickel and chromium K-edge XRA spectra were measured at the National Synchrotron Light Source (NSLS), Brookhaven National Laboratory. The electron beam was 2.5 GeV with 90 to 200 microamps of current. Data were taken on beam line X23-A2 which contains a Golovchenko-Cowan, two-crystal monochromator using silicon 220 crystals. At both facilities, data for the samples were usually taken in the fluorescence mode and data for the reference compounds and mixtures were taken in the transmission mode.

RESULTS

A few representative spectra are shown in Figures 1 to 4. Figure 1 shows a chromium, K-edge XANES spectrum for the laboratory-ashed sample, 1N2S. The pre-edge peak at about 4 eV clearly indicates the presence of Cr(VI). The dotted lines are linear combinations of a Cr(VI) spectrum and a Cr(III) spectrum, and the labels show the percent Cr(VI). These data suggest that chromium in this laboratory ashed sample is about 55% Cr(VI).

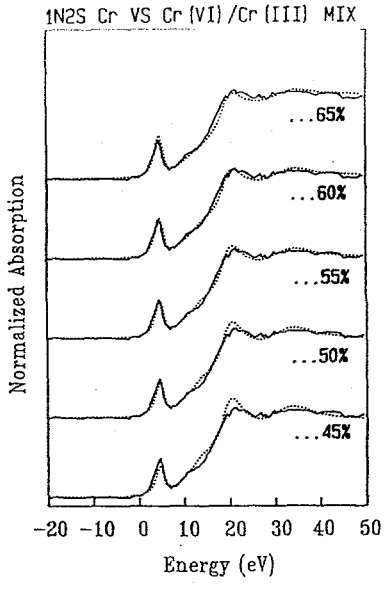

Figure 1. Solid lines are the chromium K-edge XANES spectrum for the laboratory ashed sample 1N2S. Dotted lines are spectra constructed as linear combinations of a chromium(VI) compound and a chromium(III) compound. Each curve is labeled with the Cr(VI)%.

The solid lines in Figure 2 are the experimental, chromium K-edge XANES spectrum for a mixture of $K_2Cr_2O_7$ (a Cr(VI) reference compound) and $FeCr_2O_4$ (a Cr(III) reference compound). The dotted lines are a linear combination of spectra for the two pure reference compounds. The mixture of compounds was 49.7% Cr(VI) and the linear combination spectra give the best fit to the pre-edge peak at 50% Cr(VI). These data support the analysis method assumed in the discussion of Figure 1.

Figure 3 shows the nickel K-edge XANES and first derivative spectra for the unspiked, laboratory-ashed sample, 3N2. The heavier lines are spectra from the reference compound nickel spinel, $NiFe_2O_4$. A excellent fit is seen indicating that laboratory ashing of this sample produces the nickel spinel compound.

The solid lines in Figure 4 show the nickel K-edge XANES spectrum for the incinerator outlet sample 5C-OUT which was collected on a quartz filter. The nickel concentration was a few hundred ppm by weight which accounts for the poor statistics on the edge spectrum. Dotted lines are XANES spectra for several reference compounds. It is clearly seen that the major compounds in the incinerator flyash are not the nickel subsulfide species. Additional study of these data suggest that nickel subsulfide is less than 20% of the total nickel in the sample.

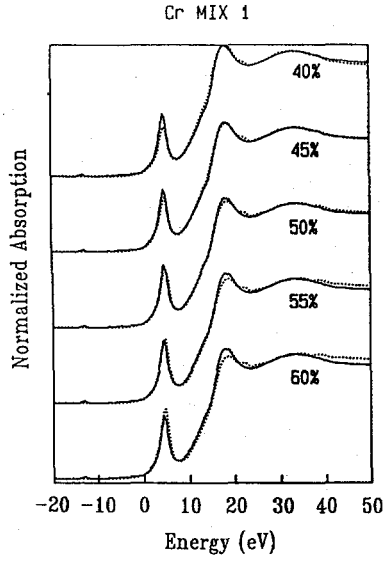

Figure 2. Solid lines are the chromium K-edge XANES spectrum of a mixture of $K_2Cr_2O_7$ and chromite ($FeCr_2O_4$) with 49.7% Cr(VI). Dotted lines are spectra constructed as linear combinations of $K_2Cr_2O_7$ and chromite spectra. Each curve is labeled with the Cr(VI)%.

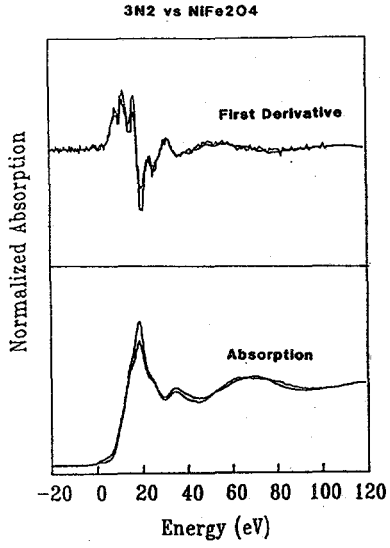

Figure 3. Light lines are the nickel K-edge XANES spectrum and its derivative for the laboratory ashed sample 3N2. Heavy lines are the nickel, K-edge XANES spectrum and its derivative for a nickel spinel ($NiFe_2O_4$) reference compound.

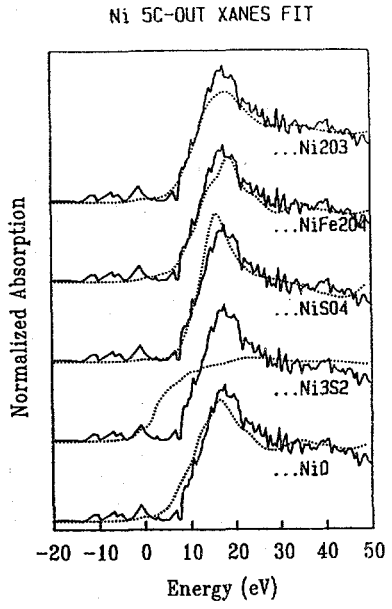

Figure 4. Solid lines are the nickel K-edge XANES spectrum for the incinerator effluent sample 5C-OUT-Ni. Dotted lines are the spectra for several reference compounds as indicated in the figure.

ACKNOWLEDGMENTS

We gratefully acknowledge the help given us at NSLS by C. E. Bouldin and Joe Woicik. We also appreciate the help from staff and crew at both SSRL and NSLS. This work was supported in part by the U.S.E.P.A., Cincinnati, OH order No. 9C6119NNEE and by Entropy Environmentalists, Inc. order No. 89-4181-01. The experiments were performed at SSRL, which is supported by DOE through the Office of Basic Energy Sciences and NIH through the Biotechnology Resources Program, and at NSLS, which is supported by the DOE through the Division of Materials Sciences.

REFERENCES

1. D.K. Berry. Environ. Sci. Technol., 20 (1986) 647-651.

2. G.L. Fisher, K.L. McNeill, B.A. Prentice and A.R. McFarland. Environ. Health Perspect., 51 (1983) 181-186.

3. C. Wei, O.G. Raabe and B.J. Kimble. Bull. Environ. Contam. Toxicol., 32 (1984) 179-186.

4. L.D. Hansen, G.L. Fisher, C.E. Chrisp and D.J. Eatough. Proceedings of the Fifth International Symposium, Polynuclear Aromatic Hydrocarbons, M. Cooke and A.J. Dennis, eds., Battelle Press, Columbus, OH, (1981) 507-517.

5. C. Wei, M.A. Al Bayati, M.R. Culberston, L.S. Rosenblatt and L.D. Hansen. J. Toxicol. Environ. Health, 10 (1982) 673-687.

S K EDGE XAS STUDIES OF PHOTOGRAPHIC MATERIALS

Jane G. DeWitt[1], Teresa A. Smith[2], Britt Hedman[3] and Keith O. Hodgson[1]

1 Department of Chemistry, Stanford University Stanford, CA 94305 USA.
2 Eastman Kodak Co., Photographic Research Laboratory Rochester, NY 14650 USA.
3 Stanford Synchrotron Radiation Laboratory, Stanford, CA 94305 USA.

Introduction

Several crucial elements of the photographic system including spectral sensitizing dyes and chemical sensitization centers contain sulfur atoms in species on the surfaces of photoactive silver halide crystals. These centers are involved in surface electron and energy transfer processes and are, therefore, of general interest for their photophysical properties. X-ray absorption studies of these important surface-active molecules may provide the first direct measure of the structure of adsorbates on the photoactive substrate.

Spectral sensitizing dyes (such as cyanine and merocyanine dyes, see figure 1) are the components of photographic materials which extend their response beyond the intrinsic blue/ultraviolet absorption of the silver halide photoconductor into the visible and infrared regions. This sensitization process involves the transfer of energy or electrons from the photoexcited state of the dyes into the conduction band of the silver halide and requires that the dye molecules exist in an adsorbed state on the surface of the silver halide grains.

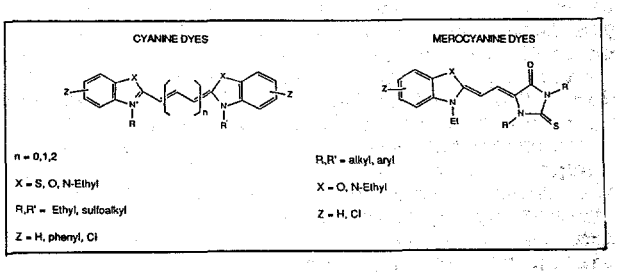

Figure 1. Generalized structures of cyanine and merocyanine sensitizing dye classes.

Chemical sensitization centers are believed to be silver sulfide specks on the surface of the silver halide grains which act as electron traps for photo-electrons [1]. This electron-trapping capability results in a reduced electron-hole recombination rate in the exposed silver halide grains and, thus, gives improved efficiency of latent image formation.

The highest degree of chemical sensitization is achieved with a combination of the sulfur compounds and gold-containing salts but the nature of these chemical sensitization centers is little understood. There has been considerable controversy surrounding the role of gold in the structure of chemical sensitization centers and in the latent image formation process [1]. Investigation of the structure of these important centers by sulfur K-edge spectroscopy could provide insight into the nature of the surface-active Ag/Au/S sites.

We have measured sulfur K-edge x-ray absorption spectra on a wide variety of dye and dye-intermediary molecules, as well as on structurally characterized Ag-S and Au-S compounds. These studies, taken together with oriented single crystal studies of dye-class molecules, reveal information about the nature and extent of intermolecular interactions between dye molecules and metals encountered in photographic systems. In addition, a variety of Au and Ag sulfide samples were measured.

Experimental

Spectra were measured in fluorescence mode at room temperature on BL 4-1 at SSRL and on BL X19A at NSLS with Si(111) crystals. Operating conditions at SSRL were 3.3 GeV and at NSLS, 2.5 GeV. Pre-oriented single crystal data were measured using a sample holder with χ fixed at 180 and allowing full ϕ rotation. Solid samples were measured as powders on mylar tape.

Results and Discussion

Sulfur K-edge x-ray absorption spectroscopic studies have revealed sharp absorption features which are highly dependent on the local geometry around and oxidation state of the absorbing atom [2-4]. The spectra of the sensitizing dye nuclei indicated a sensitivity to the local sulfur environment in these organic compounds (figure 2). The primary difference between the cyanine and merocyanine dye spectra is the sharp feature on the rising portion of the edge that is characteristic of the thiocarbonyl group of the merocyanine class dyes and has no counterpart in the spectra of the cyanine dyes.

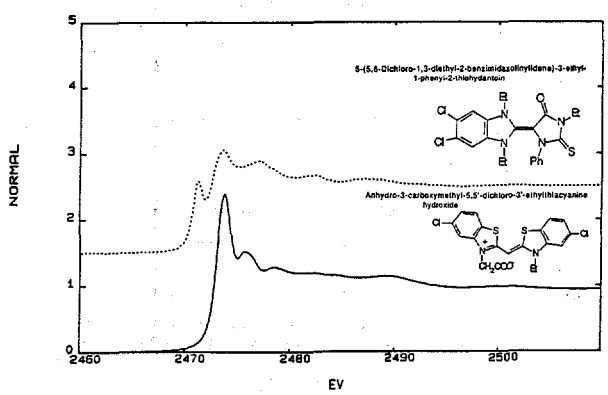

Figure 2. S K-edge spectra of representative cyanine (——) and merocyanine (· · · · ·) dye molecules.

The sharp features on the rising portion of the S K-edge reflect transitions to localized, unfilled atomic or molecular states and exhibit angular-dependent intensities in oriented samples of anisotropic centers. Oriented single crystal spectra of 2-thiohydantoin are compared to the powder spectra in figure 3. The single crystal polarized spectra suggests that the bound state feature characteristic of the thiocarbonyl group is almost entirely polarized along the Z molecular axis (normal to the plane of the molecule) and is attributed to a $1s \rightarrow p\pi^*$ transition in the terminal sulfur. The white line feature is polarized along the C=S bond in the plane of the molecule and is attributed to a $1s \rightarrow p\sigma^*$ transition.

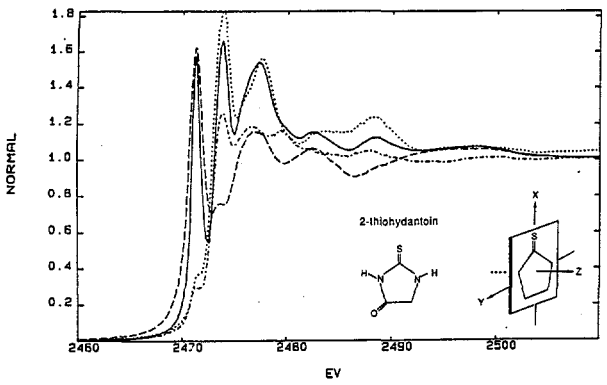

Figure 3. The powder spectra of 2-thiohydantoin (——) and the spectra corresponding to polarization along the average X (- - - -), Y (-·-·-·-) and Z (— —) molecular axis.

Direct interaction of sulfur with silver and gold atoms (in metal sulfides and other metal/sulfur complexes) results in increased intensity and broadening of predominant S K-edge features. The dramatic reduction of the thiocarbonyl feature of 3-carboxymethyl-4-methyl-4-thiazoline-2-thione upon complexation with Ag (figure 4) indicates that the metal interacts with the ligand via the thiocarbonyl group. This feature, which we have found to be polarized normal to the C=S bond, suggests that the metal/ligand interaction involves the sulfur $p\pi$ atomic orbitals and the Ag d orbitals.

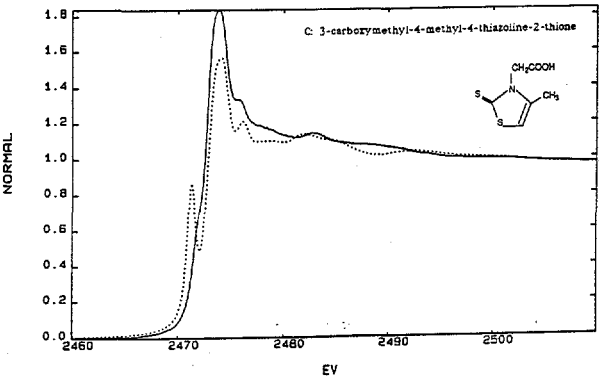

Figure 4. The powder spectra of AgC (——) and C (· · · ·). AgC is a polymeric structure with each thione S bound to 2 Ag's.

Sulfur-containing materials exhibit sharp K-absorption edge features which are polarized along specific molecular bonds and can be used to determine the orientation of dye molecules in well-characterized systems. The results from these preliminary investigations will form the basis for interpreting polarized surface XAS spectra of dyes in ordered systems, such as Langmuir-Blodgett films and dyes adsorbed to silver halide single crystals. Analysis of the EXAFS region of the K-edge spectra will provide a direct determination of the substrate-adsorber atomic distance and the first quantitative measure of the sulfur-surface distance for the adsorbed dye molecules.

Chemical sensitization centers are inherently surface active species and we intend to use a glancing-angle configuration to measure the K-edge spectra of sulfur and sulfur/gold-treated silver halide crystals. Comparison of the chemical sensitization site K-edges and EXAFS with Ag/Au/S-containing models may provide considerable insight into the structure of the elusive sensitization centers on the silver halide surface.

Acknowledgment

This work is supported by research funds from Eastman Kodak Company. The data were measured at SSRL and NSLS which are supported by the Department of Energy, Office of Basic Energy Sciences.

1. H.E. Spencer, R.E. Atwell, M. Levy, *J. Phot. Sci.*, **31**, 158 (1983).
2. Hedman, B., Frank, P., Penner-Hahn, J.E., Roe, A.L., Hodgson, K.O., Carlson, R.M.K., Brown, G., Cerino, J., Hettel, R., Troxel, T. Winick, H., Yang, J. *Nucl. Instr. and Meth.*, **A246**, 79 (1986).
3. Lytle, F.W., Greegor, R.B., Sandstrom, D.R., Marques, E.C., Wong, J., Spiro, C.L., Huffman, G.P., Huggins, F.E. *Nucl. Instr. and Meth.*, **226**, 542 (1984).
4. Sugiura, C. *J. Chem. Phys.*, **79**, 4811 (1983).

COMPARISON OF FLUORESCENT AND e-YIELD X-RAY ABSORPTION SPECTRA

F. W. Lytle and R. B. Greegor

The Boeing Company, Seattle, WA 98124

The problems inherent in preparing thin, uniform absorbers or the self absorption which occurs in fluorescent EXAFS data from concentrated samples can be avoided by using the electron yield technique. Kordesch and Hoffman (1) first demonstrated that collection of the electrons from the face of a sample in a gas filled chamber was a viable technique for measuring XAS. Later Erbil et al. (2) and Elam et al. (3) showed e-yield collection in the presence of an atmosphere provided a significant gain (up to 100) compared to collection in a vacuum. This occurs because of secondary ionization of the counter gas by Auger electrons.

The technique is most useful for low Z absorbers where the fluorescent yield is low, self-absorption of the fluorescent signal is high and thin, uniform absorbers are essentially impossible to prepare. Note that dilution of the sample with a lower Z material will do no good for either an absorber or fluorescent sample because the individual particle sizes are too large by at least a factor of 10. The effect is shown in Fig. 1 for a sample composed of a pressed disk of sulfur. All of the fluorescent data are so distorted by self absorption as to be unrecognizable as the same material. Fluorescent data from a suite of concentrated reference compounds would be useful only for comparison to similarly concentrated samples because fluorescent data from, e. g. a biological sample containing a small amount, well dispersed, would result in spectra more nearly like the e-yield spectra. The data were obtained simultaneously on BL IV-1, 3 GeV, 30 ma, Si (111) crystals detuned 90 % in a He filled detector rotated at 45° to the beam so that both signals could be collected in the same scan. The fluorescent gain was 10^{10}, e-yield gain was 10^{8}. For sulfur the fluorescent yield is 7% and the e-yield signal arises primarily from the KLL Auger electrons (2 KeV). Since the first ionization potential for He is 25 eV, each electron will create 80 ion pairs. This gas gain factor compared to the fluorescent yield and the 2 pi solid angle compared to 0.2 pi for the fluorescent detector account for the high signal level from the e-yield detector.

REFERENCES

1. M. E. Kordesch and R. W. Hoffman, Phys. Rev. B29, 491 (1984).
2. A. Erbil, G. S. Cargill, R. Frahm and R. F. Boehme, Phys. Rev. B37, 2450 (1988).
3. W. T. Elam, J. P. Kirkland, R. A. Neiser and P. D. Wolf, Phys. Rev. B38, 26 (1988).

ACKNOWLEDGEMENT

Supported in part by DOE Grant DE-FG06-84ER45121.

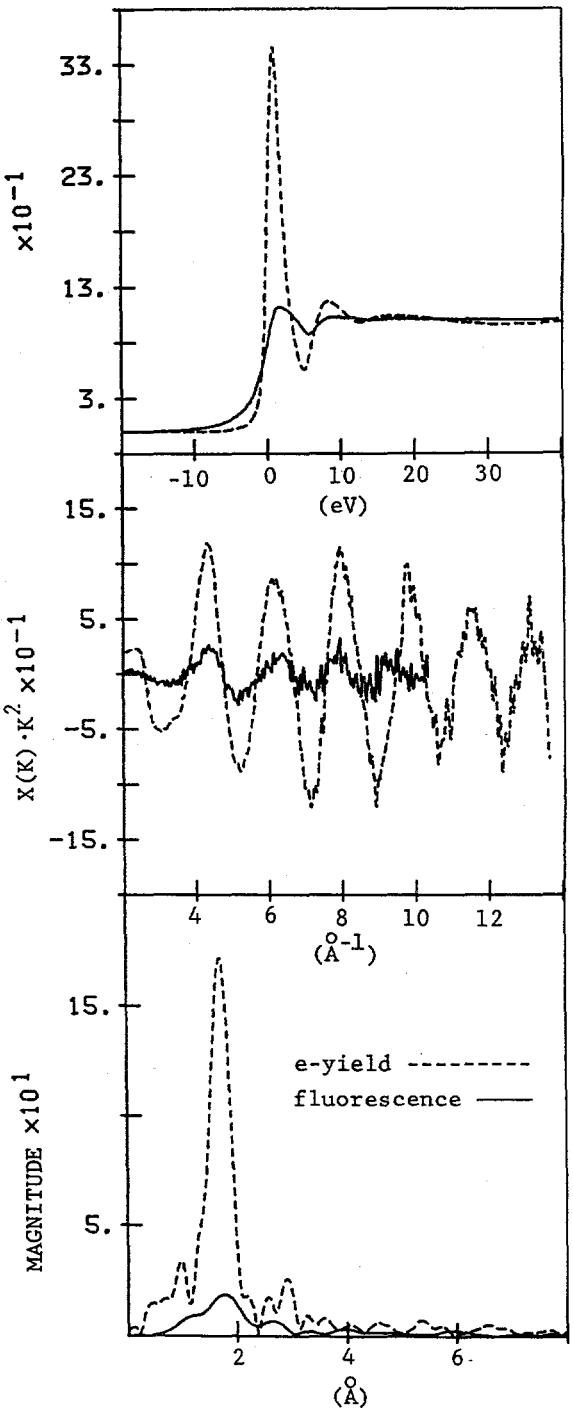

Fig. 1 The reduced amplitude in the fluorescent spectra of the edge resonance, EXAFS and FT as well as the apparent broadening at the edge are caused by the exponential diminution of the edge jump due to self absorption.

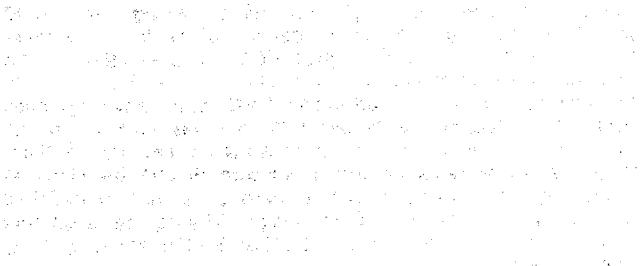

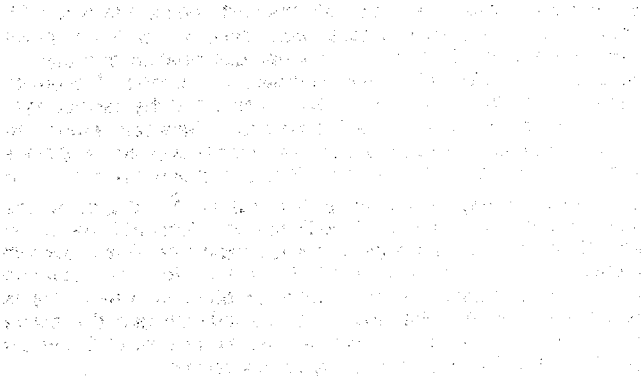

THE ENERGY DEPENDENCE OF THE PRODUCTION OF THE E' CENTER IN AMORPHOUS SiO_2

D.B. Kerwin and F.L. Galeener
Department of Physics, Colorado State University, Fort Collins, CO 80523

Introduction

The E' point defect center in amorphous SiO_2 has been studied for over 30 years. It has been determined with a high degree of accuaracy that the E' center corresponds to an electron in an sp^3 orbital of a silicon atom that is bonded to three (rather than four) oxygens. However, the mechanism of E' defect formation is not as well understood. Experiments on the desorption of oxygen from SiO_2 surfaces by Knotek[1] suggested that either a cooperative Auger transition or a Coulomb explosion[2] could produce an oxygen vacancy in the bulk when a silicon atom was photoionized. The paramagnetic version of the oxygen vacancy is just the E' center. The goal of this experiment was to determine whether the cross section for E' production differed significantly for x-irradiation below and above the k-edge of silicon.

Experimental

The samples used were high hydroxyl containing silica (1200 ppm OH) and low hydroxyl containing silica from Heraeus-Amersil (Suprasil-1 and Suprasil-W1, respectively). The samples were irradiated on beamline III-4 in March 1989. Although it had been intended to use the C-Rh multilayer synthetic crystals to monochromate the beam, the flux was too low to obtain the necessary exposures in a reasonable amount of time. Therefore, white radiation was used with Si and Be filters to produce spectral distributions that were either rich or deficient in radiation just above the silicon k-edge. The post-radiation spin signals were measured on the Brucker ER300 series ESR at Colorado State University.

Results

Several exposures were made with the white beam with only a 25 μm Be filter, and a few exposures were made with both a 5 μm Be filter and a 2 μm Si filter. The latter combination produced a spectral distribution which was deficient in photons of energies just above the k-edge of silicon. Measurement of the number of E' spins indicated no significant differences between exposures containing photons above the k-edge and those deficient in photons with energies above the k-edge. Figure 1 shows the results for Suprasil-1 for exposures up to 500 mJ cm^{-2}. Based on the difference in the absorption coefficient of silicon 200 eV below and 200 eV above the k-edge, one would expect an almost four fold increase in the production of E' centers for the radiation containing a significant distribution of photons with energies above the k-edge. Preliminary results indicate that the above mentioned mechanisms do not determine the number of E' defects observed in SiO_2 irradiated in this energy regime.

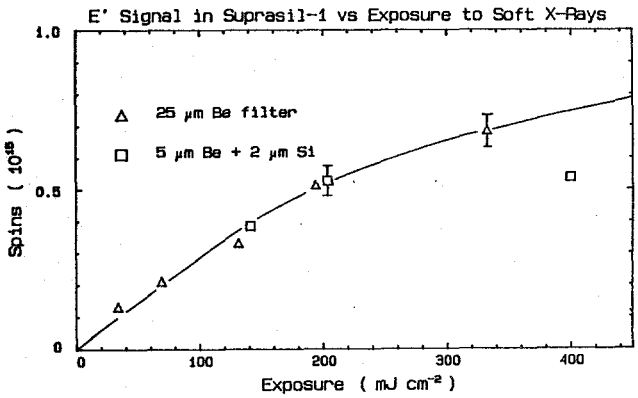

Figure 1: Number of E' spins vs exposure for Suprasil-1 samples. Circles - 25 μm Be filter, Squares - 5 μm Be + 2 μm Si filters.

REFERENCES

1. M.L. Knotek and P.L. Feibelman, Surf. Sci. 90, 78 (1979).
2. J.H.O. Varley, Nature 174, 886 (1954).

ACKNOWLEDGEMENTS

The assistance of P. Pianetta and L. Pan of SSRL was greatly appreciated. The assistance of A. Miller of Colorado State University in performing the experiments was also appreciated. This research was performed in part at SSRL, which is supported by the DOE's Office of Basic Energy Science.

Sn-related DX centers in $Ga_{0.7}Al_{0.3}As$

T.M. Hayes, D.L. Williamson, A. Outzourhit, and P. Small
Physics Department
Colorado School of Mines, Golden, CO 80401

P. Gibart and A. Rudra
Laboratory for Solid State Physics and Solar Energy, CNRS
Sophia Antipolis, 06560 Valbonne, France

The development of many promising devices based on III-V compound semiconductors has been impeded substantially by difficulties in producing highly-conductive wide-band-gap material. Dopants which yield shallowly-bound donor states in GaAs, such as Si, Se, Sn, and Te, give rise to deep levels as well in $Ga_{1-x}Al_xAs$ for $x > 0.22$. These levels, called DX centers, are associated with several deleterious materials characteristics, including both carrier freeze-out and persistent photoconductivity at low temperatures as well as reduced minority carrier lifetimes and recombination efficiency. DX centers impair the performance of any devices which incorporate n-doped wide-band-gap material, such as modulation-doped field-effect transistors (MODFET's), monolithic cascade solar cells, and multi-junction high-output-voltage photodetectors. Further progress in the engineering of these potentially important devices requires that we be able to control the occurrence of DX centers, which is not likely without a microscopic model for them.

DX centers have been extensively characterized electronically but there is little direct microscopic structural knowledge of them, due largely to the very low concentration of dopants in the materials of interest (typically 10^{17} to 10^{19} cm^{-3}). As a consequence, there are two competing classes of models for the DX center which have very different atomic-scale structures. Noting the large difference between the optical and thermal excitation energies (1.1 eV as opposed to 0.19 eV) and the large thermal capture barrier (0.1 eV), it was proposed in 1977 that neutral DX centers must be characterized by a large lattice relaxation [1,2]. There are several models incorporating such an effect [3]. Following in the tradition of substitutional donor models, the other class of models seeks to explain the properties of DX centers on the basis of the homogeneous properties of the $Ga_{1-x}Al_xAs$ host, with little or no distortion of the lattice about either neutral or ionized donor [4]. The most rudimentary knowledge of the atomic structure of the DX center would eliminate one of these classes of models.

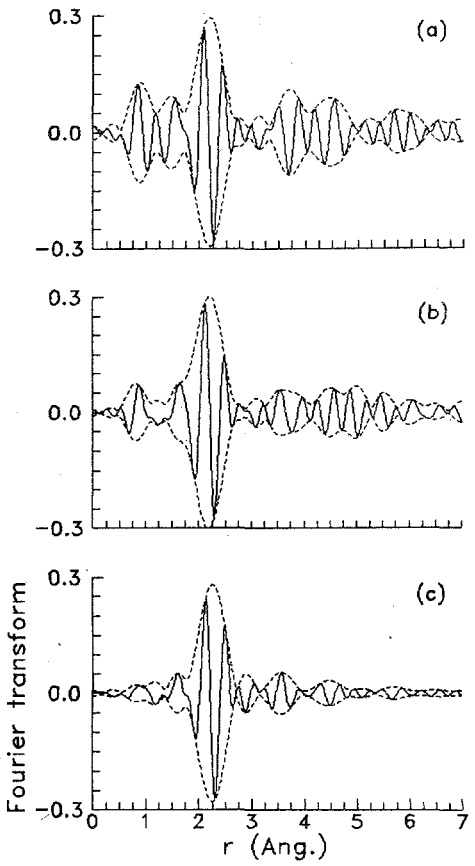

Fig.1. The real part (solid line) and the magnitude (dashed line) of the Fourier transform of the extended fine structure, $k\chi(k)$, on the Sn K-shell absorption of (a) GaAs and (b) $Ga_{0.7}Al_{0.3}As$ doped with 5×10^{18} cm^{-3} Sn and of (c) ordered $ZnSnAs_2$ at 80 K. The data were transformed using a square window with final-state electron momentum k between 2.8 and 10 $Å^{-1}$, broadened by convolution with a Gaussian of half-width 0.5 $Å^{-1}$.

A variety of samples with x between 0 and 1 and doping levels of 4 to 9×10^{18} cm^{-3} ^{119}Sn have been studied using Mössbauer effect spectroscopy (MES) [5]. Clear evidence for the DX center was found in a shifted and broadened resonance which is most prominent for x=0.3-0.4. The broadening suggests a quadrupole interaction at the Sn DX site and therefore a local distortion from cubic symmetry.

The x-ray absorption spectra associated with the Sn K shell in GaAs and $Ga_{0.7}Al_{0.3}As$ doped with 5×10^{18} cm^{-3} Sn have been measured at 80 K using fluorescence detection methods. The samples were cooled in the dark to populate the DX center. The extended fine structure in these spectra have been compared in detail with each other and with that in the spectrum from ordered $ZnSnAs_2$, in which each Sn atom is surrounded by four As atoms at 2.60 Å. The Fourier transforms of those spectra are shown in Fig. 1. We conclude that each Sn atom in the doped samples has four As neighbors at ~2.58 Å, but note that the shape of the nearest-neighbor (NN) peak in the radial distribution function does not have a simple Gaussian shape. While there are slight differences between NN peaks in the two doped samples, there is no evidence of a large shift in NN distance associated with the neutral DX center in $Ga_{0.7}Al_{0.3}As$, thereby eliminating the possibility of a large dilatory lattice relaxation in this sample. An angular distortion consistent with the MES measurements would of course be possible. Measurements of the Sn donor site under different doping conditions are in progress.

1. R.J. Nelson, Appl. Phys. Lett. **31**, 351 (1977)
2. D.V. Lang and R.A. Logan, Phys. Rev. Lett. **39**, 635 (1977)
3. See, for example, D.V. Lang, R.A. Logan, and M. Jaros, Phys. Rev. B**19**, 1015 (1979); K. Kobayashi, Y. Uchida, and H. Nakashima, Jpn. J. Appl. Phys. **24**, L928 (1985); A. Oshiyama and S. Ohnishi, Phys. Rev. B**33**, 4320 (1986); T.N. Morgan, Phys. Rev. B**34**, 2664 (1986); H. Hasegawa and H. Ohno, Jpn. J. Appl. Phys. **25**, L643 (1986)
4. See, for example, A.K. Saxena, Solid State Electron. **25**, 127 (1982); H.P. Hjalmarson and T.J. Drummond, Appl. Phys. Lett. **48**, 656 (1986); J.C.M. Henning and J.P.M. Ansems, Semicond. Sci. Technol. **2**, 1 (1987)
5. P. Gibart, D.L. Williamson, B. El Jani, and P. Basmaji, Phys. Rev. B **38**, 1885 (1988)

ELECTROCHEMICALLY DEPOSITED METAL MONOLAYERS: STRUCTURE, COMPRESSIBILITY AND GROWTH

Michael F. Toney, Joseph G. Gordon, Mahesh G. Samant, Gary L. Borges,
IBM Research Division, Almaden Research Center, 650 Harry Road, San Jose, CA
Dennis Yee and Larry B. Sorensen
Department of Physics FM-15, University of Washington, Seattle, WA 98195

The atomic structure at the solid-liquid interface is of fundamental importance in electrochemistry, since this structure strongly affects the chemical properties of the interface. While a great deal is known about surface structure at the solid-vacuum interface, our understanding of solid-liquid interfaces is still quite primitive. This is largely because standard surface structural techniques (LEED, etc.) cannot penetrate the liquid overlayer. Surface x-ray scattering is, however, ideally suited for studies of such buried interfaces and we have recently made substantial progress in determining, in-situ, the atomic structure of electrochemically adsorbed metal monolayers.[1-5]

The electrochemical deposition of many metal monolayers occurs at potentials positive of bulk deposition, and consequently, there is a potential range where only a monolayer is stable. In previous experiments at SSRL, we have determined the two-dimensional (2D) structure of the electrochemically deposited monolayer of lead on silver (111).[1, 2] This monolayer forms a 2D, incommensurate hexagonal solid that is compressed relative to bulk Pb and rotated away from the Ag($\bar{2}$11) direction by 4-5°. We also discovered that as the applied potential becomes more negative, the in-plane atomic spacing decreases.[3, 4] This increased density is a direct consequence of the decreased chemical potential of the Pb^{2+} ions in solution. Because the monolayer is in chemical equilibrium with the ions in solution, our measurements of atomic spacing enable us to calculate the 2D compressibility, κ_{2D}, of the monolayer: $\kappa_{2D} = \partial a/\partial\mu$, where a is the atomic area and μ is the chemical potential.[3, 4]

During our last run, we investigated the effect that two different counterions, perchlorate and acetate, have on the structure, atomic spacing, and compressibility of Pb/Ag(111). The acetate anion strongly adsorbs onto Pb and Ag surfaces, while the perchlorate anion only adsorbs weakly. These experiments were designed to probe how the presence of adsorbed anions affect the properties of the monolayer. The measurements were made in-situ (in contact with solution) and under potential control on beamline 7-2 with an incident x-ray energy of 9.05keV. We found that in both perchlorate and acetate solutions the Pb monolayer forms the same incommensurate, hexagonal structure. In addition, as shown in Figure 1, the potential dependence of the atomic spacing is independent of anion and in both cases $\kappa_{2D} = 1.2$Å^2/eV. This indicates that the properties of the electrochemically deposited monolayer are predominately determined by the adsorbate-adsorbate and adsorbate-substrate interactions and are not strongly influenced by adsorbed anions. Since the structure of electrochemically deposited Pb/Ag(111) is the same as vapor deposited Pb/Ag(111),[6, 7] it also appears that the metal-metal interactions are much more important than the effects of the water overlayer.

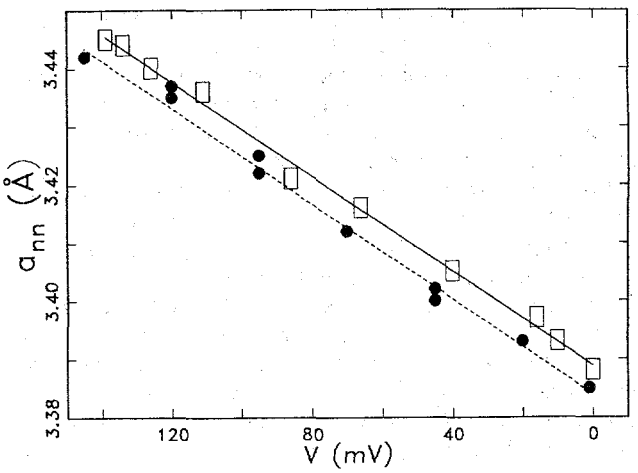

Figure 1. Potential dependence of the near-neighbor spacing, a_{nn}, for an electrochemically deposited monolayer of Pb on Ag(111). The filled circles are for Pb deposited in the perchlorate solution (0.005 M lead perchlorate, 0.1M sodium perchlorate and 0.01M perchloric acid) and the open squares are for the acetate solution (0.005 M lead acetate, 0.1M acetic acid, 0.1M sodium acetate). The lines are least-squares fits to the data; the solid line for acetate and the dashed line for perchlorate. The potentials are relative to the Nernst potential, where bulk Pb is thermodynamically stable. Since the measured accuracy of the Nernst potential is about 5mV, it is not clear if the shift between the acetate and perchlorate data (≃12mV) is significant or not.

References

1 M.G. Samant, M.F. Toney, G.L. Borges, L. Blum, and O.R. Melroy, Surf. Sci. **193**, L29 (1988).
2 M.G. Samant, M.F. Toney, G.L. Borges, L. Blum, and O.R. Melroy, J. Phys. Chem. **92**, 220 (1988).
3 O.R. Melroy, M.F. Toney, G.L. Borges, M.G. Samant, J.B. Kortright, P.N. Ross, and L. Blum, Phys. Rev. B **38**, 10962 (1988).
4 O.R. Melroy, M.F. Toney, G.L. Borges, M.G. Samant, J.B. Kortright, P.N. Ross, and L. Blum, J. Electroanal. Chem. **258**, 403 (1989).
5 M.F. Toney, J.G. Gordon, L.S. Kau, G. Borges, O.R. Melroy, M.G. Samant, D.G. Wiesler, D. Yee, and L.B. Sorensen, unpublished, 1990
6 K. Takayanagi, D.M. Kolb, K. Kambe, and G. Lehmpfuhl, Surf. Sci. **100**, 407 (1980).
7 K. Takayanagi, Surf. Sci. **104**, 527 (1981).

This work was partially supported by the Office of Naval Research.

Structural Improvements in Multilayers for Instrumentation Applications

William K. Warburton
X-ray Instrumentation Associates, 1300 Mills St., Menlo Park, CA 94025

Troy W. Barbee, Jr.
Lawrence Livermore National Laboratory, P.O. Box 808, Livermore, CA 94550

1: Introduction

When a diffraction grating is overcoated with a multilayer, a new x-ray optical element results which possesses novel,characteristics found in neither the grating nor the multilayer taken separately. [1, 2] First, the devices can be much more efficient than single metal overcoated gratings because the multilayer can be designed to be an efficient x-ray reflector at the energy of interest. Further, because of the finite multilayer bandwidth, the grating orders become discontinuous in energy. Finally, the devices act like x-ray prisms, maintaining a constant deflection for a given energy as the incident angle is changed. Barbee and collaborators have extensively observed and verified these effects in the soft x-ray regime below 1500 eV. [2, 3] Barbee has further developed an equation for the angle between the different grating orders based on the grating equation and Bragg's Law: [3]

$$\sin\phi = \frac{2\, m_D\, d}{m_d\, D}\left[1 - \frac{2\delta - \delta^2}{\sin^2\theta}\right]^{1/2} \qquad (1)$$

Here m's are reflection orders, d (D) is the multilayer (grating) spacing, and δ is the average anomalous scattering factor. Warburton has addressed the same problem using kinematic scattering theory [4] to derive an equivalent expression for the offset angles between the grating orders as:

$$\phi_{max} = \frac{2\, R\, m_D\, d}{m_d\, D}\left[1 - R\,\frac{m_D}{m_d}\,\frac{d}{D}\cot\theta\right]^{-1}, \qquad (2)$$

where R is the bracketed term to the 1/2 power in Eqn 1. The difference between the expressions becomes most important as θ approaches zero.

These devices are expected to become extremely important for instrumentation since they are not only efficient and dispersive but may also resolve many of the overlapping order problems associated with simple gratings. In the present work we are extending earlier measurements into the hard x-ray region.

2: Experimental

The data were taken in BL 2-3 in white light mode during the March 1989 run. The sample, 89037, was a 40Å d spacing Rh/C multilayer deposited on an 8 mm D spacing grating etched into a Si wafer. The sample was initially placed on the ω goniometer of a small angle diffractometer described elsewhere [5] at an angle of 1.5° and film exposures of the dispersed beam were taken with interposed elemental filters ranging from Mn through Ge. The elemental absorption edges could be clearly seen and moved across the dispersed beam with absorption edge energy in accord with the previously observed prism effect. We then proceeded to quantitative data by installing an 0.001" slit on the exit arm in front of an ion chamber so the dispersed beam could be scanned.

3: Results

Due to poor ring performance, only a few scans could be obtained, but these are extremely interesting. Figure 1 shows the white beam as dispersed by 89037. The center of the peak (0 grating order) corresponds to an energy of 5.9 keV from the Bragg relationship and the multilayer d spacing. The multilayer coated grating displays very complex behavior, particularly at low angles, which we are working to understand and will discuss below. When an Fe foil is inserted, the result is as shown in Figure 2, with the absorption edge at 7.1 keV clearly visible at about 2.5° 2θ. This is the same value of 2θ at which the multilayer would Bragg reflect 7.1 keV light, but the reflection has unequal angles of incidence and reflection in the present case. Finally, in Figure 3, we present a view of the diffraction structure in the vicinity the

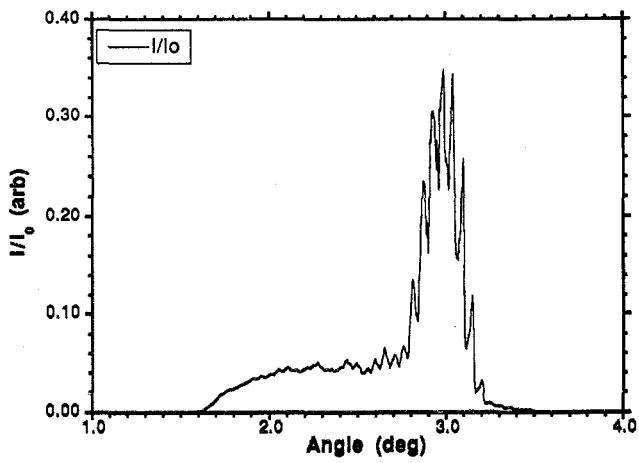

Figure 1: White light reflected from a 8 µm pitch grating coated with a 40Å d spacing multilayer.

grating 0 order which has been expanded to show the detailed structure of the peaks.

4: Discussion

The spacing of the peaks near 0 grating order is fairly well understood. From either equation 1 or 2, ignoring the correction terms in brackets, the interpeak spacing for 1st multilayer Bragg order would be $\Delta\phi = 2d/D = 0.057°$ for 89037's values of d and D. The average interpeak angle computed simply form the peak maxima is 0.056°, in good agreement. In addition, the subpeaks and shoulders seen in Fig 3 fall at intervals given approximately by 0.056°/2 and 0.056°/3, corresponding to the 2nd and 3rd Bragg orders from the multilayer.

The peak amplitudes, on the other hand, have yet to be explained. According to the kinematic theory they should fall off as $1/m_D^2$, which they clearly do not. Since we do not yet know to what extent this shape depends upon the alignment of the grating in the beam, we have postponed its interpretation until we are sure that it is not an experimental artifact. The other area of interest is the small angle shoulder region. In this region there is a transition between Bragg reflection from the multilayer and total external reflection from its surface. The cutoff at 1.5°, in fact, corresponds to an exit beam travelling parallel to the grating surface since the angle of incidence is also 1.5°. The description of the multilayer coated grating in this region will therefore be more complex than in the region near 0 grating order and its description may require combining a dynamical description of the multilayer with the grating equation.

5: References

[1] T.W. Barbee Jr., in: Multilayers: Synthesis, Properties and Non-Electronic Applications, Mat. Res. Soc. Symp. Proc. 103 (1988) 307

2] T.W. Barbee Jr., Rev. Sci. Instrum. 60 (1989) 1588.

[3] T.W. Barbee Jr., in: X-ray and Vacuum Ultraviolet Interaction Databases, Calculations and Measurements, Proc. SPIE 911 (1988)

[4] W.K. Warburton, 6th National Conference on Synchrotron Radiation Instrumentation, Nucl. Instr. and Meth. Accepted for publication. (1990)

[5] W.K. Warburton, T.W. Barbee Jr. and Z.U. Rek, 6th National Conference on Synchrotron Radiation Instrumentation, Nucl. Instr. and Meth. Accepted for publication. (1990)

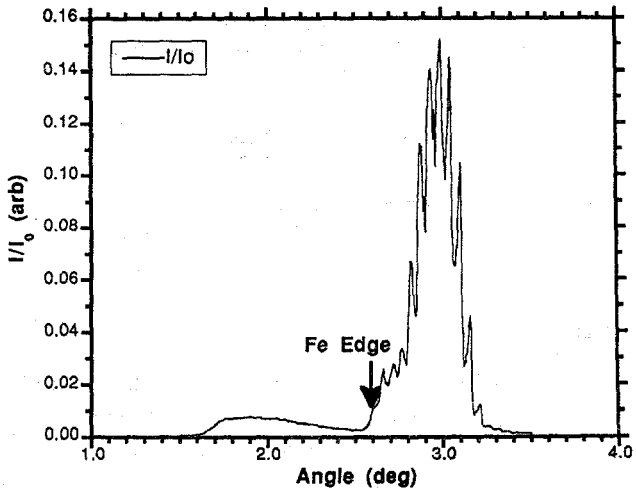

Figure 2: Identical conditions to Fig. 1 but with a 10 μm Fe foil inserted after the grating.

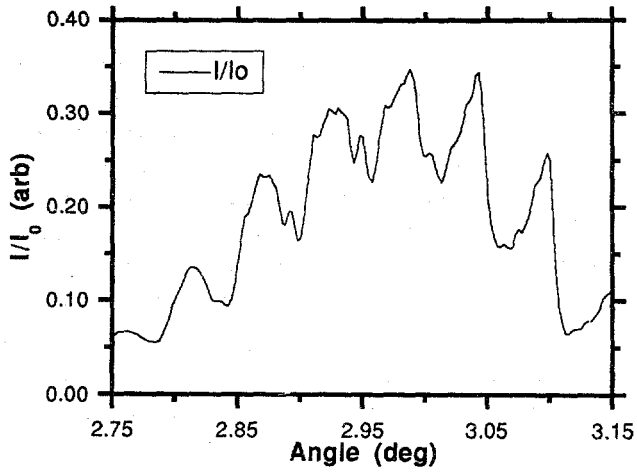

Figure 3: Enlarged view of the peak region of Fig. 1.

ANOMALOUS SMALL ANGLE X-RAY SCATTERING STUDY OF AMORPHOUS METAL-GERMANIUM ALLOYS

Marybeth Rice
Department of Electrical Engineering
Stanford University

Soichi Wakatsuki
Department of Chemistry
Stanford University

Arthur Bienenstock
Stanford Synchrotron Radiation Laboratory

INTRODUCTION

Anomalous small angle x-ray scattering (ASAXS) is emerging as a tool for detecting and characterizing phase separation in amorphous materials. In crystalline materials phase separation is shown readily by the superposition of the broadened x-ray diffraction powder patterns from each phase. Because there are no sharp diffraction peaks in an amorphous material, it is impossible to tell whether the pattern originates from a single, or from multiple, phases.

Classically, information about such phase separation is obtained from small angle x-ray scattering. SAXS is sensitive to electron density fluctuations on a scale of tens to thousands of Angstroms. Therefore, SAXS indicates the presence of inhomogeneities arising from such diverse phenomena as phase separation or cracks and voids. Unfortunately, SAXS alone cannot distinguish between these various possibilities.

Recently, investigators have begun to combine SAXS with anomalous dispersion to achieve such a distinction[1]. We are using ASAXS as a tool for understanding the structure of amorphous metal-germanium thin films. In particular, we are seeking to determine whether these films are phase separated on a very fine (2-4 nanometers) scale, the size of the single phase domains being limited by the kinetics of film formation.

The metal-germanium amorphous films, which can be prepared typically from pure Ge to approximately 70 atomic percent metal, are semiconducting for low metal concentrations and then metallic when the metal concentration reaches 10-15 atomic percent. When the metal concentration rises even more, physically interesting metallic characteristics arise. Superconductivity appears in the Mo-Ge system at 13 atomic percent Mo whereas ferromagnetism appears at approximately 40 atomic percent Fe in the Fe-Ge system. We are using ASAXS to determine whether these transitions occur via phase separation or through homogeneous alloy formation.

EXPERIMENTAL

Proposal No. 2088M

In February of 1989 we performed ASAXS experiments on a-W_8Ge_{92}, a-Mo_8Ge_{92} and a-$Fe_{12}Ge_{88}$ on SSRL beamline IV-2. We used the SSRL Biotechnology Group's SAXS camera with its position sensitive linear detector (described by Hubbard[2]). We intended to collect data at 100 eV, 20 eV, and 7 eV below the absorption edge of each element in all the three samples, but the beam conditions prohibited the collection of data at the Ge edge for the FeGe sample and at the Mo edge for the MoGe sample. For the WGe sample we collected a complete data set. The region of reciprocal space probed in these experiments runs from $s=2\sin\theta/\lambda=0.01$ to $s=0.2$ inverse Angstroms. The data shown here are scaled by the intensity of the transmitted beam and are background subtracted. To remove the contribution of the resonant Raman scattering, the three data sets at each edge are forced to coincide at $s=0.2$ inverse Angstroms where the intensity of the small angle scattering approaches its asymptotic value.

RESULTS AND DISCUSSION

Corrected ASAXS data for the a-W_8Ge_{92} sample are reproduced in Figures 1 and 2. As the W edge is approached from below the intensity of scattered radiation decreases. At the Ge edge the intensity of scattered radiation remains the same as the photon energy increases beneath the edge. This means that the Ge is not contributing to the small angle scattering. The scattering arises from fluctuations in the electron density of the W and the Ge number density is uniform across the sample. As a rough check on whether it is possible for Ge to be present in two phases in a-W_8Ge_{92} and have the same density within each phase, we investigated the density of Ge atoms in c-Ge and in c-MoGe (assuming that the metastable phases of WGe strongly resemble those of MoGe, since there are no compound in the WGe equilibrium phase diagram). As shown in Table 1, the number density of Ge in pure Ge, $MoGe_2$ and $Mo_{13}Ge_{23}$ is nearly the same. Therefore, phase separation of a-W_8Ge_{92} into a-Ge and an a-$MoGe_2$ or a-$Mo_{13}Ge_{23}$-like substance is consistent with the data.

TABLE 1.

Crystals	Number of Ge atoms per unit cell	a (Å)	c (Å)	N/V
Crystalline Ge	8	5.658	-	**0.0442**
$MoGe_2$	4	3.313	8.195	**0.0445**
$Mo_{13}Ge_{23}$	92	5.990	63.54	0.0404

Although our data sets on the a-Mo_8Ge_{92} and a-$Fe_{12}Ge_{88}$ samples are incomplete, they both exhibit small angle scattering near s=0.05 inverse Angstroms similar to that seen in the a-W_8Ge_{92} sample. As shown in Figure 3, the intensity of the small angle scattering remains constant as the photon energy is increased beneath the Ge edge in the a-Mo_8Ge_{92} sample. The a-$Fe_{12}Ge_{88}$ results for the Fe edge are shown in Figure 4. The scattered intensity decreases with increasing photon energy beneath the Fe edge. Both of these results are consistent with the a-W_8Ge_{92} results, although they are incomplete. These results suggest that there may be strong similarities in the structure of these metal-germanium films in the low metal concentration regime.

We performed more ASAXS experiments on the a-FeGe, a-WGe and a-MoGe systems at NSLS beamline X14A in December 1989. We collected data for samples of different concentrations across the broad amorphous region of each system. These data will be presented when they are analyzed.

REFERENCES

1 See, for example: P. Godeau, A. Naudon, A. Chamberod, B. Rodmacq, and C. E. Williams, Europhys. Lett. 3 (3), 269 (1987)

2 S. R. Hubbard, Ph.D. thesis, Stanford University (1987).

ACKNOWLEDGMENTS

This research is supported by the Department of Energy through the Office of Basic Energy Science.

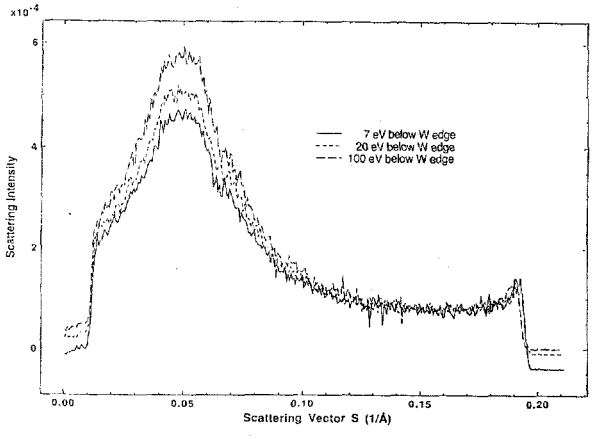

FIGURE 1.
For the a-W_8Ge_{92} sample, we observed a decrease in the intensity of the SAXS peak as the W edge was approached from below.

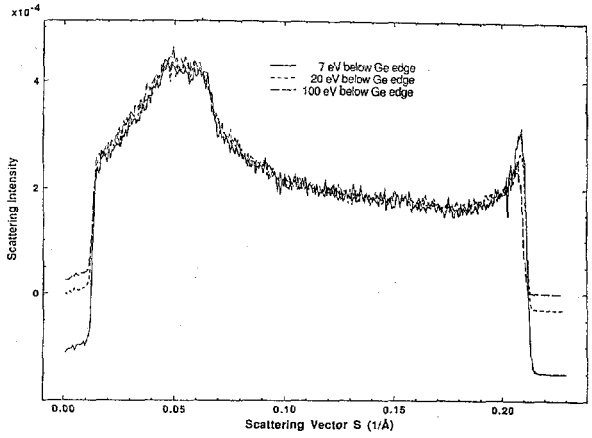

FIGURE 2.
The intensity of the SAXS peak, for the a-W_8Ge_{92} sample, remained constant as the Ge edge was approached from below.

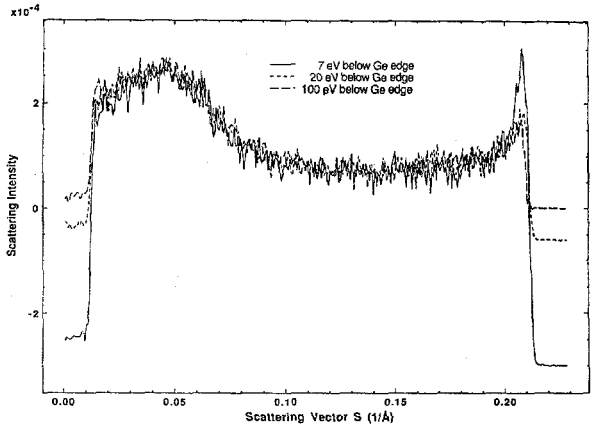

FIGURE 3.
For the a-Mo_8Ge_{92} sample, the intensity of the SAXS peak did not change as the Ge edge was approached from below.

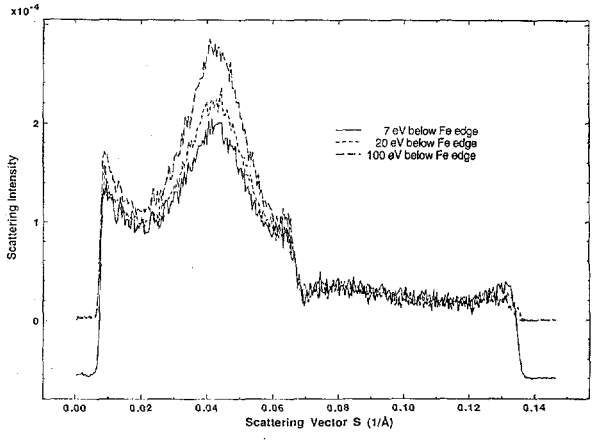

FIGURE 4.
For the a-$Fe_{12}Ge_{88}$ sample, the intensity of the SAXS peak decreased as the Fe edge was approach from below.

STUDYING HYPERFINE FIELDS WITH RESONANT NUCLEAR DIFFRACTION OF X RAYS

J. Arthur, D. E. Brown, S. L. Ruby, and G. S. Brown
Stanford Synchrotron Radiation Laboratory, Stanford, CA 94309

G. K. Shenoy
Advanced Photon Source, Argonne National Laboratory, Argonne, IL 60439

In the SSRL Activity Report for 1988 we presented some of the results of an experiment carried out in December, 1988 at the PEP 1B beam line. During 1989 we analyzed more of the data from that experiment. This report is condensed from a paper prepared for the 34th Annual Conference on Magnetism and Magnetic Materials, held in Boston in November, 1989.[1]

The use of resonant nuclear diffraction to study hyperfine fields in a crystal depends simply on the spectral and temporal characteristics of the synchrotron radiation pulse. A synchrotron source provides very short (<1 ns) pulses of radiation, with a bandwidth that is much wider than the energy range of the nuclear resonance in the sample. If the sample resonance is split by hyperfine fields, the synchrotron pulse will simultaneously and coherently excite all the levels of the split resonance (subject to the polarization selection rules discussed below). The coherence between the excited levels is preserved during the excited state lifetime, which can be much longer than the synchrotron pulse, and so the radiative decay of the excited state exhibits interference effects. The time distribution of the scattered radiation contains a beat structure determined mainly by the energy differences between the coherently excited levels.[2]

In addition to its well-defined time structure, a synchrotron source provides radiation with a well-defined polarization. If the sample is magnetic, the experiment can be designed to give specific relationships between the directions of polarization of the incident and scattered light and the magnetic field in the sample. The nuclear excitation matrix elements give polarization selection rules which can be used to simplify the experimental analysis.

X-ray diffraction selection rules can also be used to simplify the experimental analysis, in the case where a sample contains more than one crystallographically distinct group of resonant nuclei. The hyperfine field environments for the nuclei in different groups may be different, but by choosing a reflection for which only one crystallographic group has a nonvanishing structure factor, the hyperfine field for that group can be examined separately.

We observed all of these effects in our experiment using resonant diffraction from the 14.4 keV Mössbauer nuclear resonance in ^{57}Fe, in a nearly perfect crystal of yttrium iron garnet (YIG). The (002) and (0 0 10) reflections that we observed are crystallographically forbidden except for nuclear scattering from a small subgroup of the Fe nuclei. Furthermore, we could control the orientation of the nuclear moments in the magnetized crystal with a small external guide field.

Figure 1 demonstrates changes in the diffracted distribution from the same set of nuclei with no change in the hyperfine fields, when the polarization selection rules are changed. Figure 1(a) shows the beat pattern obtained with the moments oriented nearly parallel to the direction of propagation of the incident X-ray beam. In this case some of the hyperfine levels are excited by left-hand-circular (LHC) light while others are excited by right-hand-circular (RHC) light. This gives a beat pattern due to interference between the levels excited by the LHC component of the incident light, overlapped by a beat pattern due to interference between the levels excited by the RHC component. Each beat pattern contains a short period of about 12 ns and a long period of about 130 ns (note that t=0 occurs at a null in the long period beat). The decay envelope arising from the lifetime of the excited state is also clearly visible in Fig. 1(a). Fitting parameters for the calculation shown were the strengths of the magnetic field and electric quadrupole splitting at the nuclear sites, and the incident beam deviation angle.

Figure 1(b) shows the time distribution with the guide magnetic field (and therefore the internal moments as well) rotated so as to be perpendicular to the scattering plane, and parallel to the polarization direction of the incident radiation. The nuclear scattering matrix is still diagonal to good approximation, but the basis states are linearly polarized. In this case interference can occur between levels which had differing polarizations and therefore did not interfere in the case shown in Fig. 1(a). This causes the rapid beat pattern.

Figure 2 shows two distributions taken with identical diffraction conditions, but with different hyperfine fields in the sample. The data shown in Fig. 2(a) were taken with the sample at 295±2 K, while the data shown in Fig. 2(b) were taken at 150±7 K. At the lower temperature, the magnetization of the sample is nearly saturated, whereas at room temperature it is not (the Néel temperature for our sample was 550 K[3]).

The use of synchrotron radiation to excite Mössbauer resonances is still very much in the exploratory stage. The brightest beams now

available have the capability to begin to move beyond demonstration experiments and to actually do materials science. With the expectation that a significant number of even brighter beams will become available within the next few years, this area of research has great expectations.

The authors would like to thank Dr. D. M. Gualtieri, who prepared the ^{57}Fe-enriched YIG crystal used in this experiment, and Dr. E. Alp and Dr. W. Lavender, for discussions and assistance during several nuclear diffraction experiments. This research was performed at SSRL, which is operated by the Department of Energy, Office of Basic Energy Sciences, Division of Chemical Sciences. That Office's Division of Materials Sciences has provided support for this research.

[1] J. Arthur, D. E. Brown, S. L. Ruby, G. S. Brown, and G. K. Shenoy, to be published in J. Appl. Phys.

[2] G. T. Trammell and J. P. Hannon, Phys. Rev. B **18**, 165 (1978).

[3] D. M. Gualtieri, W. Lavender, and S. L. Ruby, J. Appl. Phys. **63**, 3795 (1988).

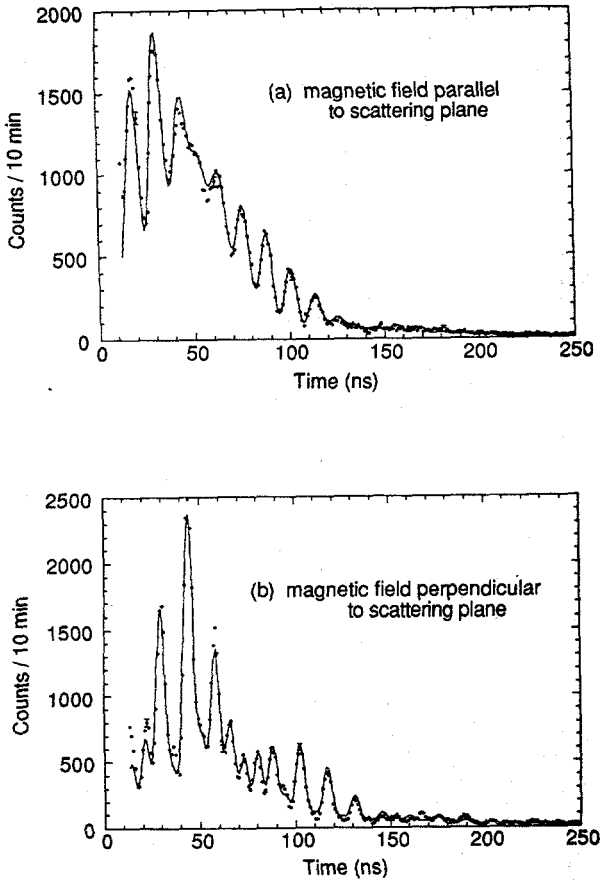

Figure 1

Time distribution of X rays resonantly diffracted from the YIG(002) planes. The solid curves are dynamical diffraction calculations. The internal magnetic field was found to be 368±2 kG, and the electric quadrupole splitting was -0.89±0.01 mm/s. (a): Magnetic field approximately parallel to the incident and scattered beams, in the scattering plane. (b): Magnetic field perpendicular to the scattering plane and parallel to the polarization direction of the incident light.

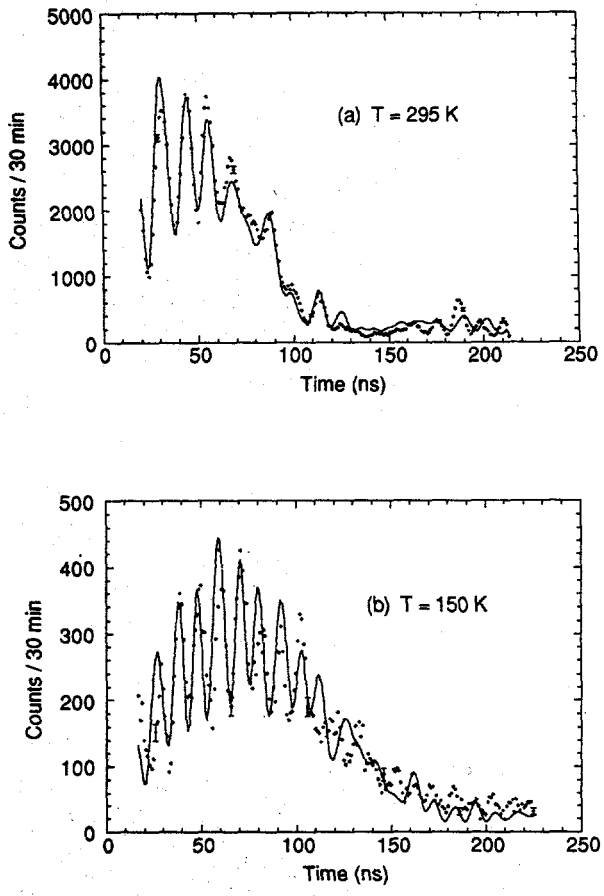

Figure 2

Time distribution of X rays resonantly diffracted from the YIG(0 0 10) planes. The fitting procedure was the same as that used for the curves in Fig. 1. (a): Sample temperature = 295±2 K. Magnetic field = 368±1 kG; electric quadrupole splitting = -0.85±0.03 mm/s. (b): Sample temperature = 150±7 K. Magnetic field = 429±4 kG; electric quadrupole splitting = -0.54±0.04 mm/s.

GRAZING INCIDENCE X-RAY DIFFRACTION STUDIES OF POLYMER FILMS

B. J. Factor
Department of Applied Physics
Stanford University

T. P. Russell
M. F. Toney
IBM Almaden Research Center

INTRODUCTION

The behavior of polymer molecules at the air/polymer interface is of both scientific and technological importance. The presence of an interface places restrictions on the conformations of the molecules near the interface, and, consequently, the structure of the polymers near the interface can be substantially altered [1]. To enable the investigation of polymer structure as a function of distance from the air/polymer interface, the technique of grazing incidence x-ray diffraction (GIXD) has been employed. The goal of this study is to examine the near surface structure of several types of polymers and compare the surface structure with that found in the bulk.

In GIXD, the x-ray beam impinges on the sample at angles close to the angle for total external reflection, typically 3mrad for polymers using $\lambda = 1.56$Å. By varying the incidence angle of the x-rays, the x-ray penetration depth can be varied from 50Å to microns [2]. For the penetration depth to be well defined, the angle of incidence must be well defined as well, and, therefore, the divergence of the the incident x-ray beam must be small, typically 1mrad or less. This requirement along with the small scattering volume and the low scattering power of hydrocarbon polymers necessitates the use of synchrotron radiation.

The polymer poly(hexyl-pentyl)silane (PHPS), containing a silicon backbone with two pendant alkyl groups, n-pentane and n-hexane, attached to each silicon atom, was investigated. Due to the silicon atoms in the backbone, PHPS scatters x-rays more strongly than the corresponding hydrocarbon analog. Steric hinderance among the sidegroups stiffens the polymer chain, changing what would be a flexible polymer without sidegroups into a stiff, rodlike polymer when the sidegroups are large. Consequently, the PHPS chains pack in a well defined manner. In contrast to other polyalkylsilane polymers, PHPS, due to the assymmetry of the sidegroups, is not crystalline at room temperature where the measurements reported herein were performed.

EXPERIMENTAL

PHPS with a molecular weight of 38,700 and a polydispersity of 1.6 was dissolved in isooctane at 2.4%. This solution was cast onto a polished 7.5cm diameter by 5mm thick Si(100) substrate, spun at 2×10^3 rpm and annealed at 90°C for 2hrs. to remove excess solvent. A film with a thickness of 2350Å and an rms roughness of 5-6Å at the air/polymer and polymer/substrate interfaces, as determined by X-ray reflectivity, was obtained.

GIXD measurements were performed in August 1989 on beam line X20C at the National Synchrotron Light Source at the Brookhaven National Laboratory. A pair of W/Si multilayers with a d-spacing of 23Å was used to monochromate the incident x-rays at a wavelength of $\lambda = 1.56$Å with a 1% bandwidth. Scattering was performed with a four circle goniometer (with standard $\theta, 2\theta, \chi$ and ϕ motions) in two different scattering geometries in order to examine electron density correlations both parallel and perpendicular to the plane of the film. In the first case, which will be referred to as "in plane" GIXD, the sample lay nearly vertical, and the angle of incidence, α, was selected by appropriate motion of χ and θ angles according to the relation $\sin\alpha = \sin\chi \sin\theta$. In the second case, which will be referred to as "out of plane" GIXD, the sample lay nearly horizontal, and the angle of incidence was chosen by movement of the θ angle In this geometry, the scattering vector tilts at an angle θ with respect to the surface normal. For both geometries, the divergence of the incidence angle was 1mrad. The data are plotted against $q = \frac{4\pi}{\lambda} \sin\frac{1}{2}(2\theta)$.

During the measurements, the sample lay in a helium environment to prevent oxidation. Nonetheless, degradation of the polysilane samples was noted during the measurements. An increased scattering background was observed, with little change in position and intensity of the diffraction peaks. The samples were translated periodically in order to ensure that undamaged portions of the sample were being observed.

RESULTS AND DISCUSSION

The PHPS powder diffraction pattern (fig. 1) from a 200μ thick film has sharp peaks at 0.492, 0.855, 0.987, and 1.31Å^{-1}. The peak positions in the pattern have a ratio of $1:\sqrt{3}:2:\sqrt{7}$ which is indicative of a hexagonal packing of the polymer chains with an interchain spacing of 14.7Å. The 1.32Å^{-1} peak is superimposed on a broad peak which arises from the packing of the hexyl and pentyl sidegroups. The sharpness of the peaks indicates the hexagonal chain packing is coherent over a large distance of at least $2\pi/\Delta q \simeq 300$Å.

"In plane" and "out of plane" GIXD were performed on the 2350Å PHPS film for several different α. For the "in plane" measurement, the diffraction in the region from 0.4-0.5Å^{-1} changes dramatically with α (fig. 2). At the

critical angle, $\alpha = 0.15°$, the peak at $0.492Å^{-1}$ has a large shoulder. With greater surface sensitivity, the shoulder develops into a separate peak located at $0.44Å^{-1}$ when $\alpha = 0.12°$, and the two peaks are almost equal in intensity when $\alpha = 0.10°$. The peak at $0.44Å^{-1}$ originates from a change in the electron density correlation parallel to the surface which could be associated with a novel structure at the surface. Modelling of the data are consistent with the notion that the novel surface structure penetrates 200-300Å into the bulk of the film.

For the "out of plane" GIXD, the $0.492Å^{-1}$ peak does not change in position or structure as α is varied, except for a small broadening due to the fact that the penetration depth approaches the same length scale as the coherence length. At the $0.492Å^{-1}$ peak, $\theta = 3.5°$. Therefore, the density correlations tilted 3.5° from the surface normal remain unchanged with changes in surface sensitivity. This indicates that the novel surface phase has the same density correlations nearly perpendicular to the surface as in the bulk of the film.

In order to precisely determine the structure of the novel surface phase, future GIXD measurements will be performed with the scattering vector positioned at arbitrary angles away from the surface normal.

REFERENCES

[1]Kumar, S.K.; Vacatello, M.; Yoon, D.Y. *J. Chem. Phys.*, 89,5206(1988).

[2]Fisher-Colbrie, A. *Ph.D. Thesis,* Stanford University, 1986.

ACKNOWLEDGEMENTS

This research is supported by the Department of Energy through the Office of Basic Energy Science, and IBM. The x-ray powder diffraction measurement of PHPS was performed by P. Iannelli at IBM.

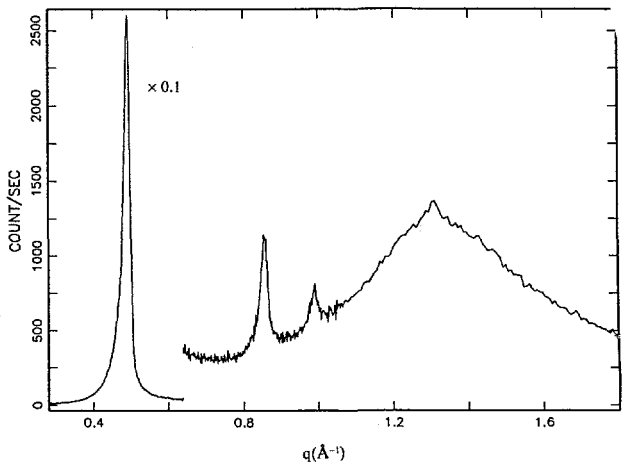

Figure 1: Plot of x-ray powder diffraction for 200μ thick film of poly(hexyl-pentyl)silane.

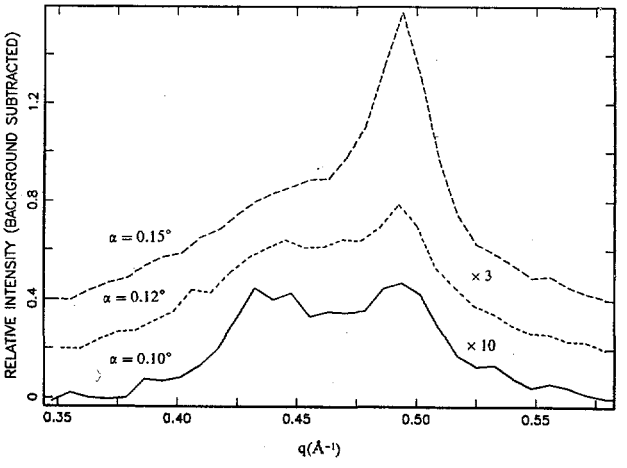

Figure 2: Plot of grazing incidence x-ray diffraction for 2350Å film of poly(hexyl-pentyl)silane for several angles of incidence. The scattering vector is parallel to the film surface. The angle for total external reflection is $\alpha = 0.15°$

Static Structures of Associating Polymers and DNA Fragments via Small Angle X-Ray Scattering

Alice P. Gast, Frans Leermakers, Kathleen Cogan, and Jennifer Raeder
Department of Chemical Engineering
Robert Pecora, John Tracy and Mark Tracy
Department of Chemistry
Stanford University, Stanford, CA 94305 USA

Introduction

Amphiphilic polymers have a tendency to associate in solution. When linear diblock copolymers are dissolved in a solvent selective for one block, they can form spherical micelles, semicrystalline aggregates or extended micellar or vesicular structures. We have been studying two such systems, poly(ethylene oxide)-polystyrene (PEO-PS), and poly(methacrylic acid)-poly(butyl methacrylate) (PMAA-PBMA), in cyclopentane, a selective solvent for polystyrene and PBMA. From light scattering studies(1) we have found that micelles from PEO-PS can be extremely sensitive to the presence of trace amounts of water in the cyclopentane solutions. Similarly, the PMAA-PBMA structures are influenced by water as well as ionic impurities.

It is our intention to study these structures in more detail with small-angle x-ray scattering, and in particular, we wish to compare the spherical structures formed from block-copolymers with those predicted for a multi-arm star polymer(2). Each arm is represented by a succession of blobs with blob size increasing from the center to the outside of the star. Single chain behavior is found within each blob with a local concentration varying inversely with blob size. Logarithmic plots of scattering intensity versus scattering vector provide information regarding concentration profiles within the polymer structures. Differences from single chain scaling behavior become more pronounced with increasing number of arms in a micelle or star polymer. Beyond the flat Guinier region, scattering from single chains decay with a slope related to the Flory swelling exponent. For star-like structures, the slope approaches -4 as the density profile approaches that of a solid sphere. The slope should eventually reflect single chain scaling behavior when q is large enough to probe within the blobs comprising the star arms.

Experimental

The polymers, described in Table 1, will be denoted by listing the number of repeat units in each block. We prepared solutions of PEO-PS block copolymers in cyclopentane with varying amounts of water as described before (1). We made similar solutions of PMAA-PBMA in cyclopentane with varying amounts of water and 1M NaCl added. The small angle scattering experiments were carried out at NSLS beamline X-12B under the guidance of Malcolm Capel, beamline supervisor. With the current configuration at this station, scattering vectors from q=0.008 to 0.1 A^{-1} were accessible.

Table 1.

Polymer	M.W.	N_A/N_B	R_h(nm)		R_g(nm)
PMAA/PBMA	6,488	6/42	6.0		4.0
(DuPont)	13,762	4/92	4.3		4.8
PEO/PS	11,140	65/80	11.6	(dry)	11.4
(Polymer Labs)			19.7	(wet)	18.5
	187,500	170/1730	47.0	(wet)	

PMMA-PBMA Results

We found from our preliminary experiments that the PMAA-PBMA copolymer exhibited a strong scattering signal, easily measurable within five minutes of beam exposure. Logarithmic plots of scattering intensity against scattering vector, shown in Figure 1, clearly distinguish between micellar solutions as in the 6/42 sample, and single chains found in 4/92 Scattering from single chains reveals near theta conditions from slope of -1.8 on log(I) vs log(q), close to minus the inverse of the Flory exponent. Micelles, having a higher density and more compact spherical structure, show a steeper slope of -4.3, typical of the Porod envelope for scattering from spheres(2). At high q we expect to see another transition to a lower slope of approximately -2 which would reflect scattering from the semidilute chains within the blobs comprising the star arms. Additional experiments probing wider q ranges are planned.

We observe a large Guinier scattering region for both polymers. Guinier plots provided radii of gyration to be compared with hydrodynamic radii found from dynamic light scattering presented in Table 1 (3). We find that the ratio of R_g to R_h changes from 0.67 for the micelles to 1.12 for the single chains; the theoretical ratio for solid spheres is 0.77 while for Gaussian chains we expect 1.4-1.5 (4).

PEO-PS Results

The PEO-PS block copolymers associate into larger micelles than those described above. Our largest sample, 170/1730, having 170 units of EO and 1730 units of styrene, forms micelles with an expected R_g on the order of 30 nm; this radius will be measurable after the scheduled improvements at X12B. Log-log slopes of approximately -2 throughout the q-range investigated reveal near theta conditions within the blobs comprising the star arms. Smaller q is necessary to measure star-like behavior.

The measured q-range corresponds to the intermediate scaling region for micelles formed by a 65/80 sample. Figure 1b) illustrates the scattering curves for 1 wt% solutions saturated and unsaturated with water. Several features indicate that the saturated micelles have a higher aggregation number; i.e., more arms. Scattering from the saturated solution exhibits a change in slope from -2.3 to -1.4 at a q~2.5×10^{-2} A^{-1}, similar to changes seen in molecular dynamics simulations(2) of star polymers with 10 or more arms. The leveling off at small q for the unsaturated solution signifies the approach to the Guinier region and hence, a smaller radius of gyration than that for the saturated micelles. The blobs comprising the outermost layer of the star decrease in size with increasing number of arms. Therefore, a larger q is necessary to probe the single chain behavior within the blobs of the saturated micelles than for the unsaturated micelles. A value of -2 is seen for the limiting slope in the unsaturated solution, as expected, since polystyrene chains are at near theta conditions in cyclopentane at room temperature.

The experimental q range included enough of the Guinier region for the 65/80 spherical micelles to estimate radii of gyration, listed in Table 1. Ratios of radius of gyration to hydrodynamic radius on the order of unity for both wet and dry micelles suggest concentration profiles intermediate to that for Gaussian chains and solid spheres.

The majority of our samples warrant scattering measurements at smaller angles. In addition to better resolving the Guinier region, we plan to extrapolate absolute intensities to q=0 to determine micelle aggregation numbers. Since polystyrene and poly(ethylene oxide) have similar electron density contrast in cyclopentane, we minimize the complications due to composition polydispersity prevalent in static light scattering measurements of this system. We also have light scattering and microscopy evidence that rod-like or lamellar structures replace the spherical micelles as we change copolymer, water and salt concentrations. We need smaller scattering vectors to measure thicknesses or diameters of these structures.

DNA Results

Preliminary analysis indicates results consistent with a rod-shaped molecule. The slope of the Log(I*G) vs Q*Q plot gives a cross-sectional R_g of 7A, achieved after 40 minutes with a sample concentration of 0.2 wt%. Higher concentrations should yield more than adequate signal. In the future, we wish to examine smaller scattering vectors in order to gain information on the persistence length of the DNA and higher moments of the scattering function. We also wish to measure the cross-sectional Rg of the super-helical form of our 2311 base pair plasmid, as this has not yet been characterized.

References

1. Cogan, K. A. and Gast, A. P., *Macromolecules*, to appear March (1990).
2. Grest, G. S., Kremer, K. and Witten, T. A., *Macromolecules*, **20**, 1376 (1987).
3. Raeder, J. and Gast, A. P., *in preparation.*
4. Xu, R. and Chu, B., *Macromolecules*, **22**, 3153 (1989).

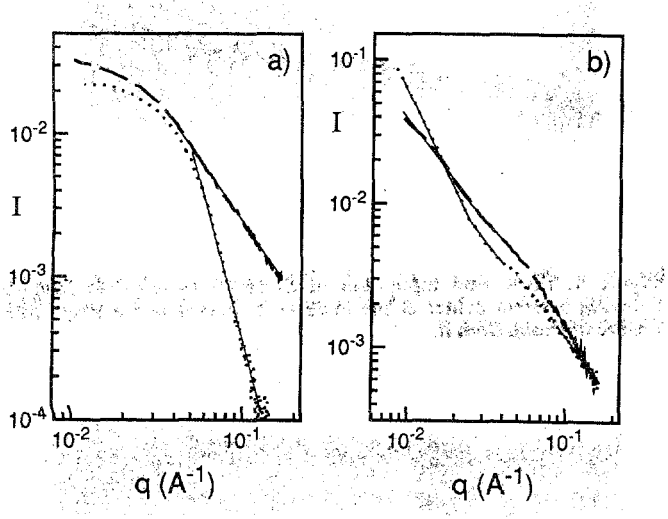

Figure 1. Log-log plots of intenstiy versus scattering vector. a) PMMA/PBMA solutions: --- 4/92 slope of -1.8 at high q indicates single chains, ... 6/42 slope of -4.3 at high q indicates compact spherical micelles. b) PEO/PS = 65/80 solutions: --- unsaturated and ... saturated with water. Slopes of -1.4 and -2.3 at low q and -2.0 and -1.5 at high q for unsaturated and saturated solutions, respectively, reveal an increase in aggregation number upon the addition of water.

Acknowledgements

This work was supported by du Pont Marshall Labs and the NSF-MRL Program through the Center for Materials Research at Stanford University. We received a travel grant through SSRL to record data at NSLS at Brookhaven National Labs. We thank Malcolm Capel for his assistance.

WHITE BEAM AND SECTION TOPOGRAPHIC SURVEY OF MO THIN FILMS ON SILICON SUBSTRATES

L. H. Lee[1], H. Y. Wang[2], H. J. Wu[3], Z. U. Rek[4], J. C. Bilello[1]

[1] Department of Materials Science and Engineering, University of Michigan, Ann Arbor, MI 48105

[2] Department of Materials, Shanghai University of Science and Technology, Shanghai, China

[3] Shanghai Research Institute of Semiconductor Devices, Shanghai, China

[4] Stanford Synchrotron Radiation Laboratory, Stanford, CA 94309

Introduction

Mo thin films are useful in a wide variety of high temperature applications. These films can be produced by sputter deposition onto a substrate followed by a heat treatment. Strains are often developed due to the deposition process, phase transformations of the deposited material, or the difference in the thermal expansion coefficient between the Mo layer and the substrate. The magnitudes of the residual strains are related to the morphology of the film and the degree of coherence, both are vital factors to the performance and reliability. In this work the quality of as-deposited Mo films on Si (100) substrates, as well as some blank Si wafers were surveyed by white beam Laue topography and section topography. The purpose was to measure the quality of the substrates to ensure good base material for future deposition work, and to compare with the coated wafers.

Experimental

Mo thin layers were deposited onto Si (100) substrates, cleaved into quarters from 3 inch wafers, at room temperature by argon plasma sputtering. The operating parameters were set at 2200 volts for target-anode acceleration voltage with 150 mTorr argon pressure. A low deposition rate of 0.6 Å/sec was maintained. Film thicknesses range from 18 to 290 Å. Projection topographs and section topographs were taken with a Mo filter on the incident slit and recorded on Kodak SR-5 single sided x-ray films. Specimen-film distance was set at 100 mm and typical exposures took 30 to 60 seconds for projection topographs, 4 to 6 minutes for single slit section topographs. These experiments were carried out at SSRL on beamline 2-2.

Results

A total of 16 bare quarter-wafers were surveyed by projection topography, usually at more than one beam-size area (typically 10 mm x 4 mm). Most of the topographs show even contrast throughout the reflection spots, whereas some show thin stripe-like feature on selected areas of a quarter wafer. These stripes could be grown-in defects in the Si boule, such as twinning or stacking faults. Slip bands were also observed. Figure 1 illustrates a typical defective Si (100) as-received sample. Observable defects have to be taken into consideration during subsequent film growth. Substrates coated with 18, 35, 65, 130, and 290 Å Mo films were inspected by projection topography in the symmetric setting, and section topography in both symmetric and asymmetric setting. Many section topographs show Pendellosung fringes (Fig. 2), which are currently being analyzed with the aid of digital image processing in the authors' laboratory.

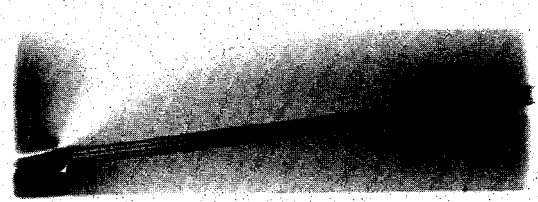

Figure 1. Projection topograph of Si (100) as-received sample showing a strain center at the lower-left corner and a stripe-like feature initiating from it.

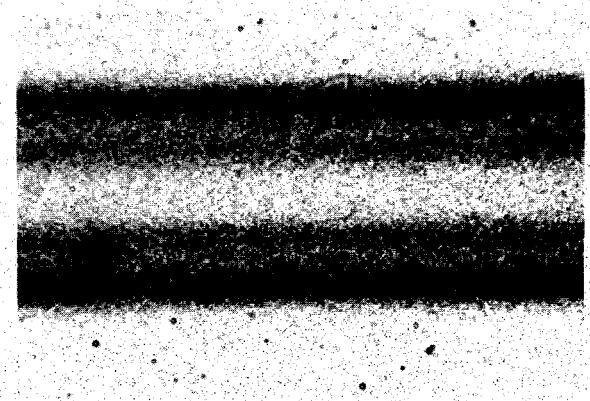

Figure 2. A segment of section topograph (x200) showing Pendellosung fringes of a Si (100) specimen coated with 18 Å Mo film.

Acknowledgements This work was supported by the Army Research Office under contract No. DAAL03-87-K-0049.

IN SITU TOPOGRAPHIC OBSERVATIONS DURING DYNAMIC LOADING OF A MO GRAIN BOUNDARY

L. H. Lee[1], J. C. Bilello[1], Z. U. Rek[2], H. Y. Wang[3]

[1] Department of Materials Science and Engineering, University of Michigan, Ann Arbor, MI 48105

[2] Stanford Synchrotron Radiation Laboratory, Stanford, CA 94309

[3] Department of Materials, Shanghai University of Science and Technology, Shanghai, China

Introduction

The early stages of plastic deformation of Mo single crystals were studied by white beam topography. In situ observations of the crystals under step-wise loading conditions were performed with a miniature tensile stage[1], while simultaneously recording transmission topographs. The objective of this work was to obtain information on slip nucleation behavior at the presence of a low angle grain boundary, as compared to the effect of other sites of stress concentration such as a crack or precipitate. In the vicinity of these regions in a sample, an enhanced intensity is observed on a white beam topograph[2]. This is directly related to the lattice distortions in the local region of the crystal which creates a severe three dimensional bending in the lattice planes. The lattice curvature in this local region can be estimated by the measured width of the enhanced contrast zone. Studies of these effects for a number of independent refections allows one to sort out the local dislocation density[3], and the symmetry of the dislocation network in the region[4].

Experimental

The tensile specimens were cut from a molybdenum single crystal sheet with surface normal near [1 1 4] and the tensile direction near [$\bar{1}$ 1 0]. The specimens were mechanically and electrolytically polished to a finished dimension 25mm x 7mm with a gauge length of 11 mm and thicknesses within 200 and 300 μm. A crater-like notch, serving as a stress concentration site, was introduced by spark-discharge at the edge of one specimen which contains no subgrain boundaries. Each exposure, which typically took 3 to 4 minutes, were taken after load relaxation had stabilized for either the loading or unloading step. The experiments were performed at SSRL on beamline 2-2.

Results

Each high resolution picture taken on Kodak SR-5 single sided x-ray film captured up to 60 (h k l) reflection spots. Analysis of the large number of topographic images was facilitated by the use of digital image processing, which allowed detailed study of the general development of microplasticity and slip nucleation in many slip systems. Lattice distortion delineated by enhanced diffraction contrast in streak shape initiating from localized region either near the notch or the subgrain boundary were observed on many reflections at a load corresponding to a fraction of the bulk yield stress (Fig. 1 and 2). The image contrast at stress concentration sites of most reflections remain unchanged upon unloading to no-load state, while some reflections move out of contrast partially or completely indicating lattice tilting and/or twisting. The lattice distortion and plastic zone curvature at each loading/unloading step are being analyzed from the large data set. The preliminary results show that the lattice near the subgrain boundary distorted to a significant extent at 24 MPa, whereas no slip bands were initiated at 60 MPa while the lattice were severely distorted without the presence of a subgrain boundary. For the single crystals, slip started at the stress concentration sites at the sample edge; whereas the presence of the low angle boundary caused strain localization and, at higher stresses, boundary breakdown.

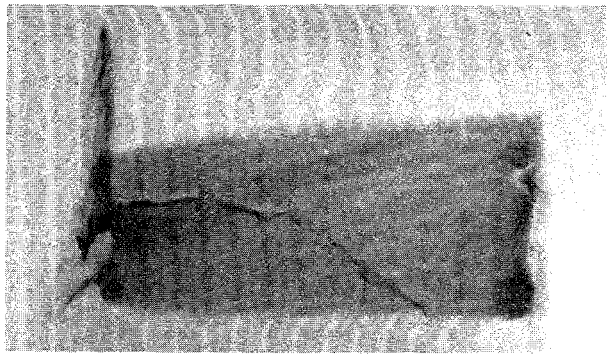

Figure 1. (3 1 0) reflection spot at 24 MPa load showing a low angle grain boundary and local enhanced-contrast streak running vertically on the left side.

Figure 2. (3 1 0) spot at 60 MPa load showing streak from the notch (center of top edge), and the severe lattice distortion of the entire speciment without the presence of a subgrain boundary.

References:

1. V. Wakharkar and J. C. Bilello, presented at the 1986 APS Spring Meeting, Las Vegas, NV., 1986 (Unpublished).
2. D. K. Bowen, A. B. Hmelo, S. T. Davies, and J. C. Bilello, Daresbury Laboratory Journal, 1982, 47.
3. A . B. Hmelo, J. C. Bilello, S. T. Davies and D. K. Bowen, in Applications of X-ray Topographic Methods to Materials Science, eds. S. Weissmann, F. Balibar, and J-F. Petroff, Plenum Press, NY, 1984.
4. J. C. Bilello, in Mechanical Properties and Behavior of Solids: Plastic Instabilities, eds. V. Balakrishnan and C. E. Bottani, World Scientific Publishing Co., Singapore, 1986. pp. 1-46.

Acknowledgements This work was supported by the U.S. Department of Energy, under contract No. DE-FG03-88ER45350.

MODELING AND EXPERIMENTAL MEASUREMENTS OF RESIDUAL STRESS USING SYNCHROTRON RADIATION

J. F. Shackelford, B. D. Brown, and J. S. Park
Department of Mechanical Engineering
University of California at Davis, CA 95616

R. W. Ryon, and Elane Flower
Engineering Sciences Division
Lawrence Livermore National Laboratory
Livermore, CA 94550

Introduction

This work was an extension of recent, related efforts by Lawrence Livermore National Laboratory (LLNL) to identify the most effective method for determining residual stress in metal components using nondestructive techniques [1-3]. These activities included neutron diffraction, x-ray diffraction, and ultrasonics. In 1988, we recognized that the newly installed UC/LLNL beam line at the Stanford Synchrotron Radiation Laboratory (SSRL) could be applied to determining lattice strains in a fashion helpful to our overall research goals. Pioneering work using synchrotron radiation for stress measurements had been reported in Japan [4]. Benefits of a synchrotron source to our studies include a highly intense and monochromatic beam with variable energies, allowing significant sample penetration, and with very low beam divergence.

Experimental Materials and Methods

The extensive time required for system development at SSRL limited experimental runs almost exclusively to one specimen. This was a ground, ball bearing steel with a highly characterized [6,7] surface-stress state (from its role in an international round robin testing program).

Much of the beam time allotted for this study (six eight-hour shifts) was devoted to experimental set-up , especially mechanical alignment, and to electronic trouble-shooting. A primary recommendation for future studies of this type is to provide for precision x-y-z translational positioning control (as well as rotational control about z) for the goniometer table. A secondary recommendation is to isolate the inlet beam slits from the goniometer table. Experimental measurements were taken with a limited number of beam energies. Most work was done using energies of either 20 or 12 keV. Useful data were taken using harmonics at 10 and 24 keV, respectively. Time did not permit obtaining useful results from other fundamental energies or from higher harmonics of the 10 and 12 keV beams.

Much of the effort, following alignment efforts, concentrated on attempting to reproduce the conventional stress measuring technique of specimen tilting. Both forward (iso-) tilting and side tilting methods were attempted. Side tilting has certain advantages especially for high beam energies and associated, smaller Bragg angles. Unfortunately, experimental results from simple tilting techniques are highly dependent on precise specimen fixturing. The alignment problems noted above made such measurements impractical. Fortunately, analytical techniques are available for measurements on untilted samples allowing for some useful results which are described in the next section. "Untilted" refers to a specimen orientation such that the specimen surface is parallel to the crystal planes responsible for a given diffraction peak. This orientation is maintained by conventional diffractometers in which the detector has twice the angular rotation rate as the specimen.

Results and Discussion

Diffraction peaks for the (211) plane of the ferritic, round robin specimen (ball bearing steel 100 Cr6) were obtained at 10, 12, 20 and 24 keV beam energies. Figure 1 shows the measured, depth-averaged stress gradient together with the true stress gradient found by an analysis method developed by us [5]. The results are in good qualitative agreement with the results of the round robin tests [6,7].

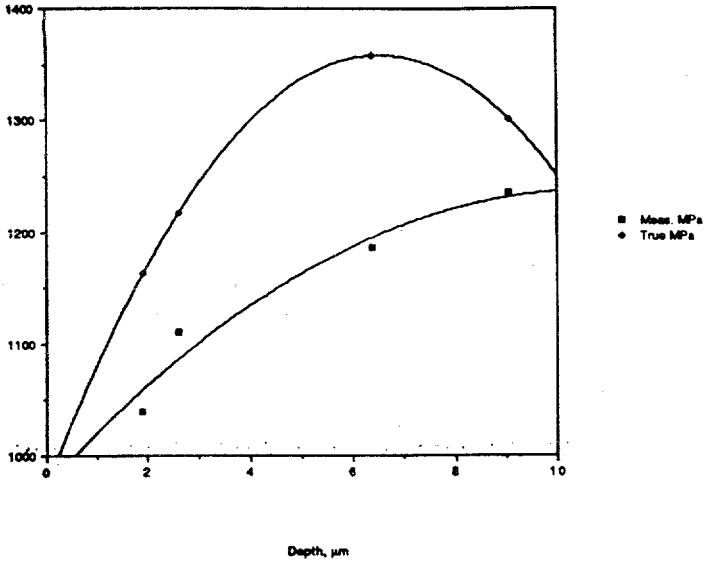

Figure 1. Measured depth-averaged stress gradient together with the true stress gradient.

Future Work

The work presented in this report indicates the preliminary useful results of the immediate, post-experiment analysis. We intend to carry on additional analysis of the results in conjunction with our ongoing studies of residual stress in cooperation with LLNL. The first effort of this type will be to carefully analyze the diffraction peak shapes for the 10, 12, 20 and 24 keV step scans of the (211) peak. Specific information about microstrain in the material is available from such analyses [10].

Finally, it is hoped that further beam time at SSRL will be available in the near future for the purpose of continuing these studies. Encouraging initial results were obtained during a relatively brief allotment of time, given that time had to be devoted to system alignment. We feel that we are poised to obtain significantly more results, given an additional block of experimental time. A primary goal would be to have sufficiently precise alignment to allow tilting measurements to be made. Equally important would be to use higher harmonics of energy to allow substantially deeper penetration of at least 50 micrometers.

ACKNOWLEDGEMENT:

Special thanks are due to Lane Wilson for his management of Beam Line X. His patience and helpfulness, under grueling circumstances, was a source of amazement to all of us.

REFERENCES:

1. E.C. Flower, S.R. MacEwen, and T.M. Holden, *FEA Predictions of Residual Stress in Stainless Steel Compared to Neutron and X-Ray Diffraction Measurements*, Lawrence Livermore National Laboratory, Livermore, California, UCRL 96643 (August 1987).
2. J.F. Shackelford and B.D. Brown, *A Critical Review of Residual Stress Technology*, Final Report, LLNL Intramural Order 5710705 (September 1987).
3. J.F. Shackelford and B.D. Brown, *Analysis of Triaxial Residual Stress Measurement Using High-Energy X-Ray Diffraction*, Final Report LLNL Intramural Order 2660503 (January 1989).
4. Y. Yoshioka, et al., "X-Ray Residual Stress Analysis in Textured Steels by Use of Synchrotron Radiation Source," *Residual Stresses in Science and Technology*, Vol 1, E. Macherauch and V. Hauk, eds., Verlag, Germany, (1987), pp. 369-376.
5. J.F. Shackelford, B.D. Brown and J.S. Park, *Modeling and Experimental Measurement of Residual Stress Using Synchrotron Radiation*, Lawrence Livermore National Laboratory, LIvermore, California, UCRL 2119 (May 8, 1989).
6. E. Brinksmeier, et al., "Residual Stresses--Measurement and Causes in Machining Processes," *Annals of the CIRP*, **31**, (2) 491-510. (1982).
7. J.F. Shackelford, *University of California Participation in the CIRP Round Robin of Residual Stress Measurement*, Lawrence Livermore National Laboratory, Livermore, California, UCID 19838 (July 1983).

X-RAY TOMOGRAPHIC MICROSCOPY OF METAL MATRIX COMPOSITES

J. H. Kinney[1], U. Bonse[2], M.C. Nichols[3], Q.C. Johnson[1], R.A. Saroyan[1], R. Nusshardt[2], and F. Busch[2]

[1]Lawrence Livermore National Laboratory, Livermore, CA 94550
[2]Department of Physics, Dortmund University, Dortmund FRG
[3]Sandia National Laboratories, Livermore, CA 94550

Introduction

Many studies have addressed the role that fibers play in impeding crack advance. In metal-matrix composites, such as aligned SiC fibers in aluminum, the fibers are sufficiently strong and the interface is sufficiently weak that the crack induces debonding along the fiber-matrix interface. As the crack opens, many unbroken fibers span the crack. This bridging process locally reduces the crack driving force if fiber motion can be restrained through interfacial friction.

Experimental observations of crack propagation in composites frequently rely on SEM observations of metallographic sections. In SEM measurements, cracks are usually held open by driving a wedge into them or by using epoxy impregnation to hold cracks open. These SEM observations are very valuable; nevertheless, there is some interest in examining unaltered cracks three-dimensionally, well away from external surfaces. Noninvasive imaging of the three-dimensional structures surrounding cracks will place SEM observations on firmer footing, as well as address such questions as: the role preexisting damage plays in crack propagation; where fibers break within the composite; and over what distance does interface debonding occur.

Experiment

X-ray Tomographic Microscopy (XTM) differs from conventional optical and electron-beam microscopy in that the sample need not be destroyed by the characterization process. There is no requirement for flat optical surfaces or thin sections, and thus it is possible to examine materials in their unaltered state. The instrument, described in detail elsewhere[1], requires a source of parallel x-rays (synchrotron radiation) and consists of a sample stage, a detector system, and an analyzing computer.

In the present study, a 1.5 x 1.5 x 10 mm specimen of an Al/SiC composite was examined with XTM on the 31-pole wiggler beamline at the Stanford Synchrotron Radiation Laboratory[2](SSRL). An x-ray energy of 21 keV was selected for good sample transparency and x-ray contrast between SiC and Al. Absorption data were collected at one degree intervals. This undersampling leads to some loss in image quality; nevertheless, the 33 μm diameter graphite cores and surrounding 140 μm diameter SiC sheaths are clearly visible.

Results

Figure 1 shows a single XTM slice of the composite from a set of 97 contiguous cross-sections obtained with the XTM. The slice thickness is 2.8 μm and the spatial resolution is ~5 μm. Cracks running longitudinally in the plane of the fiber layup are evident. These cracks, which do not penetrate the fiber, are believed to be due to incomplete consolidation and CTE mismatch between the fibers and the matrix. This explains the greater crack density near the exterior surfaces. Smaller cracks can be seen nucleating at the SiC/Al interfaces within the interior in response to these stresses.

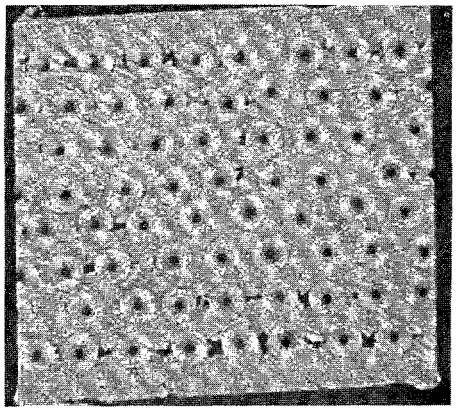

Figure 1: XTM cross-section of the Aluminum-matrix / SiC-fiber composite.

Figure 2 is a view of a single fiber showing the graphite core and the SiC sheath surrounding it. The change in columnar SiC subgrain size produced during the growth of the sheath is evident, as is the carbon-rich SCS-8 coating in the final few micrometers near the Al interface.

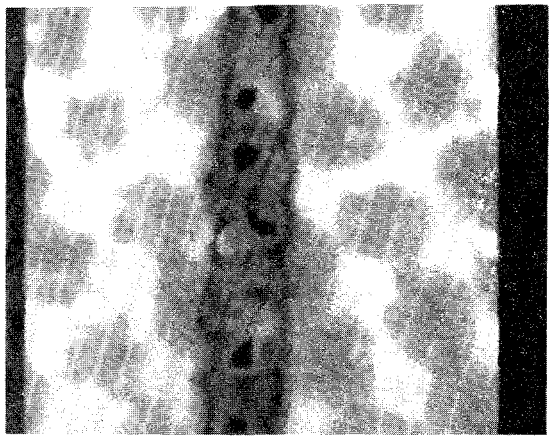

Figure 2: XTM cross-section of a single fiber.

What must be emphasized is that these XTM images have been taken of *unaltered* interior surfaces. XTM is nondestructive and no surface preparation is involved in the characterization. Because of this, direct observation of crack nucleation and growth is possible throughout *bulk* specimens *during* deformation testing. The availability of such data should have a profound effect on modeling of damage accumulation in metal matrix composites and other advanced materials.

References

1 J.H. Kinney, Q.C. Johnson, R.A. Saroyan, M.C. Nichols, U.Bonse, R. Nusshardt and R. Pahl, Rev. Sci. Instrum.,59,196 (1988).
2 The storage ring SPEAR was running at 3.3 GeV and nominally 30 mA. The wiggler field was 1.0T, only 60% of its rated field strength.

Acknowledgements

This work was performed under the auspices of the U.S. Department of Energy (DOE) by the Lawrence Livermore National Laboratory under Contract W-7405-ENG-48, by Sandia National Laboratories (Livermore) under contract AT-(29-1)-789 and by SSRL which is supported by the DOE's Office of Basic Energy Sciences and by the National Institutes of Health's Biotechnology Resource Program, Divisions of Research Resources. The work was also supported by BMFT (Bonn, West Germany) under Contract 03-B01DOR. The authors would like to thank Stuart R. Stock and T. Breunig of Georgia Institute of Technology for supplying the samples, and G. J. Mauger and W.N. Massey at Lawrence Livermore National Laboratory for their help in all phases of this work.

THIN FILM AND INTERFACE STRUCTURE

Joe Wong, Troy W. Barbee and L. M. Larson
Lawrence Livermore National Laboratory, Livermore, CA 94550

Experiments to both demonstrate sub-monolayer sensitivity and to study interfaces in the copper-tungsten binary have been performed on BL 10 at SSRL. Multilayer synthesis technology was used to sputter deposit tungsten-copper film on 3.75 cm x 10 cm x 0.25 cm superpolished fused silica x-ray optic flats. Tungsten layers 50 nm thick were deposited first and then overcoated "in situ" with copper layers designed to give surface concentrations of copper of 0.1, 0.5, 1.0, 2.0 and 5.0 monolayers (ML). Multilayer structures consisting of 5 ML tungsten/5 ML copper and 5 ML tungsten/1 ML copper were also synthesized. All structures were overcoated with 0.7 nm amorphous carbon to stabilize the film/ambient surfaces against contamination. The operating conditions at SSRL were abnormally poor [10 kG, <10 mA, 3.3 GeV]. Even under such conditions the copper EXAFS spectra from a 0.1 ML surface concentration film was easily acquired. These results demonstrate that surface coverages of 0.01 ML or less are accessible for study using this technique. In Fig. 1, the Fourier Transform of EXAFS signals for bulk copper, the 5 ML, 2 ML and 1 ML copper coverage on tungsten are given. The copper EXAFS signal at coverages of 2 ML and higher are clearly related to that of the bulk copper. At lower coverages EXAFS is significantly changed, appearing as expected for an amorphous solid. The interatomic distances derived from these data are consistent with these interpretations. Data indicate that the local environment of the copper in these very thin films is dominated by carbon from the passivating overlayer. Additionally, the near edge structure appears to change as the copper coverage decreases. This is consistent with evidence for an electronic interfacial bonding state between copper and tungsten that will dominate the low coverage samples.

EXAFS measurements were also obtained from the copper in the multilayer samples.

The copper in the 5 ML tungsten/5ML copper sample was disordered and appeared amorphous. In the 5 ML tungsten in this sample, by contrast, was disordered and appeared amorphous. In the 5 ML tungsten/1 ML copper sample the copper appeared to be body centered cubic, assuming the structure of tungsten.

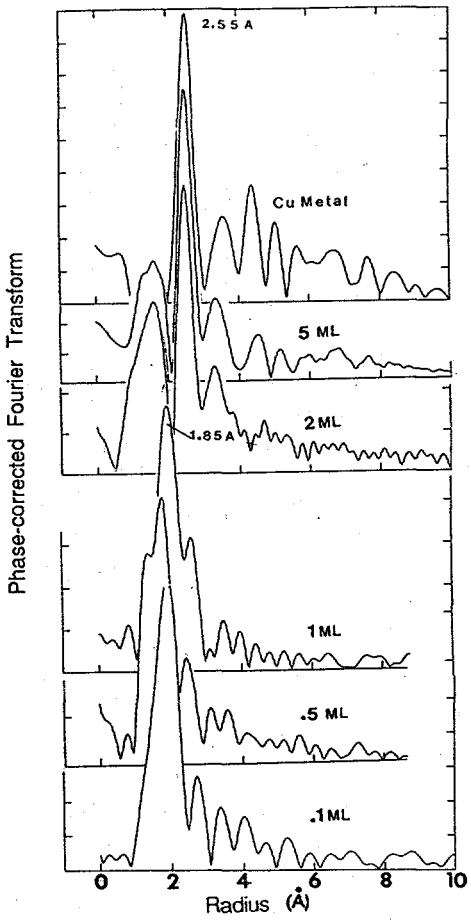

Fig. 1. Phase corrected Fourier transform of Cu K-edge EXAFS from Cu overlayers sputtered in a tungsten substrate at various coverages. A 70 A protective layer of amorphous C was sputtered on top of the Cu layer.

Biology Progress Reports

EXAFS and WAXS/DAS Analyses of Tc and Re Drugs and Tc-Metallothionein

Richard C. Elder and Edward Deutsch

Departments of Chemistry and Radiology and the Biomedical Chemistry Research Center

University of Cincinnati
Cincinnati, OH 45221-0172

Radipharmaceuticals based on technetium or radioactive isotopes of rhenium have been in use for diagnostic imaging and palliative agents (and more recently as therapeutics) for a number of years (1a,b). ^{99m}Tc, ^{186}Re and ^{188}Re are the isotopes involved, each of which provide gamma rays suitable for imaging, while the Re isotopes have short half-lives and are widely available via so-called Tc or Re "generators". These features make them attractive for use in formulating radiopharmaceuticals in a hospital setting.

Metallic complexes of Tc and Re with a variety of diphosphonate ligands ($O_3PCRR'PO_3^{4-}$) are the most useful for bone imaging agents and were the compounds studied. Depending on the method of synthesis and the identity of R and R', these complex mixtures have different biodistributions. They are in general difficult to crystallize. The crystal structure of the Tc-diphosphonate compound with R=R'=H (Technetium and methylene diphosphonate or Tc-MDP) has been determined (2) and an EXAFS structure characterization of an HPLC separated, 8 mM solution of this material was previously reported (3). More recently, studies of the compound Technetium hydroxyethylidene diphosphonate (Tc-HEDP) using EXAFS and the corresponding Re-HEDP using both EXAFS and WAXS/DAS techniques were performed at room temperature. In addition, samples of Tc bound to the liver protein metallothionein (provided by Maurice Morelock of DuPont), were also investigated with the same techniques but at 10-20K using a He flow cryostat.

EXAFS data were collected at SSRL beamline IV-3 (300K and 10K) and also at NSLS beamline X9A (at Brookhaven National Laboratory). The gross structural features of the M-HEDP compounds (M = Tc or Re) are quite similar. Each of the compounds has pronounced Fourier transform peaks in the 1.5-2.1 Å range and further peaks in the 2.3-3.4 Å range (fig. 1). The first peak (or peaks) are definitely associated with M-O bonds usually requiring two shells of oxygens for the best fits. Model parameters for these M-O bonds were taken from the KMO_4 salts, whose EXAFS were also measured. Meanwhile, the peaks at longer distances seem to result from M-M or M-P interactions (or both), but are much more difficult to extract and evaluate. Models for the latter parameters were taken from the $[M(DMPE)_3]^+$ compounds, where DMPE is the 1,2-Bis (dimethylphosphino)ethane ligand, and from metal foils.

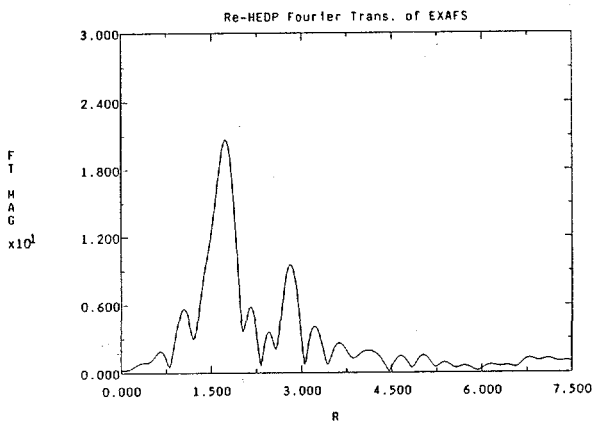

Figure 1: Fourier transform of Re-HEDP EXAFS showing the principal oxygen backscattering peak near 1.6 Å and the weaker but evident heavy metal backscatterer near 2.7 Å. The transform has not been corrected for phase shifts.

WAXS data were obtained from experiments performed at SSRL beamline VII-2 (low temperature) and at NSLS beamline X7A. These experiments were performed on Re-(HEDP) samples (provided by David Pipes and Karen Libson at Mallinckrodt Medical Inc.). Radial distribution functions (RDFs) were obtained showing peaks at roughly the same distances as suggested by the EXAFS experiment (fig. 2). However, better identification in terms of

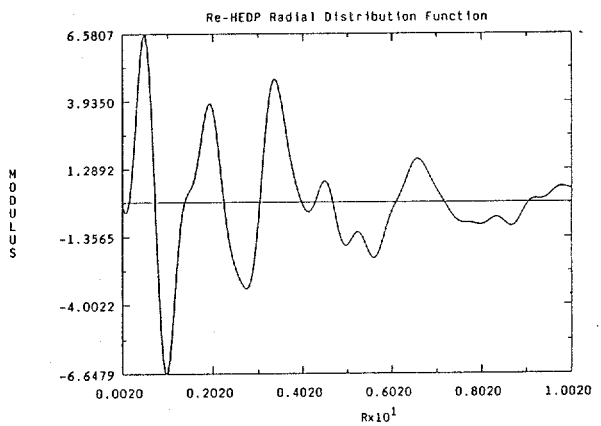

Figure 2: Radial Distribution Function calculated from X-ray scattering data of Re-HEDP. The first peak results from difficulty in normalization the peaks near 2.0 and 3.3 Å are in reasonable agreement with the conclusions of the EXAFS study.

coordination number and species bound will require cleaner, less noisy data at two energies for the extraction of differential distribution functions (DDFs) from a DAS analysis. This will require measurement of samples without crystalline impurities, at low temperature, with higher photon fluxes and/or greater beam stability, than has been available so far.

Tc metallothionein was prepared by incubating Zn metallothionien (MT) with varying amounts of Tc oxo glucoheptanoate. MT usually has seven binding sites at which a metal such as Zn or Tc may attach. Three samples of the protein were prepared: NEN1 containing 1-2 Tc atoms per MT, NEN2 with 3-4 Tc atoms per MT, and NEN3 with 5-6 Tc atoms per MT. The objective of this study is to: (1) assess protein structural changes resulting from substitu-

tion of TcO^{+3} for Zn^{+2} in Zn_7-MT and (2) determine the binding modes of Tc^{+5} to MT.

Approximately 5 mg of each sample was pressed into a pellet using coffeemate as a binder. EXAFS spectra of the compounds were then acquired about the Tc K edge at 1,047.3 ev. Full EXAFS scans were taken out to 16 $Å^{-1}$ in K space using a low temperature flowing helium cryostat. Each sample was fit for oxygen, sulfur, technetium, and zinc. Theoretical fits were used for the metal-metal interaction while empirical fits were used for the oxygen and sulfur atoms. Technetium-dioxo-tris-ethanedithiolate was used as a model for the metal-sulfur and metal-oxygen interactions but is far from adequate due to its extreme static disorder.

The calculations, at this point, give little insight as to the absolute coordination number, but a trend is evident from sample to sample. The technetium-oxygen bond distance and coordination number remain relatively constant. The technetium-sulfur coordination number decreases dramatically from NEN1 to NEN3 with coordination numbers of 2.66 atoms, 2.15 atoms, and 0.77 atoms. These trends are interesting and merit further study on subsequent trips with empirical parameters derived from better model compounds. Fits for the metal-metal interaction yield relatively consistent results of between one to one-half zinc or technetium at 2.60 Å.

In conclusion, trends throughout the series of compounds are evident. A dramatic decrease is seen in the coordination of sulfur to technetium as more metal is loaded into the protein. Further studies will be done to elucidate this phenomenon by examining both technetium and zinc EXAFS.

Support for this work is through the NIH (GM35404 and CA32863). Individuals involved in this project included W.B. Jones, J. Yuan and J. D'Amore.

REFERENCES

1a. Deutsch E., et al, Prog. Inorg. Chem. **30**, 75-139 (1983).

1b. Deutsch E., et al, Nucl. Med. Biol. **13**, 465-477 (1986).

2. Deutsch E., et al, Jour. Am. Chem. Soc. **102**, 2476 (1980).

3. Martin J.L., et al, Inorg. Chem. **28**, 2899-2901 (1989).

EXAFS, WAXS and DAS of Gold Based Drugs Used to Treat Rheumatoid Arthritis

Richard C. Elder* and Katherine Tepperman

Biomedical Chemistry Research Center
University of Cincinnati
Cincinnati, OH 45221-0172

Gold based drugs have been used for many years to combat rheumatoid arthritis. However, the form of these drugs circulating throughout the body, and the site of uptake is unknown. Gold metabolites of the oligomeric drugs enter the red blood cells (rbs's) of smoking patients but not of nonsmoking patients (1,2). Metabolites of auranofin (triethylphosphine)(2,3,4,6-tetra-O-acetyl-1-thio- -D-gluco-pyranosato-S)gold(I) enter rbc's irrespective of smoking habits (2,3). More subtle metabolic changes due to ligand exchange reactions of auranofin and HCN have not been fully investigated (4).

Cyanide binds to gold very tightly and the equilibrium competition of HCN and thiols for gold(I) favors cyanide (4). Our aim is to (1) study the competition of HCN with the phosphine and protein thiolate ligands of AlbSAuPEt$_3$, (2) determine the immediate environment around the gold center, and (3) develop a biochemical model for the metabolism of auranofin in smoking chrysotherapy patients.

X-ray absorption spectra were recorded at SSRL on beam line IV-3 about the gold L_{III} edge using a flowing liquid helium cryostat to cool the sample to 10 K. XANES studies yield the oxidation state information for gold in the samples. A hump in the XANES region at 11.928 eV is characteristic of a gold(I)-phosphorus interaction. In the sample of AlbSAuPEt$_3$ reacted with HCN, the gold was shown to be bound to a phosphorus atom and remained in the +1 oxidation state (Figure 1).

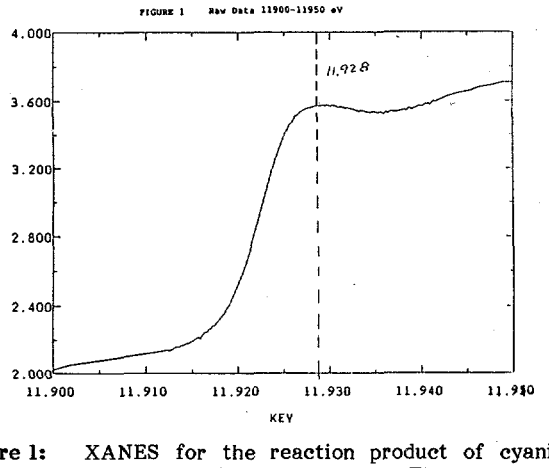

Figure 1: XANES for the reaction product of cyanide with albumin-S-AuPEt$_3$. The hump at 11.928 keV is characteristic of gold-phosphorus interactions.

Analyses of the EXAFS region of the spectra provide structural details of the average gold coordination environment. It is suspected that when HCN is reacted with AlbSAuPEt$_3$ that the gold(I) which is typically two-coordinate becomes three coordinate bound to sulfur, phosphorus and cyanide. The Fourier transform of the data shows two distinct peaks at 1.5 and 2.0 R + α (Figure 2). A backtransform of these two peaks shows a beat pattern in the reverse filtered Fourier transform. A two shell fit was performed using empirical parameters taken from a two

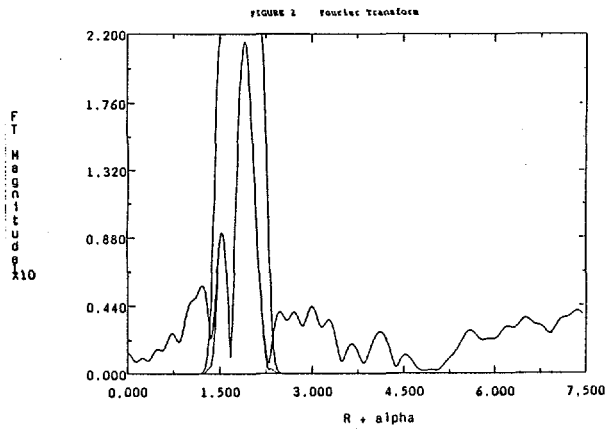

Figure 2: The Fourier transform of EXAFS for the material of Fig. 1. The peak near 1.6 Å corresponds to the Au-C interaction while that near 1.9 Å corresponds to the composite of the Au-S and Au-P interactions.

coordinate gold(I) phosphorus model compound and theoretical parameters for carbon. The fit yielded a three coordinate structure containing a carbon atom at 1.95 Å which compares well with 1.97 Å in the crystal structure of Et$_3$PAuCN. The second shell was fit with empirical parameters from the gold diphosphine structure, yielding two phosphorus atoms at 2.28 Å. However, it is impossible to determine whether this represents two phosphorus atoms or one phosphorus and one sulfur atom since EXAFS experiments can not differentiate adjacent elements in the periodic table. The crystal structure of Auranofin shows a gold-phosphorus bond at 2.26 Å and a gold-sulfur bond distance of 2.29 Å.

Our studies of this compound indicate that the gold is indeed three coordinate and that a cyanide is bound to the gold. The most probable structure would be the mixed ligand Et$_3$P and thiol-cysteine complex. However, evidence has shown that the mixed ligand complexes containing sulfur or phosphine and cyanide disproportionate in solution according to:

$$2\ Et_3PAuCN = [(Et_3P)_2Au]^+ + [Au(CN)_2]^-$$

Therefore, a structure containing two phosphines and a cyanide should be considered as well.

Gold-gold interactions due to clustering in biological systems were studied also. Three gold dimeric species were studied $[Au(dppm)_2Br]_2$, $[Au(dppm)_2PF_6]_2$, and $[Au(dppp)_2Br]_2$ at low temperature to determine whether the weak gold-gold interactions could be observed. A peak corresponding to this interaction is absent in the Fourier transform at room temperature. This can be attributed to the high thermal disorder caused by vibration of the gold atoms with respect to one another. By reducing the sample temperature to that of liquid helium, thermal disorder should be substantially reduced and a peak might appear in

the Fourier transform corresponding to the gold-gold interaction.

Two peaks are seen in the EXAFS of $[Au(dppm)_2PF_6]_2$, one at 1.82 R + α and one at 2.79 R + α (Fig. 3). Fits of the two peaks yielded two phosphorus atoms at 2.33 Å and a gold-gold interaction at 2.96 Å. These correspond very well with the crystal structure distances of 2.31 Å and 3.02 Å. Three peaks are seen in the $[Au(dppm)_2Br]_2$ corresponding to gold-phosphorus, gold-bromine, and gold-gold interactions at 2.33 Å, 2.87 Å, and 3.02 Å (Fig. 4). The structure for $[Au(dppp)_2Br]_2$ has a gold-gold interaction of 5.04 Å which is not seen in the Fourier transform.

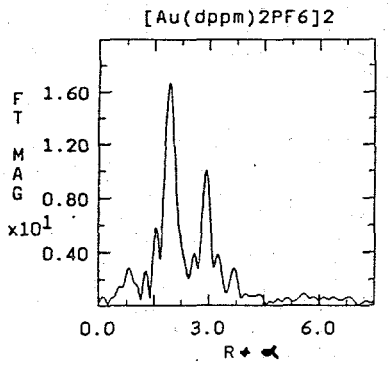

Figure 3: Fourier transform of the EXAFS data for a gold dimer showing both binding to phosphorus and also a gold-gold interaction at 3.0 Å.

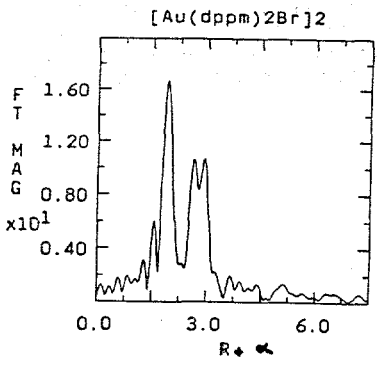

Figure 4: Fourier transform of the EXAFS of material identical to that in Fig. 3 except that noncoordinating PF_6^- has been replaced by Br^- which coordinates and results in a third peak in the transform.

At low temperature it is possible to see weak gold-gold interactions at a distance of 3.0 angstroms. These interactions are absent when data is taken at room temperature. The absence of a peak at 5.04 angstroms in the dppp structure suggests that at some distance between 3-5 angstroms evidence is lost, even in data measured at 10 K, of the metal-metal interaction. The resolution of the data suggests that two atoms with bond distances differing by as little as 0.15 Å can be refined, as in the gold-gold and gold-bromine distances for the dppmbr structure. Hence, by studying samples at liquid helium temperatures moderately long, weak interactions can be examined.

ACKNOWLEDGEMENTS

Support for this project is from the NIH (GM35404). The work reported here is largely that of W.B. Jones. All data were measured at SSRL.

REFERENCES

1. Graham, G.G., Haavisto, T.M., McNaught, P.J., Browne, C.D., Champion, G.D., J. Rheumatol. **1981**, 9, 532-535.

2. Lewis, D., Capell, H.A., McNiel, C.J., Iqbal, M.S., Brown, D.H., Smith, W.E., Ann. Rheum. Dis. **1983**, 42, 566-570.

3. Intoccia, A.P., Flanagan, T.L., Walz, D.T., Gutzait, L., Swagzdis, Bioinorganic Chemistry of Gold Coordination Compounds; Sutton, B.M., Ed., Smith Kline & French Laboratories: Philadelphia, 1983, pp. 21-22.

4. Isab, A.A., Hormann, A.L., Coffer, M.T., Shaw, C.F. J., Am. Chem. Soc. **1988**, 110, 3278-3284.

SYNCHROTRON RADIATION CORONARY ANGIOGRAPHY IN A HUMAN SUBJECT WITH A DUAL BEAM, DUAL DETECTOR IMAGING SYSTEM

E. Rubenstein[1], J.C. Giacomini[1], H.J. Gordon[1], A. C. Thompson[2], G. Brown[3], R. Hofstadter[4], W. Thomlinson[5] and H.D. Zeman[5]

[1] Stanford University School of Medicine, Stanford, California 94305, USA

[2] Lawrence Berkeley Laboratory, University of California, Berkeley, California 94720, USA

[3] Stanford Synchrotron Radiation Laboratory, Stanford University, Stanford, California 94305, USA

[4] Department of Physics, Stanford University, Stanford, California 94305, USA

[5] National Synchrotron Light Source, Brookhaven National Laboratory, Long Island, NY 11973, USA

Introduction

Two sets of prior studies of transvenous synchrotron radiation coronary angiography in human subjects have demonstrated that the approach can provide images of major portions of the human coronary anatomy [1,2]. The images acquired in these studies lacked clinical quality owing to an inadequate signal-to-noise ratio. Comparison with prior studies in anesthetized dogs indicated that an eight-fold increase in X-ray fluence is needed [1]. Several measures are being undertaken to achieve this increment, and the present report describes the implementation of the first of these, the dual beam, dual detector imaging system [3].

Experimental

These studies were conducted during March 1989 on beamline IV-2 at the Stanford Synchrotron Radiation Laboratory (SSRL). This beamline is illuminated by an eight-pole, 1.8 T wiggler. In this system the synchrotron radiation is monochromatized by diffraction off a pair of asymmetrically cut crystals which produce two X-ray beams with energy closely bracketing the K-edge of iodine (33.16 keV). The energy separation of the two beams is about 300 eV and the band width of each beam is about 15-25 eV. The beams, 125 mm in horizontal dimension, cross at the position of the subject's heart, diverge, and then impinge on the two dual arrays of 300 pixel elements of the lithium-drifted silicon detector. The efficiency of the detector for 33 keV photons is about 70%; the efficiency for the transmitted third harmonic (99 keV) is only about 5%. The dynamic range of the electronic system is 40,000:1 in a readout time < 2 ms. The pixel resolution is 0.5 mm by 0.5 mm. The detector is housed in a thermoelectrically cooled cryostat and operated at -30°C. The subject is scanned vertically, as in prior experiments, at a rate of 12 cm/s. The exposure time of each line image is 4 ms. The subject was a 62-year-old man with angina pectoris due to severe coronary artery disease. Bypass surgery (left internal mammary artery anatomosis and two vein grafts) had been done approximately four years prior to the present study.

Results

Images were recorded in two positions, left lateral (Fig. 1) and right anterior oblique (30°) (Fig. 2). The images revealed that the left internal mammary artery anastomosis was intact and that there was diminished perfusion of the distal left anterior descending coronary artery. The two vein bypass grafts appeared to be patent. The image quality was improved over that obtained in prior studies owing to an increase in X-ray fluence, and the ramus intermedius artery (Fig. 1) was visualized for the first time. Fourteen of the 600 channnels functioned improperly owing to 60-cycle noise in some and excessive leakage current in the detector in others. The signals from the channels with the 60-cycle noise were corrected by adjusting the pedestal. The signals in the channels with leakage current were replaced with the average of the two bracketing adjacent channels.

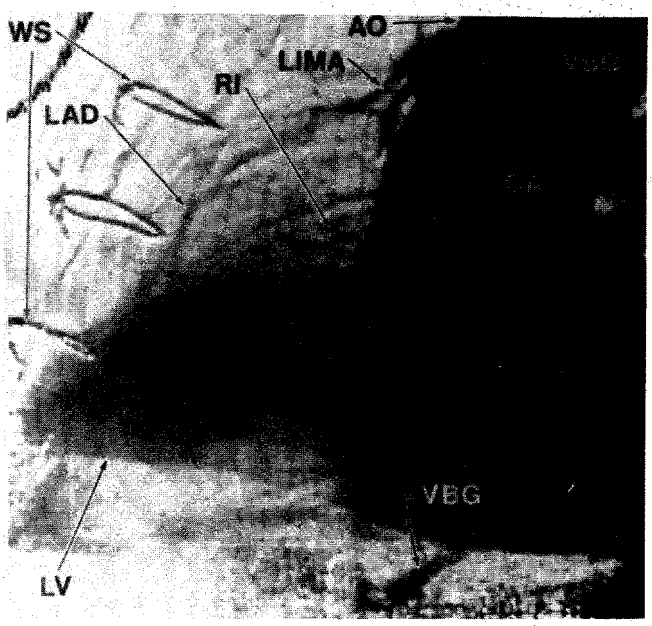

Figure 1 This is a lateral view of a transvenous synchrotron radiation angiogram performed at SSRL in March 1989 (3.3 GeV, 50 mA). The subject was a 62-year-old man who had previously undergone left internal mammary and vein bypass graft surgery. The contrast agent, Renograffin-76, was injected into the superior vena cava (50 ml, 12 ml/s). The radiation exposure was 0.49 rad for this frame. AO = aorta, LIMA = left internal mammary artery, VBG = vein bypass graft, RI = ramus intermedius artery, LAD = left anterior descending artery, LV = left ventricle, CA = catheter, CL = surgical clips, WS = wire sutures.

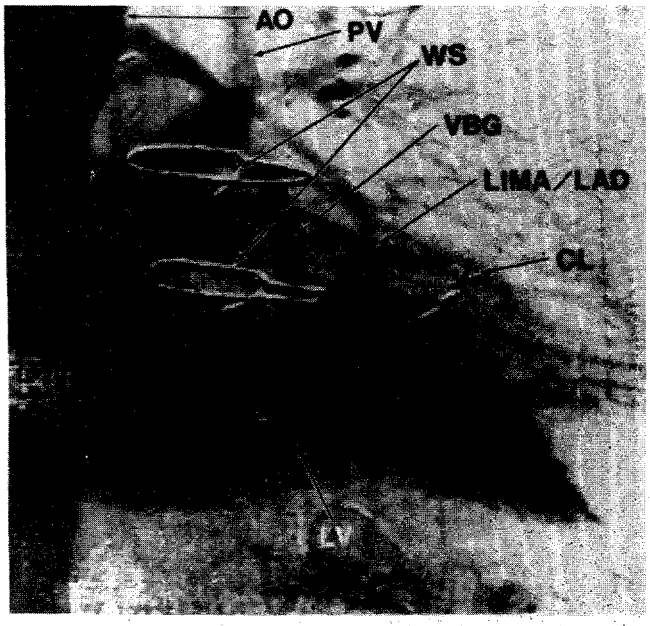

Figure 2 This is a right anterior oblique (30°) view of a transvenous synchrotron radiation angiogram done on the same patient (3.3 GeV, 47 mA). The contrast agent dose was 50 ml, 12 ml/s. The radiation exposure for this frame was 0.47 rad. PV = pulmonary vein; the other abbreviations are the same as in fig. 1.

REFERENCES:

1. Rubenstein, E., Hofstadter, R., Zeman, H.D., Thompson, A.C., Otis, J.N., Brown, G.S., Giacomini, J.C., Gordon, H.J., Kernoff, R.S., Harrison, D.C., and Thomlinson, W. (1986), Proc. Nat. Acad. Sci. USA. 83, 9724-9728.
2. Thompson, A.C., Hofstadter, R., Otis, J.N. Zeman, H.D., Kernoff, R.S., Rubenstein, E., Giacomin, J.C., Gordon, H.J., Brown, G.S., and Thomlinson, W. (1988), Nucl. Instr. and Meth. A266, 252-259.
3. Thompson, A.C., Zeman, H., Thomlinson, W., Rubenstein, E., Kernoff, R.S., Hofstadter, R., Giacomini, J.C., Gordon, H.J., Brown, G.S. (1989), Nucl. Instr.and Meth. B40/41, 407-412.

ACKNOWLEDGEMENTS

We thank the staff of SSRL for their generous efforts on behalf of this project and for their scientific and technical expertise, without which these studies would not have been possible. This work was supported by National Institutes of Health Grant 5R01 HL 39253-02 and Department of Energy Grant DE-FG03-87ER60527. The data were recorded at SSRL which is supported by the DOE's Office of Basic Energy Science.

Reactivity of the Laccase Trinuclear Copper Active Site with Dioxygen : An X-ray Absorption Edge Study

James L. Cole, Grace O. Tan, Edward K. Yang,
Keith O. Hodgson and Edward I. Solomon

Department of Chemistry, Stanford University, Stanford, CA 94305, USA.

The multicopper oxidases (laccase, ascorbate oxidase and ceruloplasmin) catalyze the four-electron reduction of dioxygen to water. Laccase contains four Cu atoms: a type 1, a type 2 and a binuclear type 3 center. Low-temperature MCD measurements have demonstrated that the type 2 and type 3 centers comprise a trinuclear Cu cluster site,[1] and this model has been supported in a recent X-ray crystal structure determination[2] of ascorbate oxidase. In the present study, X-ray absorption edge spectroscopy has been used to determine Cu oxidation states following reaction of reduced laccase derivatives with dioxygen, leading to a description of which of the Cu centers are required for reactivity.

A pre-edge 1s→4p transition near 8984 eV is present in the edge spectra of 2-coordinate and 3-coordinate Cu(I) compounds, but not in Cu(II) compounds[3]. Thus the degree of oxidation of the laccase derivatives may be determined against a scale obtained by subtracting the edge of a fully oxidized sample (reacted with H_2O_2) from that of a fully reduced sample.

The feature near 8984 eV is present in the spectra of fully reduced type 2-depleted (T2D) laccase and type 1 Hg^{2+}-substituted (T1Hg) laccase. In T2D laccase, this feature persists upon exposure to air (see Figure 1), indicating that the sample remains partially reduced. Optical spectroscopy on the T2D samples shows that the type 1 Cu is completely oxidized, enabling us to conclude that the binuclear type 3 center remains reduced. In contrast, fully reduced T1Hg laccase, which contains a valid type 2-type 3 trinuclear Cu cluster site, reacts readily with dioxygen, resulting in complete reoxidation of the type 2 and type 3 centers (see Figure 2). These results demonstrate that the type 2-type 3 trinuclear site represents the minimal active site required for the multielectron reduction of dioxygen.[4]

Acknowledgements. This work was supported by NSF Grant CHE 8817702 (KOH) and NIH Grant AM31450 (EIS). Beam time was provided by SSRL, supported by the DOE's Office of Basic Energy Sciences and the NIH's Division of Research Resources.

References

(1) (a) Allendorf, M.D.; Spira, D.J.; Solomon, E.I. *Proc. Natl. Acad. Sci. USA* **1985**, *82*, 3063-3067. (b) Spira-Solomon, D.J.; Allendorf, M.D.; Solomon, E.I. *J. Am. Chem. Soc.* **1986**, *108*, 5318-5328.
(2) Messerschmidt, A.; Rossi, A.; Ladenstein, R.; Huber, R.; Bolognesi, M; Gatti, G; Marchesini, A.; Petruzzelli, R; Finazzi-Agrò, A. *J. Mol. Biol.* **1989**, *206*, 513-529.
(3) Kau, L.-S.,; Spira-Solomon, D.J.; Penner-Hahn, J.E.; Hodgson, K.O.; Solomon, E.I. *J. Am. Chem. Soc.* **1987**, *109*, 6433-6442.
(4) Cole, J.L.; Tan, G.O.; Yang, E.K.; Hodgson, K.O.; Solomon, E.I., in press, *J. Am. Chem. Soc.*

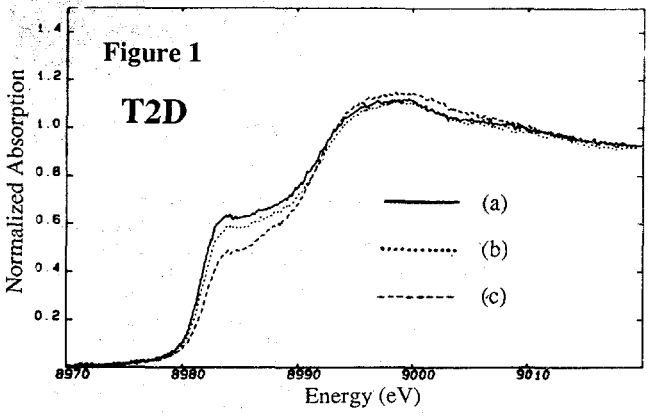

T2D	% Cu oxidized T1	T2	T3
(a) T2D fully reduced	0	---	0
(b) T2D exposed 15 min.	0	---	0*
(c) T2D exposed 63 hrs.	100	---	14

*The slight decrease at 8984 eV is due to oxidation of the 10% of native laccase present in the T2D preparation

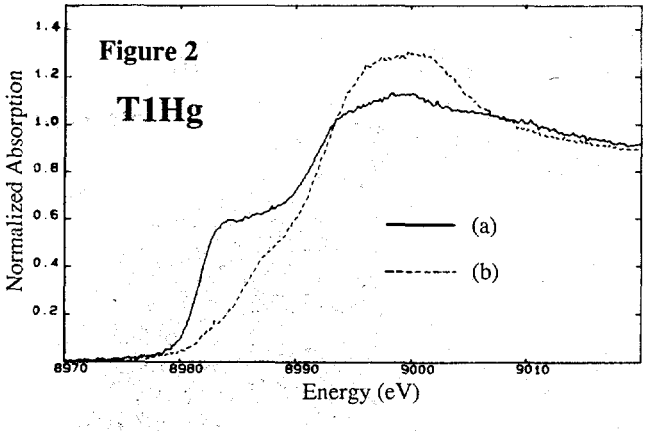

T1Hg	% Cu oxidized T1	T2	T3
(a) T1Hg reduced	---	10	10
(b) T1Hg exposed 30 min.	---	98	98

STRUCTURAL COMPARISON OF PURPLE AND BLUE FORMS OF BACTERIORHODOPSIN

Proposal No. 2035B

Soichi Wakatsuki[1], Y. Kimura[2], N. Gillis[3], D. Eliezer[4], W. Stoeckenius[2], Keith O. Hodgson[1], and S. Doniach[3]

1 Department of Chemistry, Stanford University Stanford, CA 94305.
2 Cardiovascular Research Institute, University of California, San Francisco, CA 94143.
3 Department of Applied Physics, Stanford University Stanford, CA 94305.
4 Department of Physics, Stanford University Stanford, CA 94305.

Introduction

A blue form of bacteriorhodopsin lacks some photocycle intermediates and does not function as a proton pump when it is transformed either by deionization or by acidification from the native, purple form. Therefore, the determination of conformational change that accompanies the purple-to-blue transition may give insights into how the transition deactivates the pump.

Studies of changes in x-ray diffraction patterns during the purple-to-blue transition have been controversial in part due to liable nature of the blue form giving rise to loss of 2D lattice structure. Contradictory descriptions of the structure of blue membranes have appeared: one claiming a well-preserved lattice[1,2] and one a distorted lattice[3,4]. Because of the low surface pH of the blue membranes, it has been suggested that their lattice structure is largely disordered in ultracentrifuged samples thus preventing structure determinations using x-ray diffraction from such samples.

We have reported that blue membrane samples have a distinct diffraction pattern, comparable in quality to that from a purple form, which, however, disappears after a few hours of drying[5]. In this report we describe the change of the diffraction patterns during drying and compare structures of blue and purple membranes.

Experimental

We used two different purple membranes: a mutant JW5 reconstituted with retinal and naturally produced ET1001. Purple membranes were washed carefully by centrifugation at 30000 g. After deionization according to a method described earlier[1], pellet samples were made by ultracentrifugation at 300000 g for about 10 hours into a cell with mylar windows on both sides. The size of such pellets is typically 1 mm x 1mm x 1mm. After centrifugation, the cells were sealed with Corning vacuum grease.

For drying experiments, the vacuum grease seal was removed immediately before exposure to x-ray. To verify the integrity of the blue samples, the pellets were collected after x-ray exposure in order to measure their optical spectra. In all cases reported here, the blue forms collected after the x-ray exposure had the same absorption maxima as those before. It is highly unlikely that the blue form becomes purple in the pellet form and returns to blue when resuspended into water. Therefore we strongly believe that the observed structural changes are characteristic of the blue form.

Quadrant Detector

A quadrant position sensitive detector developed by A. Gabriel of EMBL in Grenoble was purchased and fully integrated into the SSRL Small Angle X-ray Scattering/Diffraction camera with additional electronics modules and minimal software change. Its 60° fan-shape active area is suitable for acquisition of diffraction patterns from moderately oriented membranes such as pelleted purple membranes. The entire system with the quadrant detector, VAX station II, CAMAC modules, and NIM modules was sent to the National Light Source Laboratory (NSLS), Brookhaven National Laboratory and rebuilt on beamline X14A for the data acquired in December 1989.

Time-resolved x-ray diffraction of blue membranes during drying

In-plane diffraction patterns from the blue membranes were collected during drying at room temperature. Figure 1-A shows an example of continuous time-resolved x-ray diffraction patterns of the blue membranes during 4 hours of drying. The in-plane diffraction peaks whose S range is between 0.03 and 0.12 Å^{-1} were lost after about 150 minutes and an inter-membrane Bragg peak at 50.0 Å appeared about the same time. The latter arises from lamellar stacking of the membranes.

A 3D plot of the same data, Figure 1-B, shows that the in-plane diffraction peaks grew for the first 100 minutes. This is clearly seen in Figure 2 which plots changes in peak heights of the (2,1) reflection and the inter-membrane Bragg diffraction peak.

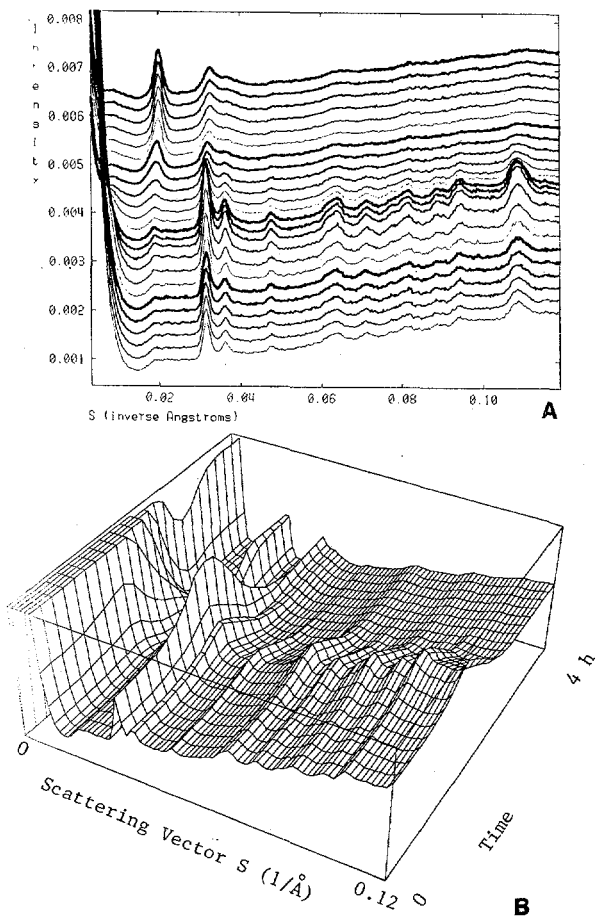

Fig. 1 Time-resolved x-ray diffraction patterns of the blue membrane during drying. (a) Calibrated data before background subtraction. Exposure of each pattern was 10 minutes and entire data set was recorded in 4 hours. (b) 3D plot of the same data showing improvement of the in-plane diffraction peaks during first 100 minutes and their disappearance thereafter.

Figure 3 demonstrates a distinction between the purple and blue forms when they are dried. The diffraction patterns of the blue membrane before drying (C) clearly shows the in-plane diffraction peaks while that after drying (D) does not. As a control experiment, the purple form was also dried and its diffraction pattern after drying (B) was compared with that before the drying (A). In this case, the in-plane diffraction peaks did not disappear. The 50.0Å inter-membrane Bragg peak was still seen after drying.

Structures of the blue and purple membranes

Intensities of the diffraction peaks were calculated from Fig.3 A and B. Structure factors of overlapping reflections, (h,k) and (k,h) were obtained using ratios of structure factors from electron microscopy data[6]. Their phases were also used for calculation of electron density maps for the purple and blue forms. Figure 4-A shows an electron density map obtained for a blue membrane sample (JW5), whereas Fig.4-B shows a difference Fourier map of the purple minus blue forms. The difference map shows one positive peak between helices 3 and 4, closer to 3 and slightly shifted toward the center, and most other peaks on the lipids. The peaks are marked in Fig.4-A as H and L respectively. A very similar difference map was obtained from a completely different sample, ET1001, which strongly indicates that these peaks are not an artifact. The peak between helices 3 and 4 is located at the same position as peak (iii) in Figure 2 of Katre et al[2]. Mitra *et al* also have found a cation binding site between helices 3 and 4, closer to 4 and shifted toward outside of the protein[7]. A detailed comparison of the difference maps with proposed bacteriorhodopsin models should help elucidate the mechanism of how deionization affects proton pumping in blue membranes.

References

1. Y. Kimura, A. Ikegami, W. Stoeckenius, *Photochem. Photobiol.* 40, 641-646 (1984).
2. N. V. Katre, Y. Kimura, R. M. Stroud, *Biophys. J.* 50, 277-284 (1986).
3. P. C. Mowery, *et al.*, *Biochem.* 18, 4100-4107 (1979).
4. M. P. Heyn, C. Dudda, H. Otto, F. Seiff, I. Wallat, *Biochemistry* 28, 9166-9172 (1989).
5. S. Wakatsuki *et al*, 1988, SSRL Activity Report for 1988, p67.
6. R. Henderson, J.M. Baldwin, K.H. Downing, F. Zemlin, *Ultramicroscopy* 19, 147-178 (1986).
7. A. Mitra and R.M. Stroud, *Biophys. J.*, in press.

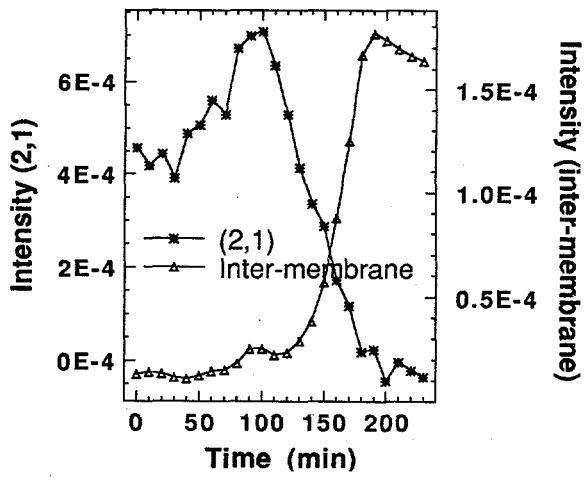

Fig. 2 Changes in peak heights of an in-plane diffraction peak (2,1) and of the inter-membrane Bragg peak at 50.0 Å during the 4 hour drying experiment.

ACKNOWLEDGEMENTS This research was supported by NIH Grant RR 1209 and data were recorded at both SSRL and NSLS which are supported by the DOE's Office of Basic Energy Science. We are grateful to Drs. Gene Ice and Paul Zschack, Mr. Mark Engbretson and Ms. Marybeth Rice for experimental assistance during the data collection at NSLS.

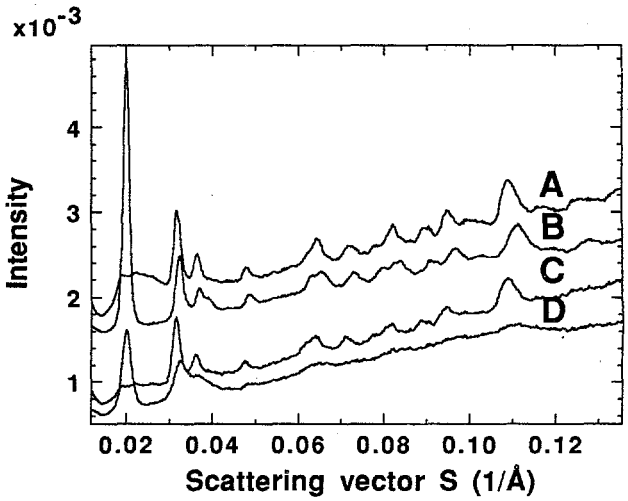

Fig. 3 Diffraction patterns of the purple and blue membranes before and after drying for 4 hours.
A: Purple before drying
B: Purple after drying
C: Blue before drying
D: Blue after drying

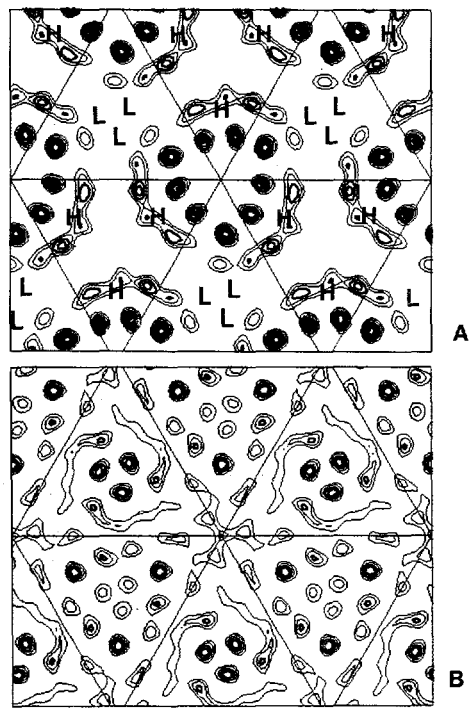

Fig.4 (A) Electron density map of the blue membrane calculated from peak intensities of Fig.3 C. (B) Difference electron density map, purple (Fig.3 A) minus blue (Fig.3 C) showing a positive peak (marked as H in (A)) between helices 3 and 4, closer to 3 and slightly shifted toward the center, and another strong peak on a lipid, which are marked as L in (A). Only positive contours are shown. Note that all the peak positions related to the 3-fold symmetry are marked.

Virus Structure

Michael Rossman, Thomas, J. Smith, Ming Luo, Sangsso Kim, John Badger
Philippe Dumas, S. krishnaswamy, Klaus Piontek
Purdue University
Dept. of Biological Science
West Lafayette, Indiana

Human Rhinovirus 1A Drug Studies

We have recently been able to obtain a structure of the HRV1A serotype (1). This virus belongs to the minor rhinovirus receptor group. Previously we had worked with HRV14 (2) which belongs to the major rhinovirus receptor group. We had studied the binding of various drugs that inhibit uncoating and attachment of HRV14 (3-5). The studies at SSRL were the first with HRV1A. The results are currently being written up for publication.

Two compounds were studied (e.g. WIN 56291)

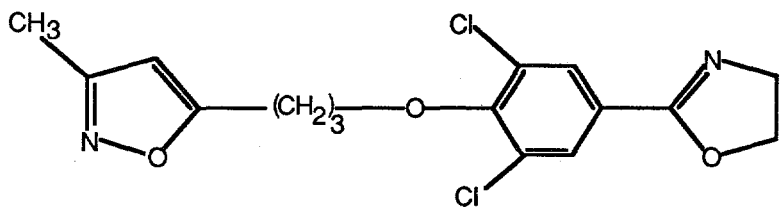

WIN 56291

Both bound in a similar manner into the "WIN pocket" of VP1 of HRV1A. However, there are substantial differences to the model of binding that occurs in HRV14. The WIN compound is displaced as much as 4 Å in places compared to its HRV14 binding site. These differences are now being analyzed.

Human Rhinovirus 14 Mutant

Data was collected on a WIN drug-resistant mutant of HRV14. Unfortunately the crystals were extremely unstable and the data was of insufficient quality.

Canine Parvovirus

Data collection of native CPV crystals (see 6) was continued. This data has been incorporated into a now fairly complete data set. We anticipate obtaining a high resolution structure perhaps in 1990. This would be the first high resolution structure of an ssDNA virus (but see ϕX174).

Phage ϕX174

We continued the data collection of native ϕX174 crystals (7). This data has been incorporated into a now fairly complete data set. We anticipate obtaining a high resolution structure in 1990. This would be the first phage structure and one of an ssDNA virus (but see CPV above).

References

1. Kim, S., T. J. Smith, M. S. Chapman, M. G. Rossmann, D. C. Pevear, F. J. Dutko, P. J. Felock, G. D. Diana, M. A. McKinlay. (1989). Crystal structure of human rhinovirus serotype 1A (HRV1A). *J. Mol. Biol.* **210**:91-111.

2. Rossmann, M. G., E. Arnold, J. W. Erickson, E. A. Frankenberger, J. P. Griffith, H. J. Hecht, J. E. Johnson, G. Kamer, M. Luo, A. G. Mosser, R. R. Rueckert, B. Sherry, G. Vriend. (1985). Structure of a human common cold virus and functional relationship to other picornaviruses. *Nature (London)*, **317**:145-153.

3. Smith, T. J., M. J. Kremer, M. Luo, G. Vriend, E. Arnold, G. Kamer, M. G. Rossmann, M. A. McKinlay, G. D. Diana, M. J. Otto. (1986). The site of attachment in human rhinovirus 14 for antiviral agents that inhibit uncoating. *Science*, **233**:1286-1293.

4. Badger, J., I. Minor, M. J. Kremer, M. A. Oliveira, T. J. Smith, J. P. Griffith, D. M. A. Guerin, S. Krishnaswamy, M. Luo, M. G. Rossmann, M. A. McKinlay, G. D. Diana, F. J. Dutko, M. Fancher, R. R. Rueckert, B. A. Heinz. (1988). Structural analysis of a series of antiviral agents complexed with human rhinovirus 14. *Proc. Natl. Acad. Sci. U.S.* **85**:3304-3308.

5. Badger, J., I. Minor, M. A. Oliveira, T. J. Smith, M. G. Rossmann. (1989). Structural analysis of antiviral agents that interact with the capsid of human rhinoviruses. *Proteins*, **6**:1-19.

6. Luo, M., J. Tsao, M. G. Rossmann, S. Basak, R. W. Compans. (1988). Preliminary X-ray crystallographic analysis of canine parvovirus crystals. *J. Mol. Biol.* **200**:209-211.

7. Willingmann, P., S. Krishnaswamy, R. McKenna, T. J. Smith, N. H. Olson, M. G. Rossmann, P. L. Stow, N. L. Incardona. (1990). Preliminary investigation of the phage ϕX174 crystal structure. *J. Mol. Biol.* In press.

CRYSTALLOGRAPHIC STUDIES OF THE NITROGENASE IRON PROTEIN FROM *AZOTOBACTER VINELANDII*

Millie M. Georgiadis, Pinak Chakrabarti and Douglas C. Rees

Division of Chemistry and Chemical Engineering 147-75CH
California Institute of Technology
Pasadena, California 91125

Introduction

The nitrogenase enzyme system provides the only biological source of fixed nitrogen, which all organisms require as an essential nutrient. The ATP dependent reduction of dinitrogen to ammonia requires two component proteins, iron (Fe-) protein and the molybdenum-iron (MoFe-) protein. We have concentrated our structural studies on Fe-protein, since it is responsible for the coupling of ATP hydrolysis to electron transfer, is highly conserved between the "standard" and "alternate" nitrogenases, and is involved in regulation of nitrogenase activity at the protein level (through ADP-ribosylation in photosynthetic bacteria). Fe-protein is a dimer of two identical, 30,000 molecular weight subunits. Each dimer contains one 4Fe:4S cluster, symmetrically liganded to each subunit through Cys-97 and Cys-132. While spectroscopic, extrusion and redox studies of Fe-protein suggest that the 4Fe:4S cluster generally resembles those found in small ferredoxins, it is quite likely that the cluster environment differs significantly between ferredoxins and Fe-protein. The most striking indication of this is the ability to generate 2Fe:2S clusters in oxidized Fe-protein in the presence of MgATP and chelator; such interconversions have not been observed in ferredoxins. In addition, the Fe-protein cluster appears to be much more exposed to solvent than in ferredoxins, as indicated by rapid D_2O exchange in pulsed EPR studies and solvent dependent spin-state interconversions in low temperature EPR studies. Exposure of the cluster almost certainly contributes to the rapid inactivation of Fe-protein by oxygen and by nitrite. We have pursued an approach towards solving the structure based on (1) native anomalous scattering measurements from the iron-sulfur cluster, (2) preparation and location of isomorphous heavy atom derivatives, (3) phase refinement by non-crystallographic symmetry averaging within and between different crystal forms and (4) atomic refinement of an initial structural model to provide the additional phase information needed to complete the polypeptide chain trace.

Experimental

Our recent crystallographic efforts have concentrated on crystals of Fe-protein from *Azotobacter vinelandii*, space group $P2_1$ with a=56.8Å, b=92.9Å,c=63.6Å,b=100.0°, and containing one dimer in the asymmetric unit. Data from 5 crystals each of the native and a gold derivative were collected at the SSRL rotation camera facility to 2.5Å resolution. The native data was reduced to 14057 unique reflections out of 29527 reflections measured, with a merging R of 0.074. The gold data was reduced to 11131 unique reflections out of 27166 measured, with a merging R of 0.102. The gold derivative contains one major site, as identified from difference Patterson studies. Phases calculated from the film data, in combination with additional native anomalous and derivative data measured from a multiwire area detector on a rotating anode x-ray source, have permitted definition of the molecular envelope, with subsequent phase refinement by non-crystallographic symmetry averaging about the dimer two-fold.

Results

Extended regions of connected chain and secondary structure are evident in the electron density maps. A general view of the secondary structure arrangement of the Fe-protein dimer is shown in Figure 1. These maps have only been recently calculated, so that a detailed fitting of amino acids to the electron density has not yet been accomplished. Several general observations about the Fe-protein structure may be noted at this stage:

(a) The Fe-protein dimer has a two-fold symmetry axis that relates the two subunits.
(b) The cluster is on the surface of the molecule and provides the principal connection between the subunits. Each subunit contains a single domain. A cleft straddling the two-fold axis separates the subunits.
(c) The chain fold of Fe-protein monomer is of the α/β type, as is generally observed in nucleotide binding proteins (i.e. the Rossmann fold).
(d) The ATP binding site is most probably located in the cleft between the two subunits.
(e) An α-helix containing residues 98 to ~115 is exposed at the top of the molecule, and may represent a major site of interaction for binding to the MoFe-protein.

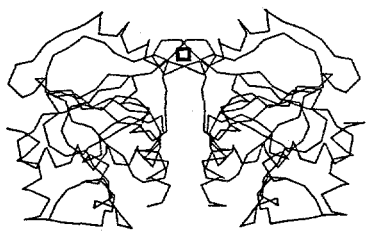

Figure 1. Chain-trace illustrating general features of the Fe-protein dimer structure.

Additional Studies of Electron Transfer Proteins

Diffraction data were collected at the SSRL rotation camera facility for the membrane protein complex *Rhodobacter sphaeroides* strain 2.4.1 photosynthetic reaction center (2.8Å resolution) and the *Rhodobacter sphaeroides* cytochrome c_2 (2.5Å resolution). Upon completion of film processing, this data will be used to refine the RC structure, and to solve the cytochrome c_2 structure by molecular replacement methods.

Acknowledgements

This research was supported by NIH grant 31299 and an NSF PYI grant. Data were recorded at SSRL which is supported by the DOE's Office of Basic Energy Science. The assistance of B.T. Hsu, M. Lewis and J.P. Allen during data collection is greatly appreciated. DCR is an A.P. Sloan research fellow.

X-RAY CRYSTALLOGRAPHY ON CRYSTALS OF *N. GONORRHOEAE* PILIN

H.E. Parge, D. Christensen, T. Hong, K. Andrews, D.E. McRee, E.D. Getzoff,and J.A. Tainer

Department of Molecular Biology, Research Institute of Scripps Clinic, La Jolla, California 92037

Introduction

Pilus fibers are long protein filaments on many pathogenic bacteria that participate in attachment to host cells (1). Although the self-assembling protein pilin is the major structural component of the *Neisseria gonorrhoeae* pilus several other proteins co-purified with pilin through the repeated solubilization-reassociation steps of the biochemical purification. Pilin solubilized in the detergent n-octyl-β-D-glucopyranoside remained an aggregate of about 100 kD at pH 9.5, but was reduced to a 40 kD dimer at pH 10.5, suggesting that assembly involves electrostatic interactions of Lys, Tyr, or other side chains with high pKa's. Pilin dimers and aggregates of higher molecular mass were partially stable even in the presence of sodium dodecyl sulfate and β-mercaptoethanol. Removal of pilus-associated proteins and stabilization of pilin multimers permitted the reproducible crystallization of pilin.

Experimental

Three-dimensional needle- and plate-shaped crystals of purified *N. gonorrhoeae* pilin (strain MS11 variant C30) grew from 36-40% polyethylene glycol 400, pH 8.0–9.0, in space group C222, with cell dimensions a = 126.4, b = 121.2, c = 26.7 Å and V_m = 2.84 Å^3/dalton for one molecule per asymmetric unit (2). Crystals were mounted in glass capillaries along with their mother liquor for experiments conducted at ambient temperatures and on glass fibres after immersion in a hydrocarbon for low temperature experiments. Data were collected on an Arndt-Wonacott rotation camera with a crystal to film distance of 10 cm, 0.2 mm collimator, and rotation increments of 2.0-3.5°

Results

Plate like crystals obtained from improved isolation procedures were examined in the spring 1989 run on the rotation camera facility at SSRL. These were shown to belong to the same space group as our earlier needle shaped crystals on which all our current data collection and heavy atom screening have be performed. Further heavy atom screening experiments were hampered by the significant downtime of the ring but experiments to test the possibility of collecting data on pilin at cryogenic temperatures were performed. The results from these tests indicated that the crystals withstand the necessary manipulations well and give satisfactory diffraction at cryogenic temperatures.

References

1. Stromberg, N., Deal, C., Nyberg, G., Normark, S., So, M. and Karlsson, K. (1988) *Proc. Natl. Acad. Sci. U.S.A.* **85**, 4902-4906.

2. Parge., H.E., Bernstein, S.L., Deal, C.D., McRee, D.E., Christensen, D., Capozza, M.A., Kays, B.W., Fieser, T.M., Draper, D., So, M., Getzoff, E.D.,and Tainer, J.A. (1990) *J. Biol. Chem.* **265**, 2278-2285.

On the Need to Account for Electron Spin when Interpreting Linearly Polarized XANES with Application to the Polarized Molybdenum L_2 and L_3 Absorption Edges of Single Crystal $MoS_2O_2^{2-}$

T. A. Tyson[1], D. A. Case[2], B. Hedman[1,3] and K. O. Hodgson[1]

[1]Department of Chemistry, Stanford University, Stanford, California 94305
[2]Department of Molecular Biology, Research Institute Scripps Clinic, La Jolla, California 92307
[3]Stanford Synchrotron Radiation Laboratory, SLAC, Bin 69, P. O. Box 4349, Stanford, California 94309

I. Introduction

We note that in the interpretation of linearly polarized XANES spectra of oriented molecules performed to date the spin or intrinsic angular momentum of the electron has been neglected. Here we discuss two models which account explicitly for electron spin.[1] In Sec. II we describe the formalism for calculation of linearly polarized XANES based on the Dirac model of the electron combined with proper treatment of the final valence levels as functions transforming under double point group irreducible representations (irreps). In Section III the same is done for the Pauli model. In Section IV we use these models to interpret the polarization dependece of the Mo L_2 and L_3 edges of $MoS_2O_2^{2-}$. It is found that the same ratio of $\hat{z}$- to $\hat{x}$ -polarized intensity (or cross section) is obtained for both the Dirac and the Pauli models. It is then possible to label the hole states by j and m, the quantum numbers of the square and the z-component of the total anglar momentum, respectively.

II. Dirac's Theory

The application of Dirac's theory to the case of particles in central potentials has been treated in the literature[2] and a rather thorough bibliography on relativistic theory of atoms and molecules has been compiled by Pyykkö.[3] The solutions of the Dirac equation for (principal quantum number n) for a central potential are four-component spinors of the form

$$\psi_{n_i K_i m_i}(\vec{r}) = \begin{pmatrix} g_{n_i K_i}(r)\,\chi_{K_i m_i}(\hat{r}) \\ i\, f_{n_i K_i}(r)\,\chi_{-K_i m_i}(\hat{r}) \end{pmatrix}.$$

These solutions are eigenstates of $\vec{J}^2$, $\vec{J}_z$, $\vec{S}^2$, K and Π corresponding to the square of the total angular momentum ($\vec{J}=\vec{L}+\vec{S}$), its z-component, the square of the intrinsic angular momentum of the electron, an angular quantum number which replaces l (K values of -1, 1, -2, 2, -3... correspond to the states $s_{1/2}$, $p_{1/2}$, $p_{3/2}$, $d_{3/2}$, $d_{5/2}$...) and the parity operator ($\Pi = \beta P_s$, P_s being space inversion), respectively. We use these spinors as core states.

Functions (four component spinors here) of the form used for the core levels are symmetry adapted for the valence states. Specifically, for the half-integer spin states which we are dealing with we construct linear combinations of Dirac spinors[4] which transform according to the extra irreps of the double point group.[5,6] It is found that for a given n and K the symmetry adapted spinors (that is to say basis functions of the extra irreps) are linear combinations of the form[7]

$$\bar{f}_{n_f K_f m_f}(\vec{r}) = a_{K_f m_f}\,\psi_{n_f K_f m_f}(\vec{r}) + b_{K_f m_f}\,\psi_{n_f K_f -m_f}(\vec{r})$$

and that the irreps are at most two dimensional. The cross section for the Cartesian component ξ is then computed via

$$\sigma_\xi(\hbar\omega) = 4\pi^2\alpha\hbar\omega \sum_{i\,f} |\langle\psi_{n_i K_i m_i}|\, \vec{r}_\xi\, |\bar{f}_{n_f K_f m_f}\rangle|^2\, \delta(E_i - E_f + \hbar\omega)$$

III. Pauli's Theory

Pauli's theory[2] of the electron represents the true nonrelativistic reduction of Dirac's theory (not Schrödinger's theory). In this case we see that the four-component theory of Dirac reduces to a two-component theory ($f_{n\kappa}(r)$ becomes negligible and $g_{n\kappa}(r)$ goes over into the Schrödinger radial function) in which the radial functions are approximated by those of the Schrödinger equation but the angular functions are the two-component spin spherical harmonics $\chi_{\kappa m}(\hat{r})$. That is to say, the nonrelativistic (NR) core states are of the form

$$\psi^{NR}_{n_i K_i m_i} = R_{n_i l_i}(r)\,\chi_{K_i m_i}(\hat{r})$$

and are eigenstates of $\vec{J}^2$, $\vec{J}_z^2$, $\vec{L}^2$, $\vec{S}^2$ and P_s.

Again linear combinations of the core type wave functions can be used to represent the valence states. We have therefore, for the nonrelativistic limit, valence states of the form

$$\bar{f}^{NR}_{n_f K_f m_f}(\vec{r}) = a_{K_f m_f}\,\psi^{NR}_{n_f K_f m_f}(\vec{r}) + b_{K_f m_f}\,\psi^{NR}_{n_f K_f -m_f}(\vec{r})$$

where the coefficients $a_{K_f m_f}$ and $b_{K_f m_f}$ are identical to those of the Dirac approach. The linearly polarized absorption cross section is now given by

$$\sigma_\xi(\hbar\omega) = 4\pi^2\alpha\hbar\omega \sum_{i\,f} |\langle\psi^{NR}_{n_i K_i m_i}|\, \vec{r}_\xi\, |\bar{f}^{NR}_{n_f K_f m_f}\rangle|^2\, \delta(E_i - E_f + \hbar\omega)$$

IV. Polarized Spectra of $MoS_2O_2^{2-}$ and Possible Interpretation

Following the method used by Kutzler et al[8] for the K-edge study of the $MoS_2O_2^{2-}$ anion, data acquisition at the Mo L_3 edges and $L_2$was performed at Stanford Synchrotron Radiation Laboratory on beam line 6-2 as discussed in ref. 9. Measurements were made for the electric field vector $\hat{e}$ along three unique molecular directions $\hat{z}$, $\overrightarrow{O\text{-}O}$ (called $\hat{x}$ below) and $\overrightarrow{S\text{-}S}$. The $\overrightarrow{S\text{-}S}$ measurement while exhibiting similar intensity behavior to the $\overrightarrow{S\text{-}S}$ measurement is not presented due to irreproducibility of the data from scan to scan as a result of a low signal-to-noise ratio at the L_3 edge.

In fig.1(a) we display the polarized Mo L_3 x-ray absorption spectrum for $\hat{x}$- polarized (solid line) and $\hat{z}$-polarized (dashed line) while in fig. 1(b) we show the L_2 spectra where the lines have the same meaning. The data are not normalized since the standard normalization methods are not easily applied here due to the fact that the Mo L-edge spectra are superimposed on the S-K-edge EXAFS (the S K-edge is located near 2470 eV). The important point to note is that the two edges differ by more than just a scale factor. Specifically, note the absence of the white line in the L_3 spectrum for $\hat{z}$-polarized radiation. Clearly any model for polarized edges which treat both edges as equivalent except for a scale factor (statistical weight) is not valid here.

In Table I we display the relative cross sections σ_z/σ_x as a function of the doubly degenerate final states labeled Γ_5, the only half-integer representation of the double group C_{2v}. The basis functions of this doubly degenerate irrep are designated by |m|. The observation of the $\hat{z}$-polarized white line of the L_2 edge combined with the cross section ratios lead us to conclude that in this anion (which has no ESR signal and hence no unpaired electrons[10]) one of the accessible d states (holes) has j=3/2 and |m|=1/2. We interpret the L_3 edge spectra as evidence for this being the only accessible hole state since it is the only transition which exhibits a weak σ_z/σ_x for the L_3 edge. The extinction implied by the transition to the j=5/2 and |m|=5/2 can not be invoked here since it would be seen only if all of the d levels are filled and hence is inconsistent with the L_2 edge measurement.

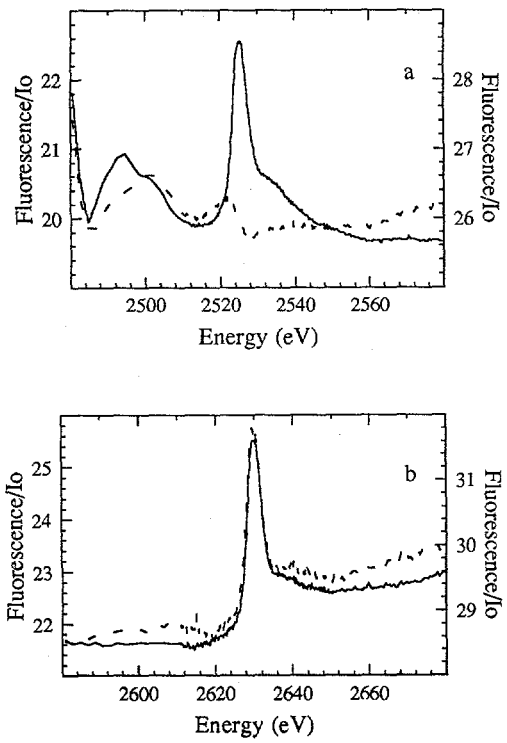

FIG 1 - Linearly polarized Mo L_2 and L_3 XANES of $MoS_2O_2^{2-}$. (a) The Mo L_3-edge spectra for $\hat{x}$-polarized (solid line) and $\hat{z}$-polarized (dashed line) absorption. The y-axis scale on the right corresponds to the dashed line. (b) The Mo L_2-edge with line types having the same meaning as in (a).

Table I - Polarized Cross Section Ratios[a].

Transition	Final State |m|	σ_z/σ_x
L_2 $p_{1/2} \rightarrow d_{3/2}$	1/2	4
	3/2	0
L_3 $p_{3/2} \rightarrow d_{3/2}$	1/2	1/7
	3/2	3
L_3 $p_{3/2} \rightarrow d_{5/2}$	1/2	3
	3/2	4/3
	5/2	0

[a]Pauli and Dirac models yield the same ratios since they depend on the angular part of the wavefunction only.

Acknowledgements

We are indebted to Dr. P. Frank (Stanford Univ. Chem. Dept.) for assistance in our experiments and for helpful discussions. This research was supported by National Science Foundation grant CHE 88-17702. The experiments were carried out at SSRL which is supported by the Department of Energy's Office of Basic Energy Science and the NIH's Division of Research Resources, Biotechnology Resource Program.

References

[1]A more thorough account of this work is in preparation.

[2] M. E. Rose, *Relativistic Electron Theory* (John Wiley and Sons, Inc., New York, 1961).

[3]P. Pyykkö, *Relativistic Theory of Atoms and Molecules* (Springer-Verlag, Berlin, 1986).

[4]J. Meyer, Int. J. Quantum Chem. 33, 445 (1988).

[5]C. J. Bradley and A. P. Cracknell, *The Mathematical Theory of Symmetry in Solids* (Clarendon Press, Oxford, 1972).

[6]H. Watanabe, *Operator Methods in Ligand Field Theory* (Prentice-Hall, Inc., Englewood Cliffs, 1966).

[7]J. Oreg and G. Malli, J. Chem. Phys. 65, 1746 (1976).

[8]F. W. Kutzler, R. A. Scott, J. M. Berg, K. O. Hodgson, S. Doniach, S. P. Cramer and C. H. Chang, J. Am. Chem. Soc. 103, 6083 (1981).

[9]T. A. Tyson, A. L. Roe, P. Frank, K. O. Hodgson and B. Hedman, Phys. Rev. B. 39, 6035 (1989).

[10]R. S. Mann and K. C. Khulbe, Bull. Chem. Soc. Jap. 48, 1021 (1975).

VUV
Progress Reports

PHOTOEMISSION SPECTROSCOPY OF ORDERED OVERLAYERS ON GaP (110)

Proposal No. 935Vp

K. E. Miyano, R. Cao, T. Kendelewicz, A. K. Wahi, I. Lindau, and W. E. Spicer

Stanford Electronics Laboratories, Stanford University, Stanford, CA 94305

The interfaces between Sn, Sb, and Bi and GaP (110) have been examined using soft x-ray photoemission, and the core level attenuation and lineshape changes confirm that these interfaces exhibit S-K growth with the first monolayer described by the zigzag chain model originally developed for Sb on GaAs (110). A model of the charge configuration at the one monolayer interface can be invoked to explain the disappearance of the surface components in the context of both charge transfers and Madelung potential differences.[1] The disappearance of the surface components is utilized to estimate intrinsic lineshape parameters of the Ga 3d and P 2p core levels. These parameters were then employed in the computer fits performed for this paper: the bulk-surface core shifts were determined to be roughly 0.32 and 0.39 for Ga 3d and P 2p, respectively. Finally, shifts of the bulk core levels as a function of Sn, Sb, and Bi coverage were examined to determine the band bending behavior and the final surface Fermi level positions at these interfaces. The position of each of the three is in the neighborhood of 1 eV above VBM, the same range as those observed for materials with significantly different work functions and electronegativities such as Au. Thus, Fermi level pinning can be discussed for the three interfaces: the pinning seems to have a correlation to the development of metallic or semimetallic character in the overlayer. This work is supported by ONR under contracts No. N00014-89-J-1083 and N00014-86-K-0736.

REFERENCES

1. K. E. Miyano, R. Cao, T. Kendelewicz, A. K. Wahi, I. Lindau, and W. E. Spicer, in *Proceedings of the Ninth International Conference on Vacuum Ultraviolet Physics*, Physica Scripta, to be published.

VACUUM ULTRAVIOLET PHOTOELECTRON SPECTROSCOPY OF $(NH_4)_2S$ TREATED GaAs (100) SURFACES

C. J. Spindt,[1] D. Liu,[2] K. Miyano,[1] P. L. Meissner,[1] T. T. Chiang,[1]
T. Kendelewicz,[1] I. Lindau,[1] and W. E. Spicer[1]

[1]Stanford Electronics Laboratories, Stanford University, Stanford, CA 94305
[2]Varian Central Research, Varian Associates, Palo Alto, CA 94303

In 1987, it was discovered by Sandroff, et al. that sulfur containing solutions such as $(NH4)_2S$ can reduce the surface recombination velocity of the GaAs surface. The surface chemistry and band bending of the ammonium sulfide treated GaAs (100) surface has been studied using surface sensitive synchrotron radiation photoemission spectroscopy on beamline III-1, the "new grasshopper". Although previous publications reported that only arsenic sulfides were found on the surface, we find that the treatment leaves the GaAs surface terminated with roughly a monolayer of sulfur bonded to both As and Ga atoms. In addition, an n-type barrier height of 0.8 eV is measured. The thermal stability of the various chemical components are studied, and it is found that the arsenic sulfide compounds desorb from the surface at ≈250 C, while the gallium sulfides are stable at temperatures of at least 400 C. In work stimulated in part by this data, we have proposed a mechanism for the reduced surface recombination velocity observed on these surfaces, based on the anti-site defect model. This model is consistent with the increase in band bending observed after treatment, and predicts that the reduced surface recombination velocity is due to the increased band bending (sweeping electrons away), and a change in the charge state of the midgap states (reducing the hole capture cross section).

This work is supported by the Defense Advanced Research Project Agency and the Office of Naval Research Contract N00014-89-J-1083.

REFERENCES

1. C. J. Spindt, D. Liu, K. Miyano, P. L. Meissner, T. T. Chiang, T. Kendelewicz, I. Lindau, and W. E. Spicer, Appl. Phys. Lett. **55** (9), 861 (1989).
2. C. J. Spindt and W. E. Spicer, Appl. Phys. Lett. **55** (16), 1653 (1989).

Proposal No. 935Vp

USE OF EPITAXIAL OVERLAYERS TO STUDY SURFACE CORE LEVEL SHIFTS AT THE CLEAVED Si, InP, AND GaP SURFACES

T. Kendelewicz, J. C. Woicik, K. Miyano, R. Cao, P. Pianetta, I. Lindau, and W. E. Spicer
Stanford Electronics Laboratories, Stanford University, Stanford CA 94305

Monolayer quantities of adsorbates are shown to quench surface components of core level photoemission spectra from cleaved semiconductor surfaces. In this work, we use selected epitaxial and nonreactive overlayers to obtain an accurate estimate of the Si 2p and P 2p bulk core level line shapes. The core hole Lorenzian widths, branching ratios, and spin orbit splittings determined by this method are then used to analyze the core level line shapes from the clean surfaces. Our analysis provides new insight to the surface core level shifts of Si(111) 2x1 and to the less studied III-V phosphides. The overlayers which we have chosen for this work are Ge and Sb for Si(111) and Sb and Bi for InP(110) and GaP(110). Our upper estimate of the Lorenzian width of 0.07 eV for both the Si 2p and P 2p core levels is one third of that used in previous high resolution photoemission studies. As a consequence, we find it impossible to fit our Si(111) 2x1 surface sensitive spectra with only two surface shifted components. An additional component finds a straightforward interpretation in the context of the chain model, while earlier photoemission results using only two surface shifted components favor the buckling model of the 2x1 reconstruction. The surface sensitive P 2p spectra show a single surface component shifted 0.29 and 0.42 eV towards lower binding energy relative to the bulk component for InP and GaP, respectively. The surface shifts of the In 4d and the Ga 3d core levels from the same surfaces are in the opposite direction and are nearly equal in magnitude (~0.3 eV).

This work is supported by the Defense Advanced Research Project Agency and the Office of Naval Research Contract No. N00014-89-J-1083.

INTERFACIAL CHEMISTRY AND BAND BENDING AT In, Al, Ag, AND Pt INTERFACES WITH CdTe AND ZnTe (110)

Proposal No. 935Vp

A. K. Wahi, K. Miyano, G. P. Carey, T. T. Chiang, I. Lindau, and W. E. Spicer

Stanford Electronics Laboratories, Stanford University, Stanford, CA 94305

Interest in examining Schottky barrier formation on II-VI semiconductors has increased in recent years. In comparison to III-V semiconductors such as GaAs, relatively little is known concerning Schottky barrier formation and interfacial chemistry at metal/II-VI interfaces.[1,2] We have investigated interfacial chemistry and morphology in conjunction with band bending behavior for In, Al, Ag, and Pt overlayers on both CdTe (E_g = 1.5 eV) and the wider bandgap ZnTe (E_g = 2.2 eV) using photoemission.[3,4] These comparative studies are also important in relation to metal/HgCdTe and metal/HgZnTe interface formation, where HgZnTe has been proposed as structurally more stable than HgCdTe.[5]

Experiments were performed on Beamline I-1 and Beamline I-3 (old and new grasshopper monochromators) at the Stanford Synchrotron Radiation Laboratory (SSRL). Photon energies were chosen to provide a range of surface sensitivities (electron escape depth, λ ~5 - 7 Å and ~10 - 20 Å). Experiments were also performed using a He discharge lamp for UPS studies (He I and He II, 21.2 and 40.8 eV). The kinetic energy of the photoemitted electrons was analyzed using a double-pass cylindrical mirror analyzer (CMA).

The metals chosen provide a range of metal-substrate reactivities: Al reacts strongly with Te, Ag moderately, and In minimally, with no evidence seen for In reaction on ZnTe. Pt exhibits strong alloying behavior with both Cd and Zn. All four metals are found to yield Schottky barriers on CdTe and ZnTe, with a narrow range of final Fermi level positions, $E_{fi} = E_f - E_{VBM}$, observed on CdTe, from 0.9 to 1.05 ± 0.1 eV, and on ZnTe from 0.65 to 1.0 ± 0.1 eV. The prediction of the MIGS model that a difference in barrier height exists for two semiconductors dependent upon their band lineup (valence band offset)[6] is examined and found to agree with experiment for Ag, Pt, and Al, but not for In. For the highly reactive Al, no evidence for the overlayer metallicity required for MIGS to operate is seen on CdTe or ZnTe until after band bending has stabilized. Reaction and intermixing for Al, Ag, and Pt overlayers on CdTe and ZnTe indicate these interfaces are not ideal. In view of the reaction and intermixing seen for Ag, Pt, and Al, and specifically the lack of metallicity seen for Al overlayers, a defect mechanism can provide a more consistent explanation for the observed barrier heights.

These results for the binaries CdTe and ZnTe are also compared to metal/HgCdTe interface formation.[4] We find that Hg loss can significantly influence the extent of reaction and/or intermixing for these overlayers, with resulting disruption either inhibiting or facilitating chemical interaction.

This work is supported by NASA/Langley under Contract No. NAG1-851 and by DARPA under Contract No. N00014-86-K-0854.

REFERENCES

1. I. M. Dharmadasa, W. G. Herrenden-Harker, and R. H. Williams, Appl. Phys. Lett. **48**, 1802 (1986).
2. D. J. Friedman, I. Lindau, W. E. Spicer, Phys. Rev. B **37**, 731 (1988).
3. A. K. Wahi, K. Miyano, G. P. Carey, T. T. Chiang, I. Lindau, and W. E. Spicer, J. Vac. Sci. Technol. A, to be published.
4. A. K. Wahi, G. P. Carey, K. Miyano, T. T. Chiang, I. Lindau, and W. E. Spicer, J. Vac. Sci. Technol. A, to be published in Mar/Apr 1990.
5. A. Sher, A.-B. Chen, W. E. Spicer, and C.-K. Shih, J. Vac. Sci. Technol. A **3**, 105 (1985).
6. J. Tersoff, Phys. Rev. Lett. **56**, 2755 (1986).

NEAR EDGE ABSORPTION FROM Yb SILICIDES

L, Braicovich, E. Puppin, M. Sancrotti
Istituto di Fisica - Politecnico di Milano
P.za Leonardo da Vinci 32 - 20133 Milano (Italy)

F. Marchetti
Istituto per la Ricerca Scientifica e Tecnologica
Povo 38050 (Italy)

G. L. Olcese
Istituto di Chimica - Fisica - Universita' di Genova
C.so Europa 30 - 16132 Genova (Italy)

I. Lindau
Stanford Electronics Laboratories - Stanford University
Stanford 94305 CA (U.S.A.)

Near edge absorption spectroscopy can be used to determine the value of valence in compounds which exhibits mixed valence behavior. In the past, this technique has been widely used in order to study the value of valence in rare earths compounds. Whitin this proposal it has been already studied the effect of chemical pressure on Yb mean valence in two families of isostructural Laves phases: $Yb_{1-x}Ca_xAl_2$ and $Yb_{1-x}Sc_xAl_2$, $0 \leq x \leq 0.8$ [1]. L_{II} and L_{III} absorption spectra clearly showed that the value of valence monotonically increases with the Yb nearest neighbor distance.

A word of caution, however, must be spent in this context since, in certain cases, the value of valence as extracted from the decomposition of the absorption spectra is considerably different with respect to Yb valences determined with other techniques. Two examples of this behavior are represented by $Yb_{0.4}Sc_{0.6}Al_2$ and $Yb_{0.2}Sc_{0.8}Al_2$ for which 4f photemission leads to estimate Yb mean valences remarkably lower than the values inferred by Yb L_{III} X-ray absorption spectroscopy [1]. For this reason it is important to compare the absorption data with other spectroscopic results.

Yb silicides (Yb_3Si_5, YbSi and Yb_5Si_3) were extensively investigated with photoelectron spectroscopy [2] and the values of valence were extracted from 4f photoemission spectra by obtaining results in good agreement with other techniques. We measured, in the present experiment, the L_{III} Yb absorption edge in all of these three compounds. We measured the edges of polycrystalline samples scraped with a diamond file in Ultra High Vacuum in order to avoid surface sample contamination. Furthermore, we repeated the experiment by using finely grounded powders (from the same samples) by obtaining the same results.

The Yb valence as a function of the nearest neighbors distance, as extracted from the absoption data, shows the same monotonic trend already observed in 4f photoemission. However, the values extracted from the absorpion spectra are sistematically higher compared to the valence photoemission results. The work is in progress in order to analyze these results.

REFERENCES

1) M. Sancrotti *et al.*, two papers in print on Solid State Communications

2) I. Abbati *et al.*, Phys. Rev B **34**, 4150 (1986); I. Abbati *et al.*, Solid State Commun. **62**, 35 (1987)

Threshold PES of Kr $4s^{-1}$ Satellites

Proposal No. 943Vp

L. J. Medhurst M. Siggel, and D.A. Shirley
Department of Chemistry,
University of California
and Materials and Chemical Sciences Division
Lawrence Berkeley Laboratory,
1 Cyclotron Road
Berkeley, CA 94720

Satellites in photoelectron spectra are the result of electron correlation. The $4s^{-1}$ satellites of Kr, which appear between the $4s^{-1}$ threshold and the $4p^{-2}$ threshold, are degenerate in energy with the doubly excited states leading up to $4p^{-2}$ ionization. In this case, it is then possible to see the results of dynamic electron-electron correlation as opposed to intrinsic correlations.[1]

Figure 1 is the Kr Threshold PES from 27.25 eV to 38.75 eV photon energy. Preliminary results indicate that the satellites with binding energies closer to the $4s^{-1}$ binding energy than the $2p^{-2}$ binding energy are enhanced near threshold as compared to their relative intensities at higher photon energies.[2]

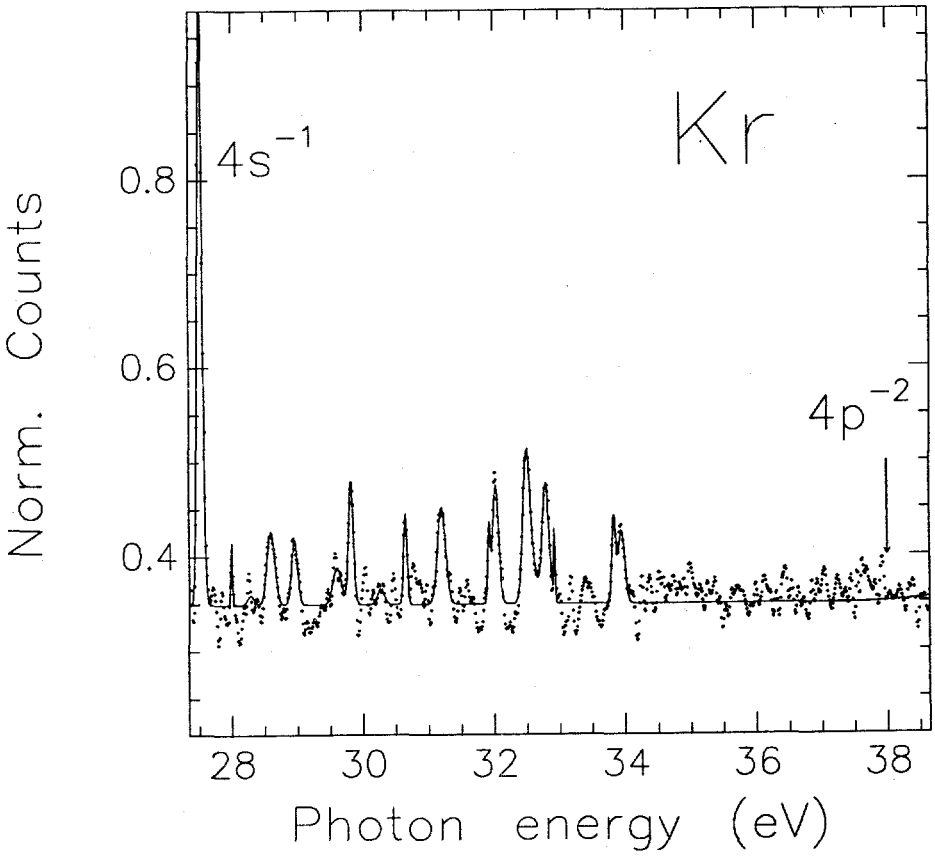

1) U. Becker, B. Langer, H. G. Kerkhoff, M. Kupsch, D. Szotak, R. Wehlitz, P. A. Heimann, S. H. Liu, D. W. Lindle, T. A. Ferrett, and D. A. Shirley, Phys. Rev. Lett. **60**, 1490 (1988).
2) S. Svensson, B. Eriksson, N. Martensson, G. Wendin, and U. Gelius, J. Electron Spectrosc. Relat. Phenom., **47**, 327 (1988).

*This work was supported by the Director, Office of Energy Research, Office of Basic Energy Sciences, Chemical Sciences Division of the U.S. Department of Energy under the Contract No. DE-AC03-76SF00098. It was performed at the National Synchrotron Light Source, which is supported by the Department of Energy's Office of Basic Energy Sciences.

TEMPERATURE DEPENDENT ARPEFS STUDY OF c(2x2)Cl/Cu(001)*

Li-qiong Wang, A.E. Schach von Wittenau, Z.G. Ji,
L.S. Wang, Z.Q. Huang, T. Shulman and D.A. Shirley

Department of Chemistry, University of California
and Materials and Chemical Sciences Division
Lawrence Berkeley Laboratory, 1 Cyclotron Road
Berkeley, CA 94720

Angle-Resolved Photoemission Extended Fine Structure (ARPEFS) is a novel technique to obtain surface structural information using photoelectron diffraction.[1]

We report the first temperature dependent ARPEFS measurements of c(2x2)Cl/Cu(001) on beam line III-3 at SSRL. The experiments were performed along two emission directions, [001] and [110], and at two temperatures, 110K and 298K. The Multiple-Scattering Spherical Wave analyses determined that the Cl atom adsorbs in the fourfold hollow site, and that the Cl-Cu bond length is 2.41±0.02Å, in agreement with LEED results.[2]

Low temperature ARPEFS has larger oscillation amplitudes and allows us to determine the reconstruction and small corrugation of the second substrate copper layer, induced by the adsorption of chlorine. Temperature dependent ARPEFS at two different emission directions also enables us to study the surface atom vibrational anisotropy.

*This work was supported by the Director, Office of Energy Research, Office of Basic Energy Sciences, Chemical Sciences Division of the U.S. Department of Energy under the Contract No. DE-AC03-76SF00098. It was performed at the National Synchrotron Light Source, which is supported by the Department of Energy's Office of Basic Energy Sciences.

1. J.J. Barton, S.W.Robey, and D.A. Shirley, Phys. Rev. B 34 (1986) 778.
2. F. Jona, D.Westphal, A.Goldmann and P.M. Marcus, J. Phys. C: Solid State Phys. 16 (1983) 3001.

LOW TEMPERATURE ARPEFS STUDY OF p(2x2)S/Ni(111) and √3x√3 R30° S/Ni(111)

A.E. Schach von Wittenau, L.Q. Wang, Z.Q. Huang,
Z. Hussain,** and D.A. Shirley

Department of Chemistry, University of California
and Materials and Chemical Sciences Division
Lawrence Berkeley Laboratory, 1 Cyclotron Road
Berkeley, CA 94720

Previous LEED[1],SEXAFS[2], and ion scattering[3] studies of p(2x2)S/Ni(111) have shown that S adsorbs into the FCC-like threefold hollow site, i.e. the site with no underlying Ni atom. Varying results for the S-Ni first layer distance and S-Ni bond length have been obtained. LEED results also indicate adsorbate-induced relaxations in the Ni surface. ARPES[4] studies of the √3x√3 R30° overlayer suggest a change of bonding site for this coverage.

We have performed low temperature (200° K) ARPEFS studies of p(2x2)S/Ni(111) and √3x√3 R30° S/Ni(111) using beamline X-24 at NSLS. Measurements were taken in the plane defined by the [111] and [O(SUP12(_),2)11] directions for both the p(2x2) coverage and in the √3x√3 R30° overlayer. Preliminary analysis of these low temperature data using multiple-scattering spherical-wave calculations indicates that in the p(2x2) case the S adsorbs 1.62 Å above the Ni surface, with reconstruction of the surface Ni layer. The S-Ni bond length is determined to be 2.16 Å.

Analysis of the √3x√3 R30° S/Ni(111) data continues.

*This work was supported by the Director, Office of Energy Research, Office of Basic Energy Sciences, Chemical Sciences Division of the U.S. Department of Energy under the Contract No. DE-AC03-76SF00098. It was performed at the National Synchrotron Light Source, which is supported by the Department of Energy's Office of Basic Energy Sciences. One of us (Z.H.) wish to acknowledge KFUPM for the grant of a sabbatical leave.

**Permanent address: Department of Physics, King Fahd University of Petroleum and Minerals, Dhahran 31261, Saudi Arabia.

1) Y.K. Wu and K.A.R. Mitchell Can. J. Chem. **67**,1975 (1989).
2) T. Ohta, Y. Kitajima, P.M. Stefan, M.L. Shek, N. Kosugi, and H. Kuroda, J. Phys. (Paris) **47** *C8*, 503 (1986).
3) T. Fauster, H. Duerr, and D. Hartwig Surace Sci. **178**, 657 (1986).
4) T.W. Capehart, C.W. Seabury, G.W. Graham and T.N. Rhodin, Surf Sci. **120**, L441 (1982).

LOW TEMPERATURE ARPEFS STUDY OF p(2x2)S/Cu(001)*

A.E. Schach von Wittenau, L.Q. Wang, Z.Q. Huang,
Z. Hussain,** Z.G. JI,
T. Shulman and D.A. Shirley

Department of Chemistry, University of California
and Materials and Chemical Sciences Division
Lawrence Berkeley Laboratory, 1 Cyclotron Road
Berkeley, CA 94720

Previous ARPEFS[1], LEED[2], and SEXAFS[3] studies of this surface, while agreeing that the S adsorbs into a fourfold hollow site, have given conflicting values for the distance between the S and the first Cu layer. They have also yielded different degrees of reconstruction of the near surface Cu layers..

We have performed low temperature (110° K) ARPEFS studies of p(2x2)S/Cu(001) using beamlines III-3 at SSRL and X-24 at NSLS. Measurements were taken in the [001] and [011] directions. Preliminary analysis of these low temperature data using multiple-scattering spherical-wave calculations indicates that the S adsorbs 1.32 Å above the Cu surface, with near surface reconstruction of the Cu layers similar to the LEED[2] results. The S-Cu bond length is determined to be 2.26 Å. We see no net vertical expansion or contraction of the Cu layers from the bulk extrapolated values.

*This work was supported by the Director, Office of Energy Research, Office of Basic Energy Sciences, Chemical Sciences Division of the U.S. Department of Energy under the Contract No. DE-AC03-76SF00098. It was performed at the Stanford Synchrotron Radiation Laboratory and National Synchrotron Light Source, which are supported by the Department of Energy's Office of Basic Energy Sciences. One of us (Z.H.) wish to acknowledge KFUPM for the grant of a sabbatical leave.

**Permanent address: Department of Physics, King Fahd University of Petroleum and Minerals, Dhahran 31261, Saudi Arabia.

1) C.C. Bahr, J.J. Barton, Z. Hussain, S.W. Robey, J.G. Tobin, and D.A. Shirley, Phys. Rev. B **35**, 3773 (1987).
2) H. C. Zeng, R. A. McFarlane, and K.A.R. Mitchell, Phys. Rev. B **39**, 8000 (1989).
3) J.R. Patel, D.W. Berreman, F. Sette, P.H. Citrin, J.E. Rowe, P.L. Cowan, T. Jach, and B. Karlin, Phys. Rev. B. **40**, 1330 (1989).

ARPEFS Study of p(2x2)K/Ni(111)

Z.Q. Huang, L.Q. Wang, A.E. Schach von Wittenau,
Z. Hussain,** and D.A. Shirley

Department of Chemistry, University of California
and Materials and Chemical Sciences Division
Lawrence Berkeley Laboratory, 1 Cyclotron Road
Berkeley, CA 94720

The adsorption of alkali metal on transition metal surfaces has been the subject of many experimental and theoretical studies because alkali additives are known to promote some major heterogeneous catalytic reactions[1]. Few surface structures have been determined, however, of these alkali-metal adsorption systems. We report the first experimental study of the geometric structure of p(2x2)K/Ni(111) using the technique of Angle_Resolved Photoemission Extended Fine Structure (ARPEFS)[2].

The p(2x2)K/Ni(111) system was prepared by evaporating K from a commercial SAES getter source onto a clean Ni(111) held at room temperature until a sharp, clear p(2x2) LEED pattern with little background was observed. K 1s angle-resolved photoemission was then measured on beamline X24A at NSLS. Results showed an energy dependent oscillation of the K 1s photoemission intensity over a kinetic energy range of 65-450 eV, arising from the photoelectron difffraction near the surface. Preliminary Fourier analysis of our data indicates that K atom most likely adsorbs on the three-fold hollow site on Ni(111)surface with a K-Ni distance of 3.2-3.3 Å. Comparison of experimental data with Multiple Scattering Spherical-Wave(MSSW) calculation is under way to reveal more structural details.

*This work was supported by the Director, Office of Energy Research, Office of Basic Energy Sciences, Chemical Sciences Division of the U.S. Department of Energy under the Contract No. DE-AC03-76SF00098.It was performed at the National Synchrotron Light Source, which is supported by the Department of Energy's Office of Basic Energy Sciences. One of us (Z.H.) wish to acknowledge KFUPM for the grant of a sabbatical leave.

**Permanent address: Department of Physics, King Fahd University of Petroleum and Minerals, Dhahran 31261, Saudi Arabia.

1) M. Grunze, in *The Chemical Physics of Solid Surfaces and Heterogeneous Catalysis*, eds. D.A. King and D.P. Woodruff (Elsevier, Amsterdam, 1982) vol.4, p.143
2) J.J. Barton, C.C. Bahr, Z. Hussain, S.W. Robey, J.G. Tobin, L.E. Klebanoff, and D.A. Shirley, Phys.Rev.Lett. 51, 272 (1983).

Photoelectron Spectroscopic Studies of CO Adsorption on the CuCl(111) Single Crystal Surface

Jian yi Lin, Paul M. Jones, Jeffrey A. Guckert, E.I. Solomon*

Introduction

CO adsorption on Cu/ZnO catalytic surfaces is an important step in the industrial synthesis of methanol. Continued interest lies in the elucidation of the bonding interaction of CO chemisorbed to such catalytic sites. Photoelectron Spectroscopic (PES) experiments involving CO adsorption on ZnO single crystal surfaces[1] indicate that σ donation from the CO 5σ orbital to the metal ion may dominate the bonding interactions in this chemisorption process. These results contrast the typical interactions of CO adsorption on a metal surface where metal-to-ligand π back-bonding generally dominates. In the present study the angular dependence of CO photoemission has been utilized to further define the electronic structure of CO chemisorbed to the CU^+ site in CuCl(111). This surface serves as a model for the Cu/ZnO surface, whose active site we have shown[2] to involve coordinatively unsaturated C3v Cu(I) sites on the (0001) and (1010) surfaces of ZnO. In addition, we have applied Auger yield NEXAFS experiments, which have been shown to be a sensitive probe of the bound C-O bond length[3], to the CO/CuCl system and calculated a C-O bond length for bound CO that is slightly shorter than that of free gaseous CO. These results support a bonding scheme for CO adsorption on CuCl(111) in which σ donation from the CO ligand dominates over the π back-bonding involved.

Experimental

All spectra were collected with synchrotron radiation from the plane grating monochromator on beam line U14A at the National Synchrotron Light Source (NSLS), Brookhaven National Laboratory. A Vacuum Generators UHV system, equipped with a double-pass cylindrical mirror analyzer (CMA), was employed and operated at a base pressure of 1×10^{-10} Torr. While the synchrotron radiation remained fixed at an angle of 88° relative to the central axis of the analyzer, the sample was rotated relative to the incident beam and the CMA to achieve various angle-dependent spectra. Accounting for all instrumentation, a final spectral resolution of 200 meV was maintained.

CuCl single crystals were polished with alumina grit and then etched with a HCl/EtOH solution. Further cleaning was performed in UHV by Ar ion sputtering followed by annealing at 360K. Surface cleanliness was monitored with core-level XPS.

Adsorption of CO on the sample surface was achieved by introducing an ambient CO atmosphere ($\sim 1 \times 10^{-5}$ Torr) into the UHV chamber for approximately ten minutes while maintaining the sample at 130K. All experiments were carried out using an electron flood gun to compensate for charging at the cold semiconducting CuCl surface.

Results and Discussion

After exposure to CO, two peaks were observed in the PES spectrum of CuCl which do not appear in the photoemission spectrum of the same surface prior to CO exposure (Figure 1). Peak I, centered at a binding energy of 12.3 eV originates from photoemission from the lone pair CO 4σ level. The peak at lower binding energy, peak II, can be assigned as overlapping photoemission from the CO 1π and CO 5σ levels through ARPES studies. In order to resolve these overlapping states, spectra were collected with two different sample orientations. With the sample positioned so that the axis of propagation of the incoming light was approximately normal to the CuCl surface, peak II was centered at a binding energy of 9.4 eV; whereas, with a grazing angle of incidence (nearly 90° off the surface normal) this same peak was centered at 9.0 eV. Having demonstrated from ARPES that the bond axis of the CO molecule is oriented perpendicular to the surface, we were able to resolve the overlapping states of peak II, assigning the state at lower binding energy as the CO 5σ and the contribution at slightly deeper binding energy as photoemission from the CO 1π level. Thus assigned, an energy separation between the 4σ and 1π levels of 2.8 eV is revealed, nearly identical to the free CO value. However, upon CO adsorption to the CU^+ active site, the 5σ orbital shifts 2.2 eV closer in energy to the 1π, indicating that the CO 5σ orbital is strongly involved in bonding. Two additional factors support a CO/CuCl bonding scheme predominantly σ in nature. First, based on the model derived by Stöhr et al[3], the broad shape resonance observed in the NEXAFS spectrum at 308.5 eV (see Figure 2) yields a C-O bond length of 0.110 ± 0.002nm for CO bound to CuCl(111), a value slightly shorter than that observed in free CO (0.113nm). Second, from He(I) PES studies the work function of the CO/CuCl surface is found to be 1.2 eV less than that of the clean surface, indicating a net charge transfer from the adsorbed CO to the surface.

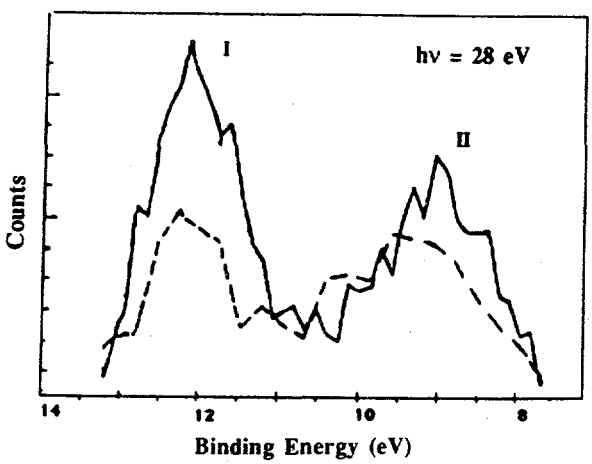

Figure 1. Angular dependence of photoemission intensity of the valence orbitals of CO/CuCl(111); (——) grazing angle of incidence; (---) near normal angle of incidence.

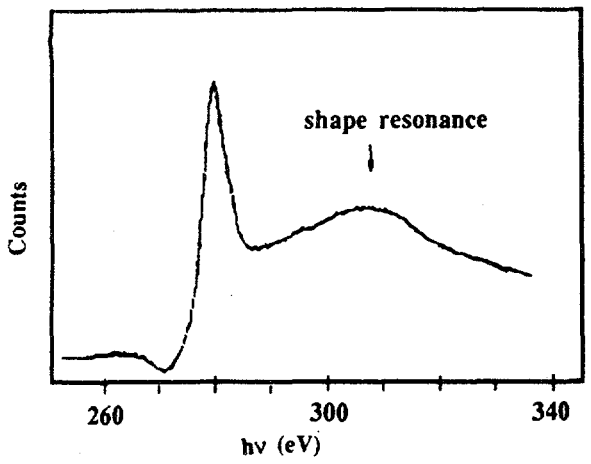

Figure 2. Normalized carbon K-edge NEXAFS spectra of CO/CuCl(111) employing a grazing angle of incidence.

References

1. (a) Gay, R.R.; Nodine, M.H.; Henrich, V.E.; Zeiger, H.J.; Solomon, E.I. J. Am. Chem. Soc. 1980, 102, 6752. (b) D'Amico, K.L.; McFeely, F.R.; Solomon, E.I. J. Am. Chem. Soc. 1983, 105, 6380.
2. Didziulis, S.V.; Butcher, K.D.; Cohen, S.L.; Solomon, E.I. Diss. Abstr. Int. B 1989, 49(7), 2666.
3. Stöhr, J. in "Chemistry and Physics of Solid Surfaces, Vol. V" ed. by Vanselow, V.R. and Howe, R., Springer-Verlag, 1984, 231.

Acknowledgements

We would like to thank Brookhaven National Laboratory for providing beam time for this study and the Stanford Synchrotron Radiation Laboratory for financial support.

PHOTOEMISSION STUDIES OF NARROW BAND MATERIALS

J.W. Allen[1], J.-S. Kang[1,2], O. Gunnarsson[3], O. Jepsen[3], T. Fujiwara[3], O.K. Andersen[3], Z.-X. Shen[4], W.P. Ellis[5], J.T. Market[2], Y. Dalichaouch[2], M.B. Maple[2], P.A.P. Lindberg[4], B.O. Wells[4], D.S. Dessau[4], A. Borg[4], K.N. Yang[2], M.S. Torikachvili[6], Y. Lassailly[7], B.B. Pate[4], I. Lindau[4], and W.E. Spicer[4]

[1] Randall Laboratory, University of Michigan, Ann Arbor, MI 48109-1120

[2] Dept. of Physics, University of California at San Diego, La Jolla, CA 92093

[3] Max-Planck Institut, D-7000 Stuttgart 80, FRG

[4] Stanford Electronic Laboratory, Stanford, CA 94305

[5] Los Alamos National Laboratory, Los Alamos, NM 87545

[6] Physics Department, San Diego State University, San Diego, CA 92182

[7] Ecole Polytechnique, 91128 Palaiseau, France

Resonant photoemission studies of Nd_2CuO_4

Using photon energies at the Cu 3p→3d edge, we have performed resonant photoemission spectroscopy (RESPES) on the Cu 3d states of ceramic samples of Nd_2CuO_4, of importance as a 'parent compound' in high temperature superconductivity. The sample temperature was about 100K, and the resolution about 0.3 eV. We have also made a theoretical calculation of the RESPES expected for this material if the 3d electrons are modeled by the impurity Anderson Hamiltonian.[1] All the model parameters for the calculation are obtained from *ab initio* calculations or atomic data. Fig. 1 shows the comparison between calculated (solid line) and measured (dots) energy distribution curves (EDC's). The upper two curves in Fig. 1 are calculated off-resonance spectra for photon polarization parallel and perpendicular to the c-axis. Overall, the main features of the calculated spectrum are in rather good agreement with the unpolarized experimental spectrum. The width of the main peak and the location of the satellites at about -10 eV and -12 eV are correct. The model predicts that the lowest lying state, the so-called local singlet, has much more weight than observed experimentally at the corresponding energies. The use of a lattice Anderson model might change the predicted weight, e.g., by giving the local singlet a dispersion. The calculation predicts that RESPES occurs only for perpendicular polarization, and that there should be a large off-resonance dependence on photon polarization for the main peak and the local singlet, offering a possible test of the Anderson model, and for the occurance of local singlet. Fig. 2 shows the calculated constant

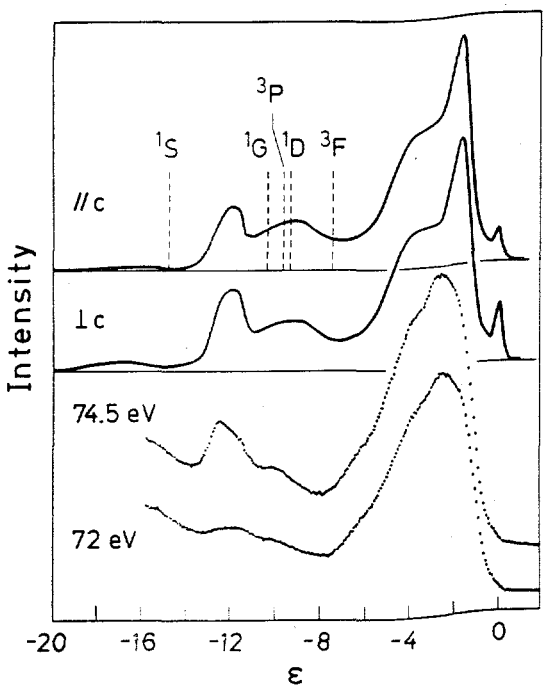

Fig. 1

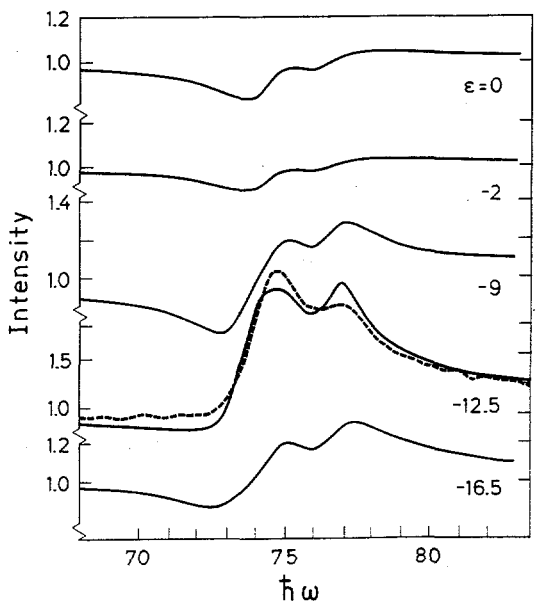

Fig. 2

initial state (CIS) spectra at various binding energies, showing antiresonance and resonance behaviors in the main band and satellite regions respectively. The experimental CIS spectrum for the largest satellite agrees well with the theory.

Angle resolved photoemission on MnO

Angle resolved photoemission spectra on the (110) surface of an MnO single crystal sample were measured. The data are being analyzed, and will be compared with a band theory calculation.

Electronic structure of $Ce(Ru_{1-x}Rh_x)_3B_2$

Beginning in 1984, under past program proposal 682VP, and continuing under the present proposal, we have made RESPES studies of the Ce 4f states in the alloy system $Ce(Ru_{1-x}Rh_x)_3B_2$, which, with increasing x, changes from a superconductor to an unusual ferromagnet. We have now constructed a complete scenario for this behavior.[2] The RESPES data have been combined with Bremstrahllung isochromat spectra (BIS) of the unoccupied Ce 4f states, as shown in Fig. 3. The peak near the Fermi energy E_F is the Kondo resonance. We have also measured the X-ray photoemission spectra (XPS) of the Ce 3d core levels (not shown). All the data have been analyzed by fitting with spectral functions for the impurity Anderson Hamiltonian, shown as solid lines in Fig. 3. The energy dependence of the hybridization matrix element in the Hamiltonian was taken to be the experimental valence band density of states, obtained in our synchrotron studies, and shown in Fig. 4. For

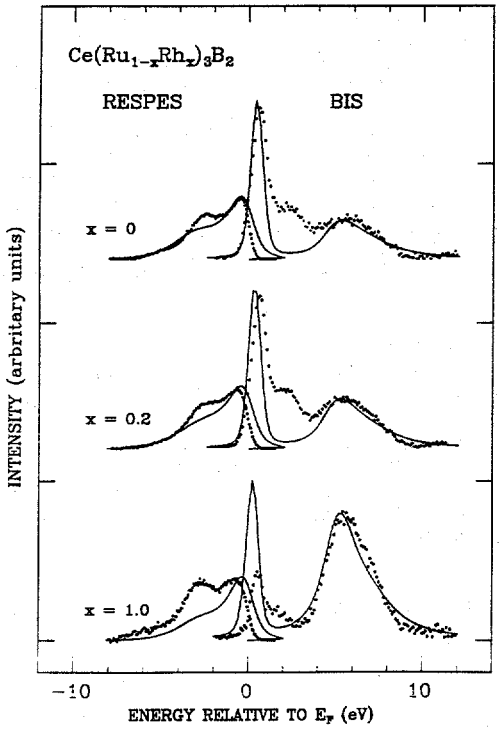

Fig. 3

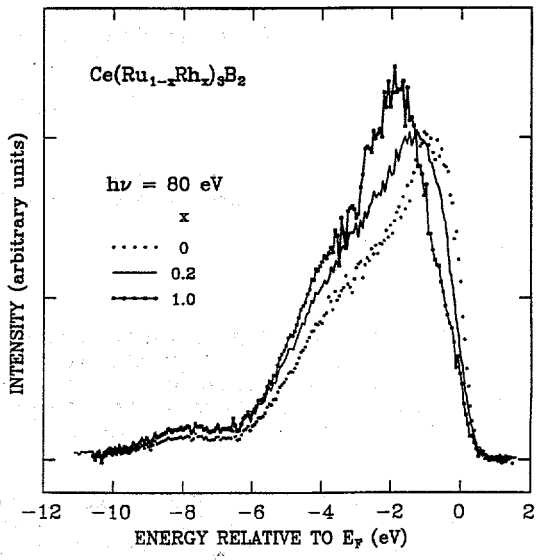

Fig. 4

x=1, we fit a recently published[3] single crystal Ce 3d XPS spectrum because our polycrystalline samples had some grain boundary oxides, as shown by the difference between the calculated and measured x=1 BIS spectra of Fig. 3. We find that the Kondo temperature T_K, calculated from the spectroscopic parameters, varies from large to small as x changes from 0 to 1, because the density of states at E_F decreases. We then argue that the change in the strength of the spin-quenching, measured by T_K, promotes the change in ground states, and that this alloy behavior comes about because of the difference in the Ru and Rh 5d states at E_F. We propose that the ferromagnetism for x=1 be understood in terms of an experimentally unresolved exchange splitting of the E_F Kondo resonance.

REFERENCES

1. O. Gunnarsson, J.W. Allen, O. Jepsen, T. Fujiwara, O.K. Andersen, C.G. Olson, M.B. Maple, J.-S. Kang, L.Z. Liu, J.-H. Park, R.O. Anderson, W.P. Ellis, R. Liu, J.T. Market, Y. Dalichaouch, Z.-X. Shen, P.A.P. Lindberg, B.O. Wells, D.S. Dessau, A. Borg, I. Lindau and W.E. Spicer, Phys. Rev. B (Rapid Commu.), accepted for publication.
2. J.W. Allen, M.B. Maple, J.-S. Kang, K.N. Yang, M.S. Torikachvili, Y. Lassailly, W.P. Ellis, B.B. Pate, and I. Lindau, Phys. Rev. B, accepted for publication.
3. M. Kasaya, A. Okabe, T. Takahashi, T. Satoh, T. Kasuya and A. Fujimori, J. Magn. Magn. Mater. **76&77**, 347 (1988).

Orientation of Submonolayer Coverages of Furan and 2,5-Dihydrofuran on Ag(110) Determined by NEXAFS

J.L. Solomon and R.J. Madix*
J. Stöhr**

*Department of Chemical Engineering, Stanford University, Stanford, CA 94305
**IBM Almaden Research Center, 650 Harry Road, San Jose, Ca 95120

We have used near-edge X-ray absorption fine-structure (NEXAFS) measurements to determine the orientation of furan and 2,5-dihydrofuran (2,5-DHF) on the surface of a silver (110) single crystal. The position of the absorption threshold or the edge-jump in the NEXAFS spectra is compared to the XPS binding energy.

Experimental

NEXAFS experiments were performed at Stanford Synchrotron Radiation Laboratory on beam line I-1 with a grasshopper monochromator (1200 lines/mm holographic grating). Spectra were recorded at the carbon K-edge with partial-electron-yield detection using a retarding voltage of -200 volts. All spectra were recorded with the surface at 100 K. The final normalized NEXAFS spectra were prepared by dividing spectra recorded for the adsorbate-covered surface by spectra recorded for the clean surface to remove the strong variation in photon intensity present in the transmission function of the monochromator. The final spectra were curvefit to determine peak positions and areas [1]. The π^* resonances were fit with symmetric Gaussian peaks, and the σ^* resonances were fit with symmetric and asymmetric Gaussian peaks [1]. A Gaussian broadened step was used to model the absorption threshold or edge-jump.

Results

The NEXAFS spectra for a submonolayer coverage of furan on Ag(110) show that the plane of the furan molecule lies nearly parallel to the plane of the surface (figure 1). At glancing incidence of the X-rays π^* resonances dominate the spectra, and the σ^* resonance are greatly diminished. At normal incidence the π^* resonances are much smaller than the large σ^* resonances. Since the π^* resonances are observed when the $\vec{E}$ is perpendicular to the plane of the furan molecule, and since the σ^* resonances are observed when the $\vec{E}$ is in the plane of the molecule, the NEXAFS spectra show clearly that the furan molecule is preferentially oriented parallel to the plane of the surface. The intensity variation of an individual resonance from glancing to normal incidence can be used to calculate the orientation of the molecule [2]. For the furan submonolayer the molecule tilts at an angle of 23±5° as determined from the average of the tilt angles of 21° and 24° calculated from the two $3b_1$ π^* resonances. The tilt angles calculated from the σ^* resonances are consistent with the values determined from the π^* resonances. The XPS binding energies for the two C(1s) levels of furan are 284.8 and 286.2 eV [3], while the lowest possible position of the edge-jump is 288.4 eV.

NEXAFS spectra for the 2,5-DHF at submonolayer coverage shows that the p-orbitals comprising the double bond are preferentially oriented perpendicular to the plane of the Ag(110) surface (figure 2). The π^* resonance is much larger at glancing incidence than at normal incidence, and the σ^*(C=C) resonance is much larger at normal incidence relative to glancing X-ray incidence. Based on the π^* intensity ratio of glancing to normal, the plane containing the π system tilts at an angle of 18±5° from the surface normal. A slight though distinct azimuthal dependence is observed for the σ^* resonances associated with the C-O and C-C single bonds for the submonolayer coverage of 2,5-DHF (figure 2, curves b and c). The resonances observed for the monolayer and submonolayer are at the same energy as the multilayer indicating only weak interaction of 2,5-DHF with the Ag(110) surface. The XPS binding energies of 2,5-DHF are 285.1 and 286.6 eV [3]. The lowest possible energy for the edge-jump is 287.8 eV.

Discussion

The XPS C(1s) binding energies of furan and 2,5-DHF are not at the same energy as the edge-jump in the NEXAFS spectra. The edge-jump in the NEXAFS spectrum corresponds to transitions from the core level (the C(1s) level for data reported here) to the a continuum of states. The continuum of states may be either the Fermi level of silver, or the vacuum level. Since the measured XPS binding energy is the energy difference between the C(1s) level and the Fermi level, the edge-jump should occur at the XPS binding energy if the edge-jump corresponds to transition to the Fermi level. The lowest possible energy position of the edge-jump for the NEXAFS spectra for furan and 2,5-DHF on Ag(110) is consistently about 2.0 eV higher in energy than the average XPS binding energy. The 0.3 eV uncertainty in the XPS binding energies and the 0.5 eV uncertainty in the energy calibration of the X-ray monochromator used in the NEXAFS experiments will not explain the difference. If, however, the edge-jump corresponds to transitions from the C(1s) level to the vacuum level, the edge-jump position would be the sum of the XPS binding energy and the work function of the silver surface, which is 4.5 eV [4]. Since we are unable to position the edge-jump at the XPS binding energy, the edge-jump has been set at the XPS binding energy plus the work function.

The observation that the edge-jump in the NEXAFS spectra corresponds to transitions from the core level to the vacuum level and not to the Fermi level is consistent with the NEXAFS results which both indicate that furan and 2,5-DHF are only weakly bound to the Ag(110) surface. Since the molecules are only weakly bound, there is very little overlap between the molecular orbitals and the metal states, so the probability of transitions to the Fermi level are small. The XPS binding energies also indicate weak adsorption. A difference 1 to 2 eV between the gas phase binding energies, E_g, and the XPS binding energies of the adsorbed molecules relative to the vacuum level (the measured XPS values, E_{ads}, plus the work function, φ) is indicative on a weakly bound, non-interacting surface species [5]. The XPS measurements are, therefore, also consistent with a weak molecular adsorption since $E_g - E_{ads} + \varphi$ is between 0.9 and 1.4 eV for the C(1s) and O(1s) levels of furan and 2,5-DHF. The difference between E_g and $E_{ads} + \varphi$ is due to surface relaxation effects [5].

Acknowledgements

The assistance of J.T. Roberts, A. Muscat, A.C. Liu, W. Jark, and D. Coulman in collecting the NEXAFS data is gratefully acknowledged. The NEXAFS experiments were performed at Stanford Synchrotron Radiation Laboratory which is funded by the Department of Energy under contract DE-AC03-82ER-13000, Office of Basic Energy Sciences, Division of Chemical Sciences. We also gratefully acknowledge the support of the Center of Material Research at Stanford.

References

[1]. D.A. Outka and J. Stöhr, J. Chem. Phys. **88** (1988) 3539.

[2]. J. Stöhr and D.A. Outka, Phys. Rev. B **36** (1987) 7891.

[3]. J.L. Solomon and R.J. Madix, in preparation.

[4]. A.W. Dweydari and C.H.B. Mee, Phys. Status Solidi A **27** (1975) 223.

[5]. C.R. Brundle and A.F. Carley, Faraday Disc. Chem. Soc. **60** (1975) 51.

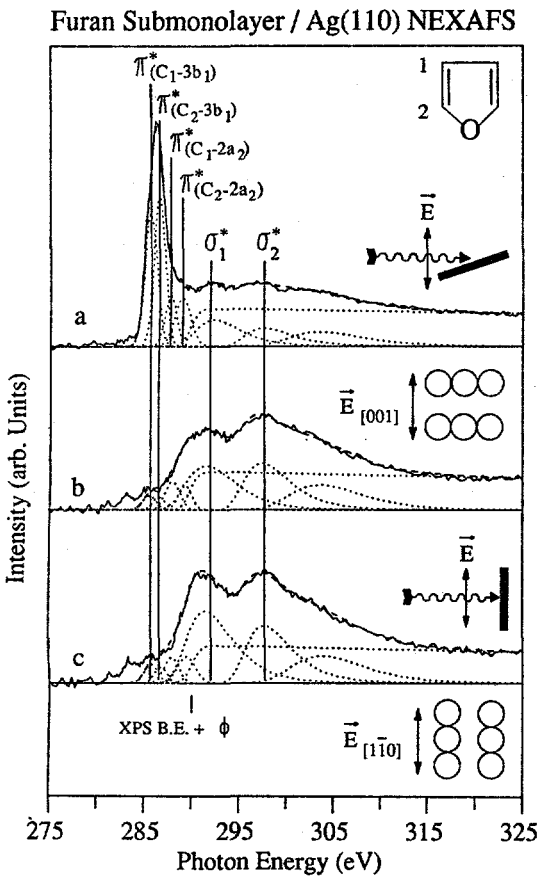

Figure 1. Carbon K-edge NEXAFS spectra of furan submonolayer are shown for glancing and normal X-ray incidence. Normal incidence spectra are shown both for the E vector of the X-rays along ([1$\bar{1}$0] azimuth) and across ([001] azimuth) the rows of the Ag(110) surface. The clear polar dependance of the π^* resonances between the glancing and normal incidence indicate the plane of the furan molecule lies nearly coplanar with the plane of the surface. At normal incidence a small yet clearly observable azimuthal dependance is also observed for the σ^* resonances.

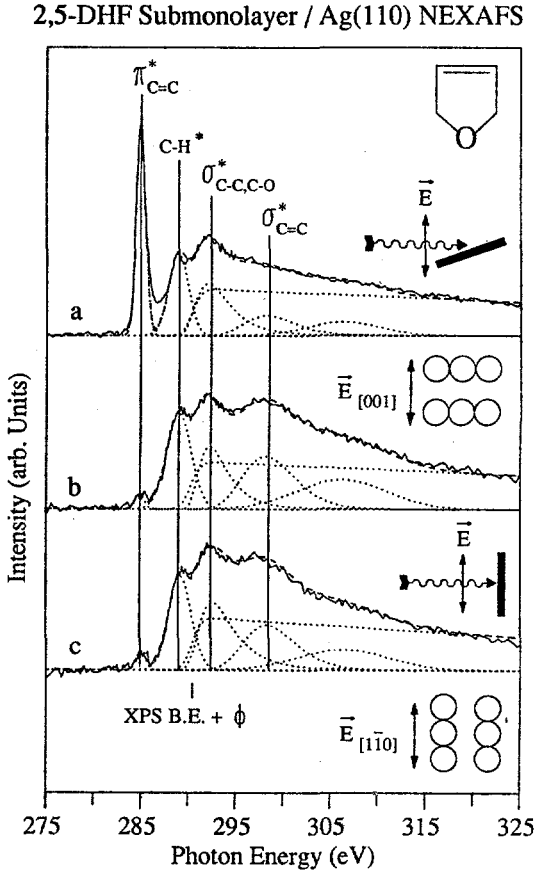

Figure 2. Carbon K-edge NEXAFS spectra of 2,5-DHF submonolayer are shown for glancing and normal X-ray incidence for the $\vec{E}$ along and across the rows of the Ag(110) surface. The double bond of the 2,5-DHF molecule lies nearly parallel to the plane of the surface, as seen by the polar dependance of the π^* resonance. A small azimuthal dependance is observed at normal incidence since the σ^* (C-C,C-O) resonance is larger when the E vector is along the rows ([1$\bar{1}$0] azimuth) than when it is across the rows ([001] azimuth).

PHOTOEMISSION STUDY OF HIGH TEMPERATURE SUPERCONDUCTORS AND RELATED MATERIALS

B.O. Wells, Z.-X. Shen, D. S. Dessau, P. A. P. Lindberg, I. Lindau, and W. E. Spicer
Stanford Electronics Laboratories, Stanford University, Stanford, CA 94305

INTRODUCTION

The recently discovered high temperature superconductors promise to be of great importance but as yet are not well understood. We performed experiments at the Stanford Synchrotron Radiation Laboratory (SSRL) on several families of these new superconductors, $Bi_2CaSr_2Cu_2O_8$, $Pb_2Sr_2PrCu_3O_8$, and $BaBiO_3$. These superconductors have very complex structures, with 5 or more types of atoms, and present new, not yet understood physics. To aid in our understanding it is useful to study simpler systems that have similar properties to the high temperature superconductors. For this reason, we have undertaken a study of transition metal oxides such as CoO, NiO, and CuO. These compounds are antiferromagnetic insulators, although traditional band theory predicts them to be conductors. The reason for this discrepancy is believed to be the presence of strong electron-electron correlations. The parent compounds of the Cu-O superconductors are antiferromagnetic insulators, and they become superconducting when doped appropriately. Thus, the attempt to understand the transition metal oxides first is an appropriate approach. Following are some examples of such efforts.

MATERIALS

1. $Bi_2CaSr_2Cu_2O_8$

a. Symmetry of Valence Band States [1]

The symmetry of the electronic states that lie near the Fermi level, and are therefore involved in the superconducting transport, is of great theoretical importance. There has been work to determine the symmetry of the unoccupied states near the Fermi level in $Bi_2CaSr_2Cu_2O_8$ [2], but we have made the first determination of the symmetry of the occupied states. We used angle resolved photoemission for this experiment. The highly polarized nature of the synchrotron radiation allows us to examine the changes in the photoemission spectra produced by changing the angle between the surface normal and the electric field of the incident light. When electrons are collected at normal emission, the symmetry selection rules are relatively straightforward. Figure 1 shows the variation of the valence band spectrum with radiation incident angle. We were able to determine that the states we measured near the Fermi level had Δ_5 crystal symmetry, while the states near the bottom of the valence band had Δ_1 symmetry. This indicates that O $2p_x$ and O $2p_y$ states lie near the Fermi level, while O $2p_z$ states lie deeper in the valence band.

b. Band Mapping [3]

Using angle resolved photoemission, we were able to map the dispersion of the bands in $Bi_2CaSr_2Cu_2O_8$. There was very little dispersion along the Γ-Z **k**-space direction (normal to the planes). The lack of dispersion indicates very little orbital overlap along the direction parallel to the planes. This confirms the highly two dimensional character of the $Bi_2CaSr_2Cu_2O_8$ material. Parallel to the planes there was dispersion, more near the bottom of the valence band than near the Fermi level. This is similar to the dispersion seen in transition metal oxides but less pronounced.

2. $Pb_2Sr_2PrCu_3O_8$ [4]

We performed the first photoemission electronic structure experiment on $Pb_2Sr_2PrCu_3O_8$. We noted that, like the other Cu-O based high T_c superconductors, correlation effects pay an important role in observed spectrum. Of particular interest was a comparison to

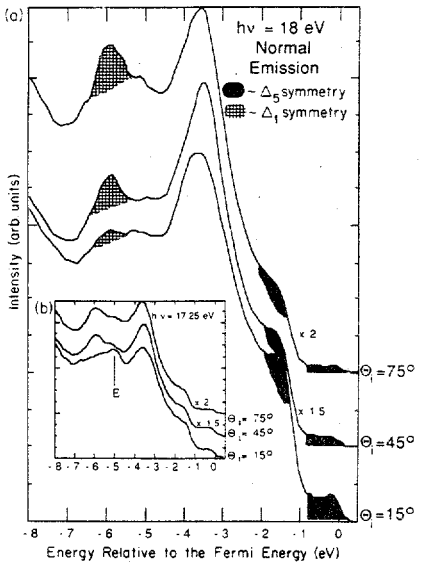

Fig. 1. Polarization-dependent EDC's for (a) 18 eV and (b) 17.25 eV radiation. The 17.25 eV spectrum is included to show feature E, which only appears for low photon energies.

the 123 ($RBa_2Cu_3O_7$) material $PrBa_2Cu_3O_7$. The two materials are very similar in structure. However, the 123 structure is a superconductor for R as any rare earth atom except Pr, while the $Pb_2Sr_2RCu_3O_8$ system is still a superconductor for R=Pr. We used resonant photoemission to determine the Pr contribution to the valence band of these compounds. Our results show that Pr 4f states are more strongly hybridized with the Cu-O states in the $PrBa_2Cu_3O_7$ compound than in the $Pb_2Sr_2PrCu_3O_8$ material (see Fig. 2). We theorize that this extra hybridization interferes with the superconductivity in the Cu-O states.

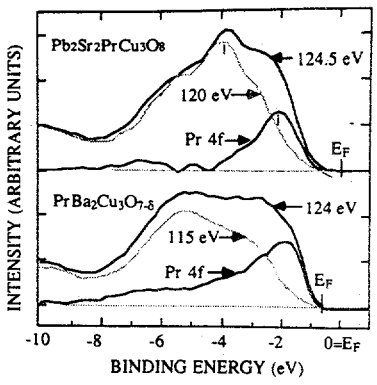

Fig. 2. Valence-band EDC's of $Pb_2Sr_2PrCu_3O_8$ and $PrBa_2Cu_3O_{7-\delta}$ [5] at photon energies just above and below the Pr 4d $\rightarrow$ 4*f* absorption edge. The valence-band maximums have been aligned for easier comparison. The normalization of the EDC's is described in the text. A subtraction of the two curves gives the extracted Pr 4*f* partial density of states. The tick marks correspond to the initial energies of the CIS curves in Fig. 3.

3. $BiBaO_3$ [5]

$BaBiO_3$ is a semiconductor and is the parent compound of the superconductors (BaK)(PbBi)O_3. $Ba_{1-x}K_xBiO_3$ has a transition temperature of about 30 K and is considered the only non Cu-O based high T_c superconductor. We performed photoemission experiments on $BaBiO_3$ in its "valence disordered" phase. The valence band total density of states looks very similar to the band calculations for this material, as shown in Fig.3. This is very different from the Cu-O based superconductors. We found evidence for an oxygen resonance in this material. There was a rapid change in the photoemission cross section of some valence band features at the same energy where there is an increase in the total x-ray absorption. The existence of an oxygen resonance has been a matter of great debate for the Cu-O based superconductors. Finally, we found that there can only be a small charge fluctuation between the unequal Bi sites, in contrast to a simple ionic picture of the compound.

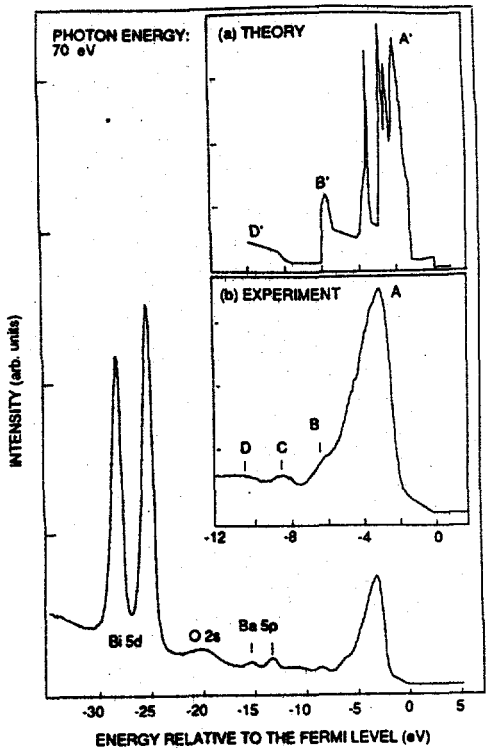

Fig.3. Valence-band and shallow core level photoemission spectrum recorded at 70 eV. The inset is a magnification of the valence-band spectrum, together with the valence band total density of states from a band calculation.

4. CoO [6]

We have performed resonance photoemission, angle resolved photoemission, and core level photoemission studies of single-crystalline CoO. On the one hand, strong correlation effects among the d electrons are observed, as signaled by a strong reduction of Co 3d bands and satellites in both the valence band and core levels. On the other hand, the oxygen states are found to be very band like, as indicated by strong dispersions of oxygen states in the valence band and the lack of oxygen satellites (see Fig.4). We give estimations of 30 and 1.5 for U/W (Coulomb interaction/band width) ratio of Co 3d bands and O 2p bands, respectively. This indicates that the density functional band calculation works well for the oxygen bands but not for the Co bands, which is verified by a comparison between the experimental and theoretical E verses k relations. We argue that CoO is not a band insulator, but a charge transfer insulator. We have also observed the effects of local magnetic order on the electronic structure. Finally, we give a general guideline on calculating the band structure of CoO by introducing a mechanism that reduces the Co 3d band width by 25%, while still retaining the other essential features of the band calculation.

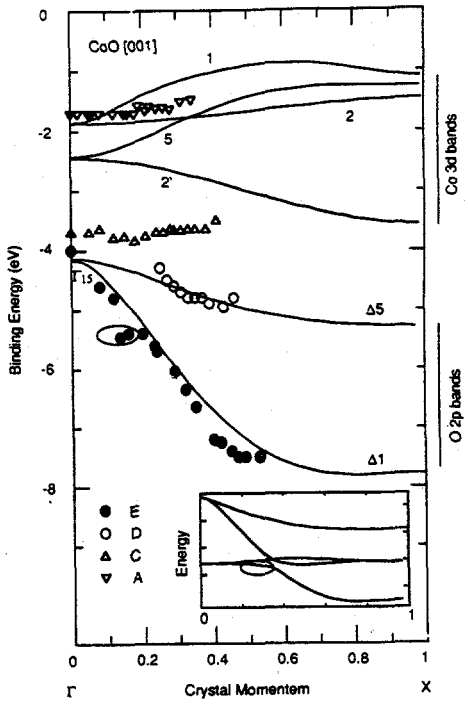

Fig. 4. Comparison of experimental E verses k relation with the results of a nonmagnetic band calculation.

This work is supported by the National Science Foundation and the Materials Research Laboratory Program at the Center for Materials Research at Stanford and the JSEP Contract DAAG29-85-K-0048.

REFERENCES

1. B.O. Wells, P.A.P. Lindberg, Z.-X. Shen, D.S. Dessau, W.E. Spicer, I. Lindau, D.B. Mitzi, and A. Kapitulnik, Phys. Rev. B **40**, 5259 (1989).
2. F.J. Himpsel, G.V. Cchandrashekar, A.B. McLean, and M.W. Shafer, Phys. Rev. B **38**, 7144 (1988); N. Nucker, H. Romberg, X.X. Xi, J. Fink, B. gegenheimer, and Z.X. Zhao, Phys. Rev. B **39**, 6619 (1989).
3. P.A.P. Lindberg, Z.-X. Shen, D.S. Dessau, B.O. Wells, D.B. Mitzi, I. Lindau, W.E. Spicer, and A. Kapitulnik, Phys Rev. B **40**, 5169 (1989).
4. D.S. Dessau, Z.-X. Shen, P.A.P. Lindberg, B.O. Wells, A. Borg, I. Lindau, W. E. Spicer, J.V. Waszczak, and L.F. Schneemeyer, Phys. Rev. B **40**, 6726 (1989).
5. Z.-X. Shen, P.A.P. Lindberg, B.O. Wells, D.S. Dessau, A. Borg, I. Lindau, W.E. Spicer, W.P. Ellis, G.H. Kwei, K.C. Ott, J.-S. Kang, and J.W. Allen, Phys Rev. B **40**, 6912 (1989).
6. Z.-X. Shen, J.W. Allen, P.A.P. Lindberg, W. Ellis, J.S. Kang, D.S. Dessau, B.O.Wells, A. Borg, S.-J. Oh, I. Lindau, and W.E. Spicer, Preprint.

A microchannel-plate-intensified, subnanosecond, x-ray imaging camera

Proposal No. 9901V

M. R. Carter, B. J. McKinley, and K. G. Tirsell

University of California, Lawrence Livermore National Laboratory
P. O. Box 808, L-43, Livermore, California 94550

Introduction

We have developed a microchannel-plate-intensified, subnanosecond x-ray detector with 400-psec time resolution and 180 micron spatial resolution for one-dimensional imaging and spectroscopic measurements of x-ray emission from laser produced plasmas.(1) An x-ray photocathode (CsI, CuI, or gold) is deposited on the MCP to enhance efficiency. Detector output is coupled to a Reticon camera or a streak camera via a fiber optic array. Efficiencies in excess of 1000 (w/cm^2 out per w/cm^2 in) have been demonstrated. We have recently measured CuI and CsI x-ray detector efficiencies using SSRL BL-VIII-2. (2)

Detector Description

Fig. 1 schematically shows the x-ray imaging detector consisting of a UV filter, an x-ray photocathode, a MCP, focusing electrodes, a fast phosphor, and a fiber optic faceplate for transmitting the light out of vacuum. Focusing electrodes compress the electron current out of the MCP in one dimension enhancing system gain by a factor of 10. The In:CdS phosphor-coated fiberoptic faceplate is biased up to +20kV to attract electrons exiting the MCP. Gains greater than 1000 can be obtained from the MCP depending on the bias voltage. The CsI detector is about six times more sensitive than the CuI detector at 700 eV. This is consistent with photocathode response data. (3)

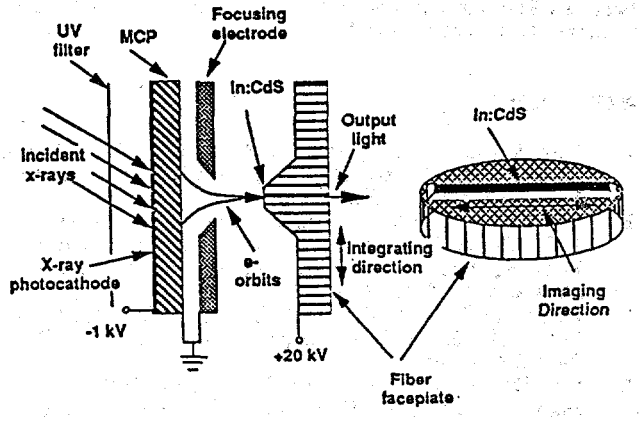

Figure 1. Schematic of an MCP-intensified x-ray detector system.

Measurements

We have measured the relative spectral response of CuI and CsI detectors at SSRL BL-VIII-2 from 450 eV to 1300 eV with the beam incident upon each detector at 35 degrees from normal. The detector was positioned so that the entire 2-mm x 20-mm beam fell on the MCP stripline. Incident x-ray flux was measured with a calibrated, gold-mesh monitor, and the detector output recorded with a Reticon camera. Our results are shown in Fig. 2.

The difference in MCP bias voltages, the measured transmission of the Al UV light shield, and the response of the gold mesh monitor have been taken into account. Each photocathode was calibrated using three different prefilters (Fe, Cu and Mg) to reduce higher-order and specularly-reflected photons exiting the monochromator. Data taken with Cu and Mg prefilters agree well in their region of overlap for both CuI and CsI and are shown as one curve. Data taken with the Fe prefilter is significantly higher than the Cu prefilter data in their region of overlap. This is not presently well understood. The CsI data shows a strong increase in sensitivity at the Cs M5-edge (726 eV) and at the I M$_{4,5}$-edge (630 eV). The CuI MCP response increases at the Cu L3-edge (932 eV) and at the I M$_{4,5}$-edge (630 eV). The Cu-edge jump is much smaller in magnitude than that determined from Eμ(E) data.(3) Another significant difference between the measured response and a simple Eμ(E) model is the gradual rise in efficiency above the Cs edge for CsI and above the I edge in the CuI case. The deviations from theory are not understood as yet.

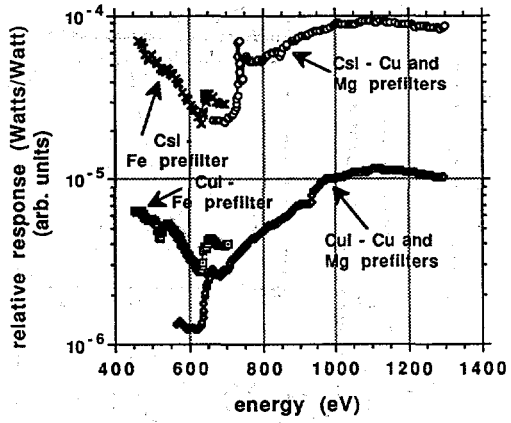

Figure 2. Relative response of CuI and CsI coated MCP imaging detectors vs x-ray energy. The vertical scale is in units of watts out per x-ray watts incident.

REFERENCES:

1. M. R. Carter, B. J. McKinley, and K. G. Tirsell, "A microchannel-plate-intensified, subnanosecond, x-ray imaging camera," Physica Scripta, to be published.
2. K. G. Tirsell and N. K. Del Grande, "Considerations for the use of synchrotron radiation sources to measure sub-keV x-ray photoabsorption cross sections in transmission," SPIE, 911, 146-156 (1988).
3. B. L. Henke, J. P. Knauer, and K. Premaratne, "The characterization of x-ray photocathodes in the 0.1-10-keV photon energy region," J. Appl. Phys. 52 (3), 1509-1520 (1981).

ACKNOWLEDGEMENTS The authors wish to thank J. Batteux, M. Bowers, C. Bruns, C. Keller, R. Mazuch, D. Price, and R. Stewart, LLNL, for their help in this research. This work was performed under the auspices of the U. S. Department of Energy by the Lawrence Livermore National Laboratory under Contract No. W-7405-Eng-48. Data were acquired at SSRL which is supported by the DOE's Office of Basic Energy Science.

Water Window Multilayer Structures

Troy W. Barbee, Jr.
Lawrence Livermore National Laboratory
Livermore, California 94550

The water window is a photon energy range extending from ~ 500 eV down to ~ 200 eV that has been proposed as useful for x-ray imaging of live biological material. This results from the very low.absorption by oxygen in the water necessary for live body observers. Reflectivities were characterized for a multilayer designed specifically for operation in the water window which was carbon free. This is important as carbon is strongly absorbing at energies greater than 283 eV.

Measurements of the reflectivity of an W/Mg_2Si (d = 62 Å, N = 30) multilayer were made over the energy range 500 to 1300 eV on BL 8-2. Mg_2Si was used in this multilayer structure as a low absorption, low scattering spacer for the tungsten layers. It was chosen as analysis showed it to be the best spacer material in this spectral range other than Li, Be, and elemental Mg and it was believed to be easier than elemental Mg to deposit as uniform thin layers. The measured reflectivities are shown as a function of energy in Figure 1 with data from the literature for a W/C (d = 58 Å, N = 30) multilayer. It is clear that the reflectivities of the W/Mg_2Si is substantially larger than that of the W/C structure. Also shown in this Figure 1 are second Bragg order (n = 2) reflectivities for the W/Mg_2Si structure. The reflectivity of the W/Mg_2Si multilayer is dominated by the optical constants of the tungsten at the lower energies. Therefore, higher reflectivities will be attained by replacing the tungsten with a more suitable material for this spectral range. The reflectivities at 900 to 1300 eV are the highest reported and make this material pair useful for proximity x-ray optic structures. Additionally, this material will allow multilayer structures to operate significantly more efficiently in the water window, a property important in biological applications of multilayer x-ray optics.

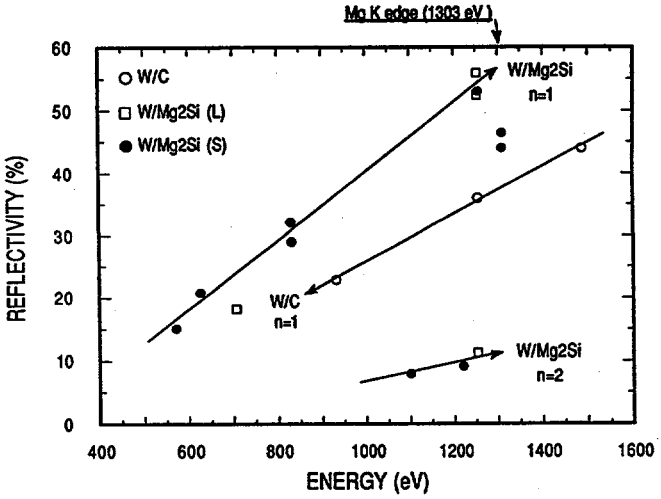

Figure 1 Measured reflectivities of a W/Mg_2Si multilayer (d = 62 Å, N = 30) deposited onto a (111) single crystal silicon wafer are compared to earlier results for a nearly equivalent W/C structure at energies of 500 to 1500 eV.

ACKNOWLEDGMENTS: This work was performed under the auspices of the U. S. Department of Energy by Lawrence Livermore National Laboratory under Contract No.W-7405-Eng-48.

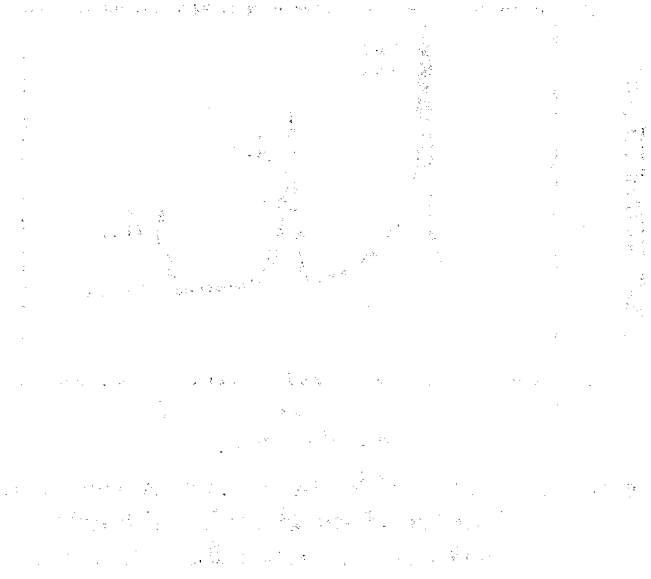

CALIBRATION OF SYNCHROTRON RADIATION GRATING MONOCHROMATORS

Troy W. Barbee, Jr., Glenn Tirsell, and Michael Moran
Lawrence Livermore National Laboratory
Livermore, California 94550

Multilayer reflectivity measurements were performed on BL 8-2. These measurements were made at fixed angles of incidance onto the multilayer samples in the Bragg-Bretano configuration using a GaAsP - Au Schottky diode detector. The energy of the incident monochromatic light was scanned over the full energy range of the monochromator grating in use. It was observed that peaks in reflectivity occurred at integer multiples of the expected first order Bragg reflection light wavelength of the multilayer. These peaks in reflectivity at the longer wavelengths are due to the higher grating order light transmitted by the grating monochromator at the monochromator wavelengths they are observed. These results therefore allow the quantitative characterization of the higher grating order effects of synchrotron radiation grating monochromators as well as demonstrating a technique for their elimination.

Data presented here are for a tungsten/carbon multilayer structure deposited on a 4 inch diameter (111) single crystal silicon wafer. The multilayer contained fifty 25.9 Å periods. The thickness of the tungsten layer was half the multilayer period, minimizing even multilayer Bragg order intensities. Also, the number of periods (50) resulted in the intensities of odd Bragg orders $n \geq 3$ being negligible. The reflectivity of this multilayer at an angle of incidence of 11.2 deg, the incident grating monochromatized light passing through a magnesium filter (~ 3μ), is shown in Figure 1 at wavelengths of 8 to 36 Å. The Mg edge is indicated by the arrows and falls to the short wavelength side of all the multilayer Bragg peaks. The Bragg peaks are all multilayer first order (n=1) and grating orders as labelled. The measured reflectivities are: n=1, m=1, R=0.166; n=1, m=2, R=0.1595; n=1, m=3, R=0.106 at monochromator wavelengths of 9.903 Å, 19.99 Å and 29.697 Å respectively. The reflectivities of the n=1, m=1 and n=1, m=2 peaks are almost equal indicating that almost all the light at a monochromator reading of 19.99 A is 9.90 Å light. The decreased reflectivity of n=1, m=3 probably results from light specularly reflected by the multilayer and the fact that the long wavelength cutoff of this grating is ~ 40 Å. It is important to note that these data show that the higher grating order contamination is appreciable for this grating monochromator.

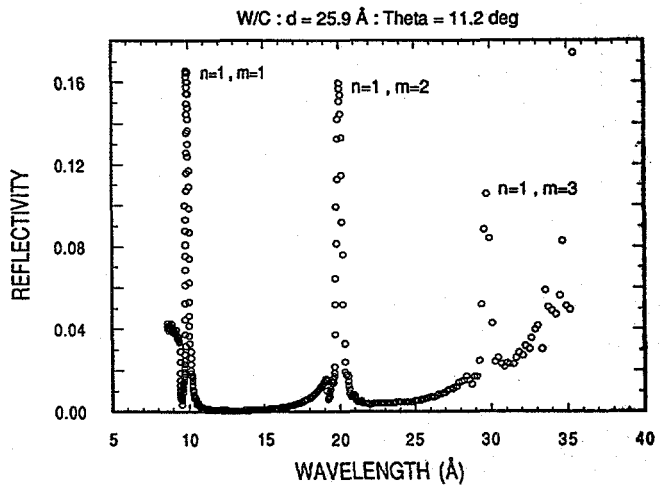

Figure 1: Reflectivity as a function of wavelength

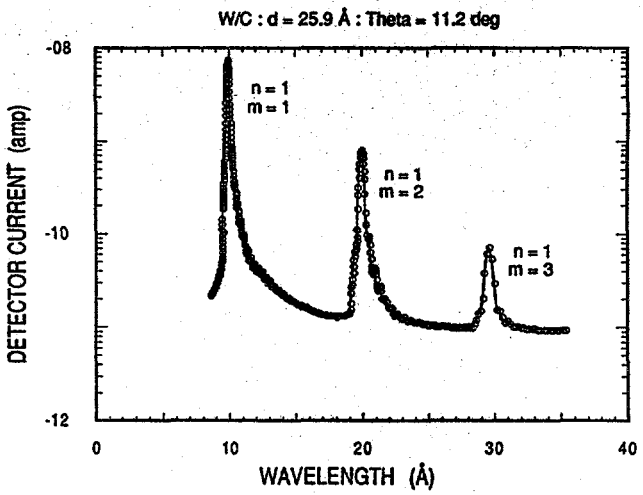

Figure 2: Diffracted beam detector current as a function of wavelength. The detector used was a GaAsP-Au Schottky diode.

It is possible to determine the relative intensities of 9.903 A light transmitted by the grating in orders m=1,2,3. This is demonstrated in Figure 2 where the Bragg diffracted light detector current is shown as a function of wavelength. The ratios of these currents give the relative intensities in the grating orders m=1,2,3. If the current for m=1 is assumed unity the intensity for m=2 is 0.107 and for m=3 is 0.0082. Absolute intensities may be derived from these results by use of a detector calibration function and consideration of filter caused attenuation. These higher grating order intensities are large and may dominate some experiments making interpretation difficult, if not impossible. It is clear from other results that multilayers also eliminate grating higher order contamination when they are operating in first Bragg order (n=1) at an angles of incidence such that m=1, m=2 or m=3 light is diffracted and no filters are used.

SUMMARY

The beamline used in this work is instrumented with a spherical grating monochromator using three separate gratings to cover the energy range 50 to 1500 eV. Earlier runs had shown that these gratings have significant higher grating order contamination of the monochromatic light delivered. This monchromatic light impurity severely limits the experimental utilization of this beamline and complicates general experimentation. Also, such higher grating order effects are present at a large number of existing beamlines in the U.S.A. and in the world imposing the same limitations on experiment. The results reported here demonstrate that multilayers may be used to **eliminate or minimize** higher grating order contamination and to allow the use of higher grating orders to **increase resolution without** the use of filters. As demonstrated above they also provide a means for quantitatively characterizing the intensities of the higher grating order so that the available intensity is known.

ACKNOWLEDGMENTS: This work was performed under the auspices of the U. S. Department of Energy by Lawrence Livermore National Laboratory under Contract No.W-7405-Eng-48.

Fluorescent EXAFS and NEXAFS in the Soft X-ray and Extreme Ultra-Violet

Troy W. Barbee, Jr.
Lawrence Livermore National Laboratory
Livermore, California 94550

The reflectivities of a 304 Stainless Steel-Silicon multilayer (d = 55Å, N = 50, $\gamma = 0.5$) were measured over the energy range 300 eV to 1500 eV. The measurements were made in the Bragg-Bretano configuration at fixed angles of incidence , θ , by scanning the energy of the incident light . A GaAsP-Au Scxhttoky diode was used as a sensitive detector. Though the reflectivities of this multilayer are of interest the important observation in this work was of the fluorescence of the components of the 304ss (75% Fe, 18% Cr, &% Ni) during a given reflectivity measurement.

Reflectivities measured are not discussed here as the significant result relates to observations of L edge fluorescence of the iron and chromium in the 304ss. In these measurements the diffracted beam detector was a GaAsP-Au Scottky diode having a 1 cm^2 active area mounted normal to the diffracted beam 17.8 cm from the illuminated area. This detector sensed the diffracted intensity and any fluorescent radiation generated by the incident beam. A reflectivity scan at θ = 9.78 deg over the energy range 500 to 800 eV is shown in Figure 1. The first order Bragg peak is at ~ 605 eV. The structure on the low energy side of this peak is due excitation of the chrome $L\alpha_{1,2}$ - 572.8 eV and the $L\beta_1$ - 582.8 eV lines. These fluorescence peaks are more intense than warranted by the chrome concentration in the 304ss. This results from the antinodes of the standing-wave field in the multilayer characteristic of Bragg reflection at the Bragg peak lying on the 304ss layers and strongly enhancing the chrome signal as well as multilayer Bragg diffraction of Cr L line radiation into the detector. Fluoresence from the iron is seen at energies of 700 to 800 eV, energies far away from any multilayer Bragg reflection.

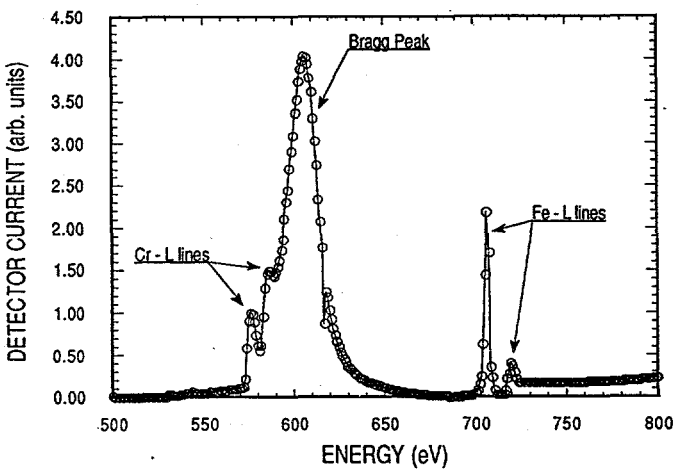

Figure 1 Reflectivity of a 304ss/Si (d=55 Å, N=50, γ=0.35) multilayer over the energy range 500 to 800 eV at θ=9.78 deg.

The peaks at ~ 700 eV are shown in more detail in Figure 2 and are from the characteristic L fluorescence lines ($L\alpha_{1,2}$ - 705 eV, $L\beta_1$ - 718.5 eV) of the iron in the 304ss layers. There is no strong Bragg diffraction from the multilayer structure at these values of energy and θ: these signals are non standing-wave enhanced fluorescence of the iron. The importance of these observations is that the solid angle of the fluorescent source subtended by the detector is very small. This solid angle may be easily increased with this type of solid state detector by increasing the active detector area and moving the detector much closer to the sample. A simple design allows this solid angle to be increased from ~ 0.003 steradian to > 1.0 steradian. This significantly increases the sensitivity of the experiment to the fluorescence of the sample and makes possible a number of scientifically and technologically significant experiments. The experiments facilitated by such a simple apparatus include: (1) fluorescence EXAFS in the soft x-ray and extreme ultra-violet (30 to 3000 eV) spectral ranges; (2) standing-wave fluorescence studies of multilayer structures in the SXR and EUV; (3) application of standing-waves in multilayers to the study of adsorbed layers on multilayer structures and other long period Bragg diffractors in the SXR; (4) sensitive x-ray fluorescence analysis (XRF) for the concentration of light elements in bulk samples; (5) detailed study of the physics of x-ray absorption/emission in the SXR by experimental determination of radiative and non-radiative decay channel strengths.

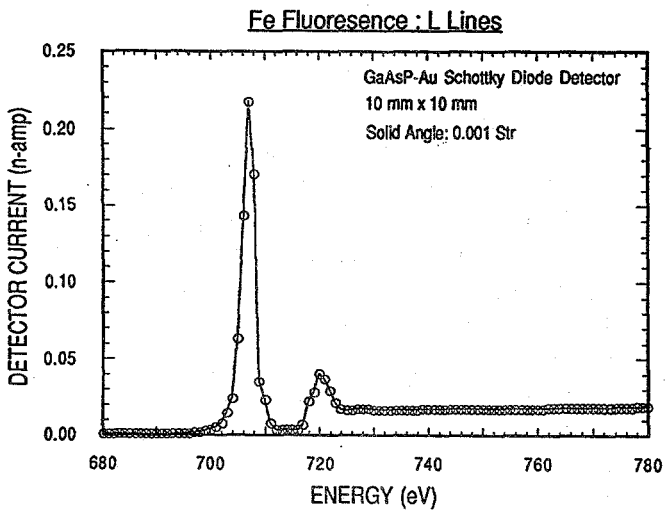

Figure 2 Characteristic L line fluoresence from iron in the 304ss of the multilayer detected using a $1cm^2$ active area GaAsP-Au Schottky diode ~ 18 cm from the fluorescing material and subtending only ~ 0.001 str. of the solid angle available.

ACKNOWLEDGMENTS: This work was performed under the auspices of the U. S. Department of Energy by Lawrence Livermore National Laboratory under Contract No.W-7405-Eng-48.

Rhodium/Carbon Multilayer Soft X-ray Reflectivity

Troy W. Barbee, Jr.
Lawrence Livermore National Laboratory
Livermore, California 94550

Multilayer reflectivity measurements were performed on BL 8-2. The measurements were made as a function of energy at fixed angles of incidence of the monochromatic light onto the multilayer samples. The energy of the incident light was scanned in the energy range 300 eV to 1600 eV during a given reflectivity measurement. The intensity of the incident beam was determined immediately prior to the reflectivity measurement using a GaAsP-Au Schottky diode so that the beam current in the storage ring was always slightly larger than during the reflectivity measurements.

BL 8-2 is a bending magnet beamline equipped with a spherical grating monochromator (SGM). SGM's exhibit substantial higher grating order contamination of the monochromatized light. Thus, reflectivity measurements made with SGM's are often of limited accuracy due to the presence of higher energy light which makes the results more uncertain. In these experiments a variety of filters designed to minimize higher order light were used. The high energy cutoff of this monochromator is ~ 1400 eV so that reflectivity measurements at energies of 700 eV or larger are not degraded.

Results for a rhodium/carbon multilayer (d = 80 Å, N = 40, $t_{Rh} = t_C$) over the energy range 400 to 1500 eV measured at angles of incidence of 3.3 to 10.5 deg are plotted as a function of energy in Figure 1. The decrease in peak reflectivity as energy decreases results from increasing absorption in the carbon as its K edge at 283 eV

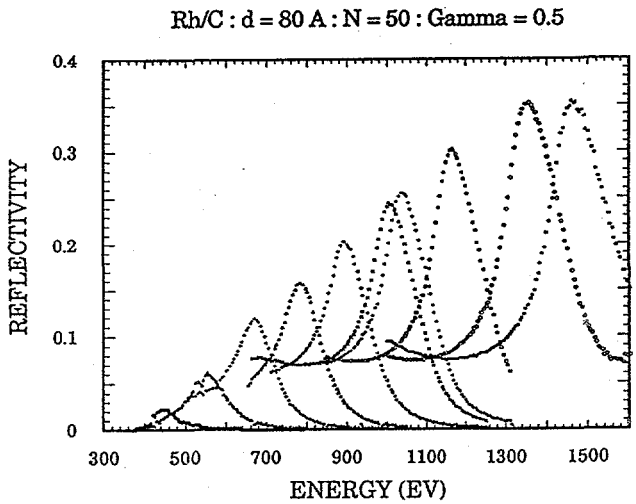

Figure 1 Experimental reflectivities as a function of incident light energy at angles of incidence of 3.3 to 10.5 deg.

is approached and a rhodium broad absorption resonance at ~ 400 eV. The broad minima in reflectivity on the low energy side of the higher energy reflectivity curves results from the onset of mirror like specular reflection at the light energy and incidence angle of measurement. The reflectivity measured at θ = 5.05 deg is compared as a function of energy to model calculations for an ideal structure made using a standard Fresnel multilayer computational code in Figure 2. The measured reflectivity at 1010 eV is 80% of that expected for an ideal multilayer. The agreement at 700 to 900 eV indicates that the ambient to multilayer surface is very smooth and that the specular reflectivity of the multilayer essentially equal to that calculated. The disagreement appearing at energies < 700 eV results from the onset of higher grating order contamination as previously pointed out.

It is important to be able to separate the multilayer diffracted light from the specularly reflected component. This is computationally, but not experimentally possible. Reflectivities calculated for the multilayer considered above using the Fresnel multilayer code that includes the multilayer diffracted and the specular surface reflected light and using a Darwin-Prins code that only calculates only the multilayer diffracted component are compared as a function of energy in Figure 3. The difference between these two calculated reflectivities is the intensity of the specularly reflected component. This analytic approach allows the reduction of broadband multilayer dispersed spectroscopic data so that signals of interest may by accurately determined. A summary comparison of the observed (see Fig. 1) and calculated peak reflectivities is shown as a function of energy in Figure 4. The important things to note from this figure are that the experimental reflectivity energy dependence is in excellent agreement with calculation and that the measured reflectivities are a constant fraction of calculation. These results demonstrate that accurate reflectivity measurements can be made on this beamline in the energy range 300 to 1600 eV and that excellent multilayers may be fabricated using rhodium and carbon.

Subsequent to these measurements reflectivities were measured at NIST over the energy range 80 to 130 eV and at LLNL using characteristic line sources ($C_{k\alpha}$ and $B_{k\alpha}$). These results were consistent with the SSRL data described above.

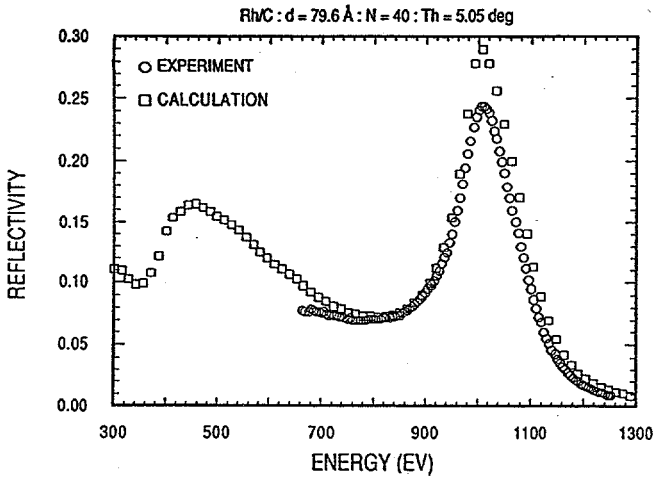

Figure 2 Experimental reflectivity at θ = 5.05 deq is compared to calculation over the energy range 600 to 1300 eV.

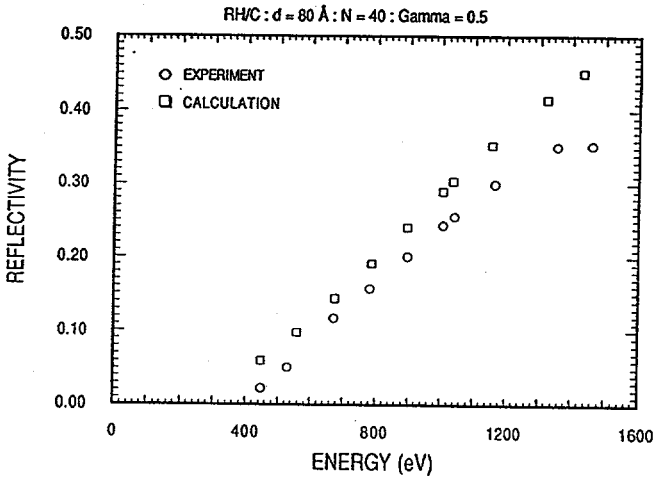

Figure 4 Experimental and calculated (Fresnel) peak reflectivities are compared as a function of energy.

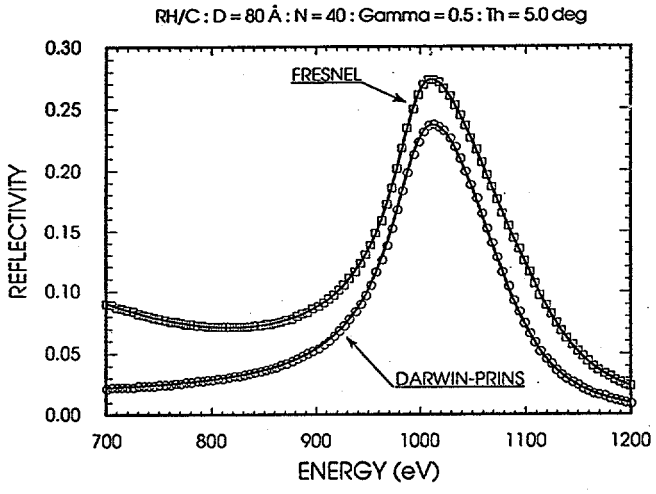

Figure 3 Reflectivities calculated using both the Fresnel and the Darwin-Prins formalisms are compared.

ACKNOWLEDGMENTS: This work was performed under the auspices of the U. S. Department of Energy by Lawrence Livermore National Laboratory under Contract No.W-7405-Eng-48.

L SHELL XANES FOR SOLID METALS: Ti, V, Cr, Fe, Ni, Cu

N.K. Del Grande

University of California, Lawrence Livermore National Laboratory
P.O. Box 808 (L-379) Livermore, CA 94550

Introduction

The *L* shell x-ray absorption near edge structure (XANES) for the 3*d* transition metals Ca-Cu is dominated by atomic-like behavior which is poorly understood.[1] It has been studied by electron energy loss spectroscopy (EELS) and bremsstrahlung isochromat spectra (BIS).[2,3] More and better photoabsorption cross-section measurements are needed over the sparsely studied 400-1500 eV region to test theoretical methodologies which fuse atomic and condensed matter theories. Progress has been made reporting absolute photoabsorption cross sections taken with the spherical grating monochromator on beamline 8-2 at SSRL in 1989. These data were used in conjunction with data taken on beamline 3-4 at SSRL and beamline U14A at NSLS.[4-7]

Experiment

Transmission data for well characterized carbon-only and carbon-metal multilayer targets (100-4000 nm thick) were recorded with a resolution of 1 eV or better for Ti, V, Cr, Fe, Ni and Cu. Absolute cross sections in Figure 1 had overall uncertainties of 10% or less. Comparisons are made with previous results.[8,9] Away from edges, targets had photon penetration depths 1/3 to 3 mean free paths thick. Thinner targets (by a factor of 3 or 4) were used to resolve XANES shown in Figure 2.

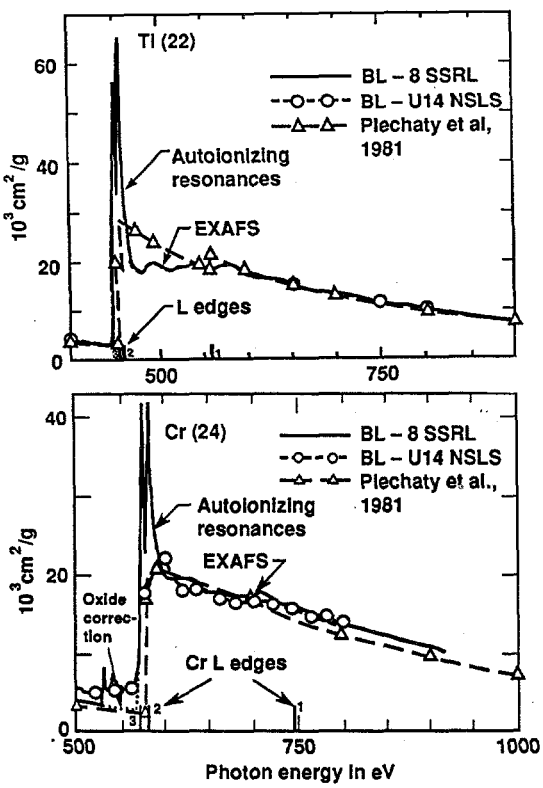

Corrections for oxide impurities were possible since synchrotron radiation sources allowed continuous coverage across the oxygen K absorption edge at 543 eV. The determination of the target metallic areal densities (mass per unit area) was known to better than ± 10%. Targets were characterized for their total as well as component element purity, weight-per-unit area, thickness and composition, using very accurate balances, ion back-scattering, and particle-induced x-ray emission.

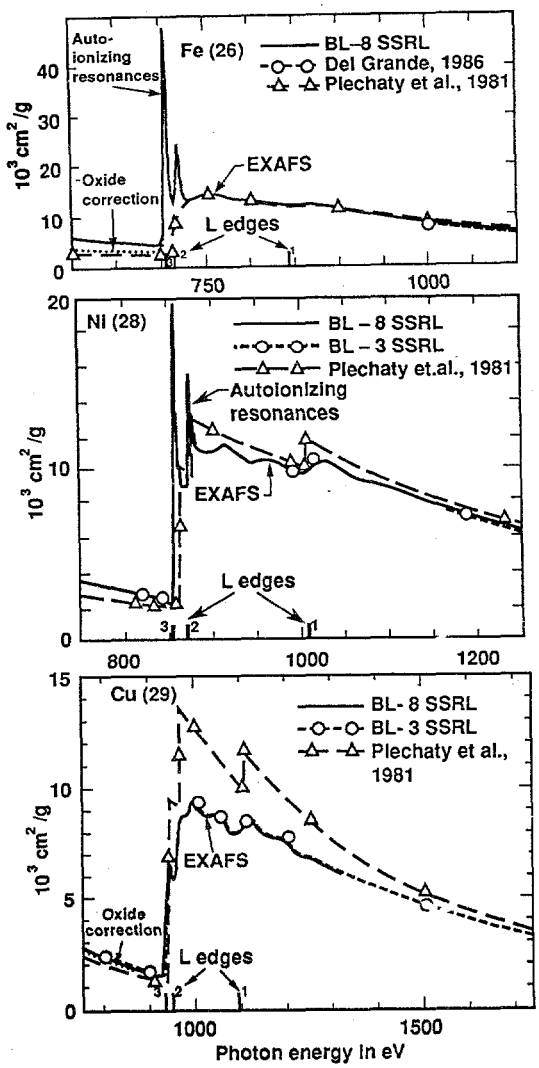

Figure 1. Photoabsorption cross section measurements in cm²/g with 10% overall uncertainties are compared with the 1981 LLNL sub-keV theoretical data base[8] and other data[9] for five 3*d* solid metals: Ti, Cr, Fe, Ni, Cu. See reference [7].

Discussion

The Figure 1 comparisons of experiment with single particle Hartree Slater (HS) theory[8] shown as a long dashed line agree for most 3*d* metals below and at twice the energy of the ionization threshold. The 2*p*-3*d* autoionizing resonances of Figure 2 are associated with bound-bound transitions which lead to non-radiative Auger decay. What is measured is a combination of the bound-bound photoabsorption and bound-free photoionization cross sections. The HS calculation [in 8] does not include the bound-bound component for the atom or band theory to address the behavior of the solid.

There is good qualitative agreement between *L* shell XANES and calculations which use a multi-configuration Dirac Fock (MCDF) model with the assumption of a statistical distribution for the initial atomic states.

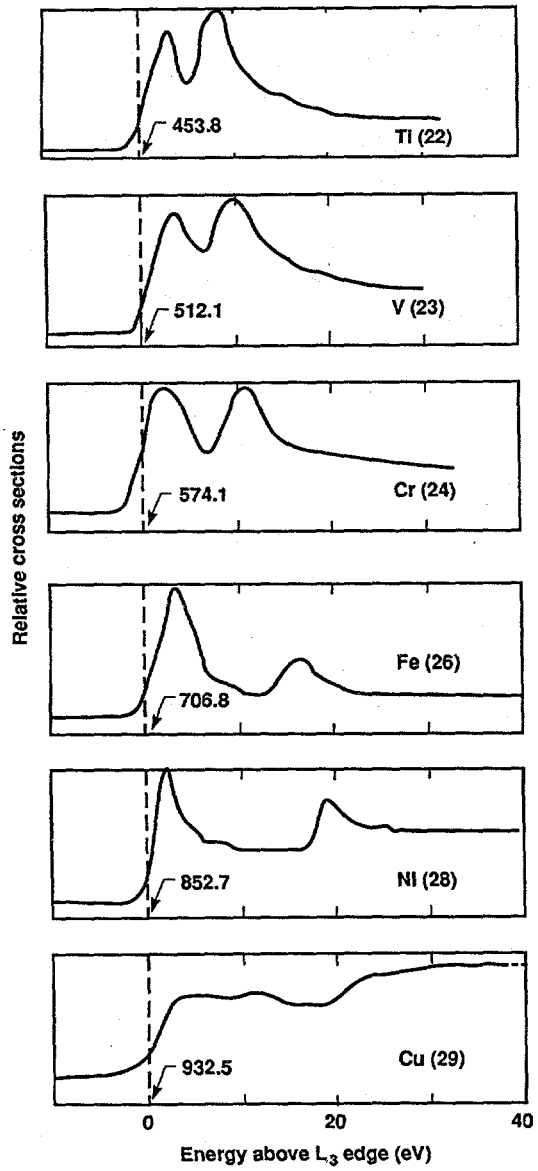

Figure 2. Measured XANES for the transition metals Ti, V, Cr, Fe, Ni and Cu showing the atomic-like 2*p*-3*d* autoionizing resonances which dominate the L_3 and L_2 edge structure.[7]

Calculations were performed in intermediate coupling with configuration interactions.[7] It is not yet clear why the statistical distribution rather than the ground state distribution for the initial states produces the measured XANES for solid metals shown in Figure 3.

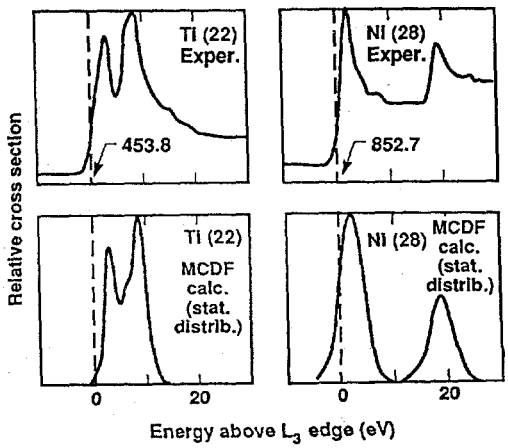

Figure 3. A comparison of measurement with calculation for *L* shell autoionizing resonances of solid metals dominated by atomic-like behavior. (Calculation by Mau H. Chen.)

REFERENCES

1. Davis, L. C. (1986), J. Appl. Phys. 59, R25-R63.
2. Fink, J., Muller-Heinzerling, M. Th., Scheerer, B., Speier, W., Hillebrecht, F.U., Fuggle, J.C., Zaanen, J. and Sawatzky, G.A., (1985), Phys. Rev. B., 32 pp. 4899-4904.
3. Zaanen, J., Sawatzky, G.A., Fink, J., Speier, W., Fuggle, J.C, (1985), Phys. Rev. B., 32, pp. 4905-4913.
4. Del Grande, N.K., Tirsell, K.G., Schneider, M.B., Garrett, R.F., Kneedler, E.M., and Manson, S.T. (1987), J. Phys. (Paris) 48, C9, pp.951-954.
5. Del Grande, N.K., and Tirsell, K.G. (1988), SPIE Vol. 911 *X-ray and VUV Interaction Data Bases, Calculations, and Measurements*, pp. 6-10.
6. Tirsell, K.G., and Del Grande, N.K. (1988), SPIE Vol 911, *X-ray and VUV Interaction Data Bases, Calculations, and Measurements*, pp. 146-156.
7. Del Grande, Nancy Kerr (1990), Physica Scripta, in press.
8. Plechaty, E., Cullen, D. and Howerton, R., (1981), Lawrence Livermore Laboratory Report, UCRL-50400, Rev. 3.
9. Del Grande, Nancy Kerr (1986), SPIE Vol. 691, *X-ray Imaging II*, pp. 2-10.

ACKNOWLEDGEMENTS

The author is indebted to K. G. Tirsell for detector improvements, to Mau H. Chen for calculations, to T. Barbee for beamline 3-4 SSRL measurements, and to P. Pianetta and his staff at SSRL for their support.

This work was performed under the auspices of the U.S. Department of Energy by LLNL under contract number W-7405-ENG-48.

Section VI

Theses Based on Research at SSRL

VI. THESES BASED ON RESEARCH AT SSRL

The following is a partial list of Ph.D and Master's theses based on experimental research at SSRL. It represents 160 theses from 22 universities.

	TITLE/ADVISOR
1990	
C.J. Chisholm-Brause *Stanford University*	**"Sorption Mechanisms of Co(II) at Oxide/Water Interfaces"** (Advisor - G.E. Brown)
W.E. Jackson *Stanford University*	**"X-Ray Absorption Analyses of Iron-Bearing Glasses and Melts: Implications for Glass-Melt Structural Differences and the Effect of Alkali and Alkaline-Earth Metals on Fe(II) Coordination"** (Advisor - G.E. Brown)
1989	
M. Ardehali *Stanford University*	**"Photoelectron Angular Distribution from the Disordered Condensed Phase: Theory and Experiment"** (Advisor - I. Lindau)
R. Cao *Stanford University*	**"Schottky Barrier Formation with Metals on III-V Semiconductor Surfaces From Thin Coverages to Thick Overlayers"** (Advisor - I. Lindau)
T. Teh-I-Chiang *Stanford University*	**"Annealing Studies of Metals and Arsenic on Gallium Arsenide"** (Advisor - W.E. Spicer)
M.P. Green *Stanford University*	**"Scanning Tunneling Microscopy Applied to the Electrochemical Deposition of Lead on the Gold (111) Surface"** (Advisor - I. Lindau)
Z.-X. Shen *Stanford University*	**"Photoemission Studies of High Temperature Superconductors and Related Materials"** (Advisor - I. Lindau)
J. C. Woicik *Stanford University*	**"Synchrotron Radiation Studies of Si and Si-Ge Interfaces"** (Advisor - P. Pianetta)
J. Hwang *Stanford University*	**"Effect of Strain on the Electronic Structure of Indium Gallium Arsenide"** (Advisor - P. Pianetta)
J.E. Benci *Univ. of Pennsylvania*	**"A Study of Creep Damage Using Microradiography and Continium Damage Mechanics"** (Advisor - D. Pope)
K.D. Butcher *Stanford University*	**"Variable Energy Photoelectron Spectroscopy on Model Catalytic Active Sites: The Electronic Structure and Bonding in Tetrahederal Iron Chlorides and Sulfides"** (Advisor - E.I. Solomon)
M. Kraitchman *UC Berkeley*	**"The Unmixing of Al_3Li in Al-Li and Al-Li-Cu Alloys"** (Master's Thesis - Advisor - D. DeFontaine)
R. Howland *Stanford University*	**"Determination of Dopant Site Occupancies in Copper-Substituted Yttirium-Barium-Copper-Oxide by a New Application of Differential Anomalous X-ray Scattering"** (Advisor - T.H. Geballe)
Y.H. Chung *Georgia Inst. of Tech.*	**"Synchrotron White Beam Topographic Study of Damage Accompanying Laser Drilling"** (Advisor - S. Stock)

A. Outrzourhit
Colorado School of Mines

"Extended X-ray Absorption Fine Structure Studies of Sn-related DX Centers in Sn-Doped $Ga_{(0.7)}Al_{(0.3)}As$" (Master's Thesis -Advisor - T.M. Hayes)

P.R.G. Small
Colorado School of Mines

"The Atomic-Scale Structure of Dilute Tin in Aluminum"
(Master's Thesis - Advisor -T.M. Hayes)

L. Emery
Stanford University

"A Wiggler Based Ultra-Low Emittance Damping Ring and its Chromatic Correction"
(Advisor - H. Wiedemann)

1988

S.V. Didziulis
Stanford University

"Photemission Spectroscopic Studies of Model Catalyst Surfaces: 1) Bonding Interactions of $3d_{10}$ Metal Ion Sites; 2) The Chemistry of Copper Overlayers on Zinc Oxide Single Crystals" (Advisor - E.I. Solomon)

G.P. Carey
Stanford University

"A Study of the Chemical and Electrical Disruption to Mercury Cadmium Telluride Upon Interface Formation and Surface Processing" (Advisor - W.E. Spicer)

P.H. Mahowald
Stanford University

"Experimental Band Alignment at Germanium, Silicon and Indiun Phosphide Heterojunctions" (Advisor - W.E. Spicer)

C.E. McCants
Stanford University

"Photoemission and Electrical Studies of the Titanium/Gallium Arsenide (110) and Platinum/Gallium Arsenide (110) Interfaces" (Advisor - W.E. Spicer)

C.-K. Shih
Stanford University

"Heterojunction Band Line-Ups and the Alloying Effect in Compound Semiconductor Alloys - A Photoemission Study" (Advisor - W.E. Spicer)

L. Hsu
UC-Los Angeles

"Electronic Properties of a $PtGa_2$ Single Crystal and Photoemission Studies of the Electron Correlation Effects in the Ni-Ga and the Ni-In Intermetallic Compounds"
(Advisor - R.S. Williams)

W.M. Lavender
Stanford University

"Observation and Analysis of X-ray Undulator Radiation from PEP"
(Advisor - G.S. Brown)

J.R. Schoonover
Arizona State University

"Time Resolved X-ray Diffraction Using Synchrotron Radiation" (Advisor - S.H. Lin)

L. Terminello
UC-Berkeley

"Surface Structures Determined Using Electron Diffraction" (Advisor - D.A. Shirley)

C.J. Chisholm
Stanford University

"Structure of Divalent Lead Complexes at the Gamma-Alumina/Water Interface"
(Master's Thesis - Advisor - G.E. Brown)

1987

R. T. Short
University of Tennessee

"Recoil-Energy Measurements of Slow Highly-Charged Ions Produced by Synchrotron Radiation and by Swift-Ion Impact" (Advisor - I.A. Sellin)

S.R. Hubbard
Stanford University

"Small-Angle X-ray Scattering Studies of Calcium-Binding Proteins in Solutions"
(Advisor - K.O. Hodgson)

L.-S. Kau
Stanford University

"Chemical and Spectroscopic Studies on Metal Active Sites in Metalloproteins and Heterogeneous Catalysts" (Advisor-K.O. Hodgson)

J. L. Cole
UC-Berkeley

"Photosynthetic Oxygen Evolution Studied by Electron Paramagnetic Resonances and X-Ray Absorption Spectroscopy" (Advisor - M.P. Klein)

A.E. McDermott
UC-Berkeley

"Structural Studies of Iron and Manganese in Photosynthetic Reaction Centers" (Advisor - M.P. Klein)

R.E. Guiles
UC-Berkeley

"X-ray Absorption with EPR Studies of the Role of Mn in the Photosynthetic Oxygen Evolving System" (Advisor - M.P. Klein)

J.J. Yeh
Stanford University

"Metal/Silicon Interfaces and Their Oxidation Behavior - A Photoemission Spectroscopy Analysis" (Advisor - I. Lindau)

D. Friedman
Stanford University

"Metal Interfaces with Mecury Cadmium Telluride" (Advisor - I. Lindau)

A. Viescas
Stanford University

"Photoemission Studies of Core Level Energy Shifts in Clean and Adsorbate Covered Tungsten and Platinum Single Crystal Surfaces" (Advisor - I. Lindau)

P. Jupiter
Stanford University

"Correlation Between the Electronic Structure and Surface Chemistry of Tungsten and Tungsten Carbide 4" (Advisor - W.E. Spicer)

K.A. Bertness
Stanford University

"Photoemission Studies of Oxgyen Chemisorption on Gallium Arsenide and Indium Phosphide Surfaces" (Advisor - W.E. Spicer)

J.N. Otis
Stanford University

"Minimally Invasive Coronary Angiography with Monochromatic X-rays: Developmental Studies Utilizing Synchrotron Radiation" (Advisor - R. Hofstadter)

Y.C. Lu
Stanford University

"Vertical Bridgman Growth and Characterization of CdTe Crystals" (Advisor - R. Feigelson)

C.W. Ponader
Stanford University

"Trace Metals in Silicate Glasses and Melts: Coordination Environments, Halogen Complexes, and Soret Diffusion" (Advisor - G.E. Brown)

K.F. Hayes
Stanford University

"Equilibrium, Spectroscopic, and Kinetic Studies of Ion Adsorption at the Oxide/Aqueous Interface" (Advisor - G.E. Brown)

1986

S.W. Robey
UC-Berkeley

"Local Surface Structures of c(2x2)S/Ni(011) and (2x2) S/Ge(111) Determined Using ARPES" (Advisor - D.A. Shirley)

J. Nogami
Stanford University

"Rare Earth Metal/Semiconductor Interfaces and Compounds" (Advisor - I. Lindau)

E.B. Sirota
Harvard University

"X-ray Scattering Study of the Thickness Dependent Phase Diagram of Liquid Crystal Films" (Advisor - P.S. Pershan)

A.L. Johnson
UC-Berkeley

"Platinum Surface Chemistry Studied by Thermal DesorptionSpectroscopy and Near Edge X-ray Absorption Fine Structure Absorbate Effects" (Advisor - D.A. Shirley)

K.F. Ludwig, Jr.
Stanford University

"Anomalous X-ray Scattering Studies of Liquids" (Advisor - A.I. Bienenstock)

R.D. Lorentz
Stanford University

"Structural Investigations of Amorphous Iron-Germanium Alloys using Synchrotron Radiation" (Advisor - A. I. Bienenstock)

J.J. Hoyt
UC-Berkeley

"An Anomalous Small Angle X-ray Scattering Study of Phase Separation in the AlZnAg System" (Advisor - D. DeFontaine)

J.C. Levin
University of Oregon

"Auger Transitions in Noble Gases Following Inner Shell Ionization by Electron Bombardment and by Synchrotron Radiation" (Advisor - B. Crasemann)

N.W. Lytle
Brigham Young Univ.

"Proton-Induced X-ray Emission, Proton-Induced Gamma-ray Emission, and X-ray Absorption" (Advisor - N.F. Mangelson)

C.C. Bahr
UC-Berkeley

"Chemisorption Geometries of Sulfur on Copper and Molybdenum Surfaces" (Advisor - D.A. Shirley)

T.A. Ferrett
UC-Berkeley

"Photoionzation of Atoms and Small Molecules using Synchrotron Radiation" (Advisor - D.A. Shirley)

P.A. Heimann
UC-Berkeley

"Near Threshold Studies of Photoelectron Satellites" (Advisor - D.A. Shirley)

M.G. Samant
Stanford University

"Atomic and Electronic Structure of Supported Monometallic and Bimetallic Clusters" (Advisor - M. Boudart)

D.J. Sajkowski
Stanford University

"Catalysis by Metals: Single Crystals, Supported or Unsupported Polycrystals, and Co-ordination Complexes" (Advisor - M Boudart)

S.L. Cohen
Stanford University

"Variable Energy Photoelectron Spectroscopic Studies of d9 and d10 Metal Chloride and Oxide Surfaces" (Advisor - E.I. Solomon)

E.D. Specht
MIT

"Synchrotron X-ray Diffraction Studies of Transitional and Orientational Order in Monolayer Krypton on Graphite" (Advisor R.J. Birgeneau)

J.A. Silberman
Stanford University

"A Photoemission Study of the Electronic Structure and Oxidation Properties of Mercury Cadmium Telluride" (Advisors - I. Lindau/W.E. Spicer)

K.K. Chin
Stanford University

"Initial Stage of the Schottky Barrier Formation of Metal/III-V Semiconductor Interfaces" (Advisor - I. Lindau)

M.D. Williams
Stanford University

"The Effect of Chemical Reactivity and Charge Transfer on Gallium Arsenide (110) Schottky Barrier Formation" (Advisors - W.E. Spicer/I. Lindau)

W.E. Jackson
Stanford University

"EXAFS Study of the Potassium Coordination Environment in Glasses from the $NaAlSi_3O_8$-$KAlSi_3O_8$ Binary: Structural Implications for the Mixed-Alkali Effect" (Master's Thesis - Advisor - G.E. Brown)

<u>1985</u>

K. Kim
Univ. of Washington

"A Study of Basic Properties and Applications of EXAFS" (Advisor - E.A. Stern)

R. Pro
UC-Berkeley

"Development of a Linear Gas-Proportional X-ray Detector System for Determination of Partial Structure Function in Al, Ag and Zn Alloys" (Advisor - D. DeFontaine)

W.G. Petro
Stanford University

"Metal and Oxygen Interactions with III-V Compound Semiconductor Surfaces" (Advisors- W.E. Spicer and I. Lindau)

E.N. Keller
Univ. of Washington

"Magnetic X-ray Study of a Gadolinium-Iron Amorphous Alloy" (Advisor - E. A. Stern)

G. Zhang
Stanford University

"Molybdenum Carbide Catalysts" (partially based on SSRL) (Advisor - M. Boudart)

T.A. Smith
Stanford University

"Single Crystal Polarization X-ray Absorption Studies of Copper Complexes" (Advisor - K.O. Hodgson)

L.E. Klebanoff
UC-Berkeley

"Photoelectron Spectroscopy Studies of Cr(001) Surface Ferromagnetism and Near-Surface Antiferromagnetism" (Advisor - D.A. Shirley)

J.G. Nelson
UC-Los Angeles

"The Electronic Structure of Gold Gallium Two and Gold Indium Two Intermetallic Compounds" (Advisor - R.S. Williams)

J.J. Barton
UC-Berkeley

"Angle-Resolved Photoemission Extended Fine Structure" (Advisor - D.A. Shirley)

T.A. Gibson
Stanford University

"Single Crystal Polarized X-ray Absorption Edge Studies of Copper Complexes" (Advisor - K.O. Hodgson)

M.A. Berding
Stanford University

"Calculation of Cu K-Edge Photoabsorption Spectra Using an Extended Continuum Multiple Scattered Wave Method" (Advisors- K.O. Hodgson/S. Doniach)

D.L. Parkhurst
Stanford University

"The Application of EXAFS and Mean-Activity Coefficient Data to Ion-Association Models for the Zinc-Chloride System" (Master's Thesis - Advisor - G.E. Brown)

1984

D.A. McKeown
Stanford University

"Spectroscopic Study of Silica-Rich Glasses and Selected Minerals within the Sodium Alumino-silicate System" (Advisor - G.E. Brown)

C.E. Bouldin
University of Washington

"An EXAFS Study of Amorphous Ge and of the Fe Impurity in Silicon Nitride" (Advisor - E.A. Stern)

J.S. Lee
Stanford University

"Catalysis of the Oxidation of Dihydrogen by Supported Gold" (partially based on at SSRL) (Advisor - M. Boudart)

K.M. Choudhary
Stevens Institute

"Surface Sensitive Photoemission EXAFS: A New Structural Tool" (Advisor - G.M. Rothberg)

S.G. Mochrie
MIT

"Structures and Transitions in Systems with Competing Interactions" (Advisor - R.J. Birgeneau)

J.E. Penner-Hahn
Stanford University

"X-Ray Absorption Studies of Metalloprotein Structure: Cytochrome P-450, Horseradish Peroxidase, Plastocyanin, and Laccase" (Advisor - K.O. Hodgson)

M.K. Eidsness
University of Cincinnati

"EXAFS and XANES Studies of Gold in Complexes of Biological Significance" (Advisor - R.C. Elder)

J.B. Kortright
Stanford University

"Structural Studies of Amorphous Mo-Ge Alloys Using Synchrotron Radiation" (Advisor - A. Bienenstock)

R.S. Moog
Stanford University

"Fluorescence Quenching of Chlorophyllide and Protoporphyrin-Protein Complexes by Electron Transfer" (Advisor - S.G. Boxer)

J.A. Guest
Stanford University

"Studies of Molecular Photoion and Photofragment Alignment" (Advisor - R.N. Zare)

B.B. Pate
Stanford University

"The Diamond Surface: Atomic and Electronic Structure"
(Advisors - W.E. Spicer/I. Lindau)

R.S. Weber
Stanford University

"Structure and Reactivity of Platinum Clusters Supported on Y-Type Zeolites"
(Advisor - M. Boudart)

G.D. Meitzner
Stanford University

"Characterization of Gold/Y-Zeolite and its Catalytic Activity in the H_2-O_2 Reaction"
(Advisor - M. Boudart)

G.B. Bunker
University of Washington

"An X-Ray Absorption Study of Transition Metal Oxides" (Advisor - E.A. Stern)

H. B. Ponader
Stanford University

"An EXAFS and X-Ray Diffraction Study of the Local Ca Environment in Anorthite ($CaAl_2Si_2O_8$) Crystal and Glass" (Master's Thesis - Advisor - G.E. Brown)

1983

J. Sanchez-Arrieta
Stanford University

"Structural Studies of Hydrodesulfurization Catalysts" (Advisor - M. Boudart)

P.H. Kobrin
UC-Berkeley

"Atomic Photoelectron Spectroscopy Studies using Synchrotron Radiation"
(Advisor - D.A. Shirley)

J. Collett
Harvard University

"X-Ray Scattering Study of Liquid Crystal Thin Films" (Advisor - P.S. Pershan)

D.W. Lindle
UC- Berkeley

"Inner-Shell Photoemission from Atoms and Molecules using Synchrotron Radiation"
(Advisor - D.A. Shirley)

P.M. Stefan
Stanford University

"A Photoemission Study of the Electronic Structure and Surface Chemical Properties of Tungsten Carbide and of a Carbonized Tungsten Model Surface for Tungsten Carbide"
(Advisor - W.E. Spicer)

A.N. Mansour
N. Carolina State

"X-Ray Absorption Studies of Silica-Supported Platinum Catalysts"
(Advisor - D.E. Sayers)

J.G. Tobin
UC-Berkeley

"Dimensionality and Its Effects Upon the Valence Electronic Structure of Ordered Metallic Systems" (Advisor - D.A. Shirley)

C. Marques
Washington State Univ.

"Thermal Motion of Surface Atoms in Silica Supported Platinum and Iridium Catalyst Clusters: An EXAFS Spectroscopy Study" (Advisor - D.R. Sandstrom)

P.R. Findley
UC-Santa Barbara

"Optical Properties of PbF_2 and PbC_{12} at High Temperatures" (Advisor - W.C. Walker)

M.R. Antonio
Michigan State

"Extended X-Ray Absorption Fine Structure of the Iron-Molybdenum Cofactor of Nitrogenase, the Three-Iron Ferredoxinll of Desulfovibrio Gigas, and of Synthetic Molybdenum and Tungsten-Iron-Sulfur and Iron-Sulfur Model Systems (Part I) and Intercalation of Tetrathiafulvalene into Iron Oxycholoride (Part II)" (Advisor - H. Eick)

G. B. Stephenson
Stanford University

"Early-Stage Phase Separation in Amorphous Solids: A Time-Resolved SAXS Study"
(Advisor - A.I. Bienenstock)

J.M. Tranquada
Univ. of Washington

"X-Ray Absorption Studies of Solids at High Pressure" (Advisor - R. Ingalls)

D. Stearns
Stanford University

"Early Photo Luminescence Decay in Amorphous Hydrogenated Silicon"
(Advisor - A.I. Bienenstock)

S. Laderman
Stanford University

"Structural Studies of Amorphous Semiconductors Containing Transition Metals"
(Advisor A.I. Bienenstock)

M.S. Co
Stanford University

"X-Ray Absorption Spectroscopy of Hemocyanin and Hemerythrin"
(Advisor - K.O. Hodgson)

S.D. Conradson
Stanford University

"X-Ray Absorption Studies of the Molybdenum Site of Nigrogenase"
(Advisor - K.O. Hodgson)

R. Miake-Lye
Stanford University

"Anomalous X-Ray Scattering as a Probe of Biological Structure"
(Advisor - K.O. Hodgson)

C.C. Parks
UC-Berkeley

"The Auger Decay Mechanism in Photon Stimulated Desorption of Ions from Surface"
(Advisor - D.A. Shirely)

D.B. Goodin
UC-Berkeley

"The Local Structure of Manganese in the Photosynthetic Apparatus and Superoxide Dismutase: An X-Ray Absorption Study" (Advisor - M.P Klein)

1982

M.G. Durrett
Rice University

"Study of KrC_1/Dr_2Cl Excited State Kinetics Using Synchrotron Radiation Excitation"
(Advisor - G.K. Walters)

M.L. Shek
Stanford University

"Electronic Structure of Platinum-Copper Surfaces and Chemisorption of Carbon Monoxide" (Advisors - I. Lindau/W.E. Spicer)

P.R. Skeath
Stanford University

"Chemical Bonding Phenomena of Column 3 and 5 Adsorbates and Fermi Energy Stabilization Mechanism on GaAs (110)" (Advisors - I. Lindau/W.E. Spicer)

M.H. Hecht
Stanford University

"Synchrotron Radiation Measurements of Subshell Photoionization Cross Sections: Techniques and Applications" (Advisor - I. Lindau)

S.-J. Oh
Stanford University

"Resonance and Relaxation Effects in Photoemission Spectroscopy"
(Advisor - I. Lindau)

S.M. Brennan
Stanford University

"Surface EXAFS of Sulphur on Nickel" (Advisor - A.I. Bienenstock)

R.O. Tatchyn
Stanford University

"The Introduction and Development of a New Method for Measuring the Optical Constants of Metals in the Soft X-Ray Range" (Advisor - I. Lindau)

P.A. Heiney
MIT

"Phase Transitions of 2D Atomic and Molecular Crystals" (Advisor - R.J. Birgeneau)

D.H. Rosenblatt
UC-Berkeley

"High Resolution Electron Energy Loss Spectroscopy and Photoelectron Diffraction Studies of the Geometric Structure of Adsorbates on Single Crystal Metal Surfaces"
(Advisor - D.A. Shirley)

J.E. Pollard
UC-Berkeley

"Photoelectron Spectroscopy of Supersonic Molecular Beams" (Advisor - D.A. Shirley)

S.H. Southworth
UC-Berkeley

"Atomic and Molecular Photoelectron and Auger Electron Spectroscopy Studies Using Synchrotron Radiation" (Advisor - D.A. Shirley)

K. Jackson
Stanford University

"Photoion Fluorescence Polarization: A Study of Molecular Ionization Dynamics" (Advisor - R.N. Zare)

V. Yachandra
Princeton University

"EXAFS Studies of Carbonic Anhydrase and Resonance Raman Spectroscopy of Iron-Sulfur Proteins" (Advisor - T. Spiro)

1981

J.M. Fine
Washington State Univ.

"Structure and Stoichiometry in Highly Concentrated Aqueous Solutions of $CuBr_2$" (Advisor - D.R. Sandstrom)

C.-Y. Su
Stanford University

"Photoemission Studies of the Interaction of Oxygen with Solid Surfaces" (Advisor - I. Lindau)

D.L. Weissman
Stanford Univesity

"Oxygen Chemisorption and Water Synthesis on Palladium and Palladium-Gold; A Study by Thermal Desorption and Photoemission" (Advisor - W.E. Spicer)

R.F. Davis
UC-Berkeley

"Angular Distribution and Atomic Effects in Condensed Phase Photoelectron Spectroscopy" (Advisor - D.A. Shirley)

F. Kutzler
Stanford University

"Electronic Structure Calculations of Germanium, Molybdenum Chromium and Erbium Compounds Predicted K and L Edge Absorption Spectra" (Advisor - K.O. Hodgson)

1980

B. Bunker
Univ. of Washington

"An X-Ray Absorption Study of Tetrahedral Semiconductors" (Advisor - E. Stern)

J.M. Lornston
Univ. of Delaware

"Characterization of $Pt/A_{12}0_3$ Catalysts by Extended X-Ray Absorption Fine Structure" (Advisors - J.R. Katzer/J.M. Schultz)

P.H. Fuoss
Stanford University

"Structural Studies of Amorphous Materials Using X-Ray Anomalous Scattering" (Advisor - A.I. Bienenstock)

D.J. Trevor
UC-Berkeley

"Photoelectron Photoion Molecular Beam Spectroscopy" (Advisor - D.A. Shirley)

S.D. Kevan
UC-Berkeley

"Normal Emission Photoelectron Diffraction: A New Technique for Determining Surface Structure" (Advisor - D.A. Shirley)

R.V. Taylor
UC-Santa Barbara

"Matrix Spectroscopy of Rare-Gas Oxides and Sulfides" (Advisor - W.C. Walker)

P. Frank
Stanford University

"The Biochemistry of Transition Metals: Copper Vanadium, and Iron" (Advisor - K.O. Hodgson)

1979

M. Breining
Univ. of Oregon

"Precision Determining of Atomic Level Energies by Absorption Spectrometry with Synchrotron Radiation" (Advisor - B. Crasemann)

F.A. de Parente
Univ. of Oregon

"Measurement of the Inelastic Scattering Cross Section of Neon with Synchrotron Radiation" (Advisor - B. Crasemann)

T.D. Bonifield *Rice University*	**"Time Resolved Spectroscopy of Krypton and Xenon Molecules Excited by Electron Impact and by Monochromatic Synchrotron Radiation"** (Advisor - G.K. Walters)
J.N. Miller *Stanford University*	**"Photoemission Studies of Adsorption and Oxidation of Selected Metals and Semiconductors"** (Advisor - I. Lindau)
D.T. Ling *Stanford University*	**"Angle-Integrated and Angle-Resolved Photoemission Studies of Chemisorption on Copper and Copper/Nickel"** (Advisors - I. Lindau/W.E. Spicer)
K.A. Mills *UC-Berkeley*	**"The Determination of Electronic State in Crystalline Semiconductors and Metals by Angle-Resolved Photoemission"** (Advisor - D.A. Shirley)
D.R. Denley *UC-Berkeley*	**"Determination of Morphology and Electronic Structure in Solids with 20-1000 eV Radiation"** (Advisor - D.A. Shirley)
E.D. Poliakoff *UC-Berkeley*	**"Time-Resolved Spectroscopy Using Synchrotron Radiation"** (Advisor - D.A. Shirley)
M.G. White *UC-Berkeley*	**"Photoelectron Spectroscopy of Heavy Molecules"** (Advisor - D.A. Shirley)
R.A. Rosenberg *UC-Berkeley*	**"Studies of Electron Correlation in the Photoionization Process"** (Advisor - D.A. Shirley)
T.D. Tullius *Stanford University*	**"Structures of Metal Complexes in Biological Systems: EXAFS Studies of Blue Copper Proteins, Xamthine Oxidase and Vanadocytes"** (Advisor - K.O. Hodgson)

1978

C.M. Garner *Stanford University*	**"Surface and Interface Studies of Oxygen on Silicon, III-V Heterojunctions, Schottky Barriers"** (Advisors - I. Lindau/W.E. Spicer)
J.C. Phillips *Stanford University*	**"Crystal Structure Determination Using Synchrotron Radiation"** (Advisor - K.O. Hodgson)
P.W. Chye *Stanford University*	**"Photoemission Studies of the Oxidation of and Schottky Barrier Formation on GaSb, InP, and GaAs"** (Advisor - W.E. Spicer)
S.P. Cramer *Stanford University*	**"Chemical Application of X-Ray Absorption Spectroscopy-Nitrogenase and Cytochrome P-450"** (Advisor - K.O. Hodgson)
T. Eccles *Stanford University*	**"X-Ray Absorption Studies of Hemocyanin"** (Advisor - K.O. Hodgson)
R.S. Williams *UC-Berkeley*	**"Angle-Resolved Photoelectron Spectroscopy Applied to the Determination of the Surface Electronic Structure of Crystalline Metals"** (Advisor - D.A. Shirley)
P.S. Wehner *UC-Berkeley*	**"Valence Band Photoemission Studies of Clean Metals"** (Advisor - D.A. Shirley)

1977

G.E. Ice *Univ. of Oregon*	**"Measurements of X-Ray Scattering Cross Sections of Hydrogen and Helium with Synchrotron Radiation"** (Advisor - B. Crasemann)

P.A. Pianetta
Stanford University

"Photoemission Studies of Solids Using Synchrotron Radiation" (Advisor - W.E. Spicer)

S.H. Hunter
Stanford University

"A Structural Study of Amorphous Copper-Arsenic Triselenide Alloys Using EXAFS" (Advisor - A.I. Bienenstock)

G.R. Apai II
UC-Berkeley

"Photoemission Studies of Clean and Adsorbate Covered Metal Surfaces Using Synchrotron and UV Radiation Sources" (Advisor - D.A. Shirley)

K.Y. Yu
Stanford University

"Photoemission and Thermal Desorption Studies of the Adsorption of Simple Molecules on Transition Metals and Alloys" (Advisor - W.E. Spicer)

F.R. McFeely
UC-Berkeley

"Relaxation and Cross Section Effects in Valence Band Photoemission Spectroscopy" (Advisor - D.A. Shirley)

1975

P.E. Gregory
Stanford University

"Ultraviolet Photoemission Studies of the Surface States and Properties of the (110) Gallium Arsenide Surface, and of the Oxidation of Cesium" (Advisor - W.E. Spicer)

B.M. Kincaid
Stanford University

"Synchrotron Radiation Studies of K-Edge X-Ray Photoabsorption Spectra: Theory and Experiment" (Advisor - S. Doniach)

1974

C.A. Ashley
Stanford University

"Extented X-Ray Absorption Fine Structure" (Advisor - S. Doniach)

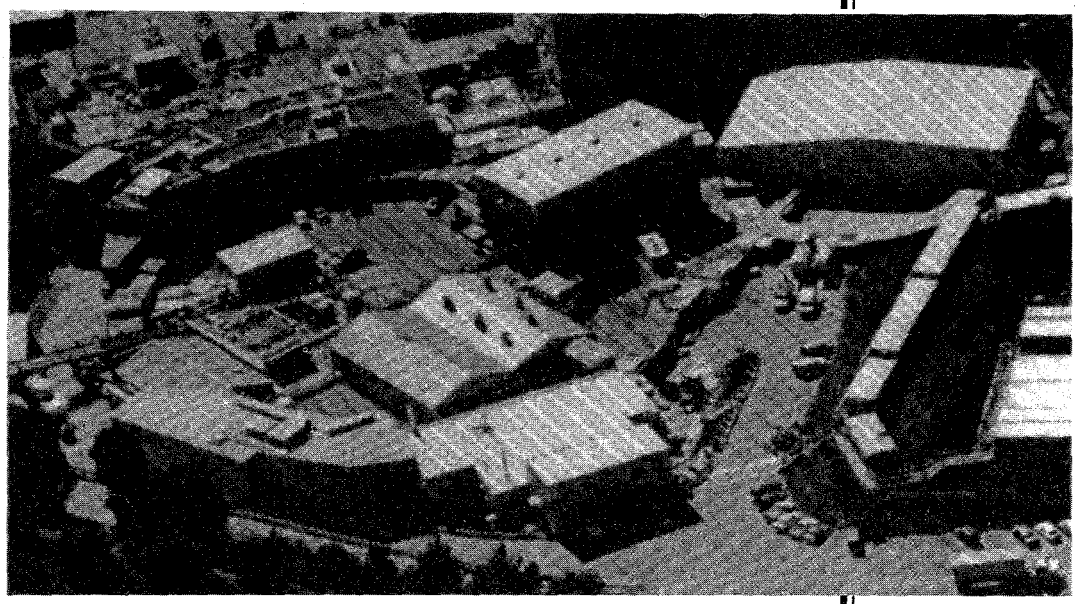

Section VII

Active Proposals

VII. ACTIVE PROPOSALS

As of December 31, 1989 there were 166 active SSRL proposals. Proposals remain active for two years after their initial rating by the Proposal Review Panel. Since October 1974 SSRL has received a total of 2107 proposals. The Spokesperson for each proposal is underlined and their institution shown in parentheses. The letter suffix appended to the proposal number indicates the sub-panel of the Proposal Review Panel to which the proposal is assigned: Materials (M), Biology (B) or Vacuum Ultra-Violet (V). The small (p) denotes a program proposal.

No.	Received	Experimenters	Title
922Bp	9/6/84	**RICHARD ELDER** KATHERINE TEPPERMAN *(UNIVERSITY OF CINCINNATI)*	**Gold-Based Antiarthritis and Anticancer Drugs and Metabolites: XAS, WAXS, DAS**
935Vp	9/20/84	**I LINDAU** DAN DESSAU ALBERTO HERRERA PAUL MEISSNER KEN MIYANO TOM KENDELEWICZ WILLIAM E SPICER CHRISS SPINDT ANITA WAHI BARRETT WELLS Z-X SHEN *(STANFORD UNIVERSITY)*	**Electronic Structure, Chemistry, and the Fermi Level at Semiconductor Surfaces**
943Vp	9/6/84	**DAVID A SHIRLEY** TONY HUFF EDDIE MOLER ZAHID HUSSAIN LI-QUING WANG ALEXIS SCHACH V WITTENAU PHILIP A HEIMANN ZHENG-QING HUANG LAURA MEDHURST *(LAWRENCE BERKELEY LABORATORY)*	**Electron Spectroscopy of Gases, Solids, and Surfaces**
956Mp	2/27/85	**G P HUFFMAN** ROBERT B GREEGOR R G JENKINS NARESH SHAH FARREL W LYTLE F E HUGGINS *(UNIVERSITY OF KENTUCKY)*	**Applications of EXAFS Spectroscopy in the Steel and Coal Industries**
957Bp	2/28/85	**DAVID H TEMPLETON** L K TEMPLETON *(LAWRENCE BERKELEY LABORATORY)*	**Anomalous Scattering of X-rays**
959Vp	3/1/85	**ROBERT Z BACHRACH** ROSS D BRINGANS *(XEROX)*	**Core Level and Near Edge Structure Study of Interface Formation**

963Vp	3/6/85	**JOACHIM STOHR** *(IBM RESEARCH LABORATORY)*	**NEXAFS and SEXAFS Studies by Means of X-ray Fluorescence Detection: Local Structure Around Low-Z Atoms**
969Bp	3/14/85	**ROBERT A SCOTT** STEPHEN P CRAMER *(UNIVERSITY OF GEORGIA)*	**X-ray Absorption Spectroscopic Studies of Nickel-Containing Metalloenzymes**
973M	4/12/85	**CHARLES E BOULDIN** E D DONOVAN R A FORMAN G K HUBLER M I BELL *(NIST)*	**EXAFS Study of Damage and Annealing of Ion Implanted Semiconductors**
981Bp	9/3/85	**JAMES O ALBEN** FRANK G FIAMINGO STEPHEN P CRAMER CRAIG F HEMANN KIMBERLY A POWELL ALLAN A CROTEAU *(OHIO STATE UNIVERSITY)*	**High Resolution EXAFS Spectroscopy of Iron and Copper Proteins**
991Bp	9/4/85	**RICHARD C ELDER** EDWARD A DEUTSCH *(UNIVERSITY OF CINCINNATI)*	**Technetium and Rhenium Imaging Agents and Therapeutic Radiopharmaceuticals**
994Mp	9/5/85	**GLENN A WAYCHUNAS** GORDON E BROWN, JR *(STANFORD UNIVERSITY)*	**High Temperature EXAFS Study of Fe and Ca in Silicate Crystals and Melts**
995Mp	9/6/85	**GORDON E BROWN, JR** GLENN A WAYCHUNAS JAMES O LECKIE GEORGE A PARKS KIM F HAYES KEITH O HODGSON *(STANFORD UNIVERSITY)*	**XAS Study of Cation Adsorption at Aqueous/Oxide Interface**
997Mp	9/10/85	**I K ROBINSON** M ALTMAN P J ESTRUP ROBERT J BIRGENEAU *(AT&T BELL LABORATORIES)*	**The Surface Phase Transition of Clean W(100)**
999Mp	9/10/85	**GORDON E BROWN, JR** C W PONADER GLENN A WAYCHUNAS W A JACKSON S ROTHFUS *(STANFORD UNIVERSITY)*	**EXAFS Study of Trace Element Environments in Quenched Silicate Melts of Geochemical Interest**
1008Mp	10/4/85	**WILLIAM K WARBURTON** KARL F LUDWIG ARTHUR BIENENSTOCK *(X-RAY INSTRUMENTATION ASSOCIATATION)*	**Binary Liquid Structures Determined by Anomalous X-ray Scattering**

1012Bp	11/4/85	**ROBERT H FAIRCLOUGH** KEITH O HODGSON STEVAN R HUBBARD SEBASTIAN DONIACH D RICHMAN *(UNIVERSITY OF CHICAGO)*	**Membrane X-Ray Diffraction Studies of the Acetylcholine Receptor**
1018Mp	3/3/86	**D DE FONTAINE** STEVE SPOONER M KRAITCHMAN JEFF J HOYT *(UNIVERSITY OF CALIFORNIA)*	**Diffusion in Ternary Multilayer Thin Films**
1021Mp	3/3/86	**WILLIAM PARRISH** CURT ERICKSON TING C HUANG MICHAEL HART MAURIZIO BELLOTTO GEORGE WILL *(IBM RESEARCH LABORATORY)*	**Synchrotron X-ray Polycrystalline Diffractometry**
1022Vp	3/3/86	**EDWARD I SOLOMON** KRISTINE BUTCHER JIAN-YI LIN *(STANFORD UNIVERSITY)*	**UPS Studies of the Coordination Chemistry of Metal Oxides, Chlorides and Sulfides**
1030Bp	3/17/86	**STEPHEN P CRAMER** J H ENEMARK M WW ADAMS W CLELAND L S SOLMONSON GRAHAM N GEORGE B E SMITH V MINAK EDWARD I STIEFEL *(BROOKHAVEN NATIONAL LABORATORY)*	**Soft X-ray Spectrocopy of Molybdenum Enzymes, Cofactors and Model Compounds**
1040B	6/3/86	**RUSSELL HILLE** STEPHEN P CRAMER *(OHIO STATE UNIVERSITY)*	**X-Ray Absorption Spectroscopy of Xanthine Oxidase**
1041B	9/3/86	**ROBERT A SCOTT** MARLY EIDSNESS *(UNIVERSITY OF GEORGIA)*	**Measurement of Metal-Metal Distances in Proteins by X-ray Anomalous Scattering**
1042B	9/3/86	**BRITTON CHANCE** LINDA S POWERS MARK CHANCE JAMES RIORDAN BARTON HOLMQUIST B VALLEE DAVID AULD *(UNIVERSITY OF PENNSYLVANIA)*	**Studies of Intermediates in the Mechanism of Carboxypeptidase-A**

1043B	9/3/86	**BRITTON CHANCE** GRANT BUNKER GUANG ZHANG PETER REICHARD BRITT-MARIE SJOBERG S M KHALID ALI NAQUI *(UNIVERSITY OF PENNSYLVANIA)*	**X-Ray Absorption Spectroscopy of Iron-Iron Interactions: Ribonucleotide Reductase**
1046B	9/3/86	**EDWARD RUBENSTEIN** HERBERT D ZEMAN GEORGE S BROWN ROBERT HOFSTADTER JOHN OTIS DONALD C HARRISON ROBERT KERNOFF ALBERT C THOMPSON W THOMLINSON *(STANFORD UNIVERSITY)*	**Iodine Dichromography with Monochromatic X-ray Beams for Angiography**
1047M	9/3/86	**ROBERT L INGALLS** DARYL CROZIER J FREUND *(UNIVERSITY OF WASHINGTON)*	**High Pressure Transition Mechanisms via EXAFS**
1048Mp	9/11/86	**CAROLINE STAHLE** ARTHUR BIENENSTOCK SEAN BRENNAN DOUGLAS OSHEROFF *(STANFORD UNIVERSITY)*	**High Resolution Compton Profiles of Iron and Silicon**
1051M	9/11/86	**GLENN A WAYCHUNAS** LAWRENCE R BERNSTEIN JAMES A DAVIS BRIDIG A REA *(STANFORD UNIVERSITY)*	**Crystal and Aqueous Chemistry of Germanium in Geochemically Important Systems**
1053B	9/15/86	**ROBERT A SCOTT** DAVID M DOOLEY ROBERT A KERTAYASA *(UNIVERSITY OF GEORGIA)*	**Copper EXAFS Spectroscopy of Non-Blue Copper Proteins. Amine Oxidases**
1055B	9/15/86	**KEITH O HODGSON** P FRANK W E NEWTON BRITT HEDMAN FRANK A SCHULTZ C STANFEL B J FELDMAN *(SSRL)*	**XAS of Iron-Molybdenum Cofactor of Nitrogenase under Electrochemical Control**
1059M	9/16/86	**MURLI H MANGHNANI** H K MAO R J HEMLEY J A XU *(UNIVERSITY OF HAWAII)*	***In Situ* High P-T Equation-of-State, Phase Transformations and Kinetics Studies on Mantle Mineral Phases using Synchrotron Radiation**

1064M	3/3/87	**J AKELLA** H K MAO G S SMITH QUINTIN C JOHNSON L C MING MURLI H MANGHNANI *(LAWRENCE LIVERMORE NATIONAL LABORATORY)*	**Static High Pressure and High Temperature X-Ray Diffraction Studies of Some Rare-Earth Elements Using Diamond-Anvil Apparatus.**
1065Mp	3/1/87	**MICHEL BOUDART** R J DAVIS *(STANFORD UNIVERSITY)*	**Characterization of Supported Pd/Au Alloys by X-Ray Absorption Spectroscopy**
1066Mp	3/1/87	**RICHARD C ELDER** WILLIAM R HEINEMAN *(UNIVERSITY OF CINCINNATI)*	**X-Ray Spectroscopy of Electrochemically Generated Species**
1067Bp	3/1/87	**ROBERT A SCOTT** SUNNEY I CHAN P MARK LI *(UNIVERSITY OF GEORGIA)*	**Active Site Structures of Cytochrome c Oxidase**
1068Bp	3/1/87	**R H FELTON** E A STERN *(GEORGIA INSTITUTE OF TECHNOLOGY)*	**Structure of Transients in the Catalytic Cycle of Dioxygenases**
1069M	3/1/87	**NOLAN MANGELSON** FARREL W LYTLE MAX W HILL *(BRIGHAM YOUNG UNIVERSITY)*	**Characterization of Vanadium, Chromium, Nickel and Arsenic in Particulate Matter**
1070M	3/1/87	**THOMAS BEIN** KARIN MOLLER *(UNIVERSITY OF NEW MEXICO)*	**Anchoring Chemistry of Transition Metal Complexes and Clusters to Intrazeolite Surfaces**
1071M	3/1/87	**MICHEL BOUDART** G P VALENCA *(STANFORD UNIVERSITY)*	**Characterization of Clusters of Pt/Y-Zeolite and Rh/γ-Al_2O_3 by X-Ray Absorption Spectroscopy**
1072M	3/1/87	**STEVE M HEALD** HEATHER CHEN *(BROOKHAVEN NATIONAL LABORATORY)*	**Glancing Angle EXAFS and Reflectivity of Aluminum-Metal Interfaces**
1073M	3/1/87	**STEVE M HEALD** J M TRANQUADA M SUENAGA *(BROOKHAVEN NATIONAL LABORATORY)*	**X-Ray Absorption Study of La CuO Based Superconductors**
1074M	3/1/87	**STEVE M HEALD** ERIC ZIEGLER DALE E SAYERS JAMES P VICCARO *(BROOKHAVEN NATIONAL LABORATORY)*	**X-Ray Absorption and Reflectivity Studies of Interfaces in Multilayer Optics**
1076B	3/1/87	**SEBASTIAN DONIACH** ROBERT M STROUD S WAKATSUKI KEITH O HODGSON *(STANFORD UNIVERSITY)*	**Study of Conformational Changes in Bacteriorhodopsin using Time-Resolved Small Angle X-Ray Diffraction**

1077M	3/1/87	**KRISHNA M CHOUDHARY** *(UNIVERSITY OF NOTRE DAME)*	**Photoemission EXAFS Studies of Surfaces and Interfaces in Compound Semiconductors**
1078M	3/1/87	**N S LEWIS** KEITH O HODGSON *(CALIFORNIA INSTITUTE OF TECHNOLOGY)*	**X-Ray Absorption Studies of Metal Ion Absorption at Semiconductor Surfaces**
1079M	3/1/87	**JAMES B BOYCE** THEODORE H GEBALLE FRANK G BRIDGES TORD CLAESON *(XEROX)*	**Local Atomic Structure of High-T_c Superconductors**
1080Vp	3/1/87	**ROBERT J MADIX** C M FRIEND J SOLOMON B FACTOR J T ROBERTS A C LIU *(STANFORD UNIVERSITY)*	**Adsorption Structure of Heteroatom-Containing Molecules on Transition Metal Surfaces**
1081M	3/1/87	**DAVID P POPE** JOHN E BENCI *(UNIVERSITY OF PENNSYLVANIA)*	**A Study of Creep Damage Using Microradiography**
1082B	3/24/87	**DAVID A LARSON** DENNIS SHRIEVE TERESA TROXEL THEODORE L PHILLIPS MICHAEL SCHELL CLIFF LING *(UNIVERSITY OF CALIFORNIA)*	**Contribution of Auger Electrons to Radiation Sensitization with IUdR**
1083B	3/1/87	**M IKEDA-SAITO** GRAHAM N GEORGE ROGER C PRINCE *(CASE WESTERN RESERVE UNIVERSITY)*	**X-Ray Absorption Spectroscopy of Myeloperoxidase and Lactoperoxidase**
1084Bp	3/1/87	**GRAHAM N GEORGE** STEPHEN P CRAMER ROGER C PRINCE *(EXXON RESEARCH & ENGINEERING)*	**Polarized X-Ray Spectroscopy of the Oriented Chloroplast Water-Oxidizing Complex**
1085Bp	3/1/87	**JAMES E PENNER-HAHN** M STERN J T GROVES W D FRASCH V L PECORARO HIM-TAI TSANG C F YOCUM D GHANOTAKIS *(UNIVERSITY OF MICHIGAN)*	**X-Ray Absorption Spectroscopic Characterization of the Manganese in Biological Systems**

1087Bp 3/1/87 **WAYNE A HENDRICKSON** **Anomalous Scattering Studies of Protein Crystal Structures**
R PAUL PHIZACKERLEY
STEVAN R HUBBARD
CRAIG OGATA
JOHN HORTON
WILLIAM E ROYER
HM KRISHNA MURTHY
MARIANNE CUFF
WEI YANG
ARNO PAHLER
(COLUMBIA UNIVERSITY)

1088M 3/1/87 **JAMES E PENNER-HAHN** **Polarized X-Ray Absorption Near Edge Structure**
GEOFFREY WALDO
SHENGKE WANG
GLENN A WAYCHUNAS
RICHARD FRONKO
(UNIVERSITY OF MICHIGAN)

1089M 3/1/87 **JAMES HOWARD** **X-Ray Absorption of Iridium in K-T Boundary Samples and Meteorites**
JULIA PECK
GRAHAM N GEORGE
STEPHEN P CRAMER
WILLIAM MURPHY
(SCHLUMBERGER DOLL RESEARCH)

1091Mp 6/6/87 **D L WILLIAMSON** **Characterization of Ion-Implanted Aluminum and Titanium**
T M HAYES
F M KUSTAS
(COLORADO SCHOOL OF MINES)

1092M 6/19/87 **JAMES HOWARD** **Structural Investigation of Interlayer Potassium and Sodium in Phyllosilicates**
S WHITTINGHAM
STEPHEN P CRAMER
N WADA
D R HINES
(SCHLUMBERGER DOLL RESEARCH)

1093Mp 8/7/87 **STEPHEN LADERMAN** **Structure of Superconducting Thin Films**
THEODORE H GEBALLE
ALICE FISCHER-COLBRIE
J Z SUN
K CHAR
B OH
N MISSERT
J MOLL
(HEWLETT PACKARD LABORATORIES)

1094M 8/20/87 **JAKOB BOHR** **X-Rays Studies of Rare Gas Inclusions in Single Crystal Aluminium**
E JOHNSON
H H ANDERSEN
L SARHOLT-KRIST
L F GRAABAEK
A JOHANSEN
I K ROBINSON
(RISO NATIONAL LABORATORY)

1095Mp 8/7/87 **PAUL H FUOSS** — **EXAFS and NEXAFS Investigation of OMPVE Growth of II-VI Compounds**
D W KISKER
LAURA NORTON
(AT&T BELL LABORATORIES)

1096Mp 8/20/87 **PAUL H FUOSS** — ***In-Situ* X-Ray Scattering Studies of OMVPE Growth of II-VI Compounds**
LAURA NORTON
D W KISKER
(AT&T BELL LABORATORIES)

1097Mp 8/20/87 **FARREL W LYTLE** — **Anti-Site Disorder in High T_c Superconductors**
ROBERT B GREEGOR
(BOEING COMPANY)

1098M 9/1/87 **DANIEL A SCHERSON** — ***In-Situ* EXAFS Transition Metal Macrocycles Absorbed on Electrode Surfaces**
PHILIP N ROSS
(CASE WESTERN RESERVE UNIVERSITY)

1099M 9/15/87 **J V ACRIVOS** — **Study of Organic Metals**
M CHEN LEI
S S P PARKIN
J SATCHER
D HELMOLDT
C BUSTILLO
S ARNOLD
R ITHNIN
(LAWRENCE BERKELEY LABORATORY)

2000M 9/15/87 **J V ACRIVOS** — **Study of Cation, Anion X-Ray Edges in S Intercalated Perovskites $[Y_1Ba_2Cu_3(O/S)_{7+\sigma}]_n$**
C BUSTILLO
S S P PARKIN
S ARNOLD
M CHEN LEI
R ITHNIN
D HELMOLDT
J SATCHER
MELVIN P KLEIN
(LAWRENCE BERKELEY LABORATORY)

2001M 9/15/87 **JEFFREY R LINCE** — **Extended X-Ray Absorption Fine Structure of Transition Metal Dischalcogenide Materials**
PAUL D FLEISCHAUER
(THE AEROSPACE CORPORATION)

2002Mp 9/15/87 **J D BROCK** — **Bond Orientational Order in Tilted Hexatic Liquid Crystal Films**
ROBERT J BIRGENEAU
J D LITSTER
(CORNELL UNIVERSITY)

2003M 9/15/87 **MIKE TONEY** — ***In-Situ* X-Ray Scattering Study of the Structure of Passive Oxides on Single Crystal Ti**
W H SMYRL
OWEN MELROY
(IBM RESEARCH LABORATORY)

2005M	9/15/87	**ROBERT L INGALLS** J M TRANQUADA E A STERN DARYL CROZIER B HOUSER *(UNIVERSITY OF WASHINGTON)*	**X-Ray Absorption Studies of Perovskites as a Function of Pressure**
2006Mp	9/15/87	**D DE FONTAINE** M KRAITCHMAN JEFF J HOYT M WIEDENMEIR S SPOONER *(UNIVERSITY OF CALIFORNIA)*	**Kinetics of Phase Separation in Al-Li**
2007B	9/15/87	**JAMES C PHILLIPS** *(ENRAF-NONIUS COMPANY)*	**Protein Folding Studied by Synchrotron X-Ray Scattering**
2008B	9/15/87	**DOUGLAS S CLARK** R MARK GUINN *(UNIVERSITY OF CALIFORNIA)*	**EXAFS of Active-Site Metals in Glucose Isomerase and Methane Monooxygenase**
2009Vp	9/17/87	**JOACHIM STOHR** THOMAS P RUSSELL *(IBM RESEARCH LABORATORY)*	**Structural Studies of Thin Polymer Films on Surfaces**
2010Bp	9/17/87	**MELVIN P KLEIN** KENNETH SAUER VICKIE DEROSE R GUILES SUSAN DEXHEIMER ANN MCDERMOTT J L ZIMMERMANN *(LAWRENCE BERKELEY LABORATORY)*	**X-Ray Spectroscopy of Manganese and Iron in Chloroplasts**
2011V	9/17/87	**DON KANIA** J TREBES PIERO PIANETTA *(LAWRENCE LIVERMORE NATIONAL LABORATORY)*	**Synchrotron Based Studies of X-Ray Induced Photoconductivity**
2012M	9/17/87	**E E ALP** PEDRO A MONTANO L SODERHOLM GOPAL K SHENOY *(ARGONNE NATIONAL LABORATORY)*	**Electronic Structure of High T_c Oxide Superconductors by X-Ray Absorption Spectroscopy**
2013M	9/17/87	**DAVE WARK** JOHN WILKERSON BERND CRASEMANN TOM BOWLES GEORGE S BROWN S B WHITFIELD ROGER J BARTLETT S L SORENSEN WALTER J TRELA JOHN HENDERSON DAVE KNAPP RICH MARTIN HAMISH ROBERTSON *(LOS ALAMOS NATIONAL LABORATORY)*	**Photoelectron Spectrometry of Correlation Satellites in Kr**

2014M 9/17/87 **ROBERT M SUTER** **Melting of Xe/TiS_2: Structure and Thermodynamics**
J D SHINDLER
R F HAINSEY
(CARNEGIE MELLON UNIVERSITY)

2015Mp 9/17/87 **S R STOCK** ***In-Situ* Synchrotron Microradiography of Delamination in Graphite/Epoxy Composites**
G WEBB
ZOPHIA U REK
S D ANTOLOVICH
(GEORGIA INSTITUTE OF TECHNOLOGY)

2016M 9/17/87 **GEORGE KWEI** **Anomalous X-Ray Powder Diffraction Studies of the Structure of Materials**
ANDREW C LAWSON
ROBERT B VON DREELE
ART WILLIAMS
JOYCE A GOLDSTONE
(LOS ALAMOS NATIONAL LABORATORY)

2017Mp 9/17/87 **BENJAMIN OCKO** **Structure and Stability of Metal Surfaces: A Proposal for X-Ray Scattering Experiments**
DAVID M ZEHNER
S G J MOCHRIE
L D GIBBS
(BROOKHAVEN NATIONAL LABORATORY)

2018M 9/21/87 **JEFFREY B KORTRIGHT** **Structural Study of Hetero-Epitaxial CaF_2 on Si(111) Using Standing Wave Fluorescence**
MARJORIE OLMSTEAD
JONATHAN DENLINGER
ROSS D BRINGANS
(LAWRENCE BERKELEY LABORATORY)

2019V 9/21/87 **MARJORIE OLMSTEAD** **Heteroepitaxial Interface Formation Between Insulators and Semiconductors**
ROSS D BRINGANS
JONATHAN DENLINGER
(UNIVERSITY OF CALIFORNIA)

2020Mp 9/21/87 **S H LIN** **X-Ray Diffraction of Solid State Reactions and Phase Transitions**
T GROY
J R SCHOONOVER
(ARIZONA STATE UNIVERSITY)

2021M 9/21/87 **NOLAN MANGELSON** **Structures of Silver(I)-Crown Complexes in Liquid and Solid Phases**
ROBERT B GREEGOR
FARREL W LYTLE
MAX W HILL
(BRIGHAM YOUNG UNIVERSITY)

2022B 9/21/87 **BRITTON CHANCE** **Structural Features of Low Temperature Recombination of Hemoproteins, Carbon Monoxide and Oxygen**
S G SLIGAR
GRANT BUNKER
KE ZHANG
HIROYUKI OYANAGI
(UNIVERSITY OF PENNSYLVANIA)

2023Mp 9/21/87 **STEVE D CONRADSON** **High T_c Superconducting Materials: Their Structural and Electronic Characterization by XAS**
ZACHARY FISK
ANTONIO REDONDO
IAN D RAISTRICK
(LOS ALAMOS NATIONAL LABORATORY)

2024Mp	9/21/87	**STEVE D CONRADSON** ALFRED SATTLEBERGER BASIL SWANSON *(LOS ALAMOS NATIONAL LABORATORY)*	**XAS Studies of Quasi-One-Dimensional Halide-Bridged Mixed Valence Platinum Compounds**
2025B	9/21/87	**BRITTON CHANCE** EDGAR DAVIDSON ROBERT POYTON KE ZHANG GRANT BUNKER TSOO E KING *(UNIVERSITY OF PENNSYLVANIA)*	**Altered Structures of Cytochrome Oxidase**
2026Mp	9/21/87	**PIERO PIANETTA** JEFF NELSON JENNCHANG HWANG RICHARD H STULEN GLENN KUBIAK *(SSRL)*	**The Bonding Behaviour in Strained Semiconductor Heterostructures**
2027M	9/22/87	**SEAN BRENNAN** ROLAND TIMSIT B FACTOR ARTHUR BIENENSTOCK *(SSRL)*	**Structural Studies of Co-Sputtered Amorphous AlTa Thin Films**
2028M	9/29/87	**HOWARD OCKEN** ZOPHIA U REK FARREL W LYTLE *(EPRI)*	**Characterization of Cobalt-Bearing Passive Oxides on Stainless Steel by EXAFS**
2029Bp	9/29/87	**KEITH O HODGSON** BRITT HEDMAN STEVEN A VAUGHN BARBARA K BURGESS *(SSRL)*	**Mo and Se XAS Studies of Small-Molecule Binding to Nitrogenase**
2030Bp	9/29/87	**KEITH O HODGSON** ROBERT H BEER BRITT HEDMAN JAMES G BENTSEN STEPHEN J LIPPARD *(SSRL)*	**XAS Structural Characterization of the Binuclear Iron-Center in Methane Monooxygenase**
2031Bp	9/29/87	**KEITH O HODGSON** EDWARD I SOLOMON GRACE TAN BRITT HEDMAN *(SSRL)*	**X-Ray Absorption Studies of Coupled Binuclear Copper Sites in Proteins**
2032Bp	9/29/87	**KEITH O HODGSON** BRITT HEDMAN JOHN H DAWSON MASANORI SONO *(SSRL)*	**XAS Studies of Heme-Iron Enzymes: Cytochrome P-450 and Peroxidases**

2033Mp	9/29/87	**TERESA A SMITH** BRITT HEDMAN KEITH O HODGSON *(EASTMAN KODAK RESEARCH LABORATORY)*	**Sulfur K Edge XAS Studies of Photographic Sensitizing Centers**
2034M	9/29/87	**KEITH O HODGSON** BRITT HEDMAN JAMES P COLLMAN MATTHEW B ZISK HITOSHI ASAHINA *(SSRL)*	**XAS Studies of Liquid Crystalline Ruthenium Phthalocyanine and Porphyrins**
2035B	9/29/87	**SEBASTIAN DONIACH** ROBERT M STROUD S WAKATSUKI U W SPANN KEITH O HODGSON *(STANFORD UNIVERSITY)*	**X-Ray Diffraction Studies of Helix Linking Regions of Bacteriorhodopsin**
2037Vp	9/29/87	**PIERO PIANETTA** DANIEL SELIGSON LAWRENCE PAN PAUL KING *(SSRL)*	**X-Ray Lithography Process Development**
2038M	10/1/87	**P G ELLER** FARREL W LYTLE ROBERT B GREEGOR E M LARSON J D PURSON *(LOS ALAMOS NATIONAL LABORATORY)*	**EXAFS Study of Actinide and Fission Product Speciation in Nuclear Waste Storage Media**
2039Vp	10/1/87	**JON ERICKSON** VICTOR REHN TSU-WIE NEE CAREY SCHWARTZ WAYNE WIEMER AROLD K GREEN SANDY LANGSJOEN PHILLIP LAROE *(NAVAL WEAPONS CENTER)*	**Superconductor-Semiconductor Heterostructure Research**
2040M	10/4/87	**FRANK G BRIDGES** JAMES B BOYCE *(UNIVERSITY OF CALIFORNIA)*	**EXAFS Study of Off-Center Behavior and Aggregation in Dilute Immissible Systems**
2041B	10/4/87	**JOHN P LANGMORE** BRIAN D ATHEY SHAWN WILLIAMS MICHAEL F SMITH *(UNIVERSITY OF MICHIGAN)*	**Synchrotron Studies of Ordered Chromatin Fibers for Model Calculations**

2042M	10/12/87	**ERIC SIROTA** N A CLARK C R SAFINYA GREG S SMITH *(EXXON RESEARCH & ENGINEERING)*	**Synchrotron Scattering Studies of Dilute Membrane Systems**
2043V	10/12/87	**PIETRO CHIARADIA** GIORGIO MARGARITONDO L J BRILLSON *(UNIVERSITA DI ROMA)*	**Schottky Barrier Formation in GaP Single Crystals**
2044Mp	11/5/87	**J KAHN** PAUL H FUOSS ARTHUR BIENENSTOCK LAURA NORTON SEAN BRENNAN *(STANFORD UNIVERSITY)*	**Direct Scattering Studies of Surface Premelting**
2045M	11/5/87	**MARYBETH RICE** ARTHUR BIENENSTOCK PAUL H FUOSS LANE C WILSON *(STANFORD UNIVERSITY)*	**Grazing Incidence X-Ray Scattering Study of Ge Epitaxy on Mo**
2046M	11/5/87	**R COLELLA** Q ZHAO *(PURDUE UNIVERSITY)*	**X-Ray Study of Charge Density Waves (CDW's) in Layer Compounds**
2047B	11/16/87	**JAMES E PENNER-HAHN** RICHARD FRONKO HIM-TAI TSANG DIANA RALSTON THOMAS V O'HALLORAN JEFF WRIGHT *(UNIVERSITY OF MICHIGAN)*	**X-Ray Absorption Spectroscopy of the MER-R Gene Product**
2048B	11/16/87	**JAMES E PENNER-HAHN** ROBERT KERTAYASA RICHARD FRONKO JAMES W WHITTAKER *(UNIVERSITY OF MICHIGAN)*	**X-Ray Absorption Spectroscopy of Galactose Oxidase**
2049Mp	3/1/88	**FARREL W LYTLE** EDWARD C MARQUES ROBERT B GREEGOR *(BOEING COMPANY)*	**Catalyst Characterization by X-ray Absorption Spectroscopy**
2050B	3/1/88	**R PAUL PHIZACKERLEY** MICHAEL SOLTIS JANOS HAJDU *(SSRL)*	**Laue Diffraction Trials with Protein Crystals on PEP**
2051Bp	3/1/88	**BRIAN J HALES** STEPHEN P CRAMER CATHY COYLE GRAHAM N GEORGE *(LOUISIANA STATE UNIVERSITY)*	**X-Ray Absorption of Vanadium and Tungsten Nitrogenases and Storage Proteins**

2053Mp 3/10/88 **G MEITZNER** — **Physical and Electronic Structure of Support Bimetallic Catalysts**
JOHN H SINFELT
GRAYSON H VIA
FARREL W LYTLE
(EXXON RESEARCH & ENGINEERING)

2055M 3/15/88 **T M HAYES** — **Shallow and Deep Donors in $Ga_{1-x}Al_xAs$ Semiconducting Alloys**
P GIBART
D L WILLIAMSON
(RENSSELAER POLYTECHNIC INSTITUTE)

2056Mp 3/15/88 **H K MAO** — **Measurements in the Terapascal Range and Hydrogen Metallization**
J H UNDERWOOD
ALBERT C THOMPSON
A P JEPHCOAT
RUSSELL J HEMLEY
Y WU
(CARNEGIE INSTITUTE)

2058M 3/15/88 **DANIEL A SCHERSON** — ***In-Situ* EXAFS Transition Metal Macrocycles Adsorbed on Electrode Surfaces**
PHILIP N ROSS
(CASE WESTERN RESERVE UNIVERSITY)

2059M 3/15/88 **MIKE TONEY** — **X-Ray Scattering of Amorphous and Hydrogenated Amorphous Carbon Thin Films**
PAUL H FUOSS
SEAN BRENNAN
(IBM RESEARCH LABORATORY)

2060Bp 3/15/88 **LINDA S POWERS** — **Structure-Function Studies of the Active Site of Lignases, Peroxidases, and Models**
M TIEN
J BUMPUS
J LI
S AUST
(UTAH STATE UNIVERSITY)

2061M 3/17/88 **OWEN MELROY** — **Electrochemically Deposited Metal Monolayers: Structure, Compressibility and Growth**
MIKE TONEY
(IBM RESEARCH LABORATORY)

2062Mp 3/17/88 **WILLIAM K WARBURTON** — **Structural Improvements in Multilayers for Instrumentation Applications**
PAUL PLAG
EDWARD FRANCO
(X-RAY INSTRUMENTATION ASSOCIATION)

2063Mp 3/17/88 **HOWARD D DEWALD** — **Characterization of Electrochemical Processes by X-Ray Absorption Spectroscopy**
(OHIO UNIVERSITY)

2064M 3/21/88 **IAN D RAISTRICK** — **X-Ray Absorption Studies of Bimetallic Electrocatalysts for C_1 Oxidation**
STEVE D CONRADSON
ANTONIO REDONDO
(LOS ALAMOS NATIONAL LABORATORY)

2065M 3/24/88 **ALBERT C THOMPSON** — **Elemental X-Ray Imaging with PEP Using an X-Ray Microscope**
ROBERT D GIAUQUE
Y WU
J H UNDERWOOD
(LAWRENCE BERKELEY LABORATORY)

2067M	4/21/88	**JAMES E PENNER-HAHN** I-WEI CHEN T Y TIEN *(UNIVERSITY OF MICHIGAN)*	**X-Ray Absorption Spectroscopy of Transformation-Toughened Zirconia Ceramics**
2068Bp	5/7/88	**JAMES E PENNER-HAHN** HIM-TAI TSANG MAX O FUNK CHRISTOPHER J BATIE DIMITRI COUCOUVANIS DAVID P BALLOU *(UNIVERSITY OF MICHIGAN)*	**X-Ray Absorption Spectroscopy of Phthalate Dioxygenase and Soybean Lipoxygenase**
2069Mp	5/7/88	**JAMES E PENNER-HAHN** M DAVID CURTIS *(UNIVERSITY OF MICHIGAN)*	**XAS of Metal-Sulfur Clusters Supported on Metal Oxide Surfaces**
2070B	9/2/88	**MARTHA LUDWIG** HENRY BELLAMY ETHAN A MERRITT R PAUL PHIZACKERLEY CARL C CORRELL *(UNIVERSITY OF MICHIGAN)*	**Multiple-Wave Length X-Ray Diffraction Analysis of Phthalate Oxygenase Reductase**
2071Bp	9/13/88	**E A STERN** AARON LEWIS DAN THIEL PETERIS LIVINS *(UNIVERSITY OF WASHINGTON)*	**Measurements on Focussed X-Rays for use with Microsecond Resolved XAFS**
2072M	9/13/88	**J KRIM** C L WANG MIKE TONEY R CHIARELLO *(NORTHEASTERN UNIVERSITY)*	**Surface Melting of Xenon Adsorbed on Au(111)**
2073Mp	8/31/88	**JEFF J HOYT** K C RUSSELL F A GARNER *(WASHINGTON STATE UNIVERSITY)*	**Phase Separation in Fe-Ni**
2074Vp	9/13/88	**BRAD PATE** INGOLF LINDAU WILLIAM E SPICER J WU *(WASHINGTON STATE UNIVERSITY)*	**Electronic and Geometric Properties of Impurities ON/IN Carbon**
2075M	9/13/88	**GLENN A WAYCHUNAS** JAMES A DAVIS BRIGID A REA CHRISTOPHER C FULLER *(STANFORD UNIVERSITY)*	**Characterization of Ferrihydrite Reactive Surface Sites and Structure**
2076Mp	9/13/88	**GLENN A WAYCHUNAS** RICHARD J REEDER CHARLES R ROSS WAYNE A DOLLASE *(STANFORD UNIVERSITY)*	**Investigation of Short Range Order in Mineralogical Solid Solutions**

2077M	2/1/89	**M SAMANT** CHARLES A BROWN GARY BORGES JOSEPH G GORDON *(IBM RESEARCH LABORATORY)*	**SEXAFS and Surface X-Ray Diffraction Study of Self-Assembled Monolayers on Gold Surfaces**
2078V	3/1/89	**DAVID B KERWIN** FRANK L GALEENER *(COLORADO STATE UNIVERSITY)*	**X-Ray Induction of Charge Trapping Defects in Amorphous SiO_2**
2079Bp	3/1/89	**KEITH O HODGSON** SCOTT ENSIGN PHILIP J STEPHENS PAUL W LUDDEN MARIE-CLAIRE MCKENNA BRITT HEDMAN *(SSRL)*	**XAS Structural Characterization of the Active Center in the *Rhodospirillum rubrum* Carbon Monooxide Dehydrogenase Enzyme**
2080M	3/1/89	**DANIEL A SCHERSON** PHILIP N ROSS *(CASE WESTERN RESERVE UNIVERSITY)*	***In-Situ* EXAFS Transition Metal Macrocycles Adsorbed on Electrode Surface**
2081Mp	3/7/89	**B FACTOR** THOMAS P RUSSELL *(STANFORD UNIVERSITY)*	**Glancing Angle Diffraction Studies on Polymer Films**
2082Vp	3/7/89	**BERND CRASEMANN** GEORGE S BROWN A F KODRE ROGER CARR J RUSCHEINSKI S J SCHAPHORST *(UNIVERSITY OF OREGON)*	**Dynamics of Atomic Inner-Shell Processes**
2083M	3/7/89	**G FARACI** A TERRASI S LA ROSA *(UNIVERSITA DI CATANIA)*	**Rare Gas Clusters**
2084M	3/7/89	**TONY RYAN** JEFF T KORBERSTEIN CHRIS MACOSKO *(UNIVERSITY OF MINNESOTA)*	**Small Angle X-Ray Studies of Phase Separation During Bulk Copolymerization**
2085M	3/14/89	**THOMAS P RUSSELL** B FACTOR *(IBM RESEARCH LABORATORY)*	**Glancing Angle Diffraction Studies on Liquid Crystalline Polymers**
2086Mp	3/15/89	**PULAK DUTTA** TOM BOHANON BINHUA LIN MINGCHIH SHIH *(NORTHWESTERN UNIVERSITY)*	**Diffraction Studies of Organic Monolayers on Water (Langmuir Films)**
2088M	3/15/89	**MARYBETH RICE** ARTHUR BIENENSTOCK S WAKATSUKI *(STANFORD UNIVERSITY)*	**Anomalous Small Angle X-Ray Scattering Study of Amorphous Metal-Germanium**

2089Mp	3/15/89	**TOM KENDELEWICZ** WILLIAM E SPICER JOE WOICIK PIERO PIANETTA INGOLF LINDAU *(STANFORD UNIVERSITY)*	**Surface EXAFS of Epitaxial Semiconductor Interfaces**
2090Mp	3/15/89	**KIN MAN-YU** W WALUKIEWICZ J JAKLEVIC *(LAWRENCE BERKELEY LABORATORY)*	**Fluorescence EXAFS Applied to the Study of Impurity Site Location in Heavily-Doped III-V Compounds**
2091Mp	3/15/89	**S R STOCK** T S GROSS J D PLUMMER A B LEE ZOPHIA U REK Y H CHUNG *(GEORGIA INSTITUTE OF TECHNOLOGY)*	**Strain Mapping and Crystal Characterization Using Synchrotron Radiation Polychromatic Topography**
2092B	3/15/89	**LINDA S POWERS** F.Y-H. WU *(UTAH STATE UNIVERSITY)*	**Structure <-> Function Studies of RNA Polymerase from *E. coli***
2093Vp	3/15/89	**JON ERICKSON** CAREY SCHWARTZ TERI COLE VICTOR REHN *(NAVAL WEAPONS CENTER)*	***In-Situ* Measurements of Quantum Well Defects and Impurities**
2094V	3/15/89	**PIERO PIANETTA** ANNE BORG PAUL KING GORDON KNAPP *(SSRL)*	**Photoelectron Microscopy**
2095V	3/15/89	**PIERO PIANETTA** X YANG *(SSRL)*	**Synchrotron Radiation Studying Ultra-thin Superlattice Band Structures**
2096B	3/30/89	**JANET L SMITH** *(PURDUE UNIVERSITY)*	**Measurement of Multiwavelength Diffraction Data from Glutamine PRPP Amidotransferase Crystals**
2097B	9/10/89	**JOHN E KUO** CONG-YUAN GUO *(UNIVERSITY OF MISSOURI-COLUMBIA)*	**Structural Investigation of Terbium Chelates in Aqueous Solution by X-Ray Absorption Spectroscopy**
2098B	9/10/89	**J H ENEMARK** M D CARDUCCI STEPHEN P CRAMER *(UNIVERSITY OF ARIZONA)*	**Mo K and L Edge Spectroscopy of Cyanide Inhibited Sulfite Oxidase and Model Compounds**
2099M	9/10/89	**GUANG ZHANG** GARY S MONDO *(CHEVRON RESEARCH COMPANY)*	**Study of Framework Demetallation of CoAPO and FAPO Molecular Sieves by X-Ray Absorption Spectroscopy, X-Ray Diffraction and Diffuse Reflectance Spectroscopy**

2100Mp	9/10/89	**GUANG ZHANG** GARY S MONDO *(CHEVRON RESEARCH COMPANY)*	**X-Ray Absorption Investigation of Metal Binding Sites in Crude Oil and Petroleum Products**
2101B	9/10/89	**SEBASTIAN DONIACH** D ELIEZER N GILLIS S WAKATSUKI KEITH O HODGSON *(STANFORD UNIVERSITY)*	**Structural Studies of the Blue Form of the Purple Membranes**
2102B	9/10/89	**KEITH O HODGSON** S WAKATSUKI N GILLIS SEBASTIAN DONIACH D ELIEZER *(SSRL)*	**Anomalous Dispersion Scattering Studies of Metal Clusters in Biological Systems**
2103Vp	9/10/89	**Z X SHEN** INGOLF LINDAU WILLIAM E SPICER *(STANFORD UNIVERSITY)*	**Photoemission Study of High T_c Superconductors and Related Materials**
2104Bp	9/10/89	**ULRICH KUSTHARDT** BRITT HEDMAN KEITH O HODGSON HANS VILTER *(TU MUNCHEN)*	**XAS Structural Characterization of Vanadium Bromoperoxidase**
2105Mp	9/19/89	**S R STOCK** T M BREUNIG S D ANTOLOVICH ZOPHIA U REK *(GEORGIA INSTITUTE OF TECHNOLOGY)*	**Damage and Crack Closure in Composite and Monolithic Materials**
2106B	9/19/89	**JEFFREY T BOLIN** NINO CAMPOBASSO WLADEK MINOR R PAUL PHIZACKERLEY *(PURDUE UNIVERSITY)*	**Measurement of Nitrogenase Multiwavelength Anomalous Diffraction Data**
2107M	9/28/89	**DANIEL A SCHERSON** PHILIP N ROSS *(CASE WESTERN RESERVE UNIVERSITY)*	***In Situ* EXAFS Transition Metal Macrocycles Adsorbed on Electrode Surfaces**

LETTERS OF INTENT

9034	6/1/88	**JOE WOICIK** PIERO PIANETTA FABIO COMIN TOM KENDELEWICZ *(NIST)*	***In Situ* Surface EXAFS Studies of Ge/Si(111), Ge/Mo(110), and Model Metal Semiconductor Interfaces**
9035	6/1/88	**THOMAS P RUSSELL** B FACTOR *(IBM RESEARCH LABORATORY)*	**Glancing Angle Diffraction Studies of Polymer Films**

9036	6/1/88	**S R STOCK** ZOPHIA U REK QUINTIN C JOHNSON MONTE NICHOLS ULRICH BONSE JOHN H KINNEY *(GEORGIA INSTITUTE OF TECHNOLOGY)*	**Microtomography of Damage in Cu-1% Sb Deformed at Elevated Temperatures**
9037	6/1/88	**R COLELLA** Q ZHAO STEPHEN M DURBIN *(PURDUE UNIVERSITY)*	**Overhauser's Theory of Charge Density Waves**
9038	6/1/88	**STUART RICE** *(UNIVERSITY OF CHICAGO)*	**Properties of Liquid Surfaces and Ampiphile Monolayers Supported on Liquid Surfaces**
9041	11/10/88	**THOMAS P RUSSELL** *(IBM RESEARCH LABORATORY)*	**Testing of 1-4 Detector as Replacement Polymers**
9042	3/23/88	**ALICE P GAST** *(STANFORD UNIVERSITY)*	**Polymer and Colloidal Structure in Solution**

PRT PROPOSALS

1001	1/1/86	**GRAHAM N GEORGE** C R SAFINYA *(EXXON RESEARCH & ENGINEERING)*	**EXXON PRT Time BL 6**
9900	1/1/85	**PHILIP N ROSS** *(LAWRENCE BERKELEY LABORATORY)*	**Lawrence Berkeley Laboratory PRT Time BL 6**
9901	1/1/85	**M J WEBER** *(LAWRENCE LIVERMORE NATIONAL LABORATORY)*	**National Labs/University of California PRT Time BL 8**
9902	9/1/88	**M J WEBER** *(LAWRENCE LIVERMORE NATIONAL LABORATORY)*	**National Labs/University of California PRT Time BL 10**

ROTATION CAMERA PROPOSALS

Access to the rotation camera facility for protein crystallography is through the submittal of a brief application which is reviewed by the Biology Sub-panel of the PRP on a short turnaround basis. The 15 rotation camera proposals active in 1989 are listed below.

1A82B	3/1/88	**MICHAEL N G JAMES** *(UNIVERSITY OF ALBERTA)*	**High Resolution Crystal Structure of Human Kidney Renin**
1A83B	3/1/88	**F SCOTT MATHEWS** LONGYIN CHEN *(WASHINGTON UNIVERSITY)*	**Methylamine Dehydrogenase-Amicyanin Complex**

1A84B	3/1/88	**WILLIAM J RAY** MAQSUD RAHMAN MICHAEL G ROSSMANN *(PURDUE UNIVERSITY)*	**Structure of an Enzyme Substrate Analog Complex**
1A86B	3/1/88	**LI LIANG** R PAUL PHIZACKERLEY DONGSHENG LIU *(IHEP)*	**Diffraction Data Collection of R-Phycoerythrin**
1A87B	3/21/88	**JOHN E JOHNSON** ZHONGGUO CHEN JEAN CAVARELLI PAUL SEHNKE JEAN-PIERRE WERY *(PURDUE UNIVERSITY)*	**Data Collection from Plant Viruses (with partially ordered RNA) and Insect Viruses**
1A88B	4/1/88	**MING LUO** S V L NARAYANA GILLIAN M AIR PAT BOSSART *(UNIVERSITY OF ALABAMA-BIRMINGHAM)*	**Structures of Viruses and Virus Proteins**
1A92B	3/1/89	**W J COOK** STEVEN EALIC *(UNIVERSITY OF ALABAMA-BIRMINGHAM)*	**Molecular Structure of Calmodulin-Melittin and Calmodulin-Trifluoroperazine Complexes**
1A93B	3/1/89	**DOUGLAS C REES** *(CALIFORNIA INSTITUTE OF TECHNOLOGY)*	**Structures of Electron Transfer Proteins**
1A94B	3/14/89	**THOMAS EARNEST** PARTHO GHOSH MICHAEL SHUSTER ROBERT M STROUD *(UNIVERSITY OF CALIFORNIA)*	**Crystal Structure of Transmembrane Ion Channels: Colicin Ia and the Nicotinic Acetylcholine Receptors**
1A95B	3/1/89	**DAVID EISENBERG** CHRIS HILL DUILIO CASCIO HERMAN SCHREUDER *(UNIVERSITY OF CALIFORNIA)*	**Structure of Crystalline Proteins**
1A96B	3/23/89	**BART DE VOS** CHARLES EIGENBROT MARK ULTSCH MIKE RANDAL *(GENENTECH, INCORPORATION)*	**Structure of Human Growth Hormone in (hGH): its Receptor and Complexs**
1A97B	3/23/89	**SUNG-HOU KIM** JAY PANDIT ANDREW BOHM CHULHEE KANG HYUNHO CHUNG *(UNIVERSITY OF CALIFORNIA)*	**LAO and Histidine J Proteins**

1A98B 3/23/89 **SUNG-HOU KIM** **GTP Complexes of Normal and Transforming ras Proteins**
HYUNHO CHUNG
WHANCHUL SHIN
MIKE MILBURN
LIANG TONG
(UNIVERSITY OF CALIFORNIA)

2A00B 3/15/89 **SUNG-HOU KIM** **Immunoregulatory Hormones (II)**
ANDREW BOHM
JAY PANDIT
LIANG TONG
(UNIVERSITY OF CALIFORNIA)

2A01B 3/23/89 **HANS E PARGE** **Proposal to Collect Cryo-crystallographic Data on Pilin, a Fibre Forming Protein from *N. gonorrhoeae***
T HONG
DUNCAN E MCREE
S MYLVAGANAM
D CHRISTENSEN
JOHN A TAINER
ELIZABETH D GETZOFF
(RESEARCH INSTITUTE OF SCRIPPS CLINIC)

RAPID TURNAROUND EXAFS

Up to 30% of the time on one of the bending magnet beam lines is reserved for rapid turnaround EXAFS experiments. Both a novice and an experienced user mode is available on the basis of a short application form.

1E00 5/1/88 **JAMES PENNER-HAHN** **Determination of the Structure of 2-cyanoethyl Zinc Iodide in THF Solutions**
PAUL KNOCHEL
(UNIVERSITY OF MICHIGAN)

1E02 5/1/88 **CRAIG E BARNES** **EXAFS Characterization of Discrete Surface Bound Rhodum Catalysts**
JAMES E PENNER-HAHN
(UNIVERSITY OF TENNESSEE)

1E03 6/1/89 **MARK R ANTONIO** **Cation Distribution and Valence in Iron-Titanium Oxides with the Pseudobrookite Structure**
R G TELLER
(BP AMERICA)

1E04 3/3/89 **BRUCE M BIWER** **Hydrated Glass Structure**
JOHN K BATES
WILLIAM L EBERT
(ARGONNE NATIONAL LABORATORY)

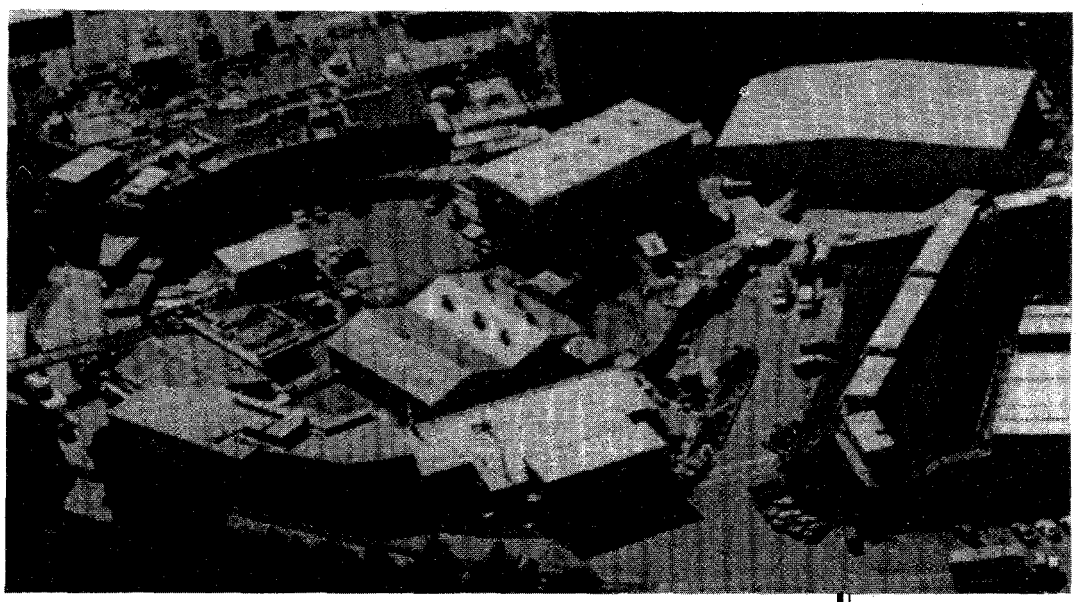

Section VIII

SSRL Experimenters and Proposals by Institution

VIII. SSRL EXPERIMENTERS AND PROPOSALS BY INSTITUTIONS

As of December 31, 1989 there were 519 experimenters from 126 institutions officially involved with active proposals at SSRL. In addition, over a 100 others (graduate students, etc.) participated in work at the laboratory in collaboration with these scientists. The 102 United States Institutions included 67 Universities, 21 private companies and 14 government laboratories.

U.S. CORPORATIONS: Amoco Corporation, ARACOR, AT&T Bell Laboratories, Becton Dickinson & Co. Rsch. Cntr., Boeing Company, BP America, Chevron Research Company, Eastman Kodak Research Laboratory, Enraf-Nonius Company, EPRI, Exxon Research & Engineering, Genentech, Inc., Hewlett Packard Laboratories, IBM Research Laboratory, Martin Marietta, Schlumberger Doll Research, Sematech, Surface Science Instruments, The Aerospace Corporation, X-Ray Instrumentation Associates, Xerox

U.S. LABORATORIES: Argonne National Laboratory, Brookhaven National Laboratory, Lawrence Berkeley Laboratory, Lawrence Livermore National Laboratory, Los Alamos National Laboratory, Naval Research Laboratory, Naval Weapons Center, National Institute and Standards of Technology, Oak Ridge National Laboratory, Pacific Northwest Laboratory, Sandia National Laboratory, Stanford Synchrotron Radiation Laboratory, US Geological Survey Water Resources Division, USDA/Western Regional Research Center

U.S. UNIVERSITIES: Amherst College, Arizona State University, Boston University, Brigham Young University, Brown University, California Institute of Technology, California State University, Carnegie Institute, Carnegie Mellon University, Case Western Reserve University, City University of New York, Colorado School of Mines, Colorado State University, Columbia University, Cornell University, Florida-Atlantic University, Georgetown University, Georgia Institute of Technology, Harvard Medical School, Harvard University, Illinois Institute of Technology, Louisiana State University, Massachusetts Institute of Technology, North Carolina State University, Northeastern University, Northwestern University, Ohio State University, Ohio University, Pennsylvania State University, Princeton University, Purdue University, Rensselaer Polytechnic Institute, Research Institute of Scripps Clinic, Stanford University, State University-New York, University City Science Center, University of Alabama-Birmingham, University of Arizona, University of California, University of Chicago, University of Cincinnati, University of Colorado, University of Connecticut, University of Georgia, University of Hawaii, University of Illinois, University of Kentucky, University of Michigan, University of Minnesota, University of Mississippi, University of Missouri-Columbia, University of New Hampshire, University of New Mexico, University of Notre Dame, University of Oregon, University of Pennsylvania, University of South Carolina, University of South Florida, University of Southern California, University of Tennessee, University of Toledo, University of Washington, University of Wisconsin, Utah State University, Washington State University, Washington University, West Virginia University

FOREIGN INSTITUTIONS Alcan International Limited, Chalmers Institute of Technology, CNRS, Electrotechnical Laboratory, European Synchrotron Radiation Facility, HC Orsted Institute, IHEP, Karolinska Institute, McGill University, Medical Nobel Institute, Mitsubishi Petrochemical Co., Ltd., Oxford University, Riso National Laboratory, Simon Fraser University, The University of Manchester, TU Munchen, Universita di Brescia, Universita di Catania, Universita di Roma, Universitat Bayreuth, Universitat Bonn, University of Alberta, Universitat Dortmund, University of Sussex

SSRL EXPERIMENTERS AND PROPOSALS BY INSTITUTION
UNITED STATES INSTITUTIONS

AMHERST COLLEGE
DAVID M DOOLEY 1053

AMOCO CORPORATION
R G TELLER 1E03

ARACOR
EDWARD FRANCO 2062
PAUL PLAG 2062

ARIZONA STATE UNIVERSITY
T GROY 2020
S H LIN 2020
J R SCHOONOVER 2020

ARGONNE NATIONAL LABORATORY
E E ALP 2012
JOHN K BATES 1E04
BRUCE M BIWER 1E04
WILLIAM L EBERT 1E04
GOPAL K SHENOY 2012
L SODERHOLM 2012
JAMES P VICCARO 1074

AT&T BELL LABORATORIES
PAUL H FUOSS 1095,1096,2044 2045,2059
D W KISKER 1095,1096
LAURA NORTON 1095,1096,2044
I K ROBINSON 997,1094

BECTON DICKINSON & CO. RSCH. CNTR.
ALI NAQUI 1043

BOEING COMPANY
ROBERT B GREEGOR 956,1097,2021 2038,2049
FARREL W LYTLE 956,1069,1097 2021,2028,2038 2049,2053
EDWARD C MARQUES 2049

BOSTON UNIVERSITY
KARL F LUDWIG 1008

BP AMERICA
MARK R ANTONIO 1E03

BRIGHAM YOUNG UNIVERSITY
MAX W HILL 1069,2021
NOLAN MANGELSON 1069,2021

BROOKHAVEN NATIONAL LABORATORY
STEPHEN P CRAMER 969,981,1030 1040,1084,1089 1092,2051,2098
L D GIBBS 2017
STEVE M HEALD 1072,1073,1074
S M KHALID 1043
BENJAMIN OCKO 2017
M SUENAGA 1073
W THOMLINSON 1046
J M TRANQUADA 1073,2005

BROWN UNIVERSITY
M ALTMAN 997
P J ESTRUP 997

CALIFORNIA INSTITUTE OF TECHNOLOGY
SUNNEY I CHAN 1067
N S LEWIS 1078
P MARK LI 1067
DOUGLAS C REES 1A93

CALIFORNIA STATE UNIVERSITY
S ARNOLD 1099,2000
C BUSTILLO 1099,2000
D HELMOLDT 1099,2000
R ITHNIN 1099,2000
M CHEN LEI 1099,2000
J SATCHER 1099,2000

CARNEGIE INSTITUTE
RUSSELL J HEMLEY 1059,2056
H K MAO 1059,1064,2056
A P JEPHCOAT 2056

CARNEGIE MELLON UNIVERSITY
R F HAINSEY 2014
J D SHINDLER 2014
ROBERT M SUTER 2014
JAMES W WHITTAKER 2048

CASE WESTERN RESERVE UNIVERSITY
M IKEDA-SAITO 1083
DANIEL A SCHERSON 1098,2058,2080 2107

CHEVRON RESEARCH COMPANY

GARY S MONDO	2099,2100
GUANG ZHANG	1043,2099,2100

CITY UNIVERSITY OF NEW YORK

PEDRO A MONTANO	2012

COLORADO SCHOOL OF MINES

N WADA	1092
D L WILLIAMSON	1091,2055

COLORADO STATE UNIVERSITY

FRANK L GALEENER	2078
DAVID B KERWIN	2078

COLUMBIA UNIVERSITY

MARIANNE CUFF	1087
WAYNE A HENDRICKSON	1087
JOHN HORTON	1087
STEVAN R HUBBARD	1012,1087
STEPHEN J LIPPARD	2030
HM KRISHNA MURTHY	1087
ARNO PAHLER	1087
WILLIAM E ROYER	1087
WEI YANG	1087

CORNELL UNIVERSITY

J D BROCK	2002
AARON LEWIS	2071
DAN THIEL	2071

EASTMAN KODAK RESEARCH LABORATORY

TERESA A SMITH	2033

ENRAF-NONIUS COMPANY

JAMES C PHILLIPS	2007

EPRI

HOWARD OCKEN	2028

EXXON RESEARCH & ENGINEERING

M WW ADAMS	1030
CATHY COYLE	2051
GRAHAM N GEORGE	1001,1030,1083 1084,1089,2051
KENG S LIANG	1001
G MEITZNER	2053
V MINAK	1030
J M NEWSAM	1001
ROGER C PRINCE	1083,1084

EXXON RESEARCH & ENGINEERING - *(Continued)*

C R SAFINYA	1001,2042
JOHN H SINFELT	1001,2053
S K SINHA	1001
ERIC SIROTA	2042
GREG S SMITH	2042
EDWARD I STIEFEL	1030
GRAYSON H VIA	1001,2053

FLORIDA-ATLANTIC UNIVERSITY

FRANK A SCHULTZ	1055

GENENTECH, INC.

BART DE VOS	1A96
CHARLES EIGENBROT	1A96
MIKE RANDAL	1A96
MARK ULTSCH	1A96

GEORGETOWN UNIVERSITY

MARK CHANCE	1042

GEORGIA INSTITUTE OF TECHNOLOGY

S D ANTOLOVICH	2015,2105
T M BREUNIG	2105
Y H CHUNG	2091
R H FELTON	1068
A B LEE	2091
S R STOCK	2015,2091,2105 9036
G WEBB	2015

HARVARD MEDICAL SCHOOL

DAVID AULD	1042
BARTON HOLMQUIST	1042
JAMES RIORDAN	1042
B VALLEE	1042

HARVARD UNIVERSITY

C M FRIEND	1080
A C LIU	1080
J T ROBERTS	1080

HEWLETT PACKARD LABORATORIES

ALICE FISCHER-COLBRIE	1093
STEPHEN LADERMAN	1093
J MOLL	1093

IBM RESEARCH LABORATORY

GARY BORGES	2077
CHARLES A BROWN	2077
CURT ERICKSON	1021

IBM RESEARCH LABORATORY - *(Continued)*

JOSEPH G GORDON	2077
TING C HUANG	1021
OWEN MELROY	2003,2061
S S P PARKIN	1099,2000
WILLIAM PARRISH	1021
THOMAS P RUSSELL	2009,2081,2085 9035,9041
M SAMANT	2077
JOACHIM STOHR	963,2009
MIKE TONEY	2003,2059,2061 2072

ILLINOIS INSTITUTE OF TECHNOLOGY

HEATHER CHEN	1072

LAWRENCE BERKELEY LABORATORY

J V ACRIVOS	1099,2000
VICKIE DEROSE	2010
SUSAN DEXHEIMER	2010
ROBERT D GIAUQUE	2065
R GUILES	2010
PHILIP A HEIMANN	943
TONY HUFF	943
ZAHID HUSSAIN	943
J JAKLEVIC	2090
MELVIN P KLEIN	2000,2010
JEFFREY B KORTRIGHT	2018
KIN MAN-YU	2090
ANN MCDERMOTT	2010
EDDIE MOLER	943
PHILIP N ROSS	1098,2058,2080 2107,9900
KENNETH SAUER	2010
DAVID A SHIRLEY	943
DAVID H TEMPLETON	957
L K TEMPLETON	957
ALBERT C THOMPSON	1046,2056,2065
J H UNDERWOOD	2056,2065
WLADYSLAW WALUKIEWICZ	2090
LI-QUING WANG	943
ALEXIS SCHACH V WITTENAU	943
Y WU	2056,2065
J L ZIMMERMANN	2010

LAWRENCE LIVERMORE NATIONAL LABORATORY

J AKELLA	1064
NANCY DEL GRANDE	9901
JOHN HENDERSON	2013

LAWRENCE LIVERMORE NATIONAL LABORATORY - *(Continued)*

QUINTIN C JOHNSON	1064,9036
DON KANIA	2011
JOHN H KINNEY	9036
DAVE KNAPP	2013
E M LARSON	2038
G S SMITH	1064
GLENN TIRSELL	9901
J TREBES	2011
C L WANG	2072
MARVIN J WEBER	9901,9902

LOS ALAMOS NATIONAL LABORATORY

ROGER J BARTLETT	2013
TOM BOWLES	2013
STEVE D CONRADSON	2023,2024,2064
P G ELLER	2038
ZACHARY FISK	2023
JOYCE A GOLDSTONE	2016
GEORGE KWEI	2016
ANDREW C LAWSON	2016
RICH MARTIN	2013
J D PURSON	2038
IAN D RAISTRICK	2023,2064
ANTONIO REDONDO	2023,2064
HAMISH ROBERTSON	2013
ALFRED SATTLEBERGER	2024
BASIL SWANSON	2024
WALTER J TRELA	2013
ROBERT B VON DREELE	2016
DAVE WARK	2013
JOHN WILKERSON	2013
ART WILLIAMS	2016

LOUISIANA STATE UNIVERSITY

BRIAN J HALES	2051

MARTIN MARIETTA

F M KUSTAS	1091

MASSACHUSETTS INSTITUTE OF TECHNOLOGY

ROBERT H BEER	2030
JAMES G BENTSEN	2030
ROBERT J BIRGENEAU	997,2002
J D LITSTER	2002
K C RUSSELL	2073

NAVAL RESEARCH LABORATORY

E D DONOVAN	973
G K HUBLER	973

NAVAL WEAPONS CENTER

TERI COLE	2093
JON ERICKSON	2039,2093
AROLD K GREEN	2039
SANDY LANGSJOEN	2039
PHILLIP LAROE	2039
TSU-WIE NEE	2039
VICTOR REHN	2039,2093
CAREY SCHWARTZ	2039,2093
WAYNE WIEMER	2039

NATIONAL INSTITUTE OF STANDARDS AND TECHNOLOGY

M I BELL	973
CHARLES E BOULDIN	973
R A FORMAN	973
JOE WOICIK	2089,9034

NORTH CAROLINA STATE UNIVERSITY

DALE E SAYERS	1074

NORTHEASTERN UNIVERSITY

R CHIARELLO	2072
J KRIM	2072

NORTHWESTERN UNIVERSITY

TOM BOHANON	2086
PULAK DUTTA	2086
BINHUA LIN	2086
THOMAS V O'HALLORAN	2047
DIANA RALSTON	2047
MING-CHIH SHIH	2086
JEFF WRIGHT	2047

OAK RIDGE NATIONAL LABORATORY

S SPOONER	1018,2006
DAVID M ZEHNER	2017

OHIO STATE UNIVERSITY

JAMES O ALBEN	981
ALLAN A CROTEAU	981
FRANK G FIAMINGO	981
CRAIG F HEMANN	981
RUSSELL HILLE	1040
KIMBERLY A POWELL	981

OHIO UNIVERSITY

HOWARD D DEWALD	2063

PACIFIC NORTHWEST LABORATORY

F A GARNER	2073

PENNSYLVANIA STATE UNIVERSITY

R G JENKINS	956
M TIEN	2060

PRINCETON UNIVERSITY

J T GROVES	1085
M STERN	1085

PURDUE UNIVERSITY

JEFFREY T BOLIN	2106
NINO CAMPOBASSO	2106
JEAN CAVARELLI	1A87
ZHONGGUO CHEN	1A87
R COLELLA	2046,9037
STEPHEN M DURBIN	9037
JOHN E JOHNSON	1A87
WLADEK MINOR	2106
MAQSUD RAHMAN	1A84
WILLIAM J RAY	1A84
MICHAEL G ROSSMANN	1A84
PAUL SEHNKE	1A87
JANET L SMITH	2096
JEAN-PIERRE WERY	1A87
Q ZHAO	2046,9037

RENSSELAER POLYTECHNIC INSTITUTE

T M HAYES	1091,2055

RESEARCH INSTITUTE OF SCRIPPS CLINIC

D CHRISTENSEN	2A01
ELIZABETH D GETZOFF	2A01
T HONG	2A01
DUNCAN E MCREE	2A01
S MYLVAGANAM	2A01
HANS E PARGE	2A01
JOHN A TAINER	2A01

SANDIA NATIONAL LABORATORY

GLENN KUBIAK	2026
JEFF NELSON	2026
MONTE NICHOLS	9036
RICHARD H STULEN	2026

SCHLUMBERGER DOLL RESEARCH

D R HINES	1092
JAMES HOWARD	1089,1092
WILLIAM MURPHY	1089
JULIA PECK	1089

SEMATECH

DANIEL SELIGSON	2037

STANFORD SYNCHROTRON RADIATION LABORATORY

HENRY BELLAMY	2070
ARTHUR BIENENSTOCK	1008,1048,2027 2044,2045,2088
ANNE BORG	2094
SEAN BRENNAN	1048,2027,2044 2059
GEORGE S BROWN	1046,2013,2082
ROGER CARR	2082
BRITT HEDMAN	1055,2029,2030 2031,2032,2033 2034,2079,2104
KEITH O HODGSON	995,1012,1055 1076,1078,2029 2030,2031,2032 2033,2034,2035 2079,2101,2102 2104
INGOLF LINDAU	935,2074,2089 2103
R PAUL PHIZACKERLEY	1087,1A86,2050 2070,2106
PIERO PIANETTA	2011,2026,2037 2089,2094,2095 9034
ZOPHIA U REK	2015,2028,2091 2105,9036
MICHAEL SOLTIS	2050
TERESA TROXEL	1082

STANFORD UNIVERSITY

MICHEL BOUDART	1065,1071
GORDON E BROWN, JR	994,995,999
KRISTINE BUTCHER	1022
K CHAR	1093
JAMES P COLLMAN	2034
R J DAVIS	1065
DAN DESSAU	935
SEBASTIAN DONIACH	1012,1076,2035 2101,2102,
D ELIEZER	2101,2102
B FACTOR	1080,2027,2081 2085,9035
P FRANK	1055
ALICE P GAST	9042

STANFORD UNIVERSITY - *(Continued)*

THEODORE H GEBALLE	1079,1093
N GILLIS	2101,2102
DONALD C HARRISON	1046
KIM F HAYES	995
ALBERTO HERRERA	935
ROBERT HOFSTADTER	1046
JENNCHANG HWANG	2026
W A JACKSON	999
J KAHN	2044
TOM KENDELEWICZ	935,2089,9034
ROBERT KERNOFF	1046
PAUL KING	2037,2094
JAMES O LECKIE	995
JIAN-YI LIN	1022
ROBERT J MADIX	1080
PAUL MEISSNER	935
N MISSERT	1093
KEN MIYANO	935
B OH	1093
DOUGLAS OSHEROFF	1048
JOHN OTIS	1046
LAWRENCE PAN	2037
GEORGE A PARKS	995
J D PLUMMER	2091
C W PONADER	999
MARYBETH RICE	2045,2088
S ROTHFUS	999
Z X SHEN	935,2103
EDWARD I SOLOMON	1022,2031
J SOLOMON	1080
WILLIAM E SPICER	935,2074,2089 2103
CHRISS SPINDT	935
CAROLINE STAHLE	1048
C STANFEL	1055
J Z SUN	1093
GRACE TAN	2031
G P VALENCA	1071
ANITA WAHI	935
S WAKATSUKI	1076,2035,2088 2101,2102
GLENN A WAYCHUNAS	994,995,999 1051,1088,2075 2076
BARRETT WELLS	935
J WU	2074
X YANG	2095
HERBERT D ZEMAN	1046
MATTHEW B ZISK	2034

STATE UNIVERSITY-NEW YORK

RICHARD J REEDER	2076
S WHITTINGHAM	1092
F.Y-H. WU	2092

SURFACE SCIENCE INSTRUMENTS

GORDON KNAPP	2094

THE AEROSPACE CORPORATION

PAUL D FLEISCHAUER	2001
JEFFREY R LINCE	2001

UNIVERSITY CITY SCIENCE CENTER

GRANT BUNKER	1043,2022,2025
TSOO E KING	2025
KE ZHANG	2022,2025

UNIVERSITY OF ALABAMA-BIRMINGHAM

GILLIAN M AIR	1A88
PAT BOSSART	1A88
W J COOK	1A92
STEVEN EALICK	1A92
MING LUO	1A88
S V L NARAYANA	1A88

UNIVERSITY OF ARIZONA

M D CARDUCCI	2098
J H ENEMARK	1030,2098

UNIVERSITY OF CALIFORNIA

ANDREW BOHM	1A97,2A00
FRANK G BRIDGES	1079,2040
BARBARA K BURGESS	2029
DUILIO CASCIO	1A95
HYUNHO CHUNG	1A97,1A98
DOUGLAS S CLARK	2008
D DE FONTAINE	1018,2006
JONATHAN DENLINGER	2018,2019
WAYNE A DOLLASE	2076
THOMAS EARNEST	1A94
DAVID EISENBERG	1A95
B J FELDMAN	1055
PARTHO GHOSH	1A94
R MARK GUINN	2008
CHRIS HILL	1A95
ZHENG-QING HUANG	943
CHULHEE KANG	1A97
SUNG-HOU KIM	1A97,1A98,2A00
M KRAITCHMAN	1018,2006
DAVID A LARSON	1082

UNIVERSITY OF CALIFORNIA - *(Continued)*

CLIFF LING	1082
LAURA MEDHURST	943
SARATH MENON	1018
MIKE MILBURN	1A98
CRAIG OGATA	1087
MARJORIE OLMSTEAD	2018,2019
JAY PANDIT	1A97,2A00
THEODORE L PHILLIPS	1082
MICHAEL SCHELL	1082
HERMAN SCHREUDER	1A95
WHANCHUL SHIN	1A98
DENNIS SHRIEVE	1082
MICHAEL SHUSTER	1A94
ROBERT M STROUD	1076,1A94,2035
LIANG TONG	1A98,2A00
STEVEN A VAUGHN	2029
M WIEDENMEIR	2006

UNIVERSITY OF CHICAGO

ROBERT H FAIRCLOUGH	1012
STUART RICE	9038
D RICHMAN	1012

UNIVERSITY OF CINCINNATI

EDWARD A DEUTSCH	991
RICHARD C ELDER	922,991,1066
WILLIAM R HEINEMAN	1066
KATHERINE TEPPERMAN	922

UNIVERSITY OF COLORADO

N A CLARK	2042
ROBERT POYTON	2025

UNIVERSITY OF CONNECTICUT

JEFF T KORBERSTEIN	2084

UNIVERSITY OF GEORGIA

MARLY EIDSNESS	1041
ROBERT KERTAYASA	2048
ROBERT A SCOTT	969,1041,1053
	1067

UNIVERSITY OF HAWAII

MURLI H MANGHNANI	1059,1064
L C MING	1059,1064
J A XU	1059

UNIVERSITY OF ILLINOIS

S G SLIGAR	2022

UNIVERSITY OF KENTUCKY

G P HUFFMAN	956
F E HUGGINS	956
NARESH SHAH	956

UNIVERSITY OF MICHIGAN

BRIAN D ATHEY	2041
DAVID P BALLOU	2068
CHRISTOPHER J BATIE	2068
I-WEI CHEN	2067
CARL C CORRELL	2070
DIMITRI COUCOUVANIS	2068
M DAVID CURTIS	2069
W D FRASCH	1085
RICHARD FRONKO	1088,2047,2048
D GHANOTAKIS	1085
JOHN P LANGMORE	2041
MARTHA LUDWIG	2070
PAUL KNOCHEL	1E00
V L PECORARO	1085
JAMES E PENNER-HAHN	1085,1088,2047 2048,2067,2068 2069, 1E00, 1E02
MICHAEL F SMITH	2041
T Y TIEN	2067
HIM-TAI TSANG	1085,2047,2068
GEOFFREY WALDO	1088
SHENGKE WANG	1088
SHAWN WILLIAMS	2041
C F YOCUM	1085

UNIVERSITY OF MINNESOTA

CHRIS MACOSKO	2084
TONY RYAN	2084
W H SMYRL	2003

UNIVERSITY OF MISSISSIPPI

W CLELAND	1030

UNIVERSITY OF MISSOURI-COLUMBIA

CONG-YUAN GUO	2097
JOHN E KUO	2097

UNIVERSITY OF NEW HAMPSHIRE

T S GROSS	2091

UNIVERSITY OF NEW MEXICO

THOMAS BEIN	1070
KARIN MOLLER	1070

UNIVERSITY OF NOTRE DAME

KRISHNA M CHOUDHARY	1077

UNIVERSITY OF OREGON

BERND CRASEMANN	2013,2082
A F KODRE	2082
J RUSCHEINSKI	2082
S J SCHAPHORST	2082
S L SORENSEN	2013
S B WHITFIELD	2013

UNIVERSITY OF PENNSYLVANIA

JOHN E BENCI	1081
BRITTON CHANCE	1042,1043,2022 2025
EDGAR DAVIDSON	2025
DAVID P POPE	1081

UNIVERSITY OF SOUTH CAROLINA

JOHN H DAWSON	2032
MASANORI SONO	2032

UNIVERSITY OF SOUTH FLORIDA

L S SOLMONSON	1030

UNIVERSITY OF SOUTHERN CALIFORNIA

MARIE-CLAIRE MCKENNA	2079
PHILIP J STEPHENS	2079

UNIVERSITY OF TENNESSEE

CRAIG E BARNES	1E02

UNIVERSITY OF TOLEDO

MAX O FUNK	2068

UNIVERSITY OF WASHINGTON

J FREUND	1047
B HOUSER	2005
ROBERT L INGALLS	1047,2005
PETERIS LIVINS	2071
ETHAN A MERRITT	2070
E A STERN	1068,2005,2071

UNIVERSITY OF WISCONSIN

SCOTT ENSIGN	2079
PAUL W LUDDEN	2079
GIORGIO MARGARITONDO	2043

US GEOLOGICAL SURVEY WATER RESOURCES DIV

JAMES A DAVIS	1051,2075
CHRISTOPHER C FULLER	2075
BRIGID A REA	1051,2075

USDA/WESTERN REGIONAL RES CTR

W E NEWTON	1055

UTAH STATE UNIVERSITY

S AUST	2060
J BUMPUS	2060
J LI	2060
LINDA S POWERS	1042,2060,2092

WASHINGTON STATE UNIVERSITY

JEFF J HOYT	1018,2006,2073
BRAD PATE	2074

WASHINGTON UNIVERSITY

LONGYIN CHEN	1A83
F SCOTT MATHEWS	1A83

WEST VIRGINIA UNIVERSITY

LANE C WILSON	2045,9902

X-RAY INSTRUMENTATION ASSOCIATES

WILLIAM K WARBURTON	1008,2062

XEROX

ROBERT Z BACHRACH	959
JAMES B BOYCE	1079,2040
L J BRILLSON	2043
ROSS D BRINGANS	959,2018,2019

SSRL EXPERIMENTERS AND PROPOSALS BY INSTITUTIONS
FOREIGN INSTITUTIONS

ALCAN INTERNATIONAL LIMITED *(Canada)*

ROLAND TIMSIT	2027

CHALMERS INSTITUTE OF TECHNOLOGY *(Sweden)*

TORD CLAESON	1079

CNRS *(France)*

P GIBART	2055

ELECTROTECHNICAL LABORATORY *(Japan)*

HIROYUKI OYANAGI	2022

EUROPEAN SYNCHROTRON RADIATION FACILITY *(France)*

FABIO COMIN	9034
ERIC ZIEGLER	1074

HC ORSTED INSTITUTE *(Denmark)*

H H ANDERSEN	1094
L F GRAABAEK	1094
A JOHANSEN	1094
E JOHNSON	1094
L SARHOLT-KRIST	1094

IHEP *(People's Republic of China)*

LI LIANG	1A86
DONGSHENG LIU	1A86

KAROLINSKA INSTITUTE *(Sweden)*

BRITT-MARIE SJOBERG	1043

MCGILL UNIVERSITY *(Canada)*

S G J MOCHRIE	2017

MEDICAL NOBEL INSTITUTE *(Sweden)*

PETER REICHARD	1043

MITSUBISHI PETROCHEMICAL CO. LTD. *(Japan)*

HITOSHI ASAHINA	2034

OXFORD UNIVERSITY *(England)*

JANOS HAJDU	2050

RISO NATIONAL LABORATORY *(Denmark)*

JAKOB BOHR	1094

SIMON FRASER UNIVERSITY *(Canada)*

DARYL CROZIER	1047,2005

THE UNIVERSITY OF MANCHESTER *(England)*
MICHAEL HART 1021

TU MUNCHEN *(West Germany)*
ULRICH KUSTHARDT 2104

UNIVERSITA DI BRESCIA *(Italy)*
MAURIZIO BELLOTTO 1021

UNIVERSITA DI CATANIA *(Italy)*
G FARACI 2083
S LA ROSA 2083
A TERRASI 2083

UNIVERSITA DI ROMA *(Italy)*
PIETRO CHIARADIA 2043

UNIVERSITAT BAYREUTH *(West Germany)*
CHARLES R ROSS 2076

UNIVERSITAT BONN *(West Germany)*
HANS VILTER 2104
GEORGE WILL 1021

UNIVERSITY OF ALBERTA *(Canada)*
MICHAEL N G JAMES 1A82

UNIVERSITAT DORTMUND *(West Germany)*
ULRICH BONSE 9036

UNIVERSITY OF SUSSEX *(England)*
B E SMITH 1030

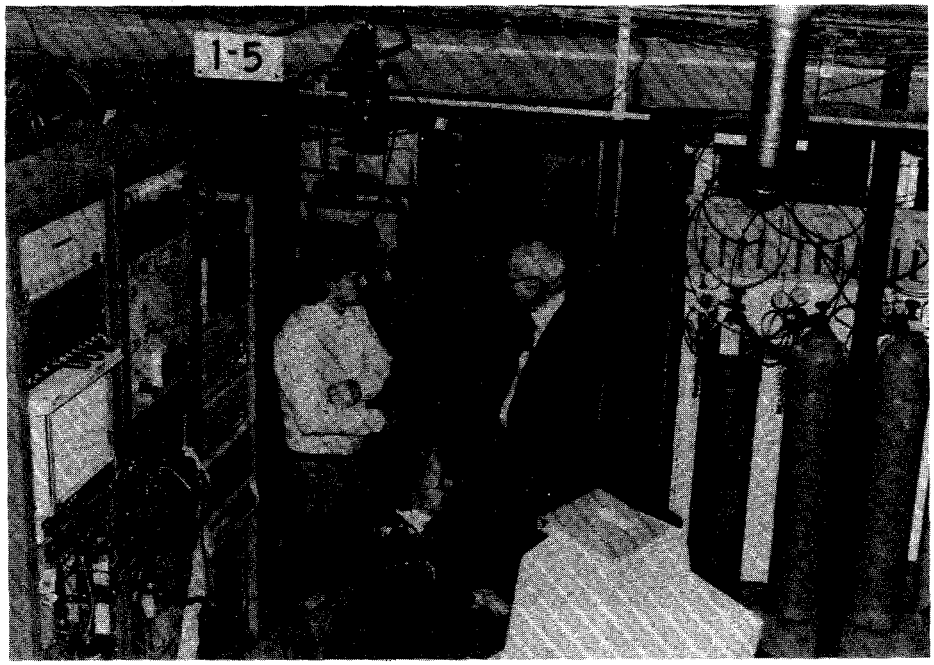

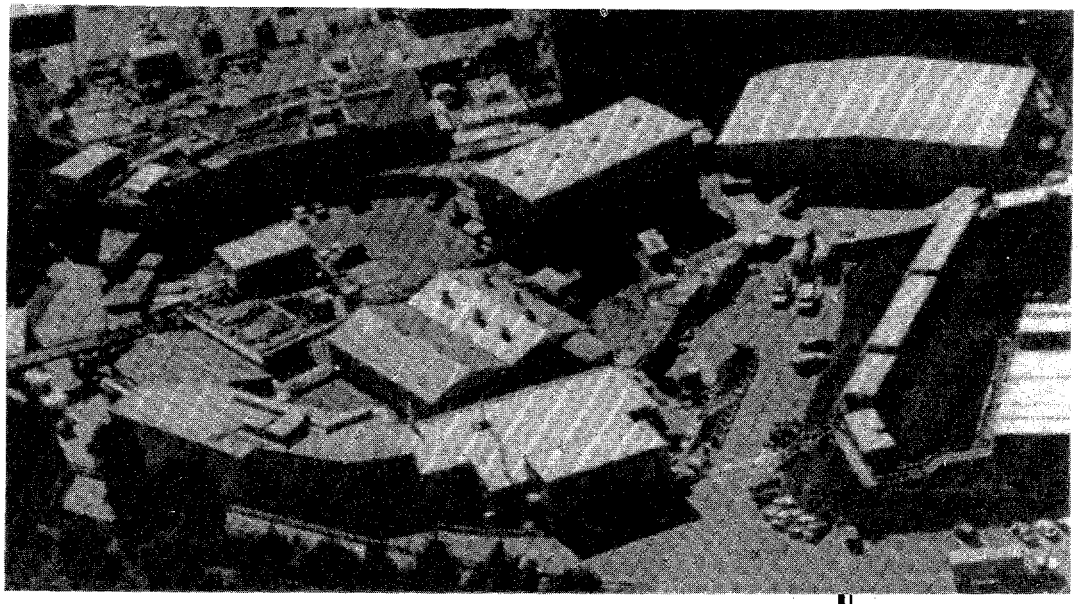

Section IX

SSRL Publications

IX PUBLICATIONS BASED ON WORK AT SSRL

S. Ahrland, K. Nilsson, I. Persson, A. Yuchi and J.E. Penner-Hahn, **Formation of Gold(I) Halide and Thiocyanate Complexes in Pyridine and Acetonitrile and the Structures of Gold(I) Solvates in These Solvents. A Thermodynamic and EXAFS Spectroscopic Study:** Inorg. Chem. 28, 1833 (1989)

N. Alberding, K.R. Bauchspiess, J.M. Tranquada, R. Ingalls and E.D. Crozier, **High Pressure EXAFS Study of High T_c Superconductors:** Physica B 158, 463 (1989)

M. Ardehali, P.H. Mahowald and I. Lindau, **Electronic Structure of the Ag/Si Interface: Angle-Resolved, Energy-Dependent Photoemission Study:** Phys. Rev. B 39, 8107 (1989)

M. Ardehali, P. Mahowald and I. Lindau, **The Energy Dependence of the 4d Partial Photoionzation Cross Section in Metallic Ag and Ag Atoms on Si at the Cooper Minimum and Near 4d Threshold:** J. Electron Spectrosc. Relat. Phenom. 48, 353 (1989)

J. Arthur, G.S. Brown, D.E. Brown and S.L. Ruby, **Resonance Energy Shifts during Nuclear Bragg Diffraction of X-rays:** Phys. Rev. Lett. 63, 1629 (1989)

J. Arthur, D.E. Brown, S.L. Ruby and G.S. Shenoy, **Studying Hyperfine Fields with Resonant Nuclear Diffraction of X-rays:** accepted by J. Appl. Phys.

J. Arthur, **The Use of Simultaneous Reflections for Precise Absolute Energy Calibration of X-Rays:** Rev. Sci. Instrum. 60, 2062 (1989)

H. Asahina, M.B. Zisk, B. Hedman, J.T. McDevitt, J.P. Collman and K.O. Hodgson, **X-ray Absorption Spectroscopic Studies of Ruthenium-Octaethylporphyrin Dimers:** J. Chem. Soc. Chem. Comm. 1360 (1989)

H. Asahina, M.B. Zisk, B. Hedman, J.T. McDevitt, J.P. Collman and K.O. Hodgson, **XAS Studies of Ruthenium Octaethylporphyrin Dimers:** Physica B 158, 217 (1989)

T.W. Barbee, **Combined Microstructure X-ray Optics:** Rev. Sci. Instrum. 60, 1588 (1989)

T.W. Barbee and J. Wong, **EXAFS of Near Monolayer Hafnium Film:** Physica B 158, 670 (1989)

T.W. Barbee, **Application of Multilayer Structures to the Determination of Optical Constants in the X-ray Constants in the X-ray and Extreme Ultra Violet Spectral Ranges:** Mat. Res. Soc. Symp. Proc. 143, 197 (1989)

K.R. Bauchspiess, E.D. Crozier and R. Ingalls, **The Valence Transition in SmSe:** Physica B 158, 492 (1989)

J.E. Benci and D.P. Pope, **Microradiography of Creep Damage in Copper:** Mat. Sci. & Eng. A 117, 51 (1989)

J.E. Benci and D.P. Pope, **A Study of High Temperature Damage Processes using Microradiography:** Mat. Res. Soc. Proc. 142, 195 (1989)

A. Bienenstock, G. Brown, H. Wiedemann and H. Winick, **PEP as a Synchrotron Radiation Source:** Rev. Sci. Instrum. 60, 1393 (1989)

O. Bisi, L. Braicovich, C. Carbone, I. Lindau, I. Iandelli, G.L. Olcese and A. Palenzona, **Chemical Bond and Electronic States in Calcium Silicides: Theory and Comparison with Synchrotron-Radiation Photoemission:** Phys. Rev. B 40, 10194 (1989)

J.B. Boyce, F. Bridges, T. Claeson and T. Geballe, **Second Neighbor Shells Around Cu in Oxygen-Deficient and Transition-Metal-Doped $Y_1Ba_2Cu_3O_{7-\delta}$:** accepted by Physica B

J.B. Boyce, F. Bridges, T. Claeson and M. Nygren, **Temperature Dependence of the Local Structure of $Y_1Ba_2Cu_3O_{7-\delta}$ with Varying Oxygen Content: An X-ray Absorption Study:** accepted by Phys. Rev. B

S. Brennan, A. Bienenstock and J.E. Keem, **Fluorescence Extended X-ray Absorption Fine Structure Study of Silicon in Neodymium Iron Boron Rare-Earth Magnets:** J. Appl. Phys. 65, 697 (1989)

S. Brennan and A. Bienenstock, **Grazing Incidence X-ray Scattering:** Res. & Dev. 31, 52 (1989)

S. Brennan, P.H. Fuoss, J.L. Kahn and D.W. Kisker, **Experimental Considerations for In-Situ X-ray Scattering Analysis of OMVPE Growth:** submitted to Nucl. Instrum. Methods

F. Bridges, J.B. Boyce, T. Claeson, T. Geballe and J.M. Tarascon, **Distorted Chain Sites for Co- and Fe-Substituted $Y_1Ba_2Cu_3O_{7-\delta}$:** accepted by Phys. Rev. B

R.D. Bringans and M.A. Olmstead, **Comparison of Interface Formation for GaAs-on-Si and ZnSe-on-Si:** Mat. Res. Soc. Symp. Proc. 145, 337 (1989)

R.D. Bringans and M.A. Olmstead, **Bonding of As and Se to Silicon Surfaces:** J. Vac. Sci. Technol. B 7 1232 (1989)

R.D. Bringans and M.A. Olmstead, **Bonding of Se and ZnSe to the Si(100) Surface:** Phys. Rev. B 39, 12985 (1989)

G.E. Brown and G.A. Parks, **Synchrotron-based X-ray Absorption Studies of Cation Environments in Earth Materials:** Reviews in Geophysics 28, 519 (1989)

G.E. Brown, G.A. Parks and C.J. Chisholm-Brause, **In-Situ X-ray Absorption Spectroscopic Studies of Ions at Oxide-Water Interfaces:** Chimia 43, 248 (1989)

R. Cao, K. Miyano, T. Kendelewicz, I. Lindau and W.E. Spicer, **Metallization and Fermi Level Movement at the Cs/GaAs (110) Interfaces:** Phys. Rev. B 39, 12655 (1989)

R. Cao, K. Miyano, T. Kendelewicz, I. Lindau and W.E. Spicer, **Duality in Fermi Level Pinning at Cu/InP (110) Interfaces:** Phys. Rev. B 39, 11146 (1989)

R. Cao, K. Miyano, T. Kendelewicz, I. Lindau and W.E. Spicer, **Fermi Level Movement at the Cs/GaAs (110) Interfaces:** Appl. Phys. Lett. 54, 1250 (1989)

R. Cao, K. Miyano, I. Lindau and W.E. Spicer, **Metal Cluster Formation on GaAs (110): A Temperature Dependence Study:** J. Vac. Sci. Technol. A 7, 1975 (1989)

R. Cao, K. Miyano, I. Lindau and W.E. Spicer, **Temperature Effects on Morphology, Reaction, and Fermi Level Movement at Ga/InP(110) Interface:** Solid State Commun. 70, 7 (1989)

R. Cao, K. Miyano, T. Kendelewicz, I. Lindau and W.E. Spicer, **Low-Temperature Alkali Metal/III-V Interfaces: A Study of Metallization and Fermi Level Movement:** J. Vac. Sci. Technol. B 7, 919 (1989)

R. Cao, K. Miyano, T. Kendelewicz, I. Lindau and W.E. Spicer, **Interaction of Thin Ga Overlayers with InP (110):** Mat. Res. Soc. Symp. Proc. 143, 103 (1989)

R. Cao, K. Miyano, I. Lindau and W.E. Spicer, **Fermi Level Pinning at the Interfaces of Sb, Sn, and Ge on GaAs (110) Surfaces:** J. Vac. Sci. Technol. A 7, 738 (1989)

R. Cao, K. Miyano, I. Lindau and W.E. Spicer, **Evidence for Two Pinning Mechanisms with Noble Metals on InP (110):** J. Vac. Sci. Technol. A 7, 861 (1989)

R. Carr and J. Yang, **Current to Frequency Converter for Electron Multiplier:** Rev. Sci. Instrum. 60, 2321 (1989)

S. Caticha-Ellis, R. Boyce and H. Winick, **Conceptual Design of Instrumentation to Measure the Diffraction Profile of a Single Crystal at Bragg Angle Near $\pi/2$ by Using Synchrotron Radiation:** accepted by Nucl. Instrum. Methods

T.T. Chiang, A.K. Wahi, I. Lindau and W.E. Spicer, **Annealing Ag on GaAs: Interplay Between Cluster Formation and Fermi Level Pinning:** J. Vac. Sci. Technol. B 7, 958 (1989)

C.J. Chisholm-Brause, G.E. Brown and G.A. Parks, **EXAFS Investigation of Aqueous Co(III) Adsorbed on Oxide Surfaces In-Situ:** Physica B 158, 646 (1989)

C.J. Chisholm-Brause, A.L. Roe, K.F. Hayes, G.E. Brown, G.A. Parks and J.O. Leckie, **XANES and EXAFS Study of Aqueous Pb(II) Adsorbed on Oxide Surfaces:** Physica B 158, 674 (1989)

J.L. Cole, G.O. Tan, E.K. Yang, K.O. Hodgson and E.I. Solomon, **Reactivity of the Laccase Trinuclear Copper Active Site with Dioxygen: An X-ray Absorption Edge Study:** accepted by J. Am. Chem. Soc.

S.D. Conradson and I.D. Raistrick, **The Axial Oxygen Atom and Superconductivity in $YBa_2Cu_3O_7$:** Science 243, 1340 (1989)

S.D. Conradson, B.K. Burgess, S.A. Vaughn, A.L. Roe, B. Hedman, K.O. Hodgson and R.H. Holm, **Cyanide and Methylisocyanide Binding to the Isolated Iron-Molybdenum Cofactor of Nitrogenase:** J. Biol. Chem. 264, 15967 (1989)

P.L. Cowan and S. Brennan, **Self-Filtering Crystal Monochromators for Synchrotron X-Radiation:** Rev. Sci. Instrum. 60, 1987 (1989)

E.D. Crozier, **Recent Topics in EXAFS Data Analysis:** Physica B 158, 14 (1989)

J. DeWitt, B. Hedman, A. Ericson, K.O. Hodgson, J. Bentsen, R. Beer, S.J. Lippard, J. Green and H. Dalton, **X-ray Absorption Spectroscopy of Protein A of Methane Monooxygenase:** Physica B 158, 97 (1989)

D.S. Dessau, Z.-X. Shen, P.A.P. Lindberg, B.O. Wells, D.B. Mitzi, I. Lindau, W.E. Spicer and A. Kapitulnik, **The Electronic Structure of $Pb_2Sr_2CaCu_3O_8$ as Studied by Resonance Photoemission:** accepted by Physica C

D.S. Dessau, Z.-X. Shen, P.A.P. Lindberg, B.O. Wells, W.P. Ellis, A. Borg, J.-S. Kang, D.B. Mitzi, I. Lindau, W.E. Spicer and A. Kapitulnik, **Electronic Structure of $Pb_2Sr_2CaCu_3O_8$:** Phys. Rev. B 40, 6726 (1989)

S.V. Didziulis, K.D. Butcher, S.L. Cohen and E.I. Solomon, **The Chemistry of Copper Overlayers on Zinc Oxide Single Crystal Surfaces: Model Active Sites for Cu/ZnO Methanol Synthesis Catalysts:** J. Am. Chem. Soc. 111, 7110 (1989)

M.K. Eidsness, R.A. Scott, B.C. Prickril, D.V. DerVartanian, J. Legall, I. Moura, J.J.G. Moura and, H.D. Peck, Jr., **Evidence for Selenocysteine Coordination to the Active Site Nickel in the [NiFeSe] hydrogenases from Desulfovibrio baculatus:** Proc. Natl. Acad. Sci. USA 86, 147 (1989)

W.P. Ellis, A.M. Boring, J.W. Allen, L.E. Cox, R.D. Cowan, B.B. Pate, A.J. Arko and I. Lindau, **Valence-Band Photoemission Intensities in Thorium Dioxide:** Sold State Commun. 72, 725 (1989)

R.D. Feldman, P.H. Fuoss, R.F. Austin, J.L. Kahn, L.J. Norton and S. Brennan, **$Hg_{1-x}Cd_xTe/Hg_{1-x}Zn_xTe$ Superlattices with Constant Hg Content:** Appl. Phys. Lett. 54, 1466 (1989)

J. Freund, R. Ingalls and E.D. Crozier, **Extended X-ray Absorption Fine-Structure Study of Copper Under High Pressure:** Phys. Rev. B 39, 12537 (1989)

J. Freund and R. Ingalls, **Inverted Isothermal Equation of State and Determination of B(0), B'(0) and B"(0):** J. Phys. Chem. Solids 50, 263 (1989)

P.H. Fuoss, D.W. Kisker, G. Renaud, K.L. Tokuda, S. Brennan and J.L. Kahn, **Atomic Nature of Organometallic-Vapor Phase-Epitaxial Growth:** Phys. Rev. Lett. 63, 2389 (1989)

P.H. Fuoss, D.W. Kisker, S. Brennan, J.L. Kahn, G. Renaud and K.L. Tokuda, **In-Situ X-ray Scattering Studies of Chemical Vapor Deposition:** accepted by J. Physique

P.H. Fuoss and S. Brennan, **Surface Sensitive X-ray Scattering:** submitted to Ann. Rev. Mat. Sci.

P.H. Fuoss, D.W. Kisker, S. Brennan and J.L. Kahn, **Application of X-ray Scattering to the In-Situ Study of Organometallic Vapor Phase Epitaxy:** Mat. Res. Soc. Symp. Proc. 131, 137 (1989)

G.N. George, W.E. Cleland, J.H. Enemark, C. Kipke, S. Roberts and S.P. Cramer, **L-Edge Spectra of Mo Compounds & Enzymes:** Physica B 158, 133 (1989)

G.N. George, N.A. Turner, R.C. Bray, F.F. Morpeth, D.H. Boxer and S.P. Cramer, **X-ray Absorption and Electron Paramagnetic Resonance Spectroscopic Studies of the Environment of Molybdenum in High-pH and Low-pH forms of Escherichia coli Nitrate Reductase:** Biochem. J. 259, 693 (1989)

G.N. George, C.A. Kipke, R.C. Prince, R.A. Sunde, J.H. Enemark and S.P. Cramer, **Structure of the Active Site of Sulfite Oxidase. X-ray Absorption Spectroscopy of the Mo(IV), Mo(V) and Mo(VI) Oxidation States:** Biochem. 28, 5075 (1989)

G.N. George, W.E. Cleland, J.E. Enemark, B.E. Smith, C.A. Kipke, S.A. Roberts and S.P. Cramer, **L-Edge Spectroscopy of Molybenum Compounds and Enzymes:** submitted to J. Am. Chem. Soc.

G.N. George, R.C. Prince and S.P. Cramer, **The Manganese Site of the Photosynthetic Water-Splitting Enzyme:** Science 243, 789 (1989)

G.N. George, R.C. Prince, K.E. Stokeley and M.W.W. Adams, **X-ray Absorption Spectroscopic Evidence for a Novel Iron Cluster in Hydrogenase II from Clostridium pasteurianum:** Biochem. J. 259, 597 (1989)

G.N. George and M.L. Gorbaty, **Sulfur K-edge X-ray Absorption Spectroscopy of Petroleum Asphaltenes and Model Compounds:** J. Amer. Chem. Soc. 111, 3182 (1989)

G.N. George, R.C. Prince, T.G. Frey and S.P. Cramer, **Oriented X-ray Absorption Spectroscopy of Membrane Bound Metalloproteins:** Physica B 158, 81 (1989)

J.A. Goodwin, L.J. Wilson, D.M. Stanbury and R.A. Scott, **Ligand-Substitution and Electron-Transfer Reactions of Pentacoordinate Copper(I) Complexes:** Inorg. Chem. 28, 42 (1989)

R.B. Greegor, F.W. Lytle, B.C. Chatoumakos, R.C. Ewing, R.J. Livak, F.W. Clinard, E.D. Crozier, N. Alberding, A.J. Seary, G.W. Arnold et al., **Application of Various EXAFS Techniques to the Investigation of Structurally Damaged Materials:** Physica B 158, 498 (1989)

M. Green, M. Richter, X. Xing, D. Scherson, K.J. Hanson, P.N. Ross, R. Carr and I. Lindau, **In-Situ Scanning Tunneling Microscopy Studies of the Underpotential Deposition of Lead on Au(111):** J. Phys. Chem. 93, 2181 (1989)

M. Hart and W. Parrish, **Polycrystalline Diffraction and Synchrotron Radiation:** Proc. Mat. Res. Soc. 143, 185 (1989)

M. Hart, R. Cernik, W. Parrish and H. Toraya, **Lattice Parameter Determination for Powders using Synchrotron Radiation:** submitted to J. Appl. Cryst.

T.M. Hayes, D.L. Williamson, A. Outzourhit, P. Small, P. Gibart and A. Rudra, **DX Centers in Sn-doped $Ga_{0.7}Al_{0.3}As$:** J. Electr. Mater. 18, 207 (1989)

T.M. Hayes, D.L. Williamson, A. Outzourhit, P. Small, P. Gibart and A. Rudra, **Sn-related DX Centers in $Ga_{0.7}Al_{0.3}As$:** Physica B 158, 581 (1989)

B. Hedman, P. Frank, S.F. Gheller, W.E. Newton, E.I. Solomon and K.O. Hodgson, **Low-Energy X-ray Absorption Edge Spectroscopy: Applications to the Nitrogenase Cofactor and Electronic Structure of S and Cl in Inorganic Solids:** Physica B 158, 71 (1989)

B. Hedman, K.O. Hodgson and E.I. Solomon, **X-ray Absorption Edge Spectroscopy of Ligands Bound to Open Shell Metal Ions:** J. Am. Chem. Soc. 112, 1643 (1990)

W.A. Hendrickson, A. Pahler, J.L. Smith, Y. Satow, E.A. Merritt and R.P. Phizackerley, **Crystal Structure of Core Strepavidin Determined from Mutliwavelength Anomalous Diffraction of Synchrotron Radiation:** Proc. Natl. Acad. Sci. USA 86, 2190 (1989)

R. Hettel, **Review of Synchrotron Beam Stability and Stabilizing Systems:** Rev. Sci. Instrum. 60, 1501 (1989)

R. Hille, G.N. George, M.K. Eidsness and S.P. Cramer, **EXAFS Analysis of Xanthine Oxidase Complexes with Alloxanthine, Violapterin, and 6-Pteridylaldehyde:** Inorg. Chem. 28, 4018 (1989)

R.S. Howland, T.H. Geballe, S.S. Laderman, A. Fischer-Colbrie, M. Scott, J.M. Tarascon and P. Barboux, **Determination of Dopant Site Occupanies in Cu-substituted $YBa_2Cu_3O_{7-\delta}$ by Differential Anomalous X-ray Scattering:** Phys. Rev. B 39, 9017 (1989)

J.J. Hoyt, B. Clark, D. DeFontaine, J.P. Simon and O. Lyon, **A Synchrotron Radiation Study of Phase Separation in Al-Zn Alloys. I. Kinetics:** Acta Metall. 15, 1597 (1989)

J.J. Hoyt and D. DeFontaine, **A Synchrotron Radiation Study of Phase Separation in Al-Zn Alloys. II. Scaling:** Acta Metall. 15, 1611 (1989)

G.P. Huffman, F.E. Huggins, A.A. Levasseur, J.F. Durant, F.W. Lytle, R.B. Greegor and A. Mehta, **Investigation of Atomic Structures of Calcium in Ash and Desposits Produced During the Combustion of Lignite and Bituminous Coal:** Fuel 68, 238 (1989)

G.P. Huffman, F.E. Huggins, S. Mitra, N. Shah, F.W. Lytle and R.B. Greegor, **Forms of Occurence of Sulfur and Chlorine in Coal:** Physica B 158, 225 (1989)

G.P. Huffman, F.E. Huggins, M. Sudipa, N. Shah, R.J. Pugmire, B. Davis, F.W. Lytle and R.B. Greegor, **Investigation of the Molecular Structure of Organic Sulfur in Coal by XAFS Spectroscopy:** Energy & Fuels 3, 200 (1989)

F.E. Huggins, G.P. Huffman, N. Shah, F.W. Lytle, R.B. Greegor and R.G. Jenkins, **In-Situ XAFS Studies of Catalyzed Pyrolysis and Gasification Reactions of Lignite:** Physica B 158, 178 (1989)

F.E. Huggins, G.P. Huffman, F.W. Lytle and R.B. Greegor, **The Form-of-Occurrence of Chlorine in U.S. Coals:** Amer. Chem. Soc. Div. of Fuel Chem. 34, 551 (1989)

J.S. Iwanczyk, N. Dorri, M. Wang, M. Szawlowski, W.K. Warburton, B. Hedman and K.O. Hodgson, **Advances in Mercuric Iodide Energy Dispersive X-ray Array Detectors and Associated Miniaturized Processing Electronics:** Rev. Sci. Instrum. 60, 1561 (1989)

W. Jark, G. Comelli, T.P. Russell and J. Stohr, **Structural Studies of Langmuir-Blodgett Multilayers by Means of Soft X-ray Diffraction:** Thin Solid Films 170, 309 (1989)

D.T. Jiang, N. Alberding, A.J. Seary, B. Heinrich and E.D. Crozier, **A Glancing-Incidence Surface EXAFS Study on Epitaxially Grown Al/Ni/Fe(001) Thin Films:** Physica B 158, 662 (1989)

G.W. Johnson, D.E. Brodie and E.D. Crozier, **EXAFS Analysis of Vacuum Deposited Amorphous Germanium:** Can J. Phys. 67, 358 (1989)

M. Kaminska, E.R. Weber, Z. Liliental-Weber and Z. Rek, **Stoichiometry-Related Defects in GaAs Grown by Molecular Beam Epitaxy at Low-Temperatures:** J. Vac. Sci. Technol. B 7, 710 (1989)

J.-S. Kang, J.W. Allen, M.B. Maple, M.S. Torikachvili, W.P. Ellis, B.B. Pate, Z.-X. Shen, J.J. Yeh and I. Lindau, **Fermi-Level Tuning in $Y_{1-x}U_xPd_3$:** Phys. Rev. B 39, 13529 (1989)

J.-S. Kang, J.W. Allen, Z.-X. Shen, W.P. Ellis, J.J. Yeh, B.-W. Lee, M.B. Maple, W.E. Spicer and I. Lindau, **Electronic Structure of the Quenched Superconductivity Materials $Y_{1-x}Pr_xBa_2Cu_3O_{7-\sigma}$:** J. Less Common Metals 148, 121 (1989)

J.S. Kang, J.W. Allen, M.B. Maple, M.S. Torikachvili, W.P. Ellis, B.B. Pate, Z.-X. Shen, J.J. Yeh and I. Lindau, **Counter-Intuitive 5f Spectral Weight Shift in $Y_{1-x}U_xPd_3$:** Phys. Rev. B 39, 13529 (1989)

V. Karpenko, J.H. Kinney, S. Kulkarni, K. Neufeld, C. Poppe, K.G. Tirsell, J. Wong, J. Cerino, T. Troxel, J. Yang et al, **Beam Line 10 - A Multipole Wiggler Beam Line at SSRL:** Rev. Sci. Instrum. 60, 1451 (1989)

L.-S. Kau, K.O. Hodgson and E.I. Solomon, **X-ray Absorption Edge and EXAFS Study of the Copper Sites in ZnO Methanol Synthesis Catalysts:** J. Am. Chem. Soc. 111, 7103 (1989)

T. Kendelewicz, K. Miyano, R. Cao, J.C. Woicik, I. Lindau and W.E. Spicer, **Surface Core Level Shifts on InP (110): Use of Sb Overlayers:** Surf. Sci. 220, L727 (1989)

T. Kendelewicz, R. Cao, K. Miyano, I. Lindau and W.E. Spicer, **Resonant Photoemission from the Ni-GaAs (110) Interface:** J. Vac. Sci. Technol. A 7, 749 (1989)

T. Kendelewicz, R. Cao, K. Miyano, I. Lindau and W.E. Spicer, **Unique Band Bending at the Sb/InP (110) Interface:** J. Vac. Sci. Technol. A 7, 765 (1989)

T. Kendelewicz, K. Miyano, R. Cao, I. Lindau and W.E. Spicer, **Abrupt Interfaces on InP (110): Cases of Sb and Sn:** J. Vac. Sci. Technol. B 7, 991 (1989)

P. King, R. Browning, P. Pianetta, I. Lindau, G. Knapp and M. Keenlyside, **Multispectral Analysis of Photoelectron Microscopy Images:** J. Vac. Sci. Technol. A 7, 3301 (1989)

P.L. King, A. Borg, C. Kim, P. Pianetta, I. Lindau, R. Browning, G.S. Knapp and M. Keenlyside, **From Small Area to Imaging Photoabsorption Spectroscopy:** submitted to Nucl. Instrum. Methods

P.L. King, R. Browning, P. Pianetta, I. Lindau, M. Keenlyside and G. Knapp, **Image Processing of Multi-spectral X-ray Photoelectron Spectroscopy Images:** J. Vac. Sci. Technol. A 7, 3301 (1989)

P.L. King, A. Borg, C. Kim, P. Pianetta, I. Lindau, G. Knapp and M. Keenlyside, **Small Area Photoemission and Photoabsorption Measurements using a Photoelectron Microscope:** accepted by Phys. Scripta

J.H. Kinney, Q.C. Johnson, M.C. Nichols, R.A. Saroyan, U. Bonse, R. Nusshardt and R. Pahl, **X-ray Micro-tomography on Beam Line 10 at SSRL:** Rev. Sci. Instrum. 60, 2471 (1989)

J.H. Kinney, S.R. Stock, M.C. Nichols, U. Bonse, T.M. Breunig, R.A. Saroyan, R. Nusshardt, Q.C. Johnson, F. Busch and S.D. Antolovich, **Nondestructive Investigation of Damage in Composites Using X-ray Tomographic Microscopy (XTM):** accepted by J. Matl. Res. (1989)

D.W. Kisker, P.H. Fuoss, K.L. Tokuda, G. Renaud, S. Brennan and J.L. Kahn, **An X-ray Analysis of GaAs Surface Reconstructions in H_2 and N_2 Atmospheres:** submitted to Appl. Phys. Lett.

D.W. Kisker, P.H. Fuoss, S. Brennan, G. Renaud, K.L. Tokuda and J.L. Kahn, **In-Situ Characterization of Organometallic Growth of ZnSe Using Grazing Incidence X-ray Scattering:** accepted by J. Cryst. Growth

W. Lavendar, G. Brown and T. Troxel, **Observation of X-ray Undulator Radiation on PEP:** Rev. Sci. Instrum. 60, 1414 (1989)

P.A. P. Lindberg, Z.-X. Shen, D.S. Dessau, B.O. Wells, D.B. Mitzi, I. Lindau, W.E. Spicer and A. Kapitulnik, **Energy Dispersions of Single Crystalline $Bi_{2.0}Sr_{1.8}Ca_{0.8}La_{0.3}Cu_{2.1}O_{8+\delta}$ Superconductors Determined Using Angle-Resolved Photoelectron Spectroscopy:** Phys. Rev. B 40, 5169 (1989)

P.A.P. Lindberg, I. Lindau and W.E. Spicer, **Quantitative Analysis of X-ray Photoemission Spectra Applied to $Bi_2Sr_2CaCu_2O_8$ High-Temperature Superconductors:** Phys. Rev. B 40, 6822 (1989)

P.A.P. Lindberg, Z.-X. Shen, B.O. Wells, D.S. Dessau, A. Borg, W. Ellis, D.B. Mitzi, I. Lindau, W.E. Spicer and A. Kapitulnik, **Spectroscopic Evidence of Two-Dimensional Character of the 90K $Bi_{2.0}Si_{1.8}Ca_{0.8}La_{0.3}Cu_{2.1}O_{8+\delta}$:** Applied Physics Lett. 55, 1141 (1989)

P.A.P. Lindberg, Z.-X. Shen, J. Hwang, C.K. Shih, I. Lindau, W.E. Spicer, D.B. Mitzi and A. Kapitulnik, **Electronic Structure of the $La1+xBa_{2-x}Cu_3O_{7+\delta}$ System Studied by Photoelectron Spectroscopy:** Solid State Commun. 69, 27 (1989)

P.A.P. Lindberg, Z.-X. Shen, B.O. Wells, D.S. Dessau, W.P. Ellis, A. Borg, J.-S. Kang, D.B. Mitzi, I. Lindau, W.E. Spicer and A. Kapitulnik, **Photoemission Study of Absorption Mechanisms in $Bi_{2.0}Sr_{1.8}Ca_{0.8}La_{0.3}Cu_{2.1}O_{8+\delta}$, $BaBiO_3$ and $Nd_{1.85}Ce_{0.15}CuO_4$:** Phys. Rev. B 40, 8840 (1989)

P.A.P. Lindberg, Z.-X. Shen, D.S. Dessau, B.O. Wells, A. Borg, W. Ellis, D.B. Mitzi, I. Lindau, W.E. Spicer and A. Kapitulnik, **The Electronic Structure of $Bi_{2.0}Sr_{1.8}La_{0.3}Ca_{0.8}Cu_{2.1}O_{8+\delta}$ Superconductors Studies using Ultraviolet and X-ray Photoelectron Spectroscopy:** Physica C 159, 649 (1989)

P.A.P. Lindberg, Z.-X. Shen, B.O. Wells, D.S. Dessau, D.B. Mitzi, I. Lindau, W.E. Spicer and A. Kapitulnik, **Reaction of Rb and Oxygen Overlayers with Single-Crystalline $Bi_2Sr_2CaCu_2O_{8+\delta}$ Superconductors:** Phys. Rev. B 39, 2890 (1989)

P.A.P. Lindberg, Z.-X. Shen, D.B. Mitzi, I. Lindau, W.E. Spicer and A. Kapitulnik, **Photoemission Study of the Electronic Structure of the $Pr_{0.2}La_{0.8}Ba_{1.875}La_{0.125}Cu_3O_{7-\delta}$ System:** Solid State Commun. 72, 575 (1989)

J.L. Martin Jr., J. Yuan, C.E. Lunte, R.C. Elder, W.R. Heineman and E. Deutsch, **Technetium-Diphosphonate Skeletal Imaging Agents: EXAFS Structure Studies in Aqueous Solution:** Inorg. Chem. 28, 2899 (1989)

N. Masciocchi and W. Parrish, **New Crystal Data for High Temperature Hexagonal Silver Sulfate:** accepted by Pow. Diff.

N. Masciocchi, H. Toraya and W. Parrish, **Structure Refinement of CuO Using Synchrotron and Focusing Powder Diffraction Data:** submitted to Mat. Sci. Eng.

A.E. McDermott, V.K. Yachandra, R. Guiles, J.L. Cole, S.L. Dexheimer, R.D. Britt, K. Sauer, M.P. Klein, K.G. Parrett and J.G. Golbeck, **EXAFS Structural Study of F_x, the Low Potential Fe-S Center in Photosystem I.:** Biochem. 28, 8056 (1989)

O.R. Melroy, M.F. Toney, G.L. Borges, M.G. Samant, J.B. Kortright, P.N. Ross and L. Blum, **An In-Situ Grazing Incidence X-ray Scattering Study of the Initial Stages of Electrochemical Growth of Lead on Silver (111):** J. Electroanal. Chem. 258, 403 (1989)

O.R. Melroy, M.F. Toney, G.L. Borges, M.G. Samant, J.B. Kortright, P.N. Ross and L. Blum, **Two-Dimensional Compressibility of Electrochemically Adsorbed Lead on Silver (111):** Phys. Rev. B 38, 10962 (1989)

K. Miyano, R. Cao, T. Kendelewicz, I. Lindau and W.E. Spicer, **Temperature Control of Morphology and Barrier Formation at the In/GaAs (110) Interface:** J. Vac. Sci. Technol. A 7, 731 (1989)

W.W. Moses and S.E. Derenzo, **Cerium Fluoride, A New Fast, Heavy Scintillator:** IEEE Trans. Nucl. Sci. 36, 173 (1989)

R. Murphy, E.W. Plummer, C.T. Chen, W. Eberhardt and R. Carr, **Dynamics of Adsorbate Core-hole Decay. II. Lifetimes:** Phys. Rev. B 39, 7517 (1989)

M.C. Nichols, J.H. Kinney, Q.C. Johnson, R.A. Saroyan, U. Bonse, R. Nusshardt and R. Pahl, **Synchrotron Microtomography of Supported Catalysts:** Rev. Sci. Instrum. 60, 2475 (1989)

J.E Penner-Hahn, R.M. Fronko, V.L. Pecoraro, C.F. Yocum and N.R. Bowlby, **XAS of Mn in the Photosynthetic Oxygen Evolving Complex:** Physica B 158, 107 (1989)

J.E. Penner-Hahn, H.T. Tsang, T.V. O'Halloran and J. Wright, **XAS of the MerR Metalloregulatory Protein:** Physica B 158, 117 (1989)

J.E. Penner-Hahn, M. Murata, K.O. Hodgson and H.C. Freeman, **Low-temperature X-ray Absorption Spectroscopy of Plastocyanin: Evidence for Copper-Site Photoreduction at Cryogenic Temperatures:** Inorg. Chem. 28, 1826 (1989)

P. Pianetta, I. Lindau, P.L. King, M. Keenlyside, G. Knapp and R. Browning, **Core Level Photoelectron Microscopy with Synchrotron Radiation:** Rev. Sci. Instrum. 60, 1686 (1989)

C.W. Ponader and G.E. Brown, **Rare Earth Elements in Silicate Glass/Melt Systems: I. Effects of Composition on the Coordination Environment of La, Gd, and Yb.:** Geochim. Cosmochim. Acta 53, 2893 (1989)

C.W. Ponader and G.E. Brown, **Rare Earth Elements in Silicate Glass/Melt Systems: II. Interactions of La, Gd and Yb with Halogens:** Geochim. Cosmochim. Acta 53, 2905 (1989)

E. Puppin and I. Lindau, **Kinetic Effects in the Overgrowth of Gd on Si: A Photoemission Study:** Solid State Commun. 71, 1015 (1989)

M. Qian, E.A. Stern, Y. Ma, R. Ingalls, M. Sarikaya, B. Thiel, R. Kurosky, C. Han, L. Hutter and I. Aksay, **Nickel Impurties in the Y-Ba-Cu-O 90K Superconductor:** Phys. Rev. B 39, 9192 (1989)

M. Qian, E.A. Stern, Y. Ma, R. Ingalls, M. Sarikaya, D. Thiel, R. Kurosky, C. Han, L. Hutter and I. Aksay, **Nickel Impurities in the 90K Superconductor:** Physica B 158, 477 (1989)

I.K. Robinson, A.A. MacDowell, M.S. Altman, P.J. Estrup, K. Evans-Lutterodt, J.D. Brock and R.J. Birgeneau, **Order-Disorder Transition of the W(001) Surface:** Phys. Rev. Lett. 62, 1294 (1989)

E. Rubenstein, J.C. Giacomini, H.J. Gordon, A.C. Thompson, G. Brown, R. Hofstadter, W. Thomlinson and H.D. Zeman, **Synchrotron Radiation Coronary Angiography with a Dual Beam, Dual Detector Imaging System:** submitted to Nucl. Instrum. Methods

T.P. Russell, W. Jark, G. Comelli and J. Stohr, **Reflectivity of Soft X-rays by Polymer Mixtures:** Mat. Res. Soc. Symp. Proc. 143, 265 (1989)

S. Sasaki, B. Youngman and H. Winick, **The Use of Single Wavelength Wiggler in PEP as Circular Polarized Hard X-ray Source:** submitted to Nucl. Instrum. Methods

A. Schmidt Klemens, D.R. McMillin, H.T. Tsang and J.E. Penner-Hahn, **Structural Characterization of Mercury Substituted Copper Proteins. Results from X-ray Absorption Spectroscopy:** J. Am. Chem. Soc. 111, 6398 (1989)

G. Scott, K. Ninomiya, C.R. Helms and I. Lindau, **Auger Analysis of Si Sputtered with Ar^+ Ions in an F_2 Ambient:** Surf. Sci. 221, 253 (1989)

R.A. Scott, W.G. Zumft, C.L. Coyle and D.M. Dooley, **Pseudomonas stutzeri N_2O Reductase Contains Cu(A)-type Sites:** Proc. Natl. Acad. USA Sci. 86, 4082 (1989)

R.A. Scott, **X-ray Absorption Spectroscopic Investigations of Cytochrome c Oxidase Structure and Function:** Ann. Rev. Biophys. Biophys. Chem. 18, 137 (1989)

R.A. Scott, **Comparative X-ray Absorption Spectroscopic Structural Characterization of Nickel Metalloenzyme Active Sites:** Physica B 158, 84 (1989)

J.R. Shapley, W.S. Uchiyama and R.A. Scott, **Bimetallic Catalysts from Alumina-Supported Molybdenum-Iridium Clusters:** accepted by J. Phys. Chem.

Z.-X. Shen, P.A.P. Lindberg, B.O. Wells, D.S. Dessau, A. Borg, I. Lindau, W.E. Spicer, W.P. Ellis, G.H. Kwei, K.C. Ott et al., **Photoemission Study of Monoclinic $BaBiO_3$:** Phys. Rev. B 40, 6912 (1989)

Z.-X. Shen, P.A.P. Lindberg, C.K. Shih, W.E. Spicer and I. Lindau, **Angle-resolved Photoemission Study of NiO and CoO:** accepted by Physica C

Z.-X. Shen, P.A.P. Lindberg, P. Soukiassian, C.B. Eom, I. Lindau, W.E. Spicer and T.H. Geballe, **Nature of the States Near the Fermi Level of the Layered Superconductors of $Bi_2Ca_1Sr_2Cu_2O_8$ and $Bi_2Sr_2CuO_6$:** Phys. Rev. B 39, 823 (1989)

Z.-X. Shen, P.A.P. Lindberg, D.S. Dessau, I. Lindau, W.E. Spicer, D.B. Mitzi, I. Bozovic and A. Kapitulnik, **Photoelectron Energy Loss Study of the $Bi_2CaSr_2Cu_2O_8$ Superconductor:** Phys. Rev. B 39, 4295 (1989)

A.K. Shiemke, W.A. Kaplan, C.L. Hamilton, J.A. Shelnutt and R.A. Scott, **Structural and Spectroscopic Characterization of Exogenous Ligand Binding to Isolated Factor F_{430} and Its Configurational Isomers:** J. Biol. Chem. 264, 7276 (1989)

A.K. Shiemke, J.A. Shelnutt and R.A. Scott, **Coordination Chemistry of F_{430}:** J. Biol. Chem. 264, 11236 (1989)

C.K. Shih, Z.-X. Shen, P.A.P. Lindberg, J. Hwang, I. Lindau, W.E. Spicer, S. Doniach and J.W. Allen, **Dispersion of One Hole Excitation in An Antiferromagnetic Mott-Insulator: An Angle-Resolved Photoemission Study:** submitted to Phys. Rev. Lett.

J.E. Silk, L.D. Hansen, D.J. Eatough, M.W. Hill, N.F. Mangelson, F.W. Lytle and R.B. Greegor, **Chemical Characteristics of Vanadium, Nickel, and Arsenic in Oil Fly-Ash Samples Using EXAFS and XANES Spectroscopy:** Physica B 158, 247 (1989)

R. Singh, J.T. Spence, G.N. George and S.P. Cramer, **Oxomolybdenum(V) Complexes with Sulfide and Hydrogensulfide Ligands: Models for the Molybdenum(V) Centers of Xanthine Oxidase and Xanthine Dehydrogenase:** Inorg. Chem. 28, 8 (1989)

M. Soncrotti, I. Abbati, E. Puppin, Z.-X. Shen, I. Lindau, R. Eggenhoffner, A. Landelli and G.L. Olcese, **Yb Mean Valence in Chemically Compressed $Yb_{1-x}Sc_xA_{12}$ Pseudobinary Alloys: An X-ray Absorption Spectroscopy Investigation:** submitted to Solid State Comm.

S. Sorenson, R. Carr, S. Schaphorst, S. Whitfield and B. Crasemann, **Coster-Kronig Yields in Silver Measured with Synchrotron Radiation:** Phys. Rev. A 39, 4198 (1989)

W.E. Spicer, R. Cao, K. Miyano, T. Kendelewicz, I. Lindau, E. Weber, Z. Liliental-Weber and N. Newman, **From Synchrotron Radiation to I-V Measurements of GaAs Schottky Barrier Formation:** Appl. Surf. Sci. 41/42, 1 (1989)

C.J. Spindt, D. Liu, K. Miyano, P.L. Meissner, T.T. Chiang, T. Kendelewicz, I. Lindau and W.E. Spicer, **Vacuum Ultraviolet Photoelectron Spectroscopy of $(NH_4)_2S$-Treated GaAs (100) Surfaces:** Appl. Phys. Lett. 55, 861 (1989)

P.A. Stevens, R.J. Madix and J. Stohr, **The Bonding of Acetonitrile and CH_2CN on Ag(110) Determined by NEXAFS: Evidence for π-donor Bonding and Aximuthal Ordering:** J. Chem. Phys. 91, 4338 (1989)

S.R. Stock, Y.H. Chung and Z.U. Rek, **A Multiple-Slit Collimator for Synchrotron White Beam Section Topography:** J. Appl. Cryst. 22, 70 (1989)

G. Tan, L.S. Kau, K.O. Hodgson and E.I. Solomon, **Edge and EXAFS Studies of Cu Coordination in Deoxy Hemocyanin:** Physica B 158, 110 (1989)

R. Tatchyn, **A Dynamic Method for Continuously Measuring Magnetic Field Profiles in Planar Microprobe Undulators with Submillimeter Gaps:** Nucl. Instrum. Methods A 279, 655 (1989)

R. Tatchyn, **A Segmented Electrostatic Undulator Design for Generating Arbitrarily Polarized Soft X-rays at the Stanford Positron Electron Project:** J. Appl. Phys. 65, 4107 (1989)

R. Tatchyn, **A Universal Classification of Optimal Undulator Types and Parameters for Arbitrary Storage Ring Environments:** Nucl. Instrum. Methods A 275, 430 (1989)

R. Tatchyn, P. Csonka and A. Toor, **Perspectives on Micropole Undulators in Synchrotron Technology:** Rev. Sci. Instrum. 60, 1796 (1989)

R. Tatchyn, **Variable-period Electrostatic and Magnetostatic Undulator Designs for Generating Polarized Soft X-rays at PEP:** Rev. Sci. Instrum. 60, 2571 (1989)

L.K. Templeton and D. Templeton, **Biaxial Tensors for Anomalous Scattering of X-Rays in Selenolanthionine:** Acta Cryst. A 44, 1045 (1989)

A. Thompson, E. Rubenstein, R. Kernoff, H. Zeman, N. Gmur, W. Thomlinson, R. Hofstadter, J. Giacomini, H. Gordon and G. Brown, **Application of Synchrotron Radiation to the Imaging of Coronary Arteries:** submitted to SPIE

A.C. Thompson, H. Zeman, W. Thomlinson, E. Rubenstein, R.S. Kernoff, R. Hofstadter, J.C. Giacomini, H.J. Gordon and G.S. Brown, **Imaging of Coronary Arteries Using Synchrotron Radiation:** Nucl. Instrum. Methods B 40/41, 407 (1989)

A.C. Thompson, H.D. Zeman, E. Rubenstein, J.N. Otis, R. Hofstadter, G.S. Brown, D.C. Harrison, R.S. Kernoff, J.C. Giacomini, H.J. Gordon and W. Thomlinson, **Coronary Angiography using Synchrotron Radiation:** Rev. Sci. Instrum. 60, 1674 (1989)

A.C. Thompson, J.H. Underwood, Y. Wu, R.D. Giauque, M.L. Rivers and R. Futernick, **X-ray Microprobe Studies Using Multilayer Focussing Optics:** Adv. X-ray Analysis 32, 149 (1989)

M.F.Toney and S. Brennan, **Measurements of Carbon Thin Films using X-rays:** J. Appl. Phys. 66, 1861 (1989)

M.F. Toney and S. Brennan, **Structural Depth Profiling of Iron Oxide Thin Films Using Grazing Incidence Asymmetric Bragg X-ray Diffraction:** J. Appl. Phys. 65, 4763 (1989)

M.F. Toney and S. Brennan, **Observation of the Effect of Refraction on X-Rays Diffracted in a Grazing Incidence Asymmetric Bragg Geometry:** Phys. Rev. B 39, 7963 (1989)

M.F. Toney and O.R. Melroy, **In-Situ X-ray Scattering of Monolayers Adsorbed at Electrochemical Interfaces:** Mat. Res. Soc. Symp. Proc. 143, 37 (1989)

A. Toor, P. Csonka and R. Tatchyn, **Micropole Undulators: Novel Insertion Devices for Synchrotron Sources:** Rev. Sci. Instrum. 60, 1439 (1989)

H. Toraya, N. Masciocchi and W. Parrish, **X-ray Structure Study of Alkali Aluminotitanate $Na_6Al_2Ti_6O_{16}$:** submitted to J. Mat. Res.

H.-T. Tsang, C.J. Batie, D.P. Ballou and J.E. Penner-Hahn, **X-ray Absorption Spectroscopy of the [2Fe-2S] Rieske Cluster in Pseudomonas cepacia Phthalate Dioxygenase. Determination of Core Dimensions and Iron Ligation:** Biochem. 28, 7233 (1989)

H.T. Tsang, C.J. Batie, D.M. Ballou and J.E. Penner-Hahn, **XAS Investigation of the Fe Sites in Phthalate Dioxygenase:** Physica B 158, 115 (1989)

T.A. Tyson, A.L. Roe, B. Hedman, P. Frank and K.O. Hodgson, **A Study of the Electronic Structure of $S_2O_6^{2-}$ by Polarized K-edge X-ray Absorption Spectroscopy:** Physica B 158, 398 (1989)

T.A. Tyson, M. Benfatto, C.R. Natoli, B. Hedman and K.O. Hodgson, **Ab Initio EXAFS and Multiple Scattering Analysis of SF_6:** Physica B 158, 425 (1989)

T.A. Tyson, A.L. Roe, P. Frank, K.O. Hodgson and B. Hedman, **Polarized Experimental and Theoretical K-Edge X-ray Absorption Studies of SO_4^{2-}, ClO_3^-, $S_2O_3^{2-}$ and $S_2O_6^{2-}$:** Phys. Rev. B 39, 6305 (1989)

A.K. Wahi, G.P. Carey, T.T. Chiang, I. Lindau and W.E. Spicer, **CdTe and ZnTe Metal Interface Formation and Fermi-Level Pinning:** J. Vac. Sci. Technol. A 7, 494 (1989)

A. Waldhauer, **Comparison of Elliptical and Spherical Mirrors for the Grasshopper Monochromators at SSRL:** Rev. Sci. Instrum. 60, 2109 (1989)

S. Wang, G.S. Waldo and J.E. Penner-Hahn, **Polarized XANES of Co(III)$(NH_3)_6$ Molecular Crystals:** Physica B 158, 253 (1989)

S. Wang, G.S. Waldo, R. Fronko and J.E. Penner-Hahn, **Polarized XANES of Iron Porphyrins:** Physica B 158, 119 (1989)

G.A. Waychunas, G.E. Brown, W.E. Jackson and C.W. Ponader, **High Temperature EXAFS Study of Fe in Crystaline and Molten Oxides and Silicates:** Physica B 158, 67 (1989)

B.O. Wells, P.A.P. Lindberg, Z.-X. Shen, D.S. Dessau, I. Lindau, W.E. Spicer, D.B. Mitzi and A. Kapitulnik, **Valence-Band States in $Bi_2Ca_1Sr_1$ $La_3Cu_2O_8$:** Phys. Rev. B 40, 5259 (1989)

J. Whitmore, Y. Ma, E.A. Stern, F.C. Brown, R.L. Ingalls, J.P. Rice, B.G. Pazol and D.M. Ginsberg, **XAFS or Oriented single Crystal of $YBa_2Cu_3O_{7-\delta}$:** Physica B 158, 440 (1989)

G. Will, N. Masciocchi, W. Parrish and H. Lutz, **Crystal Structure and Cation Distribution of $MnCrInS_4$ from Synchrotron Powder Diffraction Data:** accepted by Zeit. f Krist.

H. Winick, **A Review of Synchrotron Radiation Facilities Outside the USA:** accepted by Nucl. Instrum. Methods

J. Woicik, B. Pate and P. Pianetta, **Silicon (111) 2x1 Surface States:K-edge Transitions and Surface Selective $L_{2,3}$ VV Auger Lineshape:** Physica B 158, 576 (1989)

J. Woicik, P. Pianetta, S.L. Sorensen and B. Crasemann, **Photon Energy Sensitive Si $L_{2,3}$ VV Auger Satellite:** Phys. Rev. B 39, 8593 (1989)

J. Woicik, B.B. Pate and P. Pianetta, **Silicon (111) 2x1 Surface States: K-edge Transitions and Surface Selective $L_{2,3}$VV Auger Lineshapes:** Phys. Rev. B 39, 6048 (1989)

J.C. Woicik, P. Pianetta and T. Kendelewicz, **Si (111) 2x1 Surface Core Level Shifts Investigated by Use of Ge Overlayer:** Phys. Rev. B 40, 1246 (1989)

J. Wong and G.A. Slack, **Metals in Beta-Rhombohedral Boron:** Physica B 158, 627 (1989)

J. Wong, G. Shimkaveg, W. Goldstein, M. Eckert, T. Tanaka, Z.U. Rek and H. Tompkins, **YB_{66}: A New Soft X-ray Monochromator for Synchrotron Radiation:** accepted by Nucl. Instrum. Methods

J. Wong, W.E. Nixon, J.W. Mitchell and S.S. Laderman, **Solute-pairing in Solution-hardened Binary and Ternary FCC Alloys:** Physica B 158, 25 (1989)

BOOKS AND CONFERENCE PROCEEDINGS

M. Borland, **"Calculating Emittance from Images of Undulator Radiation"** in F. Bennet, J. Kopta , eds., Proceedings of the 1989 IEEE Particle Accelerator Conference, March 20-23, 1989, pp. 1228-1230.

M. Borland, M. Donald, **"Experimental Characterization of a PEP Low Emittance Lattice"** in F. Bennett, J. Kopta, eds., Proceedings of the 1989 IEEE Particle Accelerator Conference, March 20-23, 1989, pp. 1231-33.

F. Bridges, J.B. Boyce, T. Claeson, T. Geballe, J.M. Tarascon, **"Occupation of Distorted Cu_1 Sites by Co and Fe in $Y_1Ba_2Cu_3O_{7-\delta}$"** in J. Weaver et al., eds., Synchrotron Radiation in Materials (Materials Research Society, Pittsburgh) 1989.

L. Emery, **"Ultra Low Emittance Damping Ring"** in F. Bennett, J. Kopta, eds., Proceedings of the1989 IEEE Particle Accelerator Conference, March 20-23, 1989, pp. 1225-27.

T.C. Huang, W. Parrish, N. Masciocchi, P. Wang, **"Derivation of d-Values from Digitized X-ray and Synchrotron Diffraction Data"** in Advanced X-ray Analysis 33 (Plenum, 1989).

J.-S. Kang, J.W. Allen, B.-W. Lee, M.B. Maple, M.S. Torikachvili, W.P. Ellis, B.B. Pate, Z.-X. Shen, J.J. Yeh, I. Lindau,**"Electron Spectroscopy Studies of High Temperature Superconductors"** in Proceedings of the International Symposium for the Electronic Structure of High Tc Superconductors, Rome 5-7 October, 1988 (Pergamon, 1989).

S.L. Kramer, **"Study of Collective Effects in a Low-Emittance PEP Lattice"** in F. Bennett, J. Kopta, eds., Proceedings of the 1989 IEEE Particle Accelerator Conference, March 20-23, 1989 pp. 1208-13.

H.-D. Nuhn, R. Boyce, R. Gould, H. Winick, B. Youngman, R. Yotam, **"A 5 GeV Injector for PEP"** in F. Bennett, J. Kopta, eds., Proceedings of the 1989 IEEE Particle Accelerator Conference, March 20-23, 1989 pp. 1217-19.

W. Parrish, M. Hart,, **"Parallel Beam and Focusing X-ray Powder Diffractometry"** in Advanced X-ray Analysis, Vol. 32 (Plenum, 1989) p. 481.

W. Parrish, **"Diffraction Geometry and its Practical Realization: X-ray Powder Techniques"** in International Tables for Crystallography, Volume C.

W. Parrish, A.J.C. Wilson, **"Determination of Lattice Parameters: X-ray Powder Methods"** in International Tables for Crystallography, Volume C.

R.P. Phizackerley, **"Facilities Available for Biophysics Research at the Stanford Synchrotron Radiation Laboratory"** in R.M. Sweet, A.D. Woodhead, eds. Synchrotron Radiation in Structural Biology (Plenum Basic Life Sciences 51, 1989) pp. 19-33.

J. Safranek, **"Beam Dynamics in Wigglers: Tracking in PEP with Damping Wigglers and Measurements at SSRL"** in F. Bennett, J. Kopta, eds., Proceedings of the 1989 IEEE Particle Accelerator Conference, March 20-23, 1989 pp. 1307-09.

Z.-X. Shen, P.A.P. Lindberg, B.O. Wells, I. Lindau, W.E. Spicer, D.B. Mitzi, C.B. Eom, A. Kapitulnik, T.H. Geballe, P. Soukiassian, **"Surface and Electronic Structure of Bi- Ca-Sr-O Superconductors Studied by LEED, UPS, and XPS"** in G. Margaritondo et al., eds., High Tc Superconducting Thin Films, Devices, and Applications, AIP Conference Proceedings 182, 312-317 (1989) .

Z.-X. Shen, P.A.P. Lindberg, I. Lindau, W.E. Spicer, J.W. Allen, **"Photoemission Studies of High Temperature Superconductors"** in G. Mararitondo et al., eds., High Tc Superconducting Thin Films, Devices, and Applications, AIP Conference Proceedings Series 182, pp. 330-349 (1989).

Z.-X. Shen, P.A.P. Lindberg, W.E. Spicer, I. Lindau, J.W. Allen, **"Photoemission Study of High Temperature Superconductors"** in Proceedings of API/AVS 182, 1989.

W.E. Spicer, R. Cao, K. Miyano, C. McCants, T.T. Chiang, C.J. Spindt, N. Newman, T. Kendelewicz, I. Lindau, E. Weber, Z. Liliental-Weber, **"Disruption, Metalization, and Electrical Properties of Metal GaAs and InP Semiconductor Interfaces"** in I.P. Batra, ed., Metallization and Metal-Semiconductor Interfaces (Plenum, 1989) Vol. 195, pp. 139-161.

E. Tanabe, M. Borland, M.C. Green, R.H. Miller, L.V. Nelson, J.N. Weaver, H. Wiedemann, **"A 2-MeV Microwave Thermionic Gun"** in Proceedings of 14th Meeting on Linear Accelerators, Nara, Japan, Sept 7-9, 1989.

B.O. Wells, P.A.P. Lindberg, Z.-X. Shen, D.S. Dessau, I. Lindau, W.E. Spicer, D.B. Mitzi, A. Kapitulnik, **"Aluminum and Gold Deposition on Cleaved Single Crystals of $Bi_2CaSr_2Cu_2O_8$ Superconductor"** in G. Margaritondo et al., eds., High Tc Superconduing Thin Films, Devices, and Applications, AIP Conference Proceedings 182 (1989) pp. 391-398.

H. Winick,**"Overview of Synchrotron Radiation Facilities"** in F. Bennett, J. Kopta, eds., Proceedings of the 1989 IEEE Particle Accelerator Conference, March 20-23 1989, pp. 7-11.

H. Winick, **"A General Overview and a Review of Storage Rings, Research Facilities, and Insertion Devices"** in Physics of Particle Accelerators, AIP Conference Proceedings, 2, 1989 pp. 2138-82.

H. Winick,**"Overview of Synchrotron Radiation Facilities"** in International Conference on SR Applications, Hefei, PRC, May 9-12, 1989.

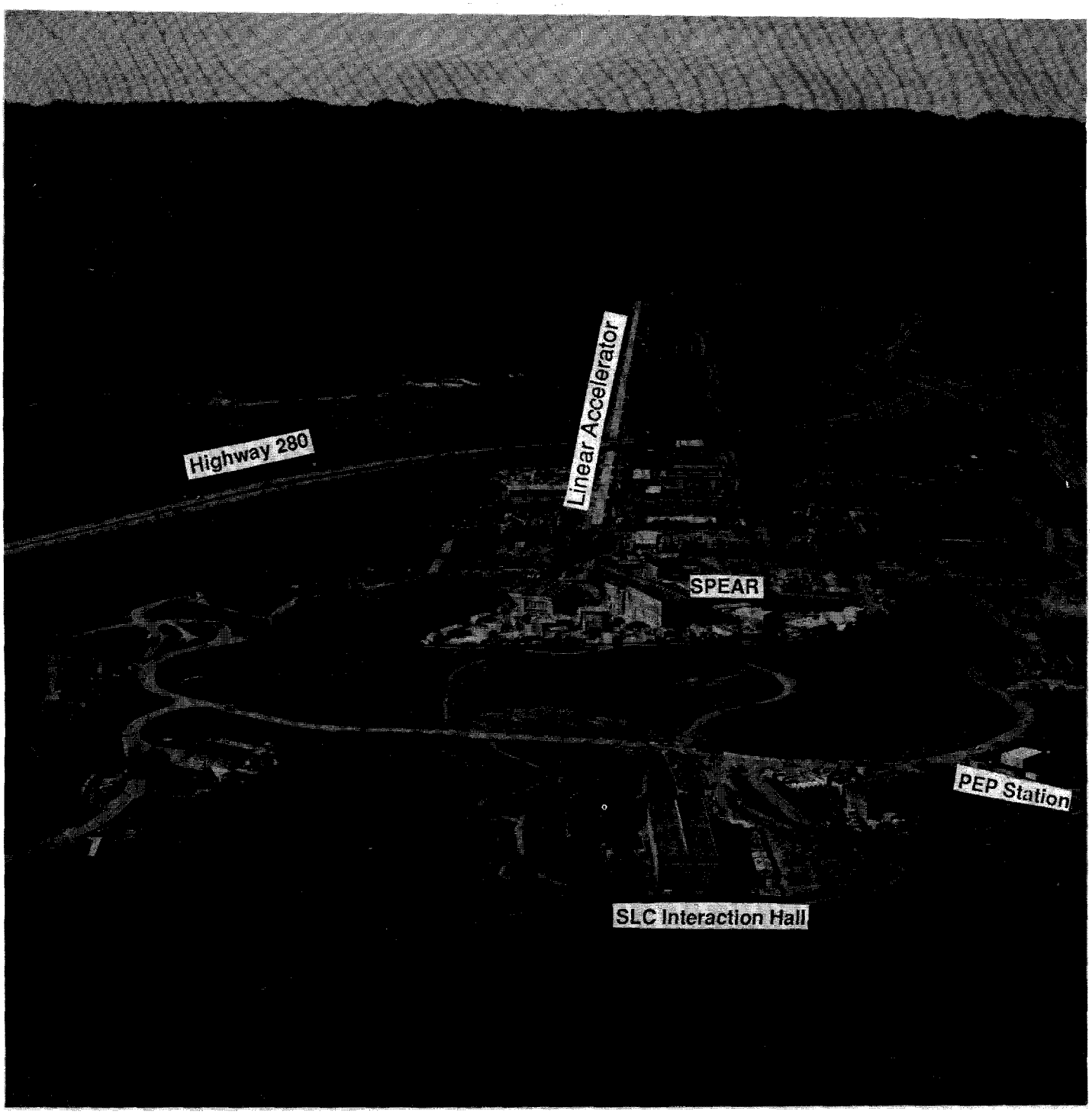

Overview of SLAC Site

☆U.S. GOVERNMENT PRINTING OFFICE:1990 -787 -676/39204